8-28-2012

Structure to function : case studies of hotdog-fold superfamily thioesterases from Escherichia coli.

John A. Latham

John A. Latham
Candidate

Chemistry and Chemical Biology
Department

This dissertation is approved, and it is acceptable in quality and form for publication:

Approved by the Dissertation Committee:

Dr. Debra Dunaway-Mariano, Chairperson

Dr. Patrick Mariano

Dr. David Bear

Dr. Charles Melançon

STRUCTURE TO FUNCTION: CASE STUDIES OF HOTDOG-FOLD SUPERFAMILY THIOESTERASES FROM *ESCHERICHIA COLI*

BY

JOHN A LATHAM

B.S., Eastern New Mexico University
M.S., Eastern New Mexico University

DISSERTATION

Submitted in Partial Fulfillment of the
Requirements for the Degree of

Doctor of Philosophy
Chemistry

The University of New Mexico
Albuquerque, New Mexico

July, 2012

ACKNOWLEDGMENTS

This dissertation is the fruit of not only hard work but also the support of colleagues, friends and family who need to be acknowledged.

I would first like to express my appreciation and gratitude to Dr. Debra Dunaway-Mariano. DDM's advice and guidance through research problems and career decisions has proven to be invaluable. More so was her willingness to allow me to work freely on many projects simultaneously and the encouragement to think independently. DDM's style of mentorship was exactly what I needed and I am forever in her debt.

I would also like to thank Dr. Patrick Mariano for the synthesis advice, the opportunity to work on the lignin peroxidase project and for his candidness. It has also been a pleasure working for Dr. Mariano as his teaching assistant and I appreciate him allowing me to try on my teaching shoes.

I gratefully acknowledge my remaining committee members Dr. David Bear and Dr. Charles Melançon for their input and their patience.

Running experiments can sometimes be monotonous and painful but I was fortunate to have worked with a wonderful bunch of people who have become like a second family to me. Thanks to all my labmates but especially Ty, Luke, Li, Min, Hua, Sarah, and Andrea for keeping things fun, for those many great conversations out of nowhere, providing me with advice, and their friendship. In addition, a good portion of the synthesis of CoA compounds and proton NMR was carried out by an outstanding undergraduate student - thank you Gabe Maestas for that hard work.

I am also grateful for the support of my parents and brothers. And finally to my wife, Kimberly, if it wasn't for her I would have never come back to school. More importantly, she sacrificed our time together so that I could work long hours to finish in a timely manner. If it wasn't for her love, support, and understanding none of this would be possible. For that I am eternally grateful.

STRUCTURE TO FUNCTION: CASE STUDIES OF HOTDOG-FOLD SUPERFAMILY THIOESTERASES FROM *ESCHERICHIA COLI*

BY

JOHN A LATHAM

B.S., Eastern New Mexico University
M.S., Eastern New Mexico University

DISSERTATION

Submitted in Partial Fulfillment of the
Requirements for the Degree of

Doctor of Philosophy
Chemistry

The University of New Mexico
Albuquerque, New Mexico

July, 2012

STRUCTURE TO FUNCTION: CASE STUDIES OF HOTDOG-FOLD SUPERFAMILY THIOESTERASES FROM *ESCHERICHIA COLI*

JOHN A. LATHAM

B.S., Chemistry, Eastern New Mexico University, 2007

M.S., Chemistry, Eastern New Mexico University, 2008

Ph.D., Chemistry, University of New Mexico, 2012

ABSTRACT

My doctoral research primarily focuses on the *Escherichia coli* hotdog-fold thioesterases *ydiI* and *ybgC*.

The *ydiI* gene is colocalized in the operon *ydi*HIJ. A substrate screen provided evidence that YdiI prefers aryl-CoA substrates and discriminated against the analogous aryl-ACP, unlike the paralog YbdB which works on 2,4-DHB-EntB in the enterobactin synthesis pathway. A bioinformatic approach showed that in some bacteria, *ydiI* is colocalized with genes from the menaquinone pathway. YdiI was shown to catalyze the hydrolysis of DHNA-CoA with physiological relevance ($k_{cat}/K_M \sim 10^5$). Furthermore, the *E. coli* YdiI⁻ strain was shown to have perturbed growth, in good agreement with other menaquinone enzyme knockout experiments. Taking into account the evidence provided, YdiI is likely the DHNA-CoA thioesterase in the menaquinone pathway.

Within the substrate binding pocket, changes to the YdiI Val68 to the YbdB equivalent of Met resulted in perturbed catalytic efficiency towards lauroyl-CoA, however not towards its physiological substrate DHNA-CoA. The YbdB M68V mutant

resulted in increase efficiency towards lauroyl-CoA and DHNA-CoA, seemingly making it a gatekeeper. Secondly, YdiI catalyzes the hydrolysis of acyl-CoA's using a Glu63, His54, and Gln48 triad determined by mutagenesis experiments. The utilization of ^{18}O incorporation and rapid-quench techniques provided insight into YdiI's catalytic mechanism. A single phase multiple turnover reaction and the incorporation of ^{18}O in single turnover reactions suggests that ydiI uses a general base catalytic mechanism where Glu63 is the activating residue.

The second *E. coli* hotdog-fold thioesterase protein discussed within is YbgC. YbgC is encoded by the first ORF of the *tol-pal* gene cluster. Previous work on the *H. influenzae* homologue demonstrated affinity for short chain acyl-CoA's and tandem affintity purificiation experiments showed *E. coli* YbgC co-purifies with ACP. No previous attempts to screen for acyl-ACP has been made. To screen YbgC for ACP activity, a method was developed to stoichiometrically construct acyl-ACP's, using *apo*ACP, BF1558 acyl-transferase and acyl-CoA. The *E. coli* YbgC demonstrated preference for long chain acyl-CoA's and their analogous acyl-ACPs. To understand the nature of ACP binding to YbgC, SAXS analysis was carried out on the complex demonstrating that 2 ACP molecules bind to 1 dimer of YbgC.

ABBREVIATIONS

A	Adenosine/Alanine
AA	Amino Acid
ADP	Adenosine 5'-diphosphate
ACP	Acyl-carrier protein
AMP	Adenosine 5'-monophosphate
ATP	Adenosine 5'-triphosphate
ArCP	Aryl-carrier protein
Arg/R	Arginine
Asn/N	Asparigine
Asp/D	Aspartic acid
ATCC	American Type Culture Collection
Bp	Base-Pair
Blast	Basic Local Alignment Search Tool
BSA	Bovine Serum Albumin
C	Cysteine
CoA/CoASH	Co-enzyme A
cDNA	Complementary Deoxynucleic acid
CV	Column volume
Da	Dalton
DHB	Dihydroxybenoate
DHNA	Dihydroxynapthoic acid

DNA	Deoxyribonucleic acid
DI H2O	Distilled and deionized water
3-D	Three dimensional
DMSO	Dimethyl sulfoxide
DTNB	5,5’-dithio-bis-(2-nitrobenzoic acid)
DTT	Dithiothreitol
E	Enzyme
EC	Enzyme Commission
E.coli	Escherichia Coli
EDTA	Disodium ethylenediamine tetraacetate
ESI-MS	Electrospray ionization Mass spectrometry
EXPASY	Expert protein analysis system
FAS	Fatty Acid synthase
FPLC	Fast Protein Liquid Chromatography
g	Gram
GC/MS	Gas chromatography/Mass spectrometry
GEO	Gene expression ominbus
Gln/Q	Glutamine
Glu/E	Glutamte
Gly/G	Glycine
h	Hour
HBA	Hydroxybenozoic acid
H-bond	Hydrogen bond

HEPES	4-(2-Hydroxyethyl)-1-piperazineethanesulfonic acid
His/H	Histidine
HPLC	High Performance Liquid Chromatography
Ile/I	Isoleucine
IPTG	Isopropylthio-β-galactoside
K	Rate constant
Kb	Kilo-base pair
kcat	Enzyme turnover rate
Kd	Dissociation constant
Km	Michaelis-Menten constant
Ki	Inhibition Constant
kob	Observed rate constant
kDa	Kilo-Dalton
L	Liter or Leucine
LB	Luria-Bertani
Lys/K	Lysine
mg	Milligram
min	Minute
ml	Milliliter
mmole	Milimole
MS	Mass spectrum
MW	Molecular Weight
mRNA	Message Ribonucleic acid

Met/M	Methionine
ng	Nanogram
NADH	β-Nicotinamide adenine dinucleotide, reduced form
NCBI	National Center for Biotechnology Information
OD	Optical density
ORF	Open reading frame
OSB	*o*-Succinylbenzoate
pfu	Plaque forming units
PDB	Protein Data Bank
PCR	Polymerase Chain Reaction
PAGE	Polyacrylamide gel electrophoresis
Phe/F	Phenylalanine
Pi	inorganic phosphate
PPi	Pyrophosphate
pI	Isoelectric point
Pro/P	Proline
PS	Polysaccharide
RNA	Ribonucleic acid
RT	Room Temperature
rpm	Rotation per minute
s	Second
S	Substrate/Serine
SAH	*S*-adenosyl-L-homocysteine

SAM	*S*-adenosyl-methionine
SAXS	Small angle x-ray scattering
SDS	Sodium dodecyl sulfate
SEPHCHC acid	2-succinyl-5-enolpyruvyl-6-hydroxy-3-cyclohexene-1-carboylic
SHCHC acid	(1*R*,6*R*)-2-succinyl-6-hydroxy-2,4-cyclohexadiene-1-carboxylic
SIE	Solvent isotope effect
S_N	Nucleophilic substitution
TAP	Tandem affinity purification
TEII	Thioesterase II
Thr/T	Threonine
Tris	Tris[hydroxymethyl]aminomethane
Trp/W	Tryptophan
Tyr/Y	Tyrosine
U	Uridine
µM	Micromolar
UV	Ultraviolet
Val/V	Valine
Vmax	Maximum Velocity
V	Volume
WT	Wild type
4HBA	4-hydroxybenzoyl-CoA
4HBAL	4-hydroxybenzoyl-CoA ligase

4HBT	4-hydroxybenzoyl-CoA thioesterase
4CBAL	4-chlorobenozyl-CoA ligase

TABLE OF CONTENTS

CHAPTER ONE
AN INTRODUCTION TO THE HOTDOG-FOLD THIOESTERASE ENZYME SUPERFAMILY

1.1 Biological significance of thioesters and thioesterases

Biological thioesters include acylated glutathione, acylated protein cysteine, acylated or aroylated coenzyme A (CoA) and acylated or aroylated *holo* acyl carrier protein (ACP) (Figure 1.1). Thioesters play important cellular roles in energy production, cell cycling, signal transduction, and gene regulation (*1*). Thioester bond hydrolysis results in the formation of the free thiol and free acid. The free acid may vary in polarity and shape, whereas the free thiol is typically either the pantothene arm of coenzyme A (CoA) or a *holo* acyl carrier protein (ACP) or the cysteine residue of a protein. Carboxylic acids are converted to thioesters for the purpose of biosynthesis (polyketide synthesis) (*2*), biodegradation (halogenated aromatic degradation) (*3*), and protein modification (S-palmitoylation of cysteine residues) (*4*).

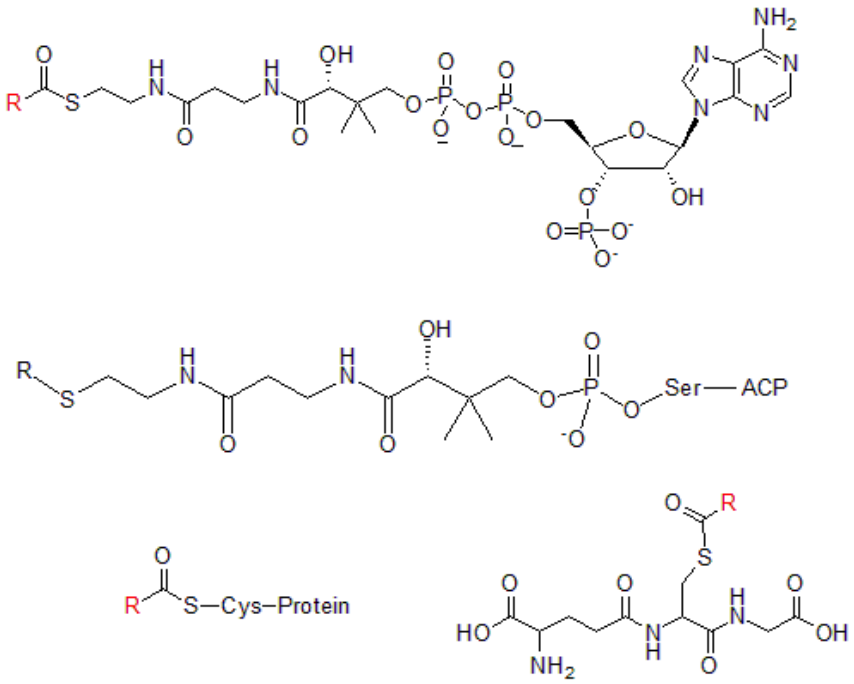

Figure 1.1: Commonly formed natural thioesters. From top to bottom: acyl-CoA, acyl-holo-ACP, acyl-cysteine, and acyl-glutathione.

The two enzyme families that have evolved to catalyze the hydrolysis of thioesters are the α/β-fold hydrolase enzyme superfamily and the hotdog-fold enzyme superfamily (*5*, *6*). Thioesterases from both enzyme superfamilies families have been found to play roles in primary and secondary metabolism. In eukaryotes, thioesterases are present in the cytosol, endoplasmic reticulum, mitochondria, or perioxisomes (*1*). Although the focus of this chapter is the hotdog-fold family, it is worthwhile to mention key aspects of the α/β-fold hydorylase fold family.

The α/β hydrolase fold was first identified by comparing five amino acid sequence and functionally divergent hydrolases (*7*). The canonical α/β hydrolase fold consists of a parallel, eight-stranded β-sheet surrounded by α-helices on both sides

(Figure 1.2.A) (5). Some α/β-fold hydrolases, *e.g.* the human acyl-CoA thioesterase 4 (Figure 1.2.B), also contain a small cap domain. The X-ray crystal structures of numerous α/β-fold thioesterases have been deposited in the Protein Data Bank (PDB). Each structure shows strict conservation of a Ser-His-Asp catalytic triad.

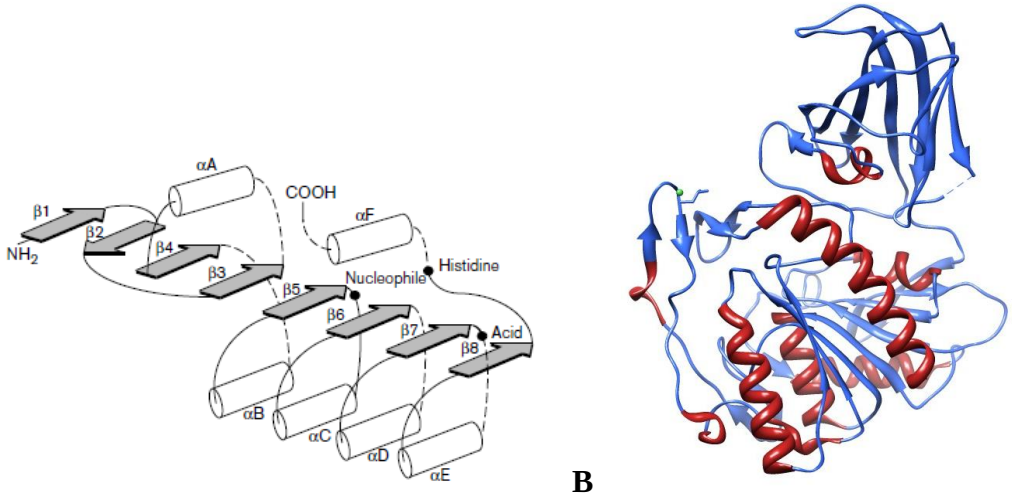

A **B**

Figure 1.2: A) Representation of the topology of the canonical α/β hydrolase fold. The β-strands are represented by grey arrows and the α-helices are represented by white cylinders. The black dots represent the location of the catalytic triad. B) The crystal structure of the human acyl-CoA thioesterase 4 (PDB ID: 3K2I). The β-strands are represented in blue and the α-helices are represented in red.

1.2 Thioesterases of the hotdog-fold enzyme superfamily

The well-conserved hotdog-fold consists of an elongated α-helix ("sausage") encompassed by 5 anti-parallel β-strands ("bun"). This fold was first observed for the dehydratase/isomerase enzyme FabA (Figure 1.3.A) (*8*). Typically, the topology of the core hotdog-fold from the N-terminus to the C-terminus is β1-α-β2-β3-β4-β5 (Figure 1.3.B). In addition to the core domain, some hotdog-fold family members contain

sequence inserts between two elements of the core fold. The minimal functional unit of the hotdog-fold family member is a homodimer. The active site is located at the interface of two subunits. The catalytic residues are located on the loop that connects with the N-terminus of the α-helix of one subunit and the middle section of the α-helix on the second subunit. The hotdog-fold enzyme superfamily includes dehydratases/isomerases, enol-CoA hydratases, and acyl-CoA and acyl-ACP thioesterases. Recently, the hotdog-fold domain of the non-reducing polyketide synthase (NR-PKS) PksA was shown to function as a cyclase/aromatase (*9*). Characteristic of hot-dog fold members is the degeneracy in sequence. Family members typically share as low as 10-15% sequence identity, while maintaining similar tertiary structures (*10*).

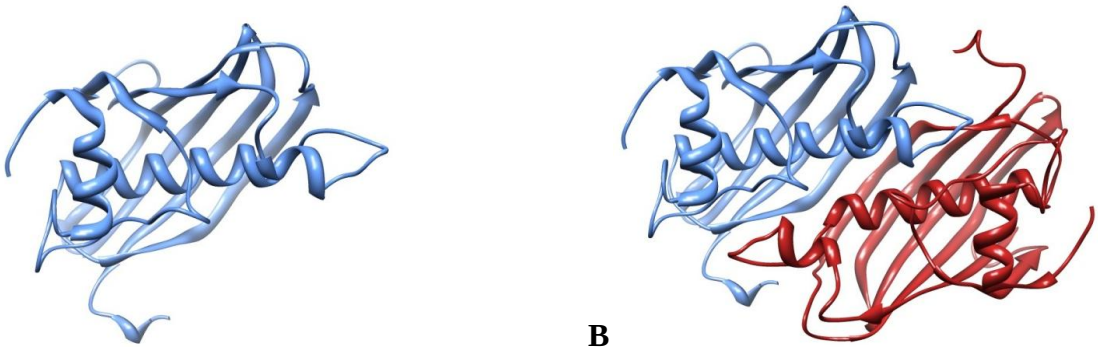

A **B**

Figure 1.3: A) The apo- monomer and (B) apo-dimer structures of *Escherichia coli* FabA (PDB ID: 1MKA).

The vast majority of the hotdog-fold family members are thioesterases. Hotdog-fold thioesterases are diverse in cellular function and span all three branches of life (6). The hotdog-fold superfamily has been divided into six subfamilies distinguished by their overall architecture (6). The largest of the six subfamilies is the acyl-CoA thioesterase subfamily, it is broadly represented throughout the prokaryotic and eukaryotic kingdoms. Members of this subfamily catalyze the hydrolysis of acyl-CoA thioesters to the

corresponding free fatty acids and the CoASH (1). Included in the acyl-CoA thioesterase subfamily are the human enzymes brown fat adipose tissue thioesterase (BFIT) and cytoplasmic acetyl-CoA hydrolase (CACH) (*11, 12*). The second subfamily is the YbgC-like subfamily. The prototype of this subfamily, *E. coli* YbgC is the topic of Chapter 5 of this thesis. Although crystal structures have been solved for YbgC (*E. coli* YbgC – PDB ID: 1S5U and *H. pylori* YbgC – PDB ID: 2PZH), the physiological role of this thioesterase remained unclear. Two studies have been performed to characterize the substrate preference of YbgC in *Haemophilus influenzae* and *Heilicobacter pylori* however, with conflicting results. The *H. influenzae* YbgC was reported to prefer short chain acyl-CoA's as substrates whereas *H. pylori* YbgC was reported to be most active with that of long chain acyl-CoA's (*13, 14*).

The third hotdog-fold subfamily is the FAT subfamily which is comprised of long chain acyl-ACP thioesterases found mainly in plants. Members of the FAT subfamily hydrolyze palmitoyl- or oleoyl-*holo*-ACP to form *holo*-ACP and the corresponding fatty acid (*15*). The fourth subfamily is the TesB-like subfamily. Members of this family possess a double hotdog fold and are known to catalyze the hydrolysis of the fatty acyl-CoA thioesters palmitoyl-CoA and myristoyl-CoA. The TesB-like subfamily is represented in eukaryotes and bacteria (*16*).

The remaining two hotdog-fold thioesterases subfamilies are the 4HBT class I (hereafter referred to as 4HBT) and the 4HBT class II (hereafter referred to as 4HBT-like). The 4HBT-like subfamily is based upon the overall structure of the *Arthrobacter sp.* strain SU 4-hydroxybenzoyl-CoA thioesterase whereas the 4HBT subfamily is based on the overall structure of the *Pseudomonas* sp. CBS3 4-hydroxybenzoyl-CoA

thioesterase. Both thioesterases catalyze the hydrolysis of 4-hydroxybenzoyl-CoA (4HBA-CoA) to the acid and CoASH within the 4-chlorobenzoate (4CBA) catabolic pathway, yet they possess a structurally divergent catalytic site architecture (*17–20*).

1.3 Structural divergence of the 4HBT and 4HBT-like hotdog-fold thioesterases clades

The 4HBT subfamily, as mentioned previously, is made up of structural homologs of *Pseudomonas* sp. CBS3 4HBT. The topology of the core structure of the 4HBT monomer, as depicted in Figure 1.4a, is β_1-α_1-α_2-β_2-β_3-β_4-β_5-β_6. Members of the 4HBT subfamily have decorated structures including the insertion of a stretch of sequence between two elements of secondary structure, which extends the length of the connecting loop. Additionally, 4HBT members differ in sequence length and/or secondary structure at the N or C-termini. However, all 4HBT members conserve the position of their respective active sites at the interface of the two hotdog-fold monomers. The catalytic scaffold consists of residues from one monomer at the N-terminus of the long α-helix, the loop between β_1 and the central α-helix and the center of the central α-helix from the other monomer (Figure 1.4 B).

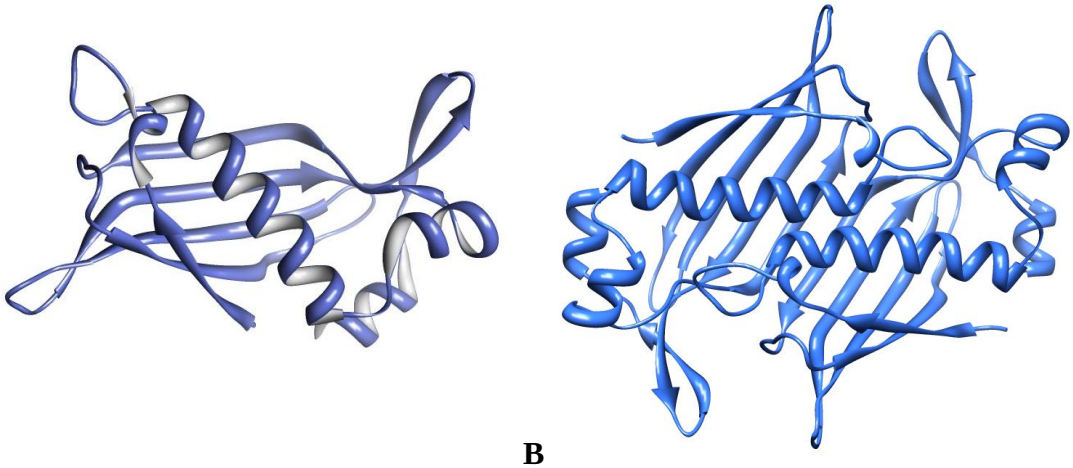

A **B**

Figure 1.4: A) Monomeric and (B) dimeric structure of *Pseudomonas* sp. CBS3 4HBT (PDB ID: 1LO8).

The catalytic site of the 4HBT thioesterase clade members is comprised of two residues that are positioned, on the same subunit, at the N-terminus of the α-helix and at the loop that connects with that N-terminus. The catalytic residues of the prototype, *Pseudomonas* sp. CBS3 4-hydroxybenzoyl-CoA thioesterase, consist of Tyr24 and Asp17. The Tyr24, located at the N-terminus of the α-helix, is responsible for the polarization of the thioester carbonyl group via hydrogen bond donation from its backbone amide NH (Figure 1.5A). The carboxylate side chain, from the nearby Asp17 (located on the loop bridging β_1 and the α-helix), functions as a nucleophile in the cleavage of the thioester C-S bond (*21*). Substrate binding is assisted by two residues: Asp32 and Trp47. Asp32, located on the α-helix of the opposing subunit, interacts with the substrate ring hydroxyl group via hydrogen bonds formed with two bridging water molecules (*23*). Trp47, which is also located on the opposing subunit, forms a hydrogen bond with the substrate benzoyl ring hydroxyl group using its indole side chain NH (see Figure 1.5B).

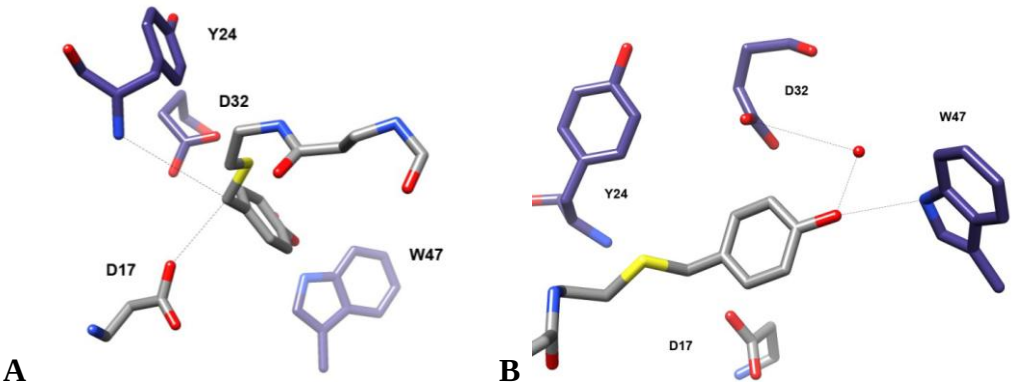

Figure 1.5: A) Active site of *Pseudomonas* sp. CBS3 4HBT shown with the truncated 4-hydroxyphenacyl-CoA substrate analog inhibitor (grey) (PDB ID: 1LO8). B) Substrate binding contributions from W47 and D32 of the same structure.

The prototype of the 4HBT-like subfamily, *Arthrobacter sp.* strain SU 4-hydroxybenzoyl-CoA thioesterase, maintains a α_1- β_1-β_2-α_2-β_3-β_4-β_5-β_6 topology and the typical hotdog-fold structure shown in Figure 1.6A. Comparison of the active site structures of the *Pseudomonas* sp CBS3 4-hydroxybenzoyl-CoA thioesterase and the *Arthrobacter sp.* strain SU 4-hydroxybenzoyl-CoA thioesterase reveals two distinct pathways of evolution (Figure 1.6B).

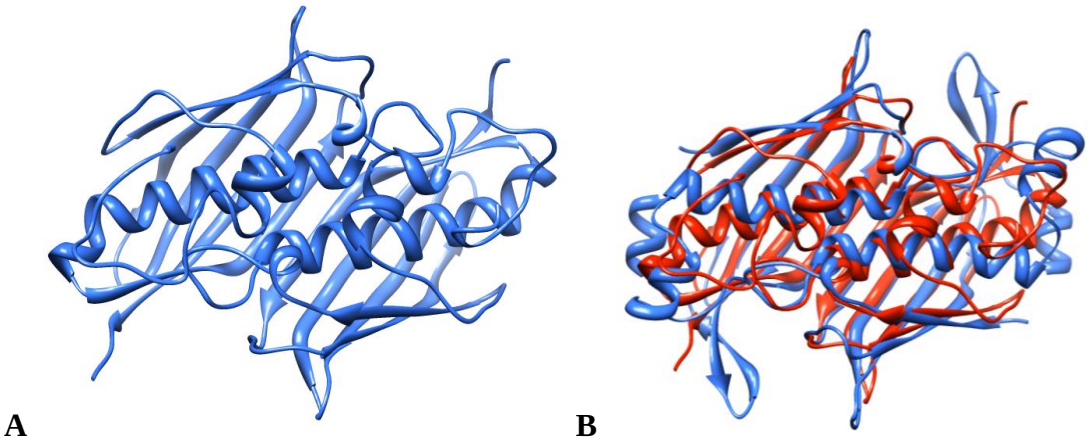

Figure 1.6: A) The dimeric structure of *Arthrobacter sp.* strain SU 4-hydroxybenzoyl-CoA thioesterase (PDB ID: 3R32). B) Superposition of the *Pseudomonas sp.* CBS3 (red) and *Arthrobacter sp.* strain SU 4-hydroxybenzoyl-CoA thioesterase (blue) dimeric structures.

The active site of 4HBT-like thioesterase catalyzes the hydrolysis of the thioester by using the α-helix N-terminus residue of one subunit to polarize the substrate thioester C=O, and a carboxylate residue (Glu or Asp), located on the long α-helix of the opposing subunit, to function in base or nucleophilic catalysis. In addition, the active site usually contains an amide residue (Asn or Gln), which is contributed by the α-helix N-terminus loop of the subunit that opposes that contributing the catalytic carboxylate residue. For example, in the case of the clade prototype *Arthrobacter sp*. strain SU 4HBT, the Gln58 (counterpart to the *Ps.* 4HBT Asp32) and Gly56 (counterpart to *Ps.* 4HBT Tyr24) activate the thioester C=O via hydrogen bonding as is shown in Figure 1.7. The Glu73, located on the α-helix of the opposing subunit functions in nucleophilic catalysis. The Thr77 located on the same subunit as the Glu73 nucleophile, orients a water molecule that attacks the anhydride intermediate, leading to product (*22*).

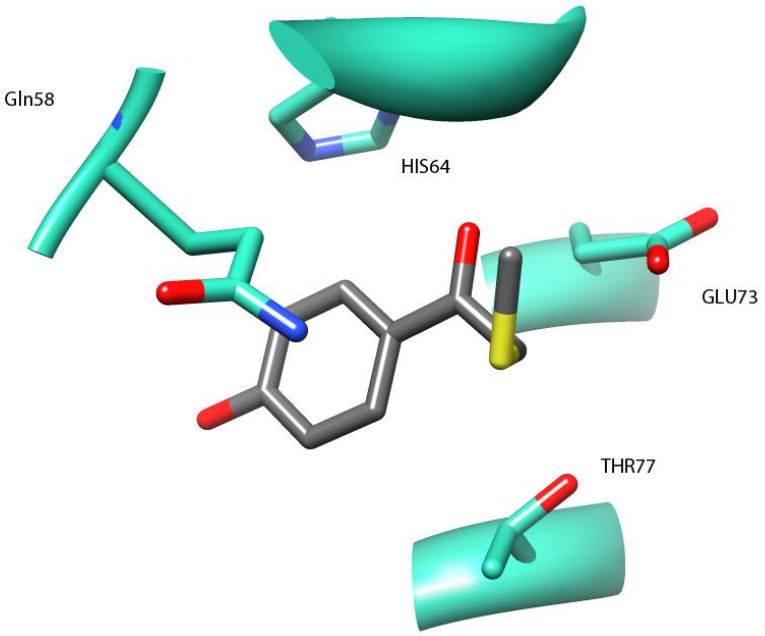

Figure 1.7: Active site of *Arthrobacter sp.* strain SU 4-hydroxybenzoyl-CoA thioesterase (blue) shown with truncated 4-hydroxyphenacyl-CoA ligand (grey) (PDB ID: 3R3F).

Remarkably, the *Arthrobacter sp.* strain SU and *Pseudomonas sp.* CBS3 4-hydroxybenzoyl-CoA thioesterases evolved from different hotdog-fold ancestors to perform catalysis in the same biochemical context, and with the same catalytic efficiency. Soil-dwelling microbes such as *Pseudomonas sp.* CBS3 and *Arthrobacter sp.* SU, are capable of surviving with 4-chlorobenzoate as their sole carbon source (*17*, *18*). The metabolic pathway of the dehalogenation of 4-chlorobenzoate is depicted in Figure 1.9. The initiating step of 4-chlorobenzoate catabolism is the 4-chlorobenzoate ligation to coenzyme A catalyzed by 4-chlorobenzoate ligase (CBAL). This step is followed by the dehalogenation of the 4-chlorobenzoyl-CoA to 4-hydroxybenzoyl-CoA catalyzed by chlorobenzoyl-CoA dehalogenase. The last step in the dehalogenation pathway is the liberation of the free 4-hydroxybenzoate from the 4-hydroxybenzoyl-CoA catalyzed by

4HBT. As previously mentioned, the 4CB pathway 4HBT from *Pseudomonas sp.* CBS and *Arthrobacter sp.* SU are the prototypes of two distinct clades of the hotdog-fold enzyme superfamily.

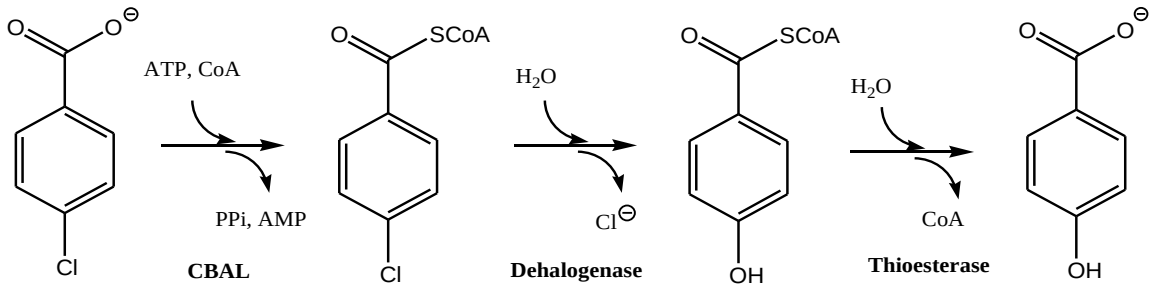

Figure 1.9: The 4-chlorobenozate degradation pathway catalyzed by 4-chlorobenzoate-CoA ligase, 4-chlorobenzoyl-CoA dehalogenase and 4-hydroxybenozoyl-CoA thioesterase.

1.4 Divergence in the Hotdog-fold Thioesterase Cellular Functions in E. coli

The genome of *Escherichia coli* encodes nine hotdog-fold thioesterases: YciA, YbgC, YbaW, PaaI, YdiI, YbdB, YigI, YiiD and TEII. All but YdiI, YigI and YiiD have been subjected to some form of functional analysis.

1.4.1 Hotdog-fold thioesterase YbdB is housekeeper of the enterobactin synthesis pathway in *E. coli*

During iron-depleted conditions, microorganisms, including bacteria and fungi, release siderophores, or iron-chelating compounds, to harvest exogenous iron (*23*). In *E. coli*, this siderophore is enterobactin. Enterobactin is synthesized by the enzymes encoded by the gene cluster *ent*CEBAH, which is under the control of the ferric uptake regulator (*fur*). The gene that encodes the hotdog-fold thioesterase EntH (YbdB) is located within this cluster (*24*). Biosynthesis of enterobactin proceeds via two pathways,

an upper pathway responsible for synthesizing 2,3-dihydroxybenzoate (2,3-DHB) from chorismate catalyzed by EntC, EntB, and EntA and the lower pathway (Figure 1.8) responsible for the construction of the cyclo-tri-2,3-DHB-peptide catalyzed by the nonribosomal peptide synthetases EntB and EntF (*25*). Although it does not appear necessary for a thioesterase to participate in the synthesis of the enterobactin, YbdB (also to become known as EntH) was shown to play an integral role in rescuing the pathway when the ArCP domain of EntB becomes misacylated (*26–28*). It was shown that holo-EntB could become misaclyated as the result of promiscuous EntD and EntE catalysis. The EntF stalls which in turn blocks the lower pathway. The thioesterase YbdB frees misacylated-holo-EntB to holo-EntB thereby ensuring unimpeded enterobactin synthesis.

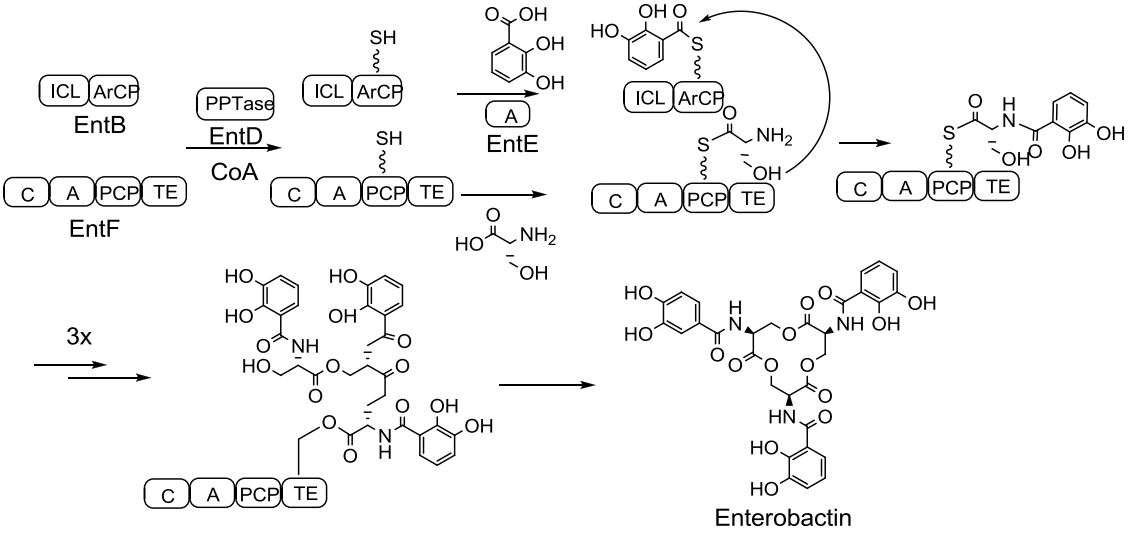

Figure 1.8: The lower chemical pathway for biosynthesis of enterobactin (*26*).

1.4.2 The phenylacetic acid degradation pathway in *E. coli*

E. coli and numerous other bacteria have been previously reported to utilize a variety of aromatic compounds, including phenylacetic acid, as its sole carbon sources (*29*). These bacteria contain the genes that encode enzymes which form the phenylacetic

acid catabolic pathway. In *E. coli* the genes are co-located in a cluster known as *paa*. This gene cluster contains 14 genes organized in multiple transcription elements. The three units transcribed are known as *paa*ABCDEFGHIJK, *paa*XY and *paa*Z (Figure 1.10A) (*30*). The gene products *paa*ABCDE are analogous to aromatic catabolic oxygenases, *paa*K is a phenylacetic acid: CoA ligase and the protein products of the *paa*FGHIJ genes have high sequence similarities to fatty acid β-oxidation pathway enzymes.

The gene product PaaI is a hotdog-fold enzyme that has demonstrated *in vitro* thioesterase activity. From the reported steady state kinetics, PaaI efficiently catalyzes the hydrolysis of phenylacetyl-CoA and various ring-hydroxylated deriviatives, however PaaI is ineffective at catalyzing benzoyl-CoA and its hydroxlated derivatives (*31*). The dead-end products of the catabolic phenylacetic acid pathway, 2- and 3-hydroxyphenylacetic acid are s formed by competing spontaneous dehydration of the putative 1,2-dihydrodiol and 2,3-dihydrodiol pathway intermediates (Figure 1.10B). PaaI is believed to rescue the CoA from phenylacetyl-CoA in the event of a stalled downstream enzyme as well as to rescue CoA from the dead-end products.

A

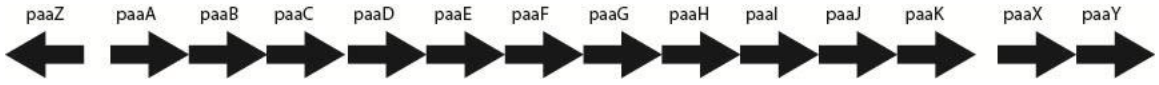

B

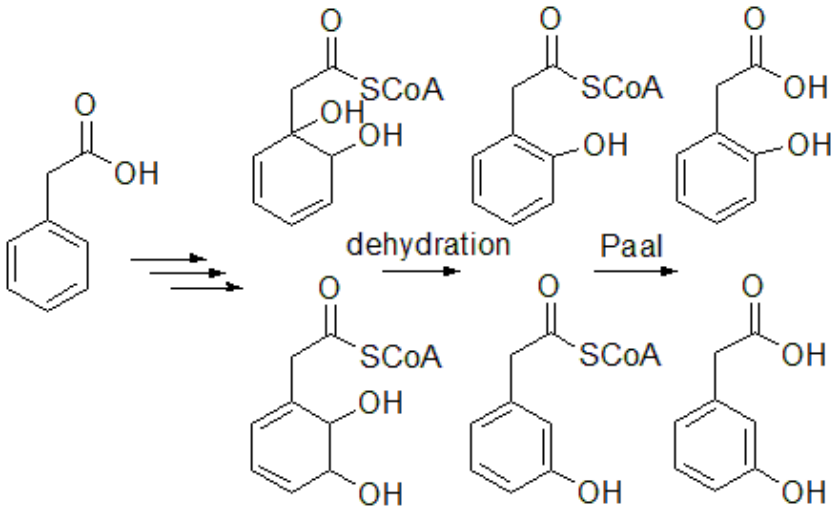

Figure 1.10: A) Gene cluster orientation of the *paa* cluster of the phenylacetic acid catabolism pathway in *E. coli*. B) The putative role of PaaI thioesterase in the phenylacetic acid catabolism pathway.

1.4.3 - *E. coli* YbaW and TEII (Thioesterase II)

When grown on oleic acid as its sole carbon source, *E. coli* has been shown to derive its energy from fatty acid β-oxidation. Recently it has been proposed that ninety percent of the oleic acid is degraded to acetyl-CoA using the classical or isomerase-dependent β-oxidation pathway, requiring enoyl-CoA isomerase (*32*). The remaining ten percent of the oleic acid is degraded partially by an alternative pathway, branching from the classical pathway, and converting the 2-*trans*,5-*cis*-tetradecadienoyl-CoA to 3,5-*cis*-tetradecadienoyl-CoA, a dead end product (see Figure 1.11) (*32*). The minor product 3,5-*cis*-tetradecadienoyl-CoA cannot be further oxidized because the required enzyme, dienoyl-CoA isomerase, is not present.

The double hotdog-fold thioesterase TesB (TEII) was initially purified from *E. coli* several decades ago and has just recently been shown to catalyze the hydrolysis of long chain acyl-CoA's having 3,5-*cis*-tetradecadienoyl-CoA as its best substrate (*33*–*35*). In addition, TEII has also been shown to hydrolyze acyl-*holo*ACP's, but 1000 times slower than the corresponding acyl-CoA (*34*). Physiologically, TEII has also been shown to increase the synthesis of 3-hydroxydecanoic acid when in the presence of (*R*)-3-hydroxydecanoyl-acyl carrier protein (3HD-ACP)–CoA transacylase (PhaG), suggesting that TEII plays a role in a *de novo* fatty acid biosynthesis (*36*). Even though its most active substrate suggests that it might play a role in the minor β-oxidation pathway, recent gene knock-out studies of TEII have shown that another thioesterase, YbaW, is responsible for the hydrolysis of dead-end product 3,5-*cis*-tetradecadienoyl-CoA (*37*, *38*).

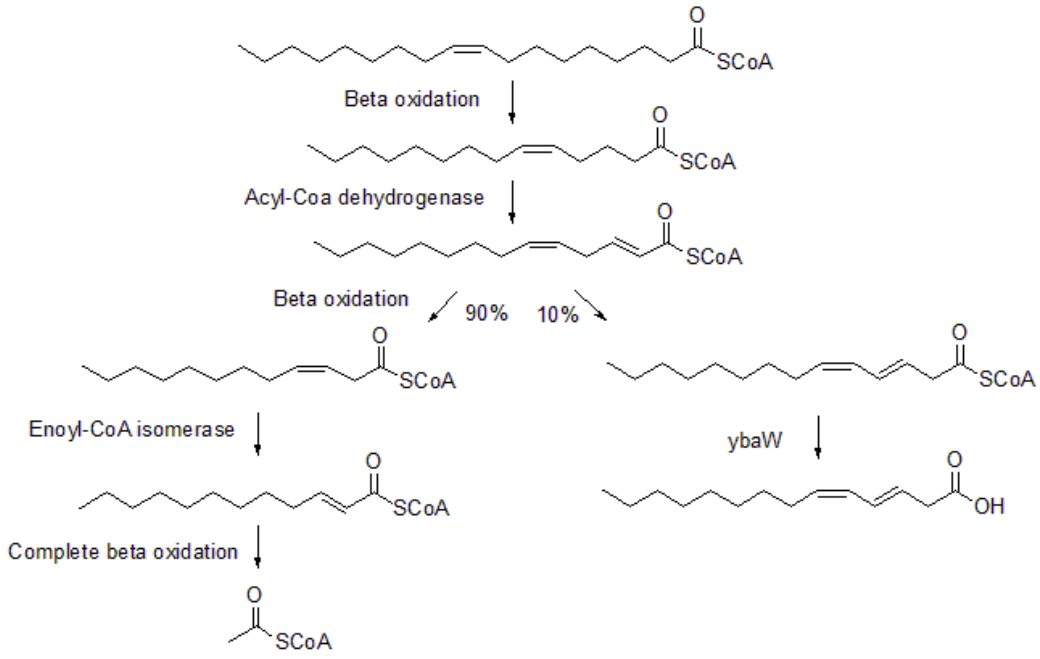

Figure 1.11: *Beta*-oxidation of oleoyl-CoA in *E. coli*. The value of 90% refers to the percentage of oleoyl-CoA that is completely degraded to acetyl-CoA via the main

pathway, while 10% indicates the flux through the minor pathway that facilitates the partial degradation of oleoyl-CoA to 3,5-tetradecadienoic acid.

YbaW is an *E. coli* hotdog-fold thioesterase that has been shown to hydrolyze the minor dead end β-oxidation product 3,5-*cis*-tetradecadienoyl-CoA to the corresponding acid, which is secreted into the medium. Kinetic analysis demonstrated that YbaW efficiently catalyzes the hydrolysis of long chain acyl-CoA thioesters with 3,5-*cis*-tetradecadienoyl-CoA being its best substrate (*37*). The YbaW$^-$ mutant was shown to display perturbed growth on oleic acid as well as on conjugated linoleic acid when compared to the growth of the YbaW$^+$ *E. coli* under the same conditions (*37*, *38*). Taken together, these results indicate that YbaW is the thioesterase necessary for the alternative β-oxidation pathway. The last piece of evidence corroborating YbaW's physiological role is gene context. Specifically, a *fad*R gene is located upstream from the *ybaW* gene (*39*). The FadR protein has a dual role in *E. coli*, acting as a repressor of the β-oxidation pathway and as an activator of the unsaturated fatty acid biosynthetic genes (*40*). Using elecrophoretic mobility assays, Feng *et. al* was able to demonstrate that FadR does bind to the *ybaW* promoter region, making YbaW the newest member of the *fad* regulon (*39*).

1.4.4 - *E. coli* YbgC

The *E. coli* hotdog-fold thioesterase YbgC a 15.6 kDa protein that has a modest level of sequence homology (21% identity) to the *Ps.* 4HBT thioesterase. The YbgC protein is encoded by the first ORF of the *tol-pal* operon found across most bacteria belonging to the α, β, and γ subdivision of proteobacteria. The proteins encoded by *tol-*

pal operon are thought to participate in the formation of the septation ring during cell division (*41*). How YbgC, a thioesterase, might assist this process is unclear.

An insight to the physiological function of YbgC has recently been established via two-hybrid tandem affinity purification (TAP), revealing a possible role in phosholipid synthesis (*42*). The TAP experiments demonstrated that YbgC co-purifies with the small acidic acyl-carrier protein, suggesting that YbgC might target an acyl-*holo*ACP (*42*). Moreover, the same study found that YbgC also co-purifies with the phospholipid synthesis proteins PlsB and PssA. Notably, PlsB is a *sn*-glycerol-3-phosphate acyltransferase that utilizes acyl-ACP as a substrate (*42*).

Substrate screens of the putative YbgC orthologs from *Heamophilus influenzae* and *Heliobacter pylori* have produced conflicting results. The *H. influenzae* YbgC (53% identity to *E.* coli YbgC) protein was shown to catalyze the hydrolysis of short chain acyl-CoA's but was inactive towards aromatic and long chain acyl-CoA's (*43*). Conversely, the *H. pylori* YbgC (37% identity to *E. coli* YbgC) was shown to favor long chain acyl-CoA's (*13*). These two conflicting results add to the mystic of YbgC's cellular role.

1.4.5 *E. coli* YciA

The last *E. coli* hotdog-fold thioesterase to be discussed, YciA, has been characterized thoroughly *"in vitro"* yet, like many other hotdog-fold thioesterases, a single distinct physiological function has yet to be assigned. A substrate screen of YciA demonstrated, like TEII, a catalytically efficient and promiscuous thioesterase activity with towards long chain acyl-CoA thioesters. On the other hand, YciA also proved to be very active towards aroyl-CoA's and short chain acyl-CoA thioesters (*10*). The *H.*

influenzae homologue of YciA was also subjected to comprehensive substrate screen to show that it too couples high catalytic efficiency with high substrate promiscuity (*10*). Crystallographic analysis of YciA shows that the acyl binding pocket is large and solvent exposed, possibly leading to its promiscuity (*44*). However, a more reasonable source might be the tight binding of the CoA unit.

The tight binding of CoA was first evident in the purification of *H. influenzae* YciA where LC-MS analysis demonstrated the presence of YciA and a small molecule with a molecular weight equivalent to coenzyme A (*10*). In addition, reactivity of the YciA protein with CoA bound demonstrated an initial lag phase corresponding to the removal of CoA from the active site (*10*). Moreover, the inhibition constant for desulfo-CoA of 0.33 μM also suggests extremely tight binding.

The tight binding of CoA and the promiscuity observed for YciA provide clues towards understanding its physiological function. An inspection of the gene context in *E. coli* shows *yciA* clustered in an operon with *yciB*, *yciC* and *yciI* and is located nearby genes encoding for the synthesis of cardiolipin (*10*). Increased expression of cardiolipin increases membrane fluidity which affects integral membrane protein functions (*45*). Cardiolipin has also been shown to organize membrane protein partners and recruit proteins to the poles and septa of inner membranes (*46*, *47*). Considering gene context, and the high activity towards long chain acyl-CoA thioesters, YciA is might involved in the biogenesis of the inner membrane for cell division or the insertion of integral membrane proteins.

1.5 Summary

The hotdog-fold protein family is ancient and has evolved to perform diverse types of chemistries. Although the tertiary fold is conserved among hotdog-fold family members, the amino acid sequence is highly divergent. Because of this divergence, the hotdog-fold protein family has been divided into subfamilies or classes based upon chemistry, catalytic core motifs, and sequence homology (*6*). Amongst the various chemistries is a niche of hotdog-fold proteins that catalyze the hydrolysis of acyl-thioester linkages. The substrates for these hotdog-fold thioesterases are typically aryl-/acyl-CoA and acyl-ACP thioesterase.

This dissertation will focus on the hotdog-fold thioesterases that catalyze acyl-CoA and acyl-ACP thioesters. The core of the thioesterase domain consists of 5 β-strands encompassing a long α-helix. The active sites of hotdog-fold thioesterase are formed at the interface of two monomers. Each thioesterase employs carboxylate residue, which functions either as a base, activating a water molecule for nucleophilic attack, or as a nucleophile, which directly attacks the thioester unit forming a mixed anhydride intermediate. Hotdog-fold thioesterases have been subdivided into clades based upon their tertiary structure and catalytic motifs.

The precise biological functions of the *E. coli* hotdog-fold thioesterase of YbdB, YbaW, TEII, and YaaI have been assigned. The biological functions of YbgC, YciA, YdiI, YigB and YiiD remained to be determined. This will require identification of the physiological substrate. Owing to substrate promiscuity *in-vitro* activity screening often falls short of identifying the physiological substrate. This coupled with the lack of meaningful gene context and an understanding of the structural elements of substrate and

protein partner recognition renders the identification of biological function challenging. The goal of the work described in this thesis is to ascertain information about the structure-function relationship of hotdog-fold thioesterases so that function might be assigned to uncharacterized thioesterases based upon known structures and/or sequence homology.

References

1. Hunt, M. C., and Alexson, S. E. H. (2002) The role Acyl-CoA thioesterases play in mediating intracellular lipid metabolism, *Progress in Lipid Research 41*, 99-130.

2. Katz, L., and Donadio, S. (1993) Polyketide synthesis: prospects for hybrid antibiotics., *Annual Review of Microbiology 47*, 875-912.

3. Scholten, Jeffrey D., Chang, Kai-Hsuan, Babbit, Patricia C., Charest, Hugues, Sylvestre, Michel, Dunaway-Mariano, D. (1991) Novel Enzymic Hydrolytic Dehalogenation of a Chlorinated Aromatic, *Science 253*, 182-185.

4. Smotrys, J. E., and Linder, M. E. (2004) Palmitoylation of intracellular signaling proteins: regulation and function, *Annual Review of Biochemistry 73*, 559-87.

5. Chemistry, B., and Groningen, A. G. (1999) α / β Hydrolase fold enzymes : the family keeps growing Marco Nardini and Bauke W Dijkstra, *Current Opinion in Structural Biology* 732-737.

6. Dillon, S. C., and Bateman, A. (2004) The Hotdog fold: wrapping up a superfamily of thioesterases and dehydratases, *BMC Boinformatics 5*, 109.

7. Ollis, D. L., Cheah, E., Cyglerl, M., Dijkstra, B., Frolow, F., Franken, S. M., Harel, M., Remington, S. J., Silman, I., Schragl, J., Sussman, J. L., and Goldmans, A. (1992) The α / β hydrolase fold, *Protein Engineering 5*, 197-211.

8. Leesong, M., Henderson, B. S., Gillig, J. R., Schwab, J. M., and Smith, J. L. (1996) Structure of a dehydratase-isomerase from the bacterial pathway for

biosynthesis of unsaturated fatty acids: two catalytic activities in one active site, *Structure 4*, 253-64.

9. Crawford, J. M., Korman, T. P., Labonte, J. W., Vagstad, A. L., Hill, E. a, Kamari-Bidkorpeh, O., Tsai, S.-C., and Townsend, C. a. (2009) Structural basis for biosynthetic programming of fungal aromatic polyketide cyclization, *Nature 461*, 1139-43.

10. Zhuang, Z., Song, F., Zhao, H., Li, L., Cao, J., Eisenstein, E., Herzberg, O., and Dunaway-Mariano, D. (2008) Divergence of function in the hot dog fold enzyme superfamily: the bacterial thioesterase YciA, *Biochemistry 47*, 2789-2796.

11. Adams, S. H., Chui, C., Schilbach, S. L., Yu, X. X., Goddard, A. D., Grimaldi, J. C., Lee, J., Dowd, P., Colman, S., and Lewin, D. A. (2001) BFIT, a unique acyl-CoA thioesterase induced in thermogenic brown adipose tissue: cloning, organization of the human gene and assessment of a potential link to obesity, *Biochemical Journal 360*, 135-142.

12. Suematsu, N., and Isohashi, F. (2006) Molecular cloning and functional expression of human cytosolic acetyl-CoA hydrolase, *Acta Biochimica Polonica 53*, 553-61.

13. Angelini, A., Cendron, L., Goncalves, S., Zanotti, G., and Terradot, L. (2008) Structural and enzymatic characterization of HP0496, a YbgC thioesterase from Helicobacter pylori, *Proteins 72*, 1212-1221.

14. Zhuang, Z., Song, F., Martin, B. M., and Dunaway-Mariano, D. (2002) The YbgC protein encoded by the ybgC gene of the tol-pal gene cluster of Haemophilus influenzae catalyzes acyl-coenzyme A thioester hydrolysis, *FEBS Letters 516*, 161-3.

15. Ohlrogge, J. B., and Jaworski, J. G. (1997) Regulation of Fatty Acid Synthesis, *Annual Review of Plant Physiology and Plant Molecular Biology 48*, 109-136.

16. Li, J., Derewenda, U., and Dauter, Z. (2000) letters Crystal structure of the Escherichia coli thioesterase II , a homolog of the human Nef binding, *Nature Structural Biology 7*, 177-180.

17. Klages, U., Markus, a, and Lingens, F. (1981) Degradation of 4-chlorophenylacetic acid by a Pseudomonas species, *Journal of Bacteriology 146*, 64-8.

18. Schmitz, a, Gartemann, K. H., Fiedler, J., Grund, E., and Eichenlaub, R. (1992) Cloning and sequence analysis of genes for dehalogenation of 4-chlorobenzoate from Arthrobacter sp. strain SU, *Applied and Environmental Microbiology 58*, 4068-71.

19. Song, F., Zhuang, Z., and Dunaway-Mariano, D. (2007) Structure-activity analysis of base and enzyme-catalyzed 4-hydroxybenzoyl coenzyme A hydrolysis, *Bioorganic Chemistry 35*, 1-10.

20. Benning, M. M., Wesenberg, G., Liu, R., Taylor, K. L., Dunaway-Mariano, D., and Holden, H. M. (1998) The three-dimensional structure of 4-hydroxybenzoyl-CoA thioesterase from Pseudomonas sp. Strain CBS-3, *The Journal of Biological Chemistry 273*, 33572-9.

21. Zhuang, Z., Latham, J., Song, F., Zhang, W., Trujillo, M., and Dunaway-Mariano, D. (2012) Investigation of the catalytic mechanism of the hotdog-fold enzyme superfamily Pseudomonas sp. strain CBS3 4-hydroxybenzoyl-CoA thioesterase, *Biochemistry 51*, 786-94.

22. Song, F., Thoden, J. B., Zhuang, Z., Trujillo, M., Holden, H. M., and Dunaway-Mariano, Debra. The catalytic mechanism of the hotdog-fold enzyme superfamily 4-hydroxybenzoyl-CoA thioesterase from *Arthrobacter sp*. strain SU, *Unpublished*.

23. Barry, S. M., and Challis, G. L. (2009) Recent advances in siderophore biosynthesis, *Current Opinion in Chemical Biology 13*, 205-15.

24. Gehring, A. M., Mori, I., and Walsh, C. T. (1998) Reconstitution and Characterization of the Escherichia coli Enterobactin Synthetase, *Biochemistry 37*, 2648-2659.

25. Lai, J. R., Fischbach, M. a, Liu, D. R., and Walsh, C. T. (2006) Localized protein interaction surfaces on the EntB carrier protein revealed by combinatorial mutagenesis and selection, *Journal of the American Chemical Society 128*, 11002-3.

26. Chen, D., Wu, R., Bryan, T. L., and Dunaway-Mariano, D. (2009) In vitro kinetic analysis of substrate specificity in enterobactin biosynthetic lower pathway enzymes provides insight into the biochemical function of the hot dog-fold thioesterase EntH, *Biochemistry 48*, 511-3.

27. Leduc, D., Battesti, A., and Bouveret, E. (2007) The hotdog thioesterase EntH (YbdB) plays a role in vivo in optimal enterobactin biosynthesis by interacting with the ArCP domain of EntB, *Journal of Bacteriology 189*, 7112-26.

28. Guo, Z.-F., Sun, Y., Zheng, S., and Guo, Z. (2009) Preferential hydrolysis of aberrant intermediates by the type II thioesterase in Escherichia coli nonribosomal enterobactin synthesis: substrate specificities and mutagenic studies on the active-site residues, *Biochemistry 48*, 1712-22.

29. Burlingame, R. P., Wyman, L., and Chapman, P. J. (1986) Isolation and characterization of Escherichia coli mutants defective for phenylpropionate degradation, *Journal of Bacteriology 168*, 55-64.

30. Ferrrandez, A., Minambres, B., Garcia, B., Olivera, E., Luengo, J., García, J., and Díaz, E. (1998) Catabolism of phenylacetic acid in Escherichia coli, *The Journal of Biological Chemistry 273*, 25974-25986.

31. Song, F., Zhuang, Z., Finci, L., Dunaway-Mariano, D., Kniewel, R., Buglino, J. a, Solorzano, V., Wu, J., and Lima, C. D. (2006) Structure, function, and mechanism of the phenylacetate pathway hot dog-fold thioesterase PaaI, *The Journal of Biological Chemistry 281*, 11028-38.

32. Ren, Y., Aguirre, J., Ntamack, A. G., Chu, C., and Schulz, H. (2004) An alternative pathway of oleate beta-oxidation in Escherichia coli involving the hydrolysis of a dead end intermediate by a thioesterase, *The Journal of Biological Chemistry 279*, 11042-50.

33. Barnes, E. M. J., and Wakil, S. J. (1957) Studies on the mechanism of fatty acid synthesis, *The Journal of Biological Chemistry 25*, 303-310.

34. Spencer, K., Greenspan, D., Cronan, E., and Ai, S. G. (1978) Thioesterases I and II of Escherchia coli Hydrolysis of Native Acyl-Acyl Carrier Protein Thioesters, *The Journal of Biological Chemistry 253*, 5922-5926.

35. Naggert, J., Narasimhang, M. L., Deveauxg, L., Chog, H., Randhawab, Z. I., Cronan, J. E., and Greenll, B. N. (1991) Cloning , Sequencing , and Characterization of Escherichia coli, *The Journal of Biological Chemistry 266*, 11044-11050.

36. Zheng, Z., Gong, Q., Liu, T., Deng, Y., Chen, G.-qiang, and Chen, J.-chun. (2004) Thioesterase II of Escherichia coli Plays an Important Role in 3-Hydroxydecanoic Acid Production Thioesterase II of Escherichia coli Plays an Important Role in 3-Hydroxydecanoic Acid Production, *Applied and Environmental Microbiology 27*, 3807-3813.

37. Nie, L., Ren, Y., and Schulz, H. (2008) Identification and characterization of Escherichia coli thioesterase III that functions in fatty acid beta-oxidation, *Biochemistry 47*, 7744-51.

38. Nie, L., Ren, Y., Janakiraman, A., Smith, S., and Schulz, H. (2008) A novel paradigm of fatty acid beta-oxidation exemplified by the thioesterase-dependent partial degradation of conjugated linoleic acid that fully supports growth of Escherichia coli, *Biochemistry 47*, 9618-26.

39. Feng, Y., and Cronan, J. E. (2009) A new member of the Escherichia coli fad regulon: transcriptional regulation of fadM (ybaW), *Journal of Bacteriology 191*, 6320-8.

40. Henry, M. F., and Cronan, J. E. (1991) Escherichia coli transcription factor that both activates fatty acid synthesis and represses fatty acid degradation, *Journal of Molecular Biology 222*, 843-849.

41. Gerding, M. a, Ogata, Y., Pecora, N. D., Niki, H., and de Boer, P. a J. (2007) The trans-envelope Tol-Pal complex is part of the cell division machinery and required for proper outer-membrane invagination during cell constriction in E. coli, *Molecular Microbiology 63*, 1008-25.

42. Gully, D., and Bouveret, E. (2006) A protein network for phospholipid synthesis uncovered by a variant of the tandem affinity purification method in Escherichia coli, *Proteomics 6*, 282-93.

43. Zhuang, Z., Song, F., Zhang, W., Taylor, K. L., Archambault, A., and Dunaway-Mariano, D. (2002) Kinetic , Raman , NMR , and Site-Directed Mutagenesis Studies of the Pseudomonas Sp. Strain CBS3 4-Hydroxybenzoyl-CoA Thioesterase Active Site, *Biochemistry 41*, 11152-11160.

44. Willis, M. A., Zhuang, Z., Song, F., Howard, A., and Dunaway-mariano, D. (2008) Structure of YciA from Haemophilus influenzae (HI0827), a Hexameric Broad Specificity Acyl-Coenzyme A Thioesterase, *Biochemistry 47*, 2797-2805.

45. Bernal, P., Segura, A., and Ramos, J.-L. (2007) Compensatory role of the cis-trans-isomerase and cardiolipin synthase in the membrane fluidity of Pseudomonas putida DOT-T1E, *Environmental Microbiology 9*, 1658-64.

46. Romantsov, T., Helbig, S., Culham, D. E., Gill, C., Stalker, L., and Wood, J. M. (2007) Cardiolipin promotes polar localization of osmosensory transporter ProP in Escherichia coli, *Molecular Microbiology 64*, 1455-65.

47. Mileykovskaya, E. (2007) Subcellular localization of Escherichia coli osmosensory transporter ProP: focus on cardiolipin membrane domains, *Molecular Microbiology 64*, 1419-22.

CHAPTER TWO
DETERMINING THE PHYSIOLOGICAL ROLE OF THE *ESCHERICHIA COLI* HOTDOG-FOLD THIOESTERASE YDII

2.1 Introduction

In the absence of oxygen, many facultative anaerobic bacteria obtain their energy through anaerobic respiration utilizing fumarate as an alternative terminal electron acceptor (*1*). The reduction of fumarate to succinate is catalyzed by the membrane protein fumarate reductase, which transfers electrons from the cofactor menaquinone (*2*). Menaquinone is lipid soluble and is composed of a napthoquinone ring to which a partially saturated polyisoprenyl side chain of varying in length is attached. Menaquinone is an essential cofactor for facultative anaerobic organisms such as *Escherichia coli*. Gene knockout mutants that are not able to produce menaquinone display inhibited growth under anaerobic conditions (*3*–*6*). Vertebrates acquire menaquinone, also known as vitamin K_2, from the intestinal flora and from ingested leafy vegetables. Vitamin K_2 functions in vertebrates as a cofactor for various carboxylases involved in blood clotting and cell cycle regulation (*7*). Because humans do not synthesize vitamin K_2, the enzymes of the biosynthetic pathway operative in pathogenic microbes are potential drug targets.

The *E. coli* menaquinone biosynthetic pathway has been extensively characterized (Figure 2.1) and is assembled by nine protein products, six of which are encoded by the *men*FDHBCE operon. Synthesis of the dihydroxnapthoic acid (DHNA) backbone begins with the conversion of chorismate to isochorismate catalyzed by MenF (*8, 9*) The three subsequent steps in which isochorismate is converted to the *o*-succinylbenzoate (OSB)

are catalyzed by the enzymes MenD, MenH, and MenC (*10–12*). The ATP-dependent enzyme MenE, activates the carbonyl group of OSB with coenzyme A (CoA) to form OSB-CoA. This intermediate undergoes a cyclization reaction cyclized by MenB to from 1,4-dihydroxynapthoyl-CoA (DHNA-CoA) (*13*, *14*). MenB was once thought to hydrolyze the DHNA-CoA to DHNA, however this was later shown to be incorrect. Until recently, it was also thought that the α/β-fold protein MenH catalyzes the hydrolysis of DHNA-CoA to DHNA, however this too was shown to be incorrect. The confusion regarding the identity of the thioesterase that catalyzes DHNA-CoA to DHNA has been nicely summarized by Widhalm *et. al*. (*26*). These investigators discovered that the *Synechocystis* sp. PCC 6803 hotdog-fold thioesterase SLR0204 is responsible for the hydrolysis of DHNA-CoA to DHNA. However, the *E. coli* menaquinone pathway thioesterase remained to be identified.

The remaining steps of the menaquinone pathway include the addition of the varying length polyisoprenyl side chain to the DHNA to form demethylmenaquinone, catalyzed by MenA and ring methylation by the *S*-adenosyl-methionine (SAM) catalyzed by MenG (*15, 16*).

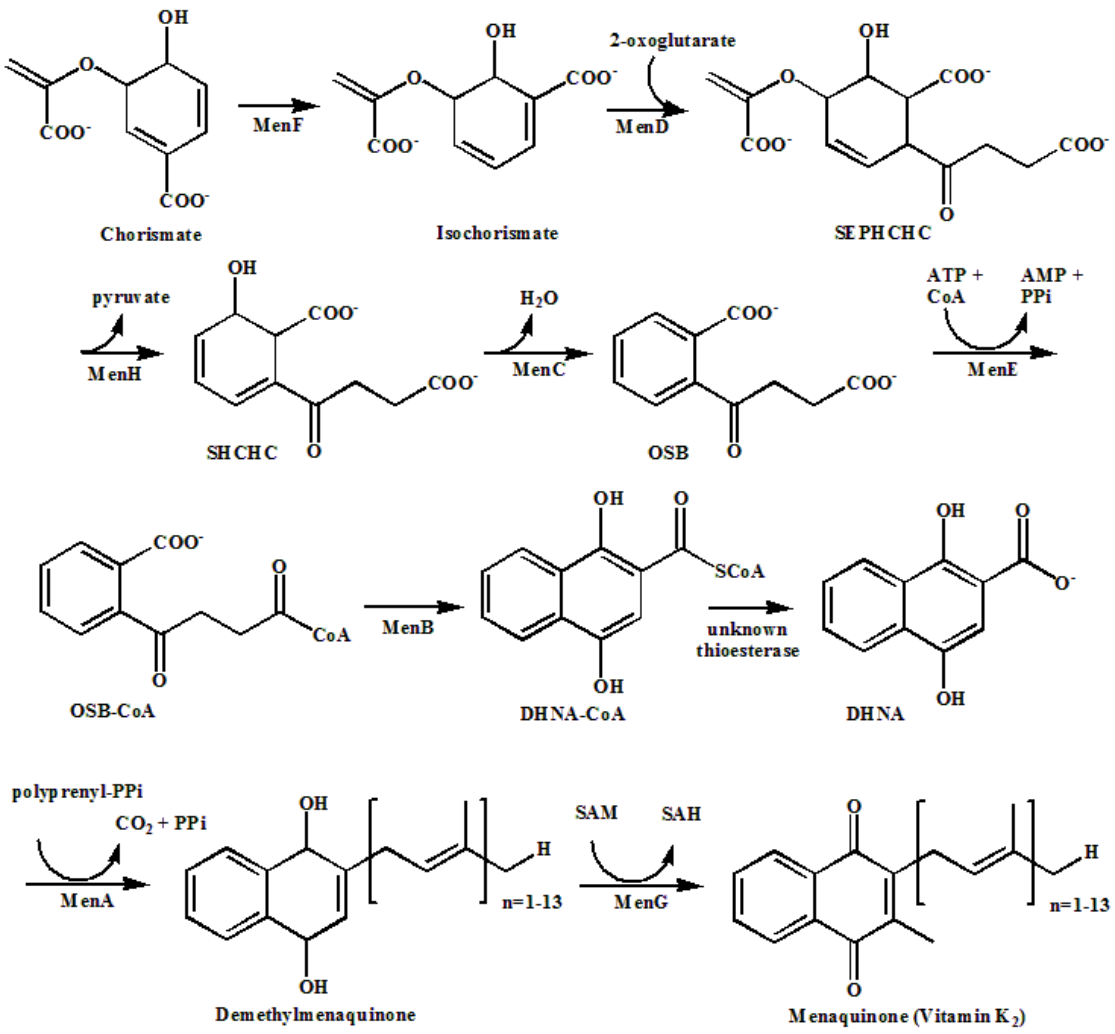

Figure 2.1. The menaquinone biosynthetic pathway in *E. coli*. The pathway enzymes are: isochorisimate synthase, MenF; SEPHCHC synthase, MenD; SHCHC synthase, MenH; OSB synthase, MenC; OSB-CoA ligase, MenE; DHNA synthase, MenB; DHNA prenyltransferase, MenA; demethylmenaquinone methyltransferase, MenG. The following acronyms are; 2-succinyl-5-enolpyruvyl-6-hydroxy-3-cyclohexene-1-carboylic acid, SEPHCHC; (1*R*,6*R*)-2-succinyl-6-hydroxy-2,4-cyclohexadiene-1-carboxylic acid, SHCHC; *o*-succinyl-benzoic acid, OSB; 1,4-dihydroxynapthoic acid, DHNA; *S*-adenosyl-methionine, SAM; and *S*-adenosyl-L-homocysteine, SAH.

The work that I describe in this chapter provides evidence that the missing thioesterase of the *E. coli* menaquinone pathway is the previously the uncharacterized *E. coli* hotdog-fold superfamily thioesterase YdiI. In *E. coli* two closely related paralogs (59% identity) of the hotdog-fold enzyme superfamily, EntH (also known as YbdB) and YdiI, have evolved to perform different cellular functions. EntH has been shown to play a housekeeping role in the enterobactin synthesis pathway by freeing misacylated-EntB (*17*, *18*). Replacement of EntH by YdiI does not restore EntH activity and thus, despite their high sequence identity, YdiI and EntH perform different functions (*19*). Whereas the gene that encodes EntH in *E. coli* is located within a gene cluster that encodes the enzymes of the enterobactin pathway, the gene that encodes YdiI in *E. coli* as well as in other species of Enterobacteriales, is co-localized with a putative oxidoreductase/dehydrogenase (YdiJ). This gene context is however, not conserved outside Enterobacteriales. For example, in *Pseudomonas aeruginosa* the YdiI (PA1618) encoding gene is adjacent to a putative ligase (Figure 2.2). Using a combination of *in vitro* substrate specificity profile determination and *in-vivo* growth curve analysis with the *E. coli* YdiI⁻ mutant, I provide evidence that the in *E. coli* YdiI functions as the menquinone pathway thioesterase. In Chapter 3, I will identify the structural basis for the divergence in EntH and YdiI function and in Chapter 4, I will show that YdiI of *P. aeruginosa* has assumed a function unique from that of the *E. coli* YdiI.

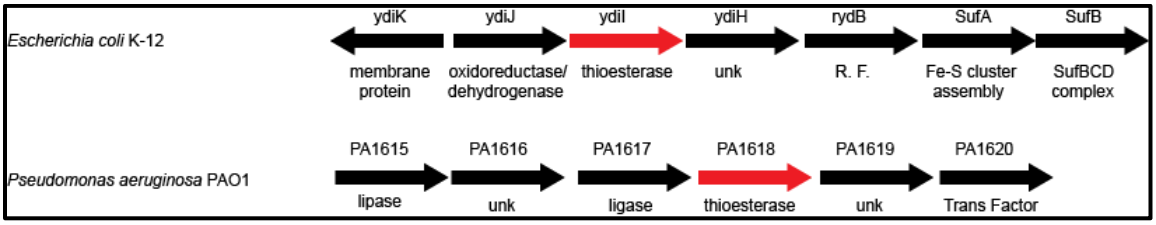

Figure 2.2: Gene context of *Escherichia coli* and *Pseudomonas aeruginosa ydiI* gene products (red).

2.2 Methods and Materials

2.2.1 Materials

All restriction enzymes and T4 DNA ligase were purchased from Invitrogen (Grand Island, NY). *Pfu Turbo* and *Deep Vent* DNA polymerases were purchased from Strategene (Santa Clara, CA). Oligonucleotide primers were custom-synthesized by Invitrogen. DNA sequencing was performed by the DNA Sequencing Facility of the University of New Mexico. Acetyl-CoA, benzoyl-CoA, propanoyl-CoA, hexanoyl-CoA, lauroyl-CoA, myristoyl-CoA, palmitoyl-CoA, oleoyl-CoA were purchased from Sigma. The thioester substrates 4-hydroxybenzyol-CoA, DHNA-CoA and coumaroyl-CoA were synthesized as previously reported (*18, 20*). *E. coli* strains JW1676 (Δ*ydiI*::*Kan*^{r}) and BW2513 (YdiI$^+$) of the Kleio collection were obtained from Yale University (*21*).

2.2.2 Preparation of wild-type *E. coli* ydiI and EntH

The wild-type EntH (YbdB) was purified as previously described (*17*). The wild-type (WT) *ydiI* gene was amplified by PCR using genomic DNA prepared from *E. coli* strain K-12 (ATCC) as template, commercial oligonucleotides as primers, and *Deep Vent* as the polymerase. The PCR-products were digested by the restriction enzymes *NdeI* and *XhoI* and then purified by polyacrylamide gel electrophoresis. The genes were ligated to a *NdeI* and *XhoI- digested* pET-23a vector (Novagen) using T4 DNA ligase. The cloned genes were verified by DNA sequencing. The cloned plasmids were used to transform

competent *E. coli* BL21(DE3) cells (Invitrogen) for gene expression. The *ydiI*/pET-23a transformed *E. coli* BL21(DE3) cells were grown aerobically at 37 ^{o}C in LB media containing 50 µg/ml ampicillin. Production of C-terminal His_6-tagged YdiI was induced with 0.4 mM isopropyl-β-$_D$-galactopyranoside (IPTG) once the cell density had reached A_{600} ~ 0.6. Following a 12 h induction period at 19 ^{o}C, the cells were harvested by centrifugation at 6,500 rpm for 10 min and then resuspended in 100 mL of 50 mM Tris buffer (pH 8.4), 50 mM imidazole, and 500 mM NaCl (Lysis Buffer). The cells were lysed using a French press at 1,200 psi and the lysate was centrifuged at 20,000 rpm for 15 min. The supernatant was loaded onto a 5 mL HisTrap FF e column (GE Life Sciences) and the column was eluted at 4 ^{o}C with Lysis Buffer to remove non-tagged protein and then with 50 mM Tris (pH 8.4), 500 mM imidazole, and 500 mM NaCl (Elution Buffer) to elute the tagged protein. Column fractions were monitored by measuring solution absorbance at 280 nm and by carrying out SDS-PAGE analysis. The YdiI-containing fractions were combined and dialyzed at 4 ^{o}C against three changes of 1 L of 50 mM Tris (pH 8.4)/50 mM NaCl. Yield: YdiI ~10 mg protein/g of wet cells.

2.2.3 Determination of the steady state kinetic constants

Thioesterase activity was measured using the 5,5'-dithio-bis-(2-nitrobenzoic acid) (DTNB) coupled assay. Reactions were monitored at 412 nm ($\Delta\varepsilon$ = 13.6 $mM^{-1}\bullet cm^{-1}$) using a Beckman 640U Spectrometer. Reactions were carried out 25 ^{o}C with 0.5 mL solutions containing 50 mM K^{+}HEPES (pH 7.5), 1 mM DNTB, a catalytic amount of thioesterase and varying concentrations of thioester (0.5 – 5 x K_m). The catalyzed

hydrolysis of 4-hydroxybenzoyl-CoA (4-HB-CoA) in 50 mM K^+ HEPES (pH 7.5) was directly monitored at 300 nm ($\Delta\varepsilon = 11.8\ mM^{-1} \bullet cm^{-1}$).

The initial velocity data, measured as a function of substrate concentration, were analyzed using Enzyme Kinetics v 1.4 and equation 1:

$$V = V_{max}[S]/([S]+K_m) \quad (1)$$

where V is initial velocity, V_{max} is maximum velocity, [S] is substrate concentration, and K_m is the Michaelis constant. The k_{cat} was calculated from $V_{max}/[E]$ where [E] is the total enzyme concentration as determined by the Bradford method.

2.2.4 Growth curve measurements for wild-type and YdiI knockout *Escherichia coli* strains

Aerobic growth curves were carried out in sterile vented flasks (Nalgene) each containing 50 mL of M9 Minimal Media supplemented with 4% glucose, sodium succinate, or sodium fumarate as the sole carbon source and with or without added kanamycin. An aliquot of saturated overnight culture of JW1676 ($YdiI^-$) or BW2513 ($YdiI^+$) *E. coli* cells in LB broth was added to the media to make an initial $A_{600} \sim 0.01$. Cultures were incubated at 37 ^oC with orbital shaking at 180 rpm. The culture A_{600} was determined at 1 h intervals for 14 h. Anaerobic growth curves were carried out in a similar fashion using 50 mL of M9 Minimal media supplemented with double the amount of phosphate and with 4% glucose plus 4% fumarate. The sterile flasks were capped with sterilized butyl stoppers and purged for 2 min with N_2 gas passed through a sterile 0.2µm in-line filter. Aliquots were removed by syringe, hourly over a 12 h period, for A_{600} determination.

2.3 RESULTS AND DISCUSSION

2.3.1 YdiI substrate screen for determination of biochemical function

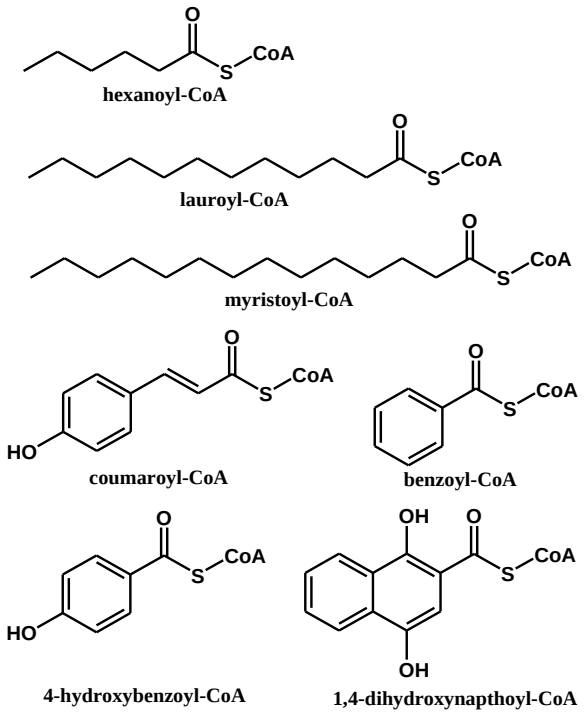

Figure 2.3: The molecular structure of selected acyl/aryl-coenzyme compounds for the YdiI substrate screening.

The YdiI substrate specificity profile was determined by measuring the steady-state k_{cat} and K_m values for a panel of acyl-CoA, benzoyl-CoA and napthoyl-CoA thioesters. The results are reported in Table 2.1 along with the steady-state kinetic constants measured for EntH (*22*). Both thioesterases are promiscuous however, each has its own unique specificity profile that differ in ways which suggest specialization for targeting the physiological substrate. EntH displays low activity with the C6-C18 aliphatic (fat-like) acyl-CoA thioesters: k_{cat} ~0.1-0.03 s^{-1} and k_{cat}/K_m ~ 1 x 10^3 M^{-1} s^{-1}.

EntH is significantly more active with substrates that possess a phenyl ring. The coumaroyl-CoA k_{cat} = 0.8 s^{-1} and the k_{cat}/K_m ~ 1 x 10^5 M^{-1} s^{-1}. Benzoyl-CoA and 4-hydroxybenzoyl-CoA are very good substrates (k_{cat} ~2 s^{-1} and k_{cat}/K_m ~1 x 10^5 M^{-1} s^{-1}) whereas the 1,4-dihydroxynapthoyl-CoA is not (k_{cat} = 0.01 s^{-1} and k_{cat}/K_m ~ 6 x 10^2 M^{-1} s^{-1}). *In-vivo*, EntH catalyzes the hydrolysis of dead-end, misacylated *holo*EntB adducts, which in turn, are not processed by EntF (for details see Chapter 1). Consistent with this function, 2,4-dihydroxybenzoyl-holoEntB is a very active substrate (k_{cat} = 4 s^{-1} and k_{cat}/K_m = 1 x 10^5 M^{-1} s^{-1}), in fact, as active as the 4-hydroxybenzoyl-CoA thioester (2,4-dihydroxybenzoyl-CoA was not synthetically accessible. In contrast, the benzoyl-holoACP (the ACP that functions in *E. coli* fatty acid synthesis; see Chapter 5 for details) is considerably less active than is benzoyl-CoA or 2,4-dihydroxybenzoyl-holoEntB (~200-fold reduction in k_{cat} and 1000-fold reduction in k_{cat}/K_m).

	EntH			YdiI		
Substrate	**k_{cat} (s^1)**	**K_M (μM)**	**k_{cat}/K_M (M^{-1} s^{-1})**	**k_{cat} (s^1)**	**K_M (μM)**	**k_{cat}/K_M ($M^{-1}s^{-1}$)**
Acetyl-CoA	$(4.4 \pm 0.2) \times 10^{-3}$	800 ± 90	5.5		ND	
Hexanoyl-CoA	$(1.36 \pm 0.03) \times 10^{-1}$	260 ± 20	5.2×10^2	0.30 ± 0.01	21 ± 1	1.4×10^4
Lauroyl-CoA	$(2.81 \pm 0.03) \times 10^{-2}$	44 ± 2	6.2×10^2	0.74 ± 0.01	2.2 ± 0.2	3.4×10^5
Myristoyl-CoA	$(7.8 \pm 0.3) \times 10^{-2}$	11 ± 1	7.1×10^2	0.63 ± 0.01	1.5 ± 0.2	4.1×10^5
Oleoyl-CoA	$(3.0 \pm 0.1) \times 10^{-2}$	13 ± 2	2.3×10^3	$(1.16 \pm 0.01) \times 10^{-1}$	1.3 ± 0.1	8.7×10^4
Benzoyl-CoA	2.2 ± 0.1	12 ± 1	1.8×10^5	18 ± 1	25 ± 3	7.2×10^5
4-HB-CoA	1.6 ± 0.1	21 ± 2	7.3×10^4	5.2 ± 0.2	9 ± 1	5.9×10^5
1,4-DHN-CoA	$(9.3 \pm 0.2) \times 10^{-3}$	17 ± 1	5.8×10^2	1.58 ± 0.03	8 ± 1	2.0×10^5
Coumaroyl-CoA	$(8.2 \pm 0.2 \times 10^{-1}$	10 ± 1	8.4×10^4	8.4 ± 0.2	30 ± 2	2.8×10^5
2,4-DHB-EntB	3.7 ± 0.1	25 ± 1	1.4×10^5	3.6×10^3	200 ± 20	3.6×10^3
Benzoyl-ACP	$(1.3 \pm 0.1) \times 10^{-2}$	57 ± 10	2.41×10^2	$(8.3 \pm 0.7) \times 10^{-2}$	54 ± 5	1.5×10^3

[a] Data was taken from reference (*22*).

Table 2.1: Steady state kinetic parameters of EntH and YdiI-catalyzed hydrolysis of various acyl-CoA, acyl-holo-ACP, or acyl-holo-EntB substrates monitored by direct absorbance change or DTNB coupled reactions in 50 mM K^+HEPES at pH 7.5.

YdiI displays a modest yet physiologically significant level of activity with the C6-C18 aliphatic fatty acyl-CoA thioesters: k_{cat} = 0.7-0.1 s^{-1} and $k_{cat}/K_m \sim 1 \times 10^4$ to 1×10^4 M^{-1} s^{-1}. Like EntH, YdiI prefers substrates having a phenyl ring: k_{cat} = 5-18 s^{-1} and the $k_{cat}/K_m \sim 1 \times 10^5$ to 1×10^6 M^{-1} s^{-1}. In contrast to the EntH, YdiI is very active in catalysis of 1,4-dihydroxynapthoyl-CoA (k_{cat} = 1.6 s^{-1} and $k_{cat}/K_m = 2 \times 10^5$ M^{-1} s^{-1}), 300-

fold more active than is EntH. Another notable difference between the two thioesterases is that ydiI is significantly more active with the CoA thioesters. Comparison of the kinetic constants for 2,4-dihydroxybenzoyl-*holo*EntH to those measured for 4-hydroxybenzoyl-CoA reveals a ~100-fold drop in activity. Likewise, benzoyl-CoA is ~100-fold more active as a substrate than is benzoyl-*holo*ACP. Whereas EntH prefers the holoEntB thiol unit over the holoACP unit, YdiI makes no distinction.

The inability of YdiI to complement the EntH gene knockout mutant suggests that the differences in their respective substrate activity profiles is sufficient to alter *in vivo* function. The source of the divergence in substrate specificity in these two paralogs must derive from divergence in their structures, and in particular the topological features of their respective active sites. From the deposited crystal structure of *apo* YdiI (1VH5) and *apo* EntH (1VH9) it appears that YdiI has a larger substrate pocket, which might account for its ability to better accommodate the napthoyl ring of the 2,4-dihydroxynapthoyl-CoA (Figure 2.4).

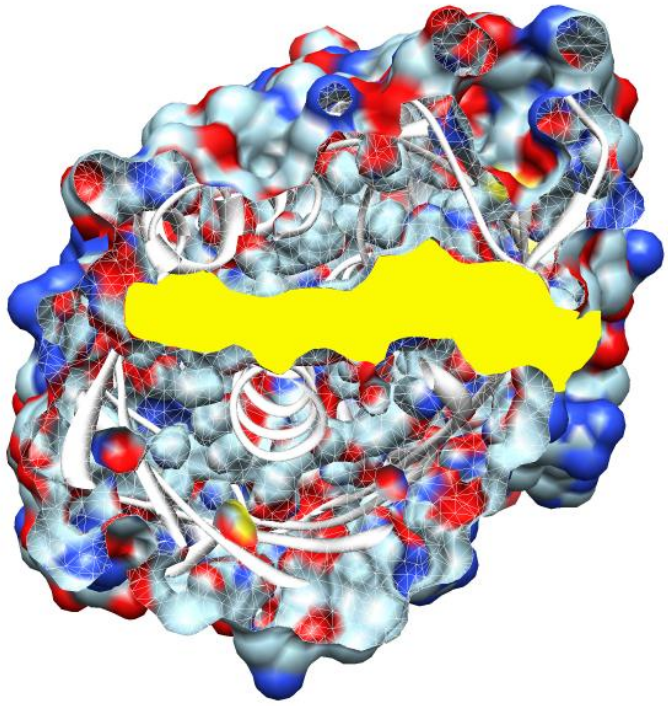

A

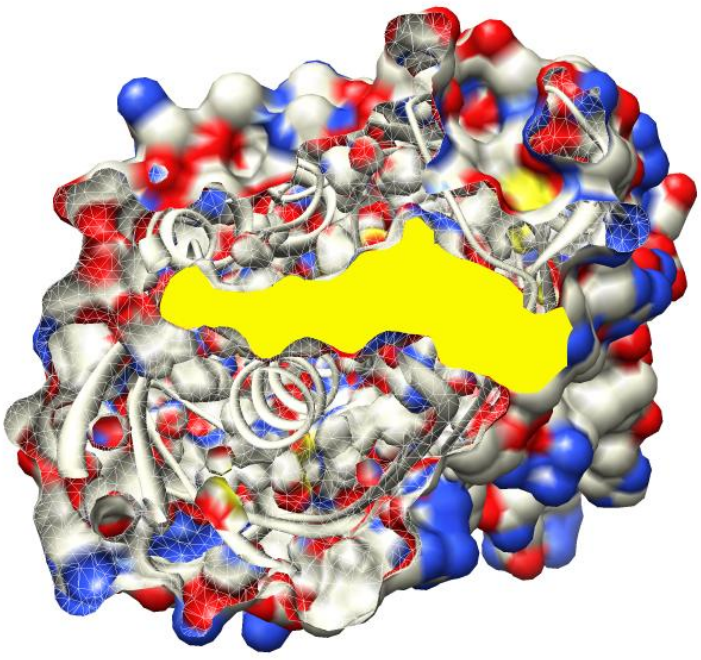

B

Figure 2.4: Surface representation of YdiI (**A -** PDB ID: 1VH5) and EntH (**B -** PDB ID: 1VH9) generated with Chimera showing the shape of the substrate binding pocket colored in yellow.

2.3.2 Wild-type and *ydiI* gene knockout aerobic and anaerobic growth curves

A potential lead that prompted the investigation of the *E. coli* growth curves came from the NCBI GEO Profiles for *ydiI*, which showed a large increase in expression of the *ydiI* gene when *E. coli* cells were grown anaerobically with glucose and fumarate as carbon sources (*23*). When grown aerobically with glucose, the *E. coli* YdiI$^-$ (JW1676) and the *E. coli* YdiI$^+$ (BW2513) strains demonstrate similar growth curves (Figure 2.6A**)**. However, when grown aerobically on gluconeogenic substrates such as succinate and fumarate, inhibition of *E. coli* YdiI$^-$ growth can be observed. The lack of complete shutdown of growth can be accounted for by the fact that the quinone dependent succinate dehydrogenase might perform the same reaction however, in a limited manner (*24*, *25*).

Anaerobic growth of the YdiI$^+$ and of the YdiI$^-$ strains on glucose and fumarate demonstrated much more dramatic results. It should be noted that the use of unmodified M9 minimal media led to a reduction in pH over time under the anaerobic conditions utilizing glucose and fumarate as sole carbon sources. The growth of the YdiI$^+$ strain peaked at an OD_{600} ~ 1.2. The doubling the concentration of the buffer in the culture did alter the growth curve obtained. Therefore the results shown are of the latter of the two conditions. As shown in Figure 4B, the YdiI$^+$ strain grew sigmoidally to a maximum OD_{600} ~ 1.2 whereas the YdiI$^-$ strain grew linearly to a maximum OD_{600} ~ 0.4 in the same timeframe. As mentioned earlier, fumarate can be utilized as the terminal electron acceptor when grown under anoxic conditions. The utilization of fumarate reductase, as well as the electron donating cofactor menaquinone, to transfer electrons to fumarate is

necessary for growth. In good agreement with other menaquinone synthesizing gene knockout experiments, the YdiI$^-$ genotype severely inhibits growth of *E. coli* under anaerobic conditions (3-6).

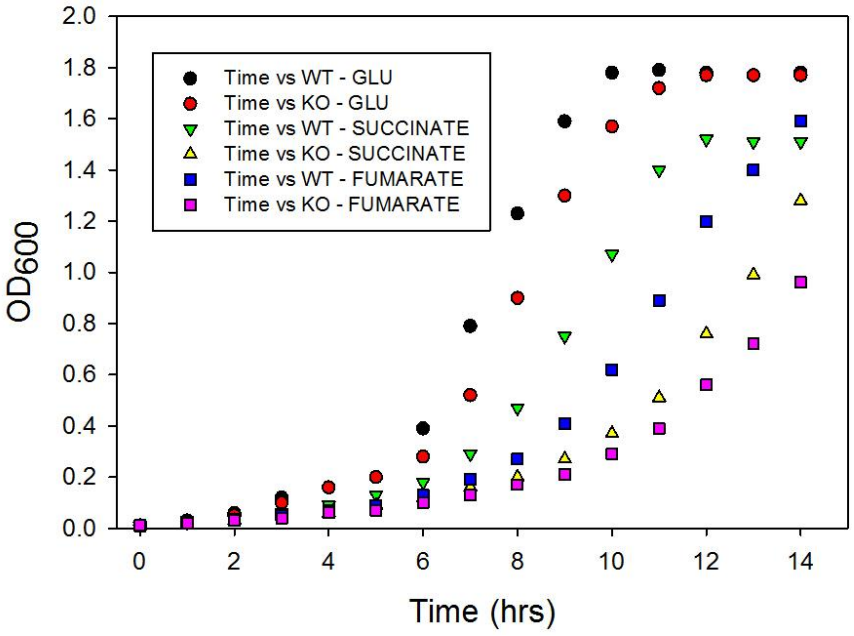

A

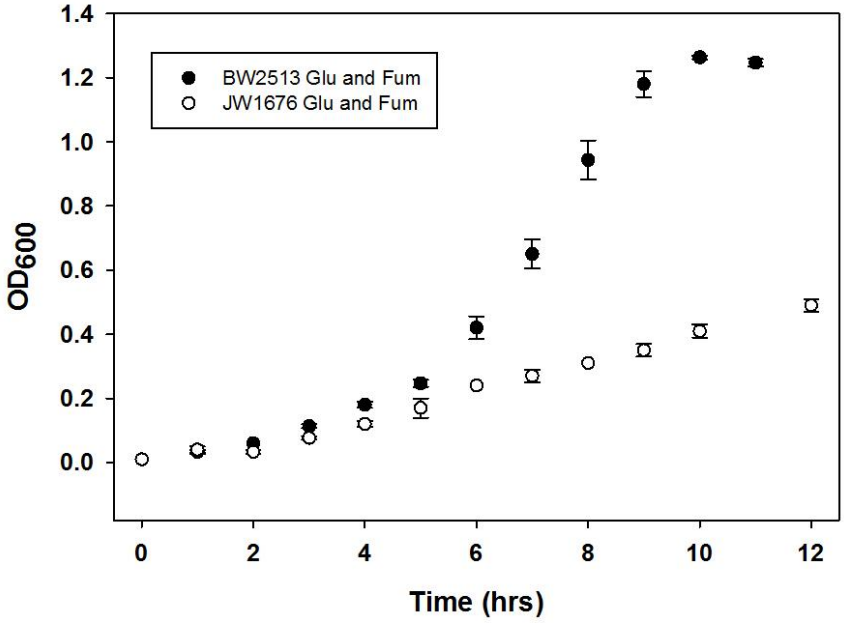

B

Figure 2.6: A) Aerobic growth curve of BW2513 (wild type *Escherichia coli*) and JW1676 (Δ*ydiI*::*Kan*^{r}) grown in M9 Minimal Media utilizing 4% of either glucose, succinate, or fumarate as the sole carbon source at 37 ^oC. Growth curves were performed in triplicate and the OD_{600} where plotted versus time and error bars represent standard deviations. **B)** Anaerobic growth curve of BW2513 and JW1676 in buffer adapted M9 Minimal Media utilizing 4% glucose and fumarate as sole carbon sources under a N_2 atmosphere at 37 ^oC. Growth curves were performed in triplicate and the OD_{600} where plotted versus time and error bars represent standard deviations.

2.4 Conclusions

A steady-state kinetic analysis of YdiI substrate specificity demonstrated a large range of substrates with physiologically relevant k_{cat}/K_M values. Even though YdiI is promiscuous towards acyl-/aroyl-CoA substrates, it readily discriminates aroyl-holo-ACP or aroyl-holo-EntB whereas the YdiI paralog EntH does not. Systemic structural changes such as the length of the substrate binding pocket may help to explain the differences in substrate preferences of the closely related paralog however, a detailed examination will be necessary to identify key changes in structural features.

Although not exclusively located in one gene context, the co-localization of *ydiI* to the menaquinone pathway in several bacterial species in addition to the NCBI GEO Profiles of *ydiI* led to the investigation of its involvement in the menaquinone synthesis pathway. Among the substrates YdiI was capable of catalyzing, the hydrolysis of DHNA-CoA to DHNA occurred with high efficiency. Taking into account that *ydiI* is up-regulated under anaerobic conditions with glucose and fumarate as carbon sources, it was

apparent that gene knockout studies were warranted. The aerobic growth of *E. coli* YdiI$^-$ on fumarate or succinate demonstrated perturbed growth rates as compared to the *E. coli* YdiI$^+$. This can be explained by the need to undergo gluconeogenesis for biomolecule synthesis, utilizing the menaquinone dependent enzyme fumarate reductase. Additionally, the anaerobic growth of *E. coli* YdiI$^-$ on glucose plus fumarate demonstrated almost complete inhibition of growth as compared to *E. coli* YdiI$^+$. In anaerobic conditions, fumarate can be used as the terminal electron acceptor and is the substrate for fumarate reductase. Both growth curves provide evidence that the YdiI$^-$ strain disrupts menaquinone synthesis. In combination with bioinformatics, an inclusive substrate screen, and gene knockout growth curves, I have provided strong evidence that YdiI is the DHNA-CoA thioesterase in the *E. coli* menaquinone synthesis pathway.

References

1. Kröger, A., Geisler, V., Lemma, E., Theis, F., and Lenger, R. Bacterial fumarate respiration, *Archives of Microbiology 158*, 311-314.

2. Hirsch, C. A., Rasminsky, M., Davis, B. D., and Lin, E. C. C. (1963) A Fumarate Reductase in Escherichia coli Distinct from Succinate Dehydrogenase, *The Journal of Biological Chemistry 238*, 3770-3774.

3. Guest, J. R. (1977) Menaquinone biosynthesis: mutants of Escherichia coli K-12 requiring 2-succinylbenzoate., *Journal of Bacteriology 130*, 1038-46.

4. Guest, J. R. (1979) Anaerobic Growth of Escherichia coli K12 with Fumarate as Terminal Electron Acceptor. Genetic Studies with Menaquinone and Fluoroacetate-resistant Mutants, *Journal of General Microbiology 115*, 259-271.

5. Lamden, P. R., and Guest, J. R. (1976) Mutants of Escherichia coli K12 Unable to use Fumarate as an Anaerobic Electron Acceptor, *Journal of General Microbiology 97*, 145-160.

6. Wallace, B. J., and Young, I. G. (1977) Role of quinones in electron transport to oxygen and nitrate in Escherichia coli. Studies with a ubiA− menA− double quinone mutant, *Biochimica et Biophysica Acta (BBA) - Bioenergetics 461*, 84-100.

7. Ichikawa, T., Horie-Inoue, K., Ikeda, K., Blumberg, B., and Inoue, S. (2006) Steroid and xenobiotic receptor SXR mediates vitamin K2-activated transcription

of extracellular matrix-related genes and collagen accumulation in osteoblastic cells., *The Journal of Biological Chemistry 281*, 16927-34.

8. Daruwala, R., Kwon, O., Meganathan, R., and Hudspeth, M. E. S. (1996) A new isochorismate synthase specifically involved in menaquinone (vitamin K2) biosynthesis encoded by the menF gene, *FEMS Microbiology Letters 140*, 159-163.

9. Daruwala, R., Bhattacharyya, D. K., Kwon, O., and Meganathan, R. (1997) Menaquinone (Vitamin K 2) biosynthesis :overexpression , purification , and characterization of a new isochorismate synthase from Escherichia coli., *Journal of Bacteriology 179*, 3133.

10. Jiang, M., Cao, Y., Guo, Z.-F., Chen, M., Chen, X., and Guo, Z. (2007) Menaquinone biosynthesis in Escherichia coli: identification of 2-succinyl-5-enolpyruvyl-6-hydroxy-3-cyclohexene-1-carboxylate as a novel intermediate and re-evaluation of MenD activity., *Biochemistry 46*, 10979-89.

11. Jiang, M., Chen, X., Guo, Z.-feng, Cao, Y., Chen, M., and Guo, Z. (2008) Identification and Characterization of Menaquinone Biosynthesis of Escherichia coli, *Biochemical Journal 47*, 3426-3434.

12. Popp, J. L., Berliner, C., and Bentley, R. (1989) Vitamin K (menaquinone) biosynthesis in bacteria: High-performance liquid chromatographic assay of the overall synthesis of o-succinylbenzoic acid and of 2-succinyl-6-hydroxy-2,4-cyclohexadiene-1-carboxylic acid synthase, *Analytical Biochemistry 178*, 306-310.

13. Kwon, O., Bhattacharyya, D. K., and Meganathan, R. (1996) Menaquinone (vitamin K2) biosynthesis: overexpression, purification, and properties of o-succinylbenzoyl-coenzyme A synthetase from Escherichia coli., *Journal of Bacteriology 178*, 6778-81.

14. Sharma, V., Suvarna, K., Meganathan, R., and Hudspeth, M. E. (1992) Menaquinone (vitamin K2) biosynthesis: nucleotide sequence and expression of the menB gene from Escherichia coli., *Journal of Bacteriology 174*, 5057-62.

15. Suvarna, K., Stevenson, D., Meganathan, R., and Hudspeth, M. E. S. (1998) Menaquinone (Vitamin K 2) Biosynthesis : Localization and Characterization of the menA Gene from Escherichia coli Menaquinone (Vitamin K 2) Biosynthesis : Localization and Characterization of the menA Gene from Escherichia coli, *Journal of Bacteriology 180*, 2782.

16. Lee, P. T., Hsu, A. Y., Ha, H. T., Clarke, C. F., Lee, P. T., Hsu, A. Y., Ha, H. T., and Clarke, C. F. (1997) A C-methyltransferase involved in both ubiquinone and menaquinone biosynthesis : isolation and identification of the Escherichia coli ubiE gene . A C-Methyltransferase Involved in Both Ubiquinone and Menaquinone Biosynthesis : Isolation and Identification, *Journal of Bacteriology 179*, 1748.

17. Chen, D., Wu, R., Bryan, T. L., and Dunaway-Mariano, D. (2009) In vitro kinetic analysis of substrate specificity in enterobactin biosynthetic lower pathway

enzymes provides insight into the biochemical function of the hot dog-fold thioesterase EntH., *Biochemistry 48*, 511-3.

18. Guo, Z.-F., Sun, Y., Zheng, S., and Guo, Z. (2009) Preferential hydrolysis of aberrant intermediates by the type II thioesterase in Escherichia coli nonribosomal enterobactin synthesis: substrate specificities and mutagenic studies on the active-site residues., *Biochemistry 48*, 1712-22.

19. Leduc, D., Battesti, A., and Bouveret, E. (2007) The hotdog thioesterase EntH (YbdB) plays a role in vivo in optimal enterobactin biosynthesis by interacting with the ArCP domain of EntB., *Journal of Bacteriology 189*, 7112-26.

20. Merkel, S. M., Eberhard, a E., Gibson, J., and Harwood, C. S. (1989) Involvement of coenzyme A thioesters in anaerobic metabolism of 4-hydroxybenzoate by Rhodopseudomonas palustris., *Journal of Bacteriology 171*, 1-7.

21. Baba, T., Ara, T., Hasegawa, M., Takai, Y., Okumura, Y., Baba, M., Datsenko, K. a, Tomita, M., Wanner, B. L., and Mori, H. (2006) Construction of Escherichia coli K-12 in-frame, single-gene knockout mutants: the Keio collection., *Molecular Systems Biology 2*, 2006.0008.

22. Chen, D. (2010) Divergence of Thioesterase Function: Human BFIT2, Escherichia Coli EntH and ydiI. The University of New Mexico.

23. Sangurdekar, D. P., Srienc, F., and Khodursky, A. B. (2006) A classification based framework for quantitative description of large-scale microarray data., *Genome Biology 7*, R32.

24. Hirst, J., Sucheta, A., Ackrell, B. A. C., and Armstrong, F. A. (1996) Electrocatalytic Voltammetry of Succinate Dehydrogenase : Direct Quantification of the Catalytic Properties of a Complex Electron-Transport Enzyme, *Journal of the American Chemical Society 7863*, 5031-5038.

25. Maklashina, E., Berthold, D. a, and Cecchini, G. (1998) Anaerobic expression of Escherichia coli succinate dehydrogenase: functional replacement of fumarate reductase in the respiratory chain during anaerobic growth., *Journal of Bacteriology 180*, 5989-96.

26. Widhlam, J., Van Oostende, C., Furt, F., and Basset, J. A dedicated thioesterase of the Hotdog-fold family is required for the biosynthesis of the naphthoquinone ring of vitamin K1.., *Proceedings of the National Academy of Sciences, 106*, 5599-603.

CHAPTER THREE
FROM FORM TO FUNCTION: A STRUCTURAL APPROACH TO EXAMINE THE DIVERGENCE OF YDII AND YBDB THIOESTERASES FROM *ESCHERICHIA COLI*

3.1 Introduction

The structure-function relationships is an important goal in the understanding of enzymes. The ability to deduce the substrate, product and chemical mechanism of an enzyme without the need of experimentation will aide in the annotation of the rapidly increasing number of genomes (*1*). The elucidation of the structure-function relationship in an *in vitro* or *in silico* environment may be provide a deeper understanding of the metabolic processes within the cell. One strategy of defining the structure-function relationship is to examine how evolution has chosen certain fold families to perform biochemical processes (*2*). As previously mentioned in Chapter 1, the hotdog-fold family has been associated with various types of chemistries and have largely divergent amino acid sequences. Examining the divergence in the structure-function relationship of two closely related paralogs such as the *Escherichia coli* paralogs YdiI and YbdB (EntH), may aide in defining how the placement of keys amino acid residues within a fold family alters substrate binding, protein-protein interaction, or overall chemistry. Furthermore, understanding how the structure-function relationship of two closely related paralogs translates to physiological function may aide in a more accurate annotation of the accumulating sequenced genes.

The physiological functions of YbdB and YdiI have been described in detail in the previous chapters however, a brief summary is presented here. The *E. coli* thioesterase YbdB has previously been reported to rescue the enterobactin synthesis pathway, essential for ferric uptake under iron starvation conditions, by cleaving mis-acylated molecules on the ArCP domain of the nonribosomal peptide synthetase EntB (*3*, *4*). In addition to rescuing the mis-acylated EntB, YbdB has also been reported to catalyze the hydrolysis of various aryl-CoA's *in vitro* and to a lesser degree, fatty acid-CoA's (*5*). The strikingly high sequence identity to YbdB prompted the investigation of YdiI's capability to replace YbdB in the enterobactin synthesis pathway (Δ*ybdB::ydiI*). The inability of YdiI protein to replace the function of the YbdB protein suggested that YdiI and YbdB have distinctly different *in-vivo* roles (*3*). The YdiI thioesterase was shown in the previous chapter through kinetic evaluation and gene knockout experiments to be involved in the synthesis of menaquinone (vitamin K_2), an essential cofactor for anaerobic respiration. Within the pathway, YdiI hydrolyzes 1,4-dihydroxynapthoyl-CoA (DHNA-CoA) to form 1,4-dihydroxynapthoic acid (DHNA) and CoA. DHNA is further processed by the addition of a polyisoprenyl side chain to form the final product of menaquinone (vitamin K_2).

Although YdiI and YbdB perform very different cellular functions, their structural homology would indicate otherwise. As shown in Figure 3.1, YdiI and YbdB share a high sequence identity (59%) and high sequence similarity (75%), uncommon to hotdog-fold thioesterases.

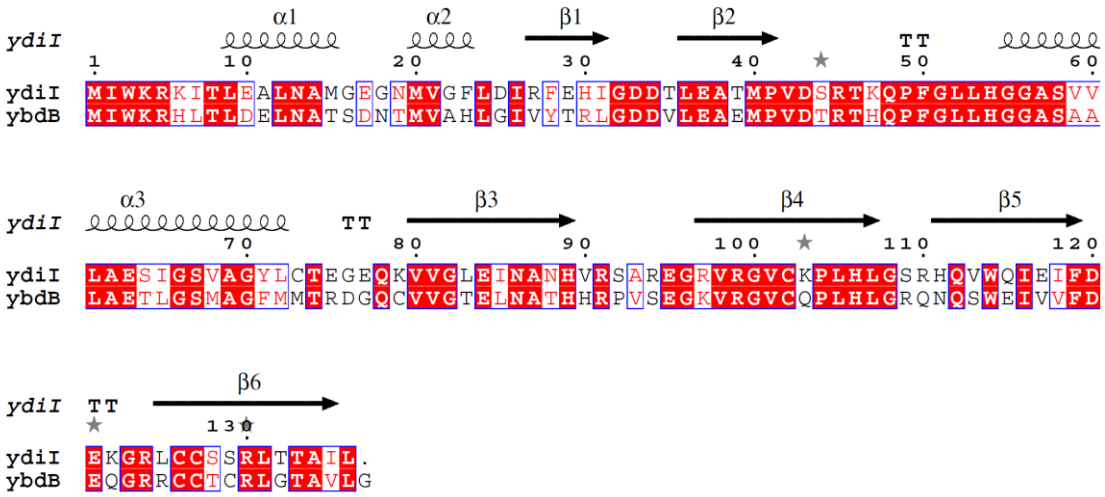

Figure 3.1: Amino acid sequence alignment of YdiI and YbdB with secondary structures generated by ESPript. Sequence identities are shown in the red background, similarities are shown with red font, α-helices are depicted by loops and β-strands are depicted by arrows.

The close sequence identity also translates into similar tertiary structures. Both YdiI and YbdB contain an indistinguishable PaaI-like hotdog fold as shown in Figure 3.2-A (*6*). The active site for both proteins lies at the interface of the monomers. The catalytic site is comprised of a glutamate and serine residue from the α-helix of one monomer and a histidine, glutamine and backbone glycine from the loop of the opposing monomer (Figure 3.2-B). The nearly identical catalytic site suggests that both YdiI and YbdB share a common catalytic mechanism.

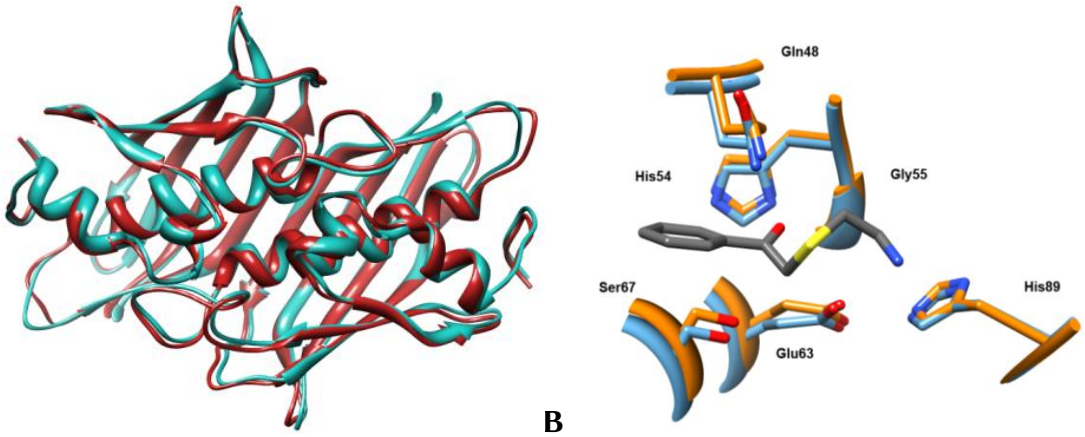

Figure 3.2: A) Crystal structure overlay of YdiI (blue (unpublished PDB: Solved by Rui Wu at Boston University)) and YbdB (red (unpublished PDB: Solved by Rui Wu at Boston University)) generated by Chimera. **B)** Active site overlay of YdiI (blue (unpublished PDB: Solved by Rui Wu at Boston University)) and YbdB (orange (unpublished PDB: Solved by Rui Wu at Boston University)) with co-crystallized phenacyl-CoA ligand (grey) generated by Chimera.

In this chapter, I will explore how the closely related YdiI and YbdB evolved to perform their individual cellular functions. To do this, I will report on the mechanism by which both YdiI and YbdB catalyze the hydrolysis of their substrate thioesters. The mechanism for thioesterases is limited to either base or nucleophilic catalysis as depicted in Figure 3.3. For base catalysis the active site glutamate activates the water nucleophile that hydrolyzes the thioester whereas for nucleophilic catalysis the glutamate attacks the thioester to form a mixed anhydride which, in a subsequent step hydrolyzed by water. The mechanism was probed through the use of active site mutants, solvent ^{18}O incorporation experiments, solvent kinetic isotope effects and pre-steady-state kinetics. Additionally, I will report on the structural properties that enable each protein to

distinguish their substrates through kinetic analysis of substrate binding pocket mutants and by examining the liganded YbdB and YdiI X-ray crystal structures.

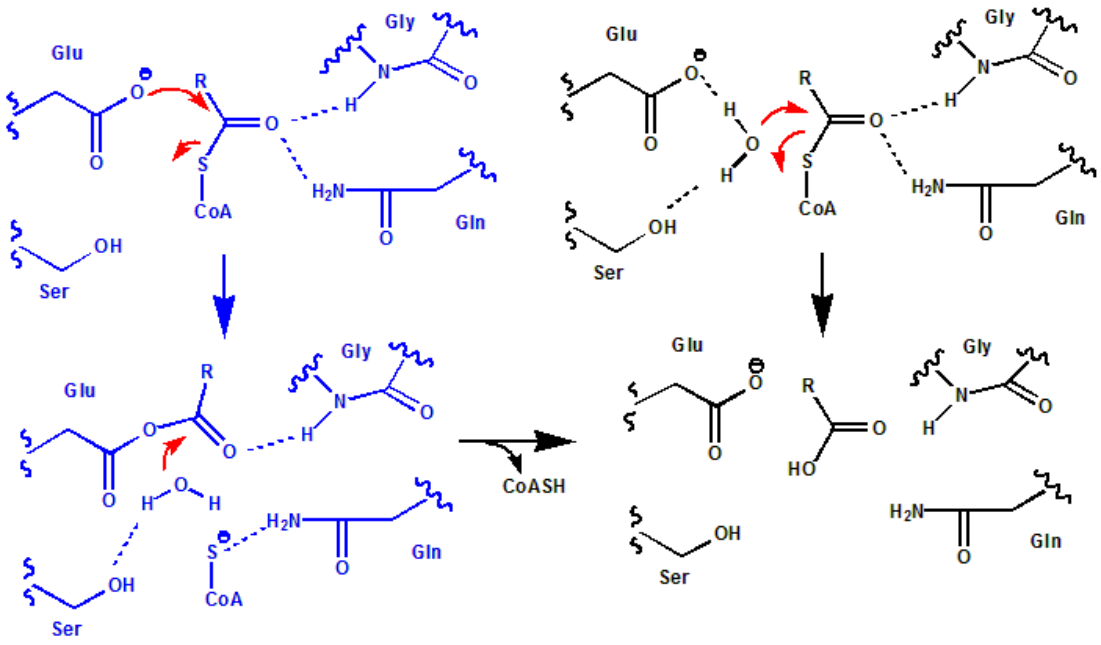

Figure 3.3: Possible catalytic mechanisms (nucleophilic catalysis [blue] or base catalysis [black]) for YdiI and YbdB.

3.2 Materials and Method

3.2.1 Materials

All restriction enzymes and T4 DNA ligase were purchased from Invitrogen. *Pfu Turbo and Deep Vent* DNA polymerases were purchased from Strategene. Oligonucleotide primers were custom-synthesized by Invitrogen. DNA sequencing was performed by the DNA Sequencing Facility of the University of New Mexico. Benzoyl-CoA was purchased from Sigma. 4-hydroxybenzyol-CoA was synthesized as previously reported (*7*). The wild-type (WT) YdiI and WT YbdB were prepared as described in Chapter 2.

3.2.2 Site-directed mutagenesis

Site-directed mutagenesis was carried out using the Quick Change PCR strategy (Stratagene) containing the WT *ydiI*/pET-23a or WT *ybdB*/pET-23a plasmid as template, commercial primers, and *Pfu Turbo* as the polymerase. The sequence of the mutated gene was confirmed by DNA sequencing. The recombinant mutant plasmids were used to transform competent *E. coli* BL21 Star (DE3) cells (Invitrogen). The mutant proteins were purified to homogeneity (as determined by SDS-PAGE analysis) using the same method reported in Chapter 2 for the wild-type proteins. Yield: 25 – 40 mg/g wet cell paste.

3.2.3 Steady-state kinetic analysis

The k_{cat} and K_m values for wild-type and mutant YdiI and YbdB-catalyzed hydrolysis of thioester substrates were determined as described in Chapter 2.

3.2.4 Inhibition of the WT enzyme-catalyzed hydrolysis of 4-hydroxybenzoyl-CoA

For 2,4-dihydroxyphenacyl-CoA inhibition, the WT YdiI or WT YbdB catalyzed hydrolysis of benzoyl-CoA was monitored using the DTNB assay as described in Chapter 2. The assay solution contained WT enzyme, varying concentrations of substrate benzyol-CoA, and varying concentrations of inhibitor (0, 20, and 50 μM). For CoASH inhibition, the WT YdiI enzyme-catalyzed hydrolysis of 4-hydroxybenzoyl-CoA (4-HB-CoA) was directly monitored at 300 nm as described in Chapter 2. The assay solution contained WT enzyme, varying concentrations of 4HB-CoA, and varying concentrations

of CoASH. The inhibition constant K_i was obtained by fitting the initial rates to equation (1):

$$V = V_{max}[S]/[K_m (1+[I]/K_i) + [S]] \quad (1)$$

Where [I] = concentration of inhibitor and K_i = inhibition constant.

3.2.5 ^{18}O-Solvent labeling experiments.

A 4.0 mL solution containing 88.9 μM WT ydiI in 50 mM Tris and 50 mM NaCl (pH 8.4) was lyophilized. To the resulting powder, 370 μL of 99.2% $H_2{}^{18}O$ were added. After 15 min incubation on ice, the enzyme was assayed to confirm retention of catalytic activity. To the 370 μL solution, 30 μL of lyophilized (30 μL of 10 mM stock concentration in normal isotopic water) benzoyl-CoA resuspended in 99.2% $H_2{}^{18}O$ water was added so that the final enzyme concentration was 889 μM and the final substrate concentration was 750 μM. The reaction was allowed to incubate at room temperature for 15 min. The reaction mixture was filtered using a 10 kDa micro separation filter (Millpore). The filtrate was acidified with 10 μL of 6 M HCl and extracted with 1 mL of ethylacetate four times. The extract was dried over anhydrous sodium sulfate and the solvent was evaporated *in vacuo*. The solid was resuspended in 10 μL of anhydrous methyl alcohol and then subjected to GC/MS analysis. The same procedure was carried-out with YdiI S67A. In this case 2.0 mL of 93.3 μM YdiI S67A lyophilized and reconstituted in 182 μL of 99.2% $H_2{}^{18}O$. To the reconstituted protein was added 18 μM benzoyl-CoA for a final enzyme concentration of 933 μM and substrate concentration of 900 μM.

For the (multi-turnover) control experiment, 20 μL of 88.9 μM YdiI solution was lyophilized. The powder was resuspended in 370 μL of 99.2% $H_2{}^{18}O$ and to it was added 30 μL of reconstituted 10 mM benzoyl-CoA in 99.2% $H_2{}^{18}O$. The final concentration of YdiI was 45 μM and the final concentration of substrate was 750 μM.

GC/MS analysis was conducted with the extract on an Agilent 5975C Series GC/MS with a Triple-Axis Detector. The temperature program for the analysis was as follows: 250 ^{o}C inlet, 80 ^{o}C intial temperature held for 1 min and ramped to 180 ^{o}C at a rate of 7 ^{o}C/min, then ramped to 250 ^{o}C at a rate of 20 ^{o}C/min and held for 6 min. The mass analyzer was set to detect in the range of 50-450 m/z. The product of benzoic acid eluted in the timeframe of 7.5 – 8.0 min.

3.2.6 Synthesis of ^{14}C radiolabled benzyol-CoA

[^{14}C]-benzoyl-CoA was synthesized enzymatically by using 4-hydroxybenozoic acid ligase (4HBAL) from *Rhodopseudomonas palustris.* 4HBAL was purified by a modification of a previously described procedure (*8*). In short, the *4HBAL*/pET3a was used to transform competent *E. coli* BL21 (DE3) cells (Invitrogen). A single colony was used to inoculate 10 mL LB media containing 50 μg/ml ampicillin. The culture was scaled, the gene expression induced, the cells were harvested described about. The cells were resupended in 50 mM K^{+}HEPES (pH 7.5) lysis buffer then lysed as described above. The cleared supernant was fractioned by ammonium-sulfate induced precipitation. The protein precipitated with 0-35 % ammonium sulfate and was harvested by centrifugation at 20,000 rpm for 15 min. The protein pellet was resuspended in 10X its weight of 50 mM K^{+}HEPES buffer pH 7.5 containing 1 M ammonium sulfate (Buffer

A) and loaded onto a FPLC attached 30 x 1 cm butyl sepharose column equilibrated with 5 CV of Buffer A. The column was washed until the A_{280} reached baseline and the protein was eluted with a gradient of 0-50% 50 mM K^+HEPES pH 7.5 (Buffer B). The protein eluted at 35% Buffer B and the fractions were combined, concentrated and dialyzed 3 times against Buffer B.

[^{14}C]-Benzoyl-CoA was synthesized in a 1 mL reaction solution containing 100 mM K^+HEPES, 5 mM $MgCl_2$, 13 mM CoA, 13 mM ATP, and 5 µM 4HBAL. [^{14}C]-Benzoic acid with a specific activity of 56 mCi/mol (American Radiolabeled Chemicals Inc.) was made into the sodium salt by the addition of 150 µL 0.1 M NaOH before adding it to the reaction for a final concentration of 9 mM. The reaction was allowed to incubate at room temperature overnight and then quenched by the addition of 1 M HCl. The precipitated protein was harvested by centrifugation. [^{14}C]-Benzoyl-CoA was purified from the crude reaction over a semi-prep Ultra Aqueous C-18 reverse phase HPLC column (RESTEK) eluted with a 50% linear gradient of 20 mM KH_2PO_4 (pH 6.1) (Buffer A) and 80% CH_3CN (Buffer B) over 35 min. The desired compound eluted at ~ 14 min. The fractions containing the final compound were combined and lyophilized to powder.

3.2.7 Rapid-quench studies of the wild-type ydiI catalyzed hydrolysis of benzoyl-CoA under single and multiple turnover conditions

Rapid-quench experiments were carried out at 25 ^{o}C using a rapid-quench instrument from KinTek Instruments. For the multiple turnover reaction of WT YdiI catalyzed hydrolysis of [^{14}C]- benzoyl-CoA, the final concentration of enzyme is 10 µM

and the substrate is 50 μM. For the single turnover reaction, the final concentration of enzyme is 50 μM and the substrate is 5 μM. The reactions were initiated by mixing the enzyme with the [^{14}C]-benzoyl-CoA in 10 mM K^+HEPES buffer (pH 7.5) containing 0.1 M NaCl and then quenched after a specific time with 0.2 M HCl. Protein was separated from the quenched reaction mixture using a 10,000 MWCO centrifuge column (Millipore). The [^{14}C]-benzoyl-CoA and [^{14}C]-benzoic acid were separated on an analytical C18 column (RESTEK) by HPLC using the same procedures as described above and quantified using an in-line β-RAM4 (Lab Logic) scintillation counter. Peak integrations were performed by Laura software (Lab Logic) and the relative ratios were used to calculate the substrate and product concentrations. The plotted time course concentrations were fitted by simulation using KinTek Corp. Global Kinetic Explorer.

3.2.8 Stopped-flow kinetic experiments of wild-type ydiI

A DX.17MV sequential stopped-flow spectrometer (Applied Photophysics, Leatherhead, U.K.) with a dead time of 3 ms was used for measurement of transient rate constants of WT YdiI thioesterase hydrolysis of 4-HB-CoA. All experiments were carried out in 50 mM K^+HEPES buffer (pH 7.5) at 25 ^oC and were run in triplicate. Substrate consumption was monitored at 300 nm ($\Delta\varepsilon$ = 11.8 $mM^{-1}cm^{-1}$). A single-turnover reaction mixture consisted of 60 μL of 124 μM WT YdiI mixed with 60 μL of 100 μM 4-HBA-CoA to give a final concentration of 62 μM YdiI and 50 μM substrate. The measured data was fitted to the single exponential decay equation 3. The multiple-turnover reactions contained 60 μL of 200 μM 4-HB-CoA mixed with 60 μL of 20, 32,

and 40 μM WT YdiI. The final concentration of 4-HBA-CoA was 100 μM and the final enzyme concentrations were 10, 16, or 20 μM.

$$f = a*\exp(-b*x) \qquad (3)$$

3.2.9 Solvent kinetic isotope effects on WT ydiI and ybdB

The steady-state kinetic constants of WT YdiI and YbdB thioesterase catalyzed hydrolysis of 4-HB-CoA at pL 7.0 and 7.5 were determined by direct monitoring at 300 nm as described above. Deuterated solvent was made by dissolving 50 mM K^+HEPES in D_2O and adjusted to the according pD by 30% DCl or 30% NaOD in D_2O. Kinetic constants determined at different pLs were used to calculate k_H/k_D.

3.3 Results and Discussion

3.3.1 Steady-state kinetics of the active site mutants E63A, Q48A, H54A, H89A, and S67A

The X-ray crystal structure of the wild-type *E. coli* YbdB and YdiI revealed numerous interactions between the ligand and the enzyme. As shown in Figure 3.4 A, the YdiI Glu63 is poised to hydrolyze the thioester carbonyl with the possible assistance from His89. The distance of the Glu63 (3.8 Å) suggests that the residue is within striking distance for nucleophilic catalysis. Additionally, as was reported for *Arthrobacter sp.* SU 4-hydroxybenzoyl-CoA thioesterase (4HBT), a glutamine (Gln48) might activate the carbonyl through hydrogen bonding to the carbonyl oxygen provide the side chain rotates into a closer position (distance from the amine to the oxygen of 4.7 Å provided that the substrate analog is in the absolute postioin) (*9*). Also within hydrogen bonding distance to the carbonyl oxygen is His54 (3.2 Å) which could also contribute to the activation of the carbonyl (Figure 3.4 B).

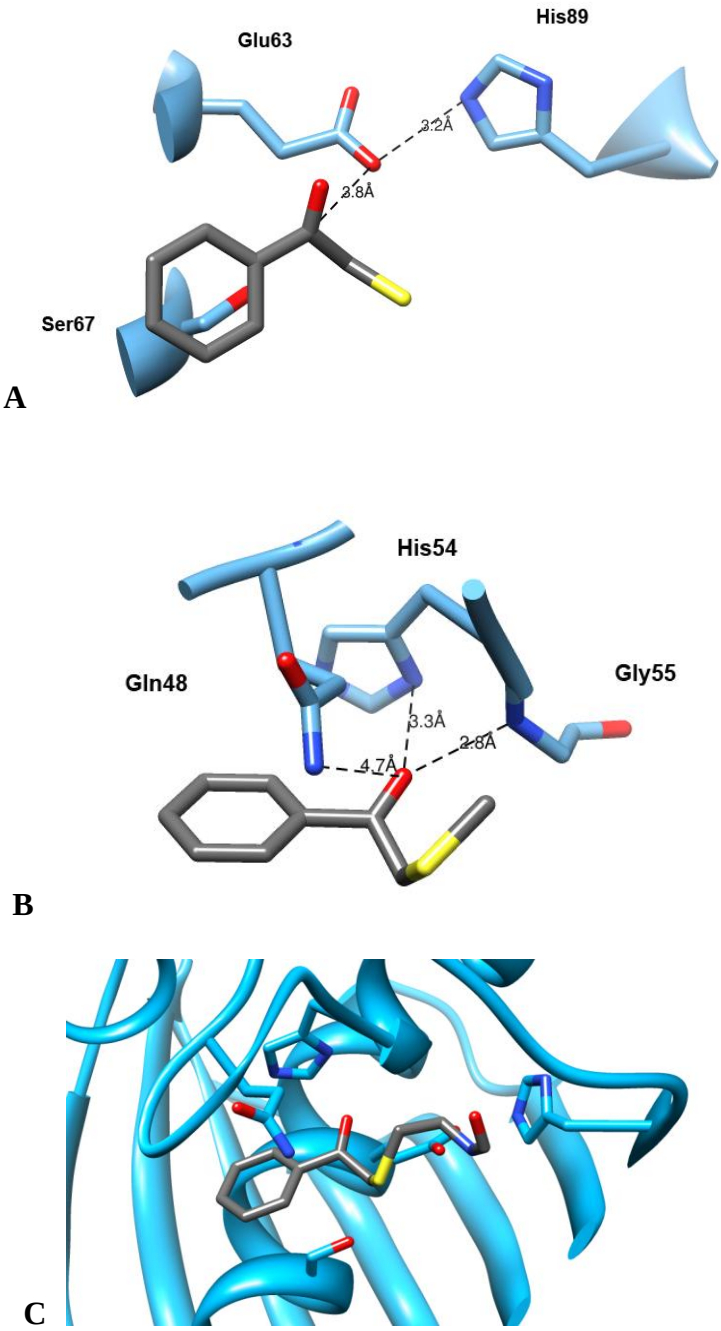

Figure 3.4 A: Active site distances of Glu63 to the carbonyl and His89 to Glu63 in YdiI (blue (unpublished PDB: Solved by Rui Wu at Boston University)) with the bound ligand phenacyl-CoA (grey) in truncated form. **B -** Active site distances of Gln48 and His54 to the carbonyl in YdiI (blue (unpublished PDB: Solved by Rui Wu at Boston University))

with the bound ligand phenacyl-CoA (grey) in truncated form. **C -** General orientation of the YdiI active site with bound ligand phenacyl-CoA (grey)

Because the phenacyl-CoA substrate analog might, owing to the added "CH_2" between the carbonyl carbon and the sulfur atom, bind in a nonproductive conformation, the enzyme-ligand interactions suggested by the X-ray structure must be tested. Therefore, to probe these enzyme interactions and as well as the catalytic mechanism, mutants were made by replacing the active site residue with alanine (the methyl side chain is chemically inert) and the steady-state constants for the mutants were measured using the benzoyl-CoA thioester as substrate. The results are reported in Table 3.1. The YdiI E63A mutant was completely inactive, in line with reported results from a previously reported mutagenesis study of YbdB (*3*). Because the crystal structure containing the ligand was devoid of an ordered active site water molecule and because of the close distance of Glu63 to the reaction site, it was thought that the glutamate residue acted as a nucleophile. Switching the residue to an aspartate should increase the spanning distance by one carbon length (total distance ~ 5 Å) but not completely abolish the enzyme from activity. The YdiI E63D mutant does retain activity as compared to the WT YdiI but at a penalty of ~ 2 x 10^3 reduced efficiency. The YdiI E63Q mutant was prepared and found to be devoid of activity. The YdiI H89A mutant was found to have a 100-fold reduction in catalytic activity. YdiI His89 may align Glu63 for either nucleophilic attack or water activation via hydrogen bonding.

YbdB				YdiI			
Mutants	**k_{cat} (s^1)**	**K_M (μM)**	**k_{cat}/K_M ($M^{-1}s^{-1}$)**	**Mutants**	**k_{cat} (s^1)**	**K_M (μM)**	**k_{cat}/K_M ($M^{-1}s^{-1}$)**
WT	2.2 ± 0.1	12 ± 1	1.8×10^5	WT	18 ± 1	25 ± 3	7.2×10^5
E63A	$< 10^{-4}$			E63A	$<10^{-4}$		
E63D*				E63D	0.040 ± .002	120 ± 10	3.39×10^2
E63Q*				E63Q	$<10^{-4}$		
Q48A	$< 10^{-4}$			Q48A	0.051 ± .002	12 ± 1	4.40×10^2
S67A*				S67A	2.5	12.6	1.98×10^5
H89A*				H89A	0.82 ± 0.02	180 ± 10	2.5×10^3
H54A	$< 10^{-4}$			H54A	0.14 ± .01	100 ± 10	1.41×10^3

Table 3.1: Steady-state kinetic constants for YbdB or YdiI mutant catalyzed hydrolysis of benzoyl-CoA; measured using DTNB spectrophotometric assay at pH 7.5 and 25 ^oC. The * represents mutant data not obtained.

Other active site mutants were also prepared to probe enzyme interactions with the substrate. As mentioned previously, the catalytic scaffold loop glutamine of the *Arthrobacter sp.* strain SU 4HBT is known to activate the thioester carbonyl by hydrogen bonding to the oxygen atom. Because YdiI also contained a similarly positioned glutamine, the YdiI Q48A mutant was prepared for evaluation. The Ala replacement of the glutamine residue diminished the efficiency of catalysis by ~1000-fold (k_{cat} decreased from 18 s^{-1} to 0.05 s^{-1}) reflecting its importance its putative activation of the thioester carbonyl. This same mutation in YbdB resulted in total loss of catalytic activity. YdiI His54 is another active site residue that was queried because of its potential role in

interacting with the thioester carbonyl. The YdiI H54A mutant displayed a 100-fold decrease in catalytic activity. The last key residue located in the active site is YdiI Gly55 however, because it is the backbone amine that possibly contributes to the activation of the carbonyl, its role could not be probed by site-directed mutagenesis

3.3.2 Comparing the pH profiles of YbdB and YdiI

All steady-state kinetic parameters were carried out at pH 7.5. To verify that this pH was within the optimum range of catalysis for YdiI and YybdB a pH profile of catalyzed 4-HB-CoA hydrolysis was measured. As illustrated in Figure 3.5**,** the YdiI the k_{cat} pH profile reflects increasing turnover rate as the pH is increased from 5 to 6, at which point it begins to plateau at and remains flat to approximately pH 8.5 (apparent pKa ~ 6.7). The k_{cat} pH profile for ybdB similarly begins to level at approximately pH 6.7 however, unlike YdiI, the turnover rate begins to drop taper off at ~pH 7.8. The profiles for both YdiI and YbdB suggest that the optimal range for catalysis is between pH 7.0 ~ 8.0.

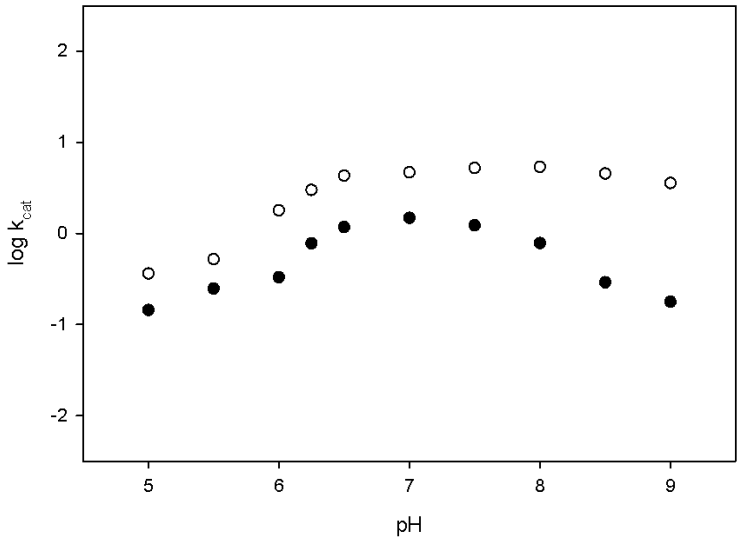

Figure 3.5 - Profile of pH dependence showing log k_{cat} vs. pH for the WT YdiI (○) and WT YbdB (●) catalyzed hydrolysis of 4-hydroxybenzoyl-CoA measured by direct assay at 300 nm and at 25^{o}C.

3.3.3 ^{18}O incorporation into benzoic acid by WT YdiI and the mutants S67A and E63D

To distinguish between the general base and nucleophilic catalysis mechanisms the solvent ^{18}O-oxygen labeling experiment was conducted. The premise of this experiment is highlighted in Figure 3.6. If the thioesterase Glu functions in base catalysis, a single turnover reaction carried out in 99.2% $H_2{}^{18}O$ will result in the incorporation of the ^{18}O into the carboxylic acid product. Thus the level of ^{18}O incorporated will reflect the solvent isotopic composition (99.2% ^{18}O and 0.8% ^{16}O). Only if the Glu carboxylate functions in nucleophilic catalysis is the incorporation of the ^{16}O-derived from Glu possible. Unfortunately, if the ^{18}O-labeled water nucleophile is positioned to attack the anhydride intermediate at the substrate carbonyl carbon rather than the Glu carbonyl

carbon, then one would not observe ^{16}O transfer to the carboxylic acid product but instead would observe ^{18}O-incorporation.

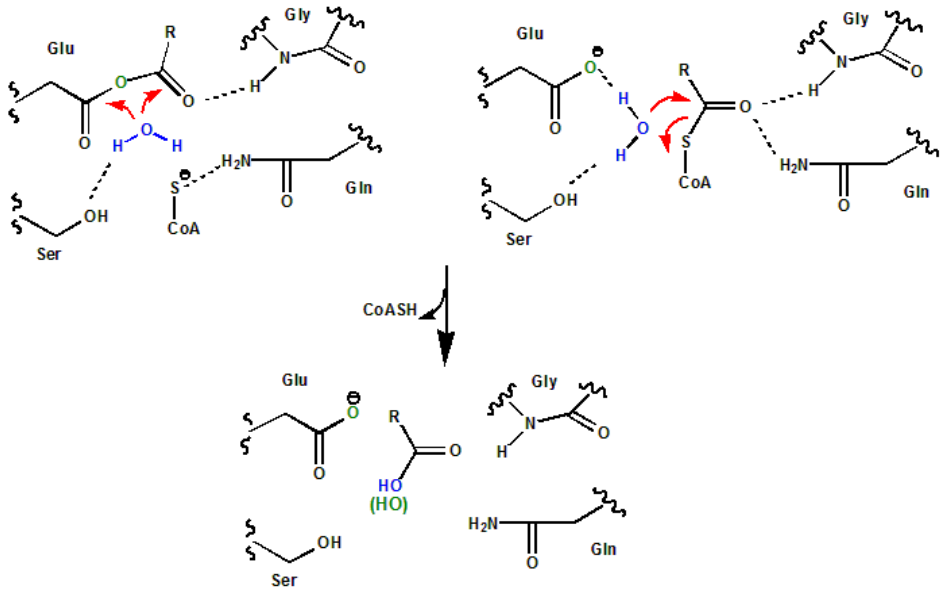

Figure 3.6 – Depiction of solvent ^{18}O (green and blue) incorporation pathways for nucleophilic catalysis (left) or base catalysis (right).

Benzoyl-CoA was utilized in this experiment because it is a very active substrate and because the product, benzoic acid (MW = 121.1) is easily isolated by organic solvent extraction for GC-MS analysis (Figure 3.7). The benzoic acid generated in the control experiment gave a single m/z peak at 121.1 with fragmentation peaks correlating to the loss of hydroxide (m/z = 16) at 105.1 and the remaining fragmentation of the $^{+}C{=}O$ (m/z = 28) at 77.1 (not shown). The single turnover experiment utilizing WT YdiI yielded a mass spectrum containing two benzoic acid peaks at m/z = 122.1 and 124.1 suggesting the incorporation of ^{18}O into the product. The ^{16}O: ^{18}O peak ratio was approximately 1:6. The fragmentation peaks suggest the ratio of ^{16}O: ^{18}O was conserved through the loss of

hydroxide yielding two peaks at 105.1 and 107.1 at a ratio of 1.1:1, ^{16}O: ^{18}O respectively. The further loss of the $^{+}C=O$ yielded only one peak at 77.1 which confirms the incorporation of ^{18}O.

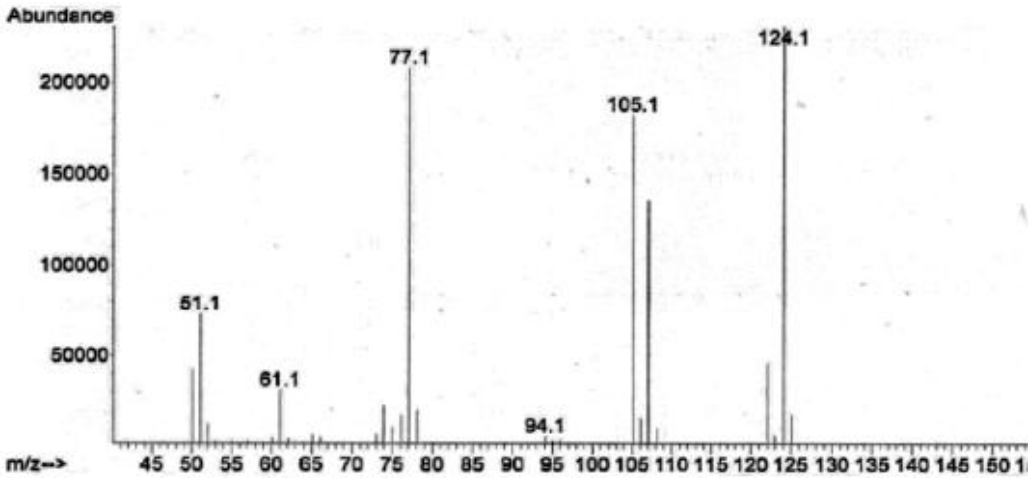

Figure 3.7 - GC-MS spectra of the product of WT YdiI thioesterase-catalyzed hydrolysis of benzoyl-CoA in 99.2% ^{18}O water under single-turnover conditions.

The benzoic acid isolated from multiple turnover reaction showed two peaks, again at m/z of 122.1 and 124.1 with a ratio of ^{16}O: ^{18}O at 1:17 (Figure 3.8) also suggesting the incorporation of ^{18}O. This control was executed to determine if the experimental ^{16}O: ^{18}O ratio was correct by showing the diminished ratio due to multiple turnovers. However, the ^{16}O peak only diminished to 1:17 suggesting that the previous experimental ^{16}O peak may be less significant.

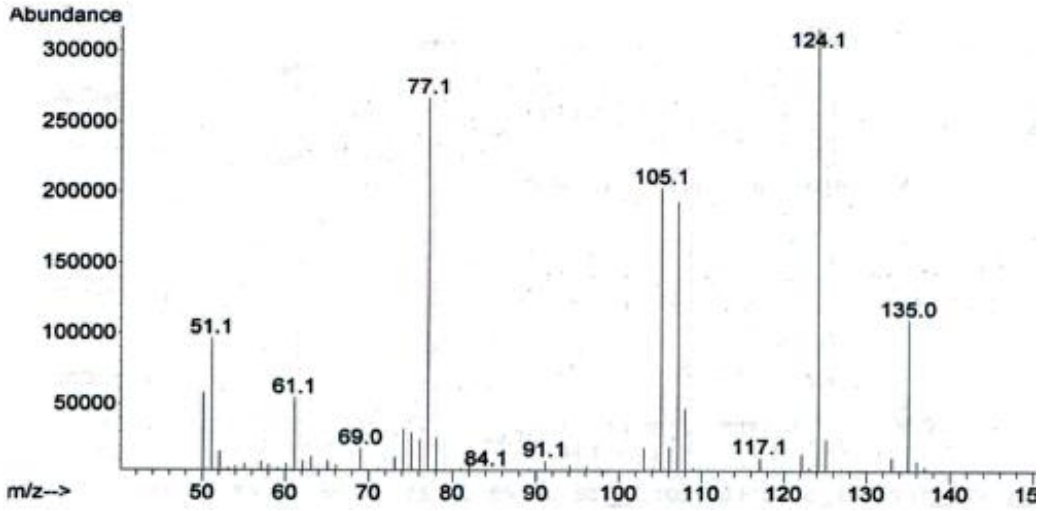

Figure 3.8 - GC-MS spectra of the product of WT YdiI thioesterase-catalyzed hydrolysis of benzoyl-CoA in 99.2% ^{18}O water under multiple-turnover conditions.

Using the mutant YdiI S67A for the^{18}O exchange could help clarify the mechanism if the residue is in fact positioning a water molecule during catalysis. As prior, if the Ser67 is prevented from directing the attack of the water nucleophile at the benzoyl carbonyl carbon by mutation to Ala the ^{16}O: ^{18}O incorporation might increase, reflecting increased attack at the Glu carbonyl carbon. The single turnover reaction was repeated with YdiI S67A and the benzoic acid product isolated and analyzed to reveal the peaks at m/z of 122.1 and 124.1 which defined the ^{16}O: ^{18}O ratio as 1:9 (Figure 3.9). The lack of an increase in the ^{16}O peak indicates that Ser67 may not play a significant role in water positioning. This is contrary to what was observed for the single turnover reaction carried out with *Arthrobacter sp*. SU 4HBT mutant T77A. In this thioesterase the 4HBT Thr77 occupies the same position on the catalytic scaffold as does the Ser67 in YdiI. The single turnover experiment carried out with *Arthrobacter sp*. SU 4HBT mutant T77A under similar conditions gave an increased amount of ^{16}O incorporation (near 50%)

suggesting that the Thr77 does serve to position water for attack on the acyl group rather than the enzyme (*10*).

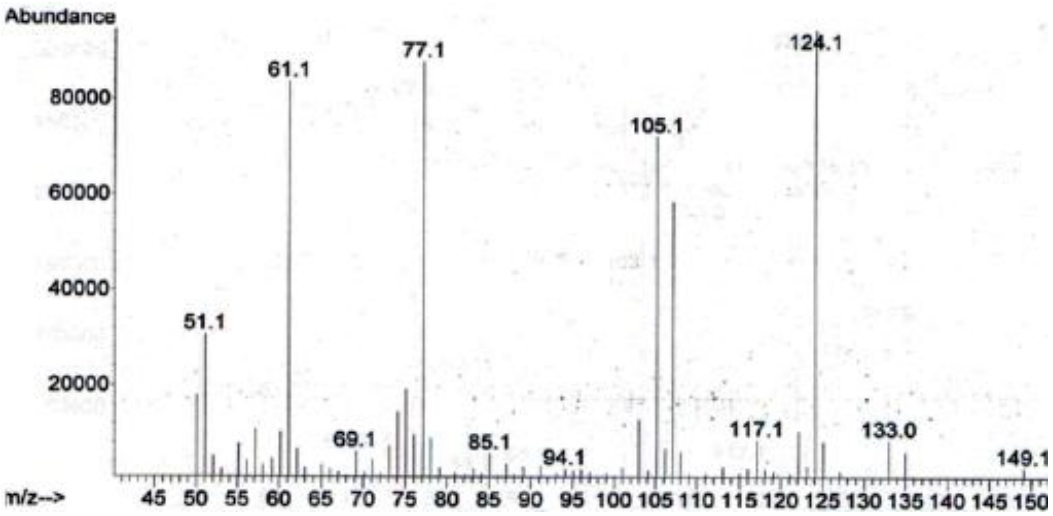

Figure 3.9 - GC-MS spectra of the product of YdiI S67A thioesterase catalyzed hydrolysis of benzoyl-CoA in 99.2% ^{18}O water under single-turnover conditions.

In an attempt to manipulate the catalytic mechanism from the assumed nucleophilic catalysis to base catalysis the YdiI E63D mutant was used in the ^{18}O experiment. In contrast to what was seen in the WT YdiI single turnover experiment, the level of ^{16}O incorporation was found to be insignificant (Figure 3.10), consistent with no anhydride intermediate formation by the Glu63.

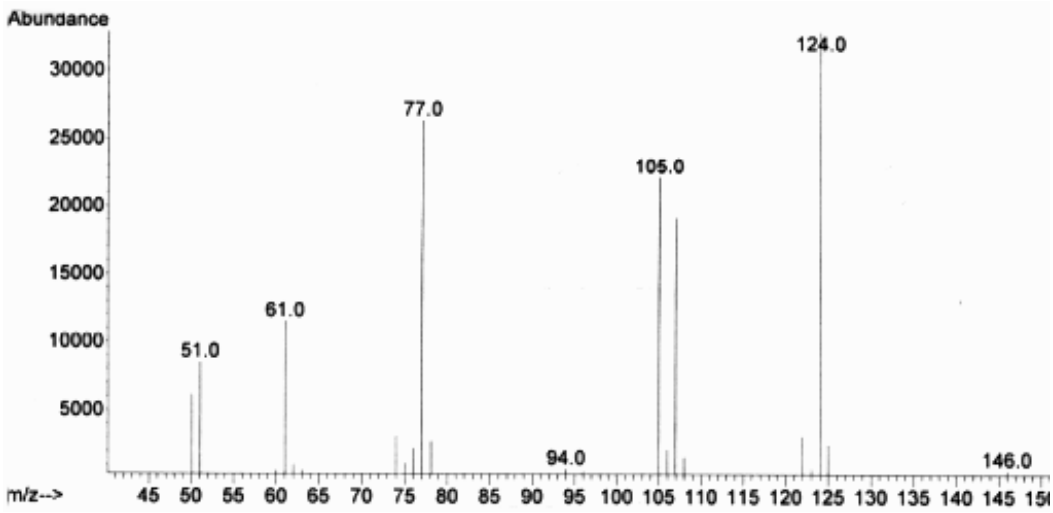

Figure 3.10 - GC-MS spectra of the product of YdiI E63D thioesterase-catalyzed hydrolysis of benzoyl-CoA in 99.2% ^{18}O water under single-turnover conditions.

3.3.4 Solvent kinetic isotope effects on ydiI and ybdB

Because the k_{cat} pH profile for both YdiI and YbdB indicated that the k_{cat} value is invariant within the pH range of 7.0 - 7.5, the deuterium solvent isotope effect (SIE) was determined for pH 7.0 and 7.5. A secondary SIE (k_H/k_D >1) would suggest that the chemistry is rate limiting whereas a primary SIE (k_H/k_D <1) would suggest that substrate binding or product leaving would be rate limiting. The results are reported in Table 3.2. The SIE for YbdB measured at pH 7.0 and 7.5 are k_H/k_D = 2.2 and k_H/k_D = 2.5, respectively. The SIE measured for YbdB at pH 7.0 and 7.5 are k_H/k_D = 2.2 and k_H/k_D = 2.5, respectively. The SIE measured for YdiI at pH 7.0 and 7.5 are k_H/k_D = 1.7 and k_H/k_D = 1.9, respectively. The SIE for YdiI and YbdB suggest that the chemical step is rate limiting.

	pH (D) 7.5			pH (D) 7.0		
	H_2O	D_2O	k_H/k_D	H_2O	D_2O	k_H/k_D
YbdB	1.2 ± 0.1	0.55 ± 0.05	2.2	1.2 ± 0.1	0.46 ± 0.03	2.5
YdiI	5.2 ± 0.2	3.1 + 0.1	1.7	2.9 ± 0.1	1.60 ± 0.03	1.9

Table 3.2. D_2O solvent kinetic isotope effects on the YbdB and YdiI-catalyzed hydrolysis of 4-hydroxybenzyol-CoA at 25 ^oC pH (D) = 7.5 or 7.0 monitored at 310 nm.

3.3.5 Pre-steady-state kinetics analyzed by stopped-flow absorbance

A single turnover reaction was performed to verify the steady-state k_{cat}. As shown in Figure 3.11, fitting to a single exponential decay provided a k_{obs} of 5.8 s^{-1} which is in reasonable agreement to the steady-state k_{cat} value of 5.2 s^{-1}. To detect if YdiI displays pre-steady state "burst" kinetics, a multiple-turnover reaction was performed. As shown in Figure 3.12, there is no apparent burst of substrate consumption associated with the first catalytic turnover. If a "burst" phase was present, the first turnover, equivalent to the concentration of enzyme, would be followed by a slow linear phase associated with subsequent turnovers. The apparent lack of a "burst" phase is consistent with a single rate-limiting chemical step, as expected for the base catalysis pathway. It is also consistent with the two-step chemical pathway associated with nucleophilic catalysis provided that the first step, *viz*. formation of the anhydride intermediate is rate-limiting. That said, the absence of the burst phase might also be attributed to an experimental artifact. Specifically, the ~5 ms delayed response to the decrease in absorbance at 300 nm

observed for the single-turnover reaction (Figure 3.12**)** is problematic in that it indicates a "dead-time" associated with solution mixing or with absorbance detection. On the other hand, the lag is not apparent in the multiple-turnover time courses measured for reaction solutions containing significantly lower enzyme concentrations. High enzyme concentration results in a high background absorbance at 300 nm.

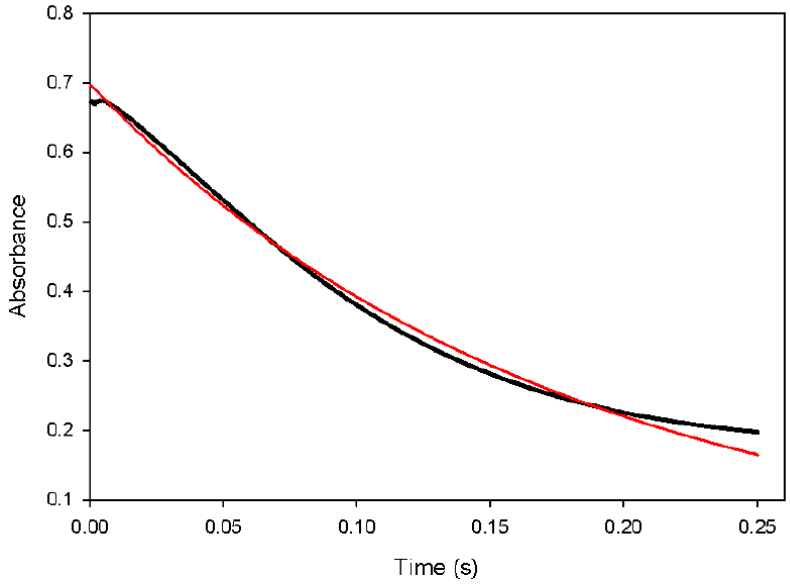

Figure 3.11 - Single turnover reaction trace (black) containing a final concentration of 50 µM 4HB-CoA and 62 µM YdiI measured by stopped flow at 300 nm and fitted to single exponential decay (red).

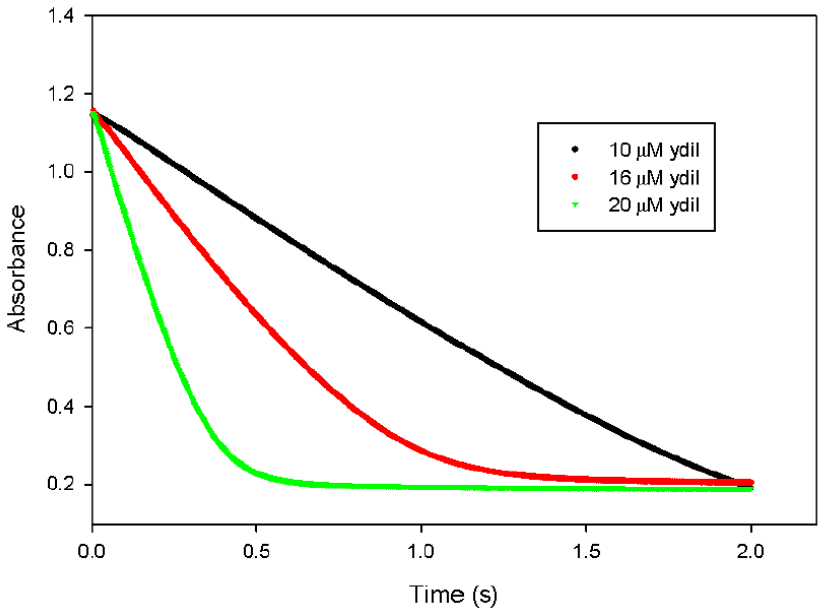

Figure 3.12: Multiple turnover reaction containing a final concentration of 100 µM 4HBA-CoA and 10, 16, and 20 µM YdiI measured by stopped flow at 300 nm.

3.3.6 Reaction time course analysis

For global kinetic fitting to be perfromed, ideally several sets of time course measurements (*e.g.*, for single-turnover, multiple-turnover, steady-state and substrate-binding reactions) are required. The substrate binding reaction is typically monitored using stopped-flow fluorescence techniques, wherein the fluorescence emanating from a binding site Trp residue is quenched as the result of substrate binding. Unfortunately, YdiI does not contain a Trp residue within its substrate binding pocket. Thus, only the steady-state time course data could be used to supplement to the stopped-flow absorbance curves. Accordingly, the YdiI (0.022 µM) catalyzed hydrolysis of 20 and 30 µM benzoyl-CoA was monitored at 412 nm using the DTNB-coupled assay. The absorbance was converted to concentration using the molar extinction coefficient (13.1 $mM^{-1}cm^{-1}$) and the

resulting time courses were fitted by simulation to the kinetic model shown in Scheme 1 using the KinTeK Corp. Global Kinetic Explorer program and setting the rate constants: $k_{1,}$ k_{-3}, and k_{-4} = 1000 s^{-1} (rate of diffusion) and k_{-2} = 0 s^{-1} (**Figure 3.13**)

$$\mathbf{E + S} \underset{k_{-1}}{\overset{k_1}{\rightleftharpoons}} \mathbf{ES} \underset{k_{-2}}{\overset{k_2}{\rightleftharpoons}} \mathbf{EPQ} \overset{k_3}{\rightarrow} \mathbf{Q} \quad \mathbf{EP} \underset{k_{-4}}{\overset{k_4}{\rightleftharpoons}} \mathbf{E + P} \qquad \textbf{(Scheme 1)}$$

$$k_{-3}\,\mathbf{(Q)}$$

The K_m (k_{-1}/k_1) was calculated to be ~7 µM, substantially less than K_m determined in the substrate screen (K_m = 25 µM). The K_i for CoA ((Q) (k_3/k_{-3})) was calculated to be ~6 µM, approximately half of the value determined for its competitive inhibition constant (*vide infra*) and the K_d (k_4/k_{-4}) for benzoic acid (P) was calculated to be ~100 µM. The k_{cat} (18 s^{-1}) was in agreement to the fitted k_2 of 17 - 20 s^{-1}.

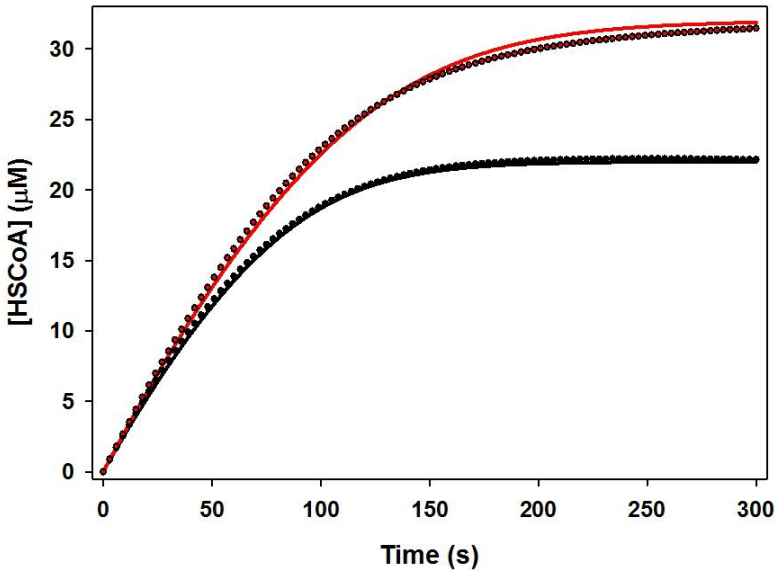

Figure 3.13: Experimental and simulated time courses for the steady-state reaction containing 0.022 µM wild type YdiI and 20 (●) or 30 µM (●) benzoyl-CoA in 50 mM

K^+HEPES (pH 7.5, 25 ^oC). The simulated curves were generated using the kinetic model in Scheme 1.

Rapid quench techniques were used in conjunction with [^{14}C]-benzoyl-CoA as an independent method to measure the time courses for single and multiple-turnover reactions. The single turnover time course measured for a reaction solution initially containing 50 µM WT YdiI and 20 µM [^{14}C]-benzoyl-CoA (Figure 3.14); was fitted by simulation using to the kinetic model shown in Scheme 1. The value of k_2 was restricted to 0 s^{-1}. For the single turnover reaction, only the rates k_1, k_{-1}, k_2, and k_{-2} had an effect on the fitting. The following set of rate constants were obtained from fitting the single turnover reaction k_1 = 50-125 $\mu M^{-1}s^{-1}$, k_{-1} = 400-650 s^{-1}, k_2 = 15 - 19.5 s^{-1}, and k_{-2} = 0 s^{-1}. The value of the rate constant k_2, was in good agreement to value of the steady-state k_{cat} (18 s^{-1}).

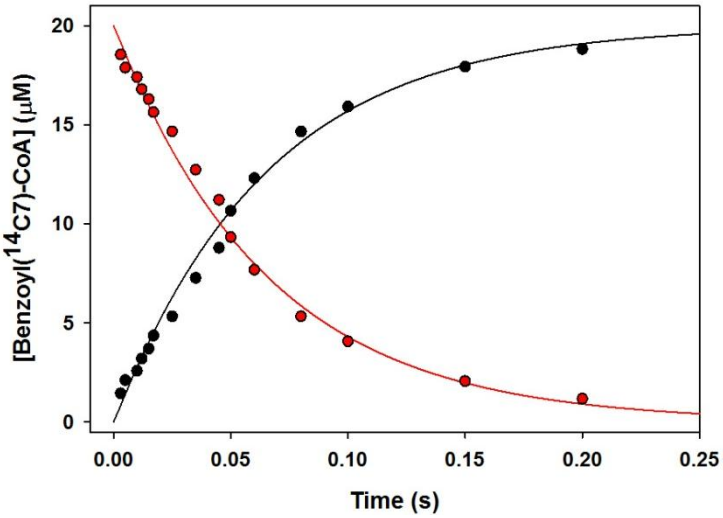

Figure 3.14: Experimental and simulated time courses for the single turnover reaction containing 50 µM wild type YdiI and 20 µM [^{14}C] benzoyl-CoA in 50 mM K^+HEPES

(pH 7.5, 25 ^{o}C). The time point data [^{14}C]-benzoyl-CoA (●) and [^{14}C]-benzoic acid (●) were calculated from the fraction of [^{14}C]-benzoyl-CoA and [^{14}C]-benzoic acid present in the acid quenched reaction. The simulated curves were generated using the kinetic model shown in Scheme 1.

The time course for the reaction of 50 µM [^{14}C]-benzoyl-CoA with 4 and 20 µM YdiI are shown in Figure 3.15. No burst phase was observed nor could the time course data be fitted by simulation using the kinetic model (Scheme 2) that incorporates the formation of a chemical intermediate prior to the rate-limiting step.

$$\mathbf{E + S} \underset{k_{-1}}{\overset{k_1}{\rightleftharpoons}} \mathbf{ES} \underset{k_{-2}}{\overset{k_2}{\rightleftharpoons}} \mathbf{EIQ} \underset{k_{-3}}{\overset{k_3}{\rightleftharpoons}} \mathbf{EPQ} \underset{k_{-4}}{\overset{k_4}{\rightleftharpoons}} \mathbf{EP} \underset{k_{-5}}{\overset{k_5}{\rightleftharpoons}} \mathbf{E + P} \quad \mathbf{Q} \qquad \textbf{(Scheme 2)}$$

Subsequently, the kinetic model was employed in curve simulation in the same manner used to simulate the single-turnover time course data. In good agreement with the rate constants defined by the single-turnover data and the steady-state kinetic data, the k_1 = 90-180 µM^{-1}s^{-1}, k_{-1} = 550-650 s^{-1}, k_2 =15.5-19 s^{-1}, the k_3 = 670-900 s^{-1}, k_{-3} = 90-130 µM^{-1}s^{-1} (k_3/k_{-3} ~ 7 µM), k_4 = 160-400 s^{-1} and k_{-4} = 3 µM^{-1}s^{-1} (k_4/k_{-4} ~ 100 µM).

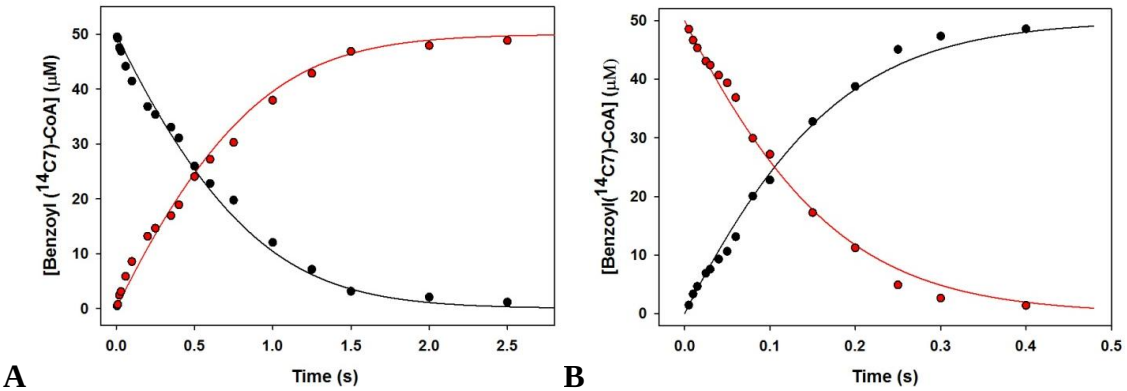

Figure 3.15: Experimental and simulated time courses for the multiple turnover reaction containing 4 μM wild type YdiI and 50 μM [^{14}C]-benzoyl-CoA (**A**) or 20 μM wild type ydiI and 50 μM [^{14}C]-benzoyl-CoA (**B**) in 50 mM K^+HEPES (pH 7.5, 25 ^{o}C). The time point data [^{14}C]-benzoyl-CoA (●) and [^{14}C] benzoic acid (●) were calculated from the fraction of [^{14}C] benzoyl-CoA and [^{14}C] benzoic acid present in the acid quenched reaction. The simulated curves were generated using the kinetic model in Scheme 1.

3.3.7 Kinetic analysis of substrate binding residues

When comparing the substrate binding pocket of YbdB to YdiI, only one significant residue change is found: YbdB Met68 vs YdiI Val68. The Met68 residue appears to protrude into the binding pocket whereas the Val68 does not. The conserved aromatic residues Phe50 and Tyr/Phe71 provide a cap to the binding pocket and in combination with the Met/Val68 residue, are posited to function in substrate discrimination. To test this proposal, site-directed mutants YbdB M68V, YdiI V68M, Y71A, and Y71A/F50A were prepared for kinetic analysis. In addition, the mutants YbdB M68V and YdiI V68M were prepared for the purpose of determining if residue swapping results in specificity exchange.

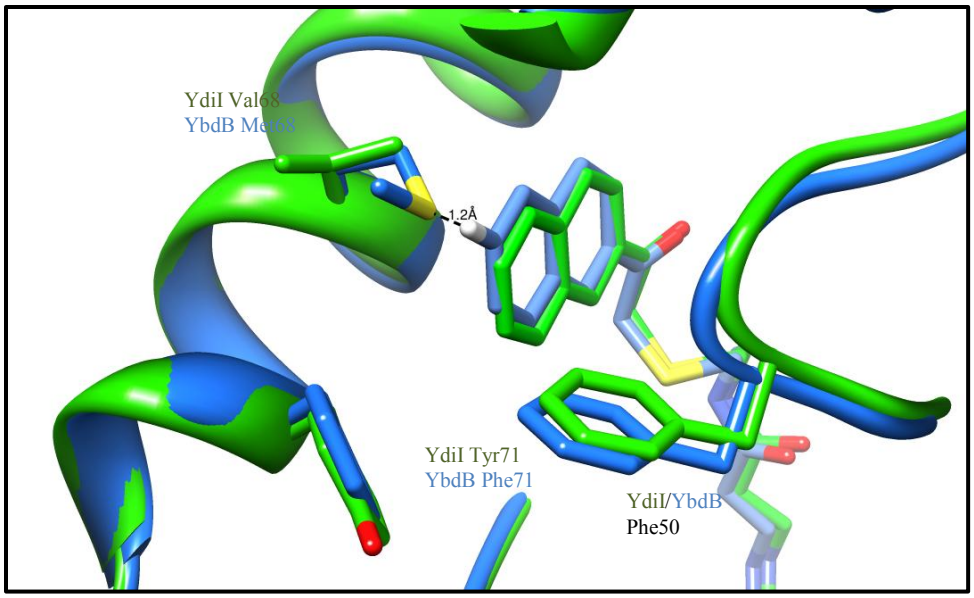

Figure 3.16: Crystal structure overlay of YdiI (green) and YbdB (blue) complexed with napthoyl-CoA. Napthoyl-CoA was modeled from the existing phenacyl-CoA substrate analog inhibitor using Chimera.

The YdiI V68M mutant displayed close to WT k_{cat}/K_m values for benzoyl-CoA, however for the substrate lauroyl-CoA the K_m was increased 10-fold suggesting that the Met68 residue does indeed protrude into the binding pocket (Table 3.3). On the other hand, the YbdB M68V mutant displayed a marginal decrease in activity towards benzoyl-CoA. However, with luaroyl-CoA serving as substrate, YbdB M68V displayed a decrease in K_m by 75% and a marginal increase in $k_{cat,}$ resulting in a 10-fold increase in k_{cat}/K_m. In addition to the changes in lauroyl-CoA turnover, the both mutants were screened against DHNA-CoA. As shown in Figure 3.16**,** the YbdB Met68 is within close proximity to the substrate napthoyl-CoA (1.2 Å). It was posited that this residue restricts the binding pocket thereby limiting YbdB's capacity to bind and turnover with DHNA-CoA. The mutant YbdB M68V did display an ~100-fold increase in k_{cat}/K_m. Although

promising, the reverse mutant YdiI V68M saw an increase in efficiency by ~ 2 fold. The essential lack of change in efficiency may be explained by the increased distance (1.8 Å) between the YdiI M68V mutant to the napthoyl substrate as compared to wild type YbdB (Figure 3.17), an unexpected possibility.

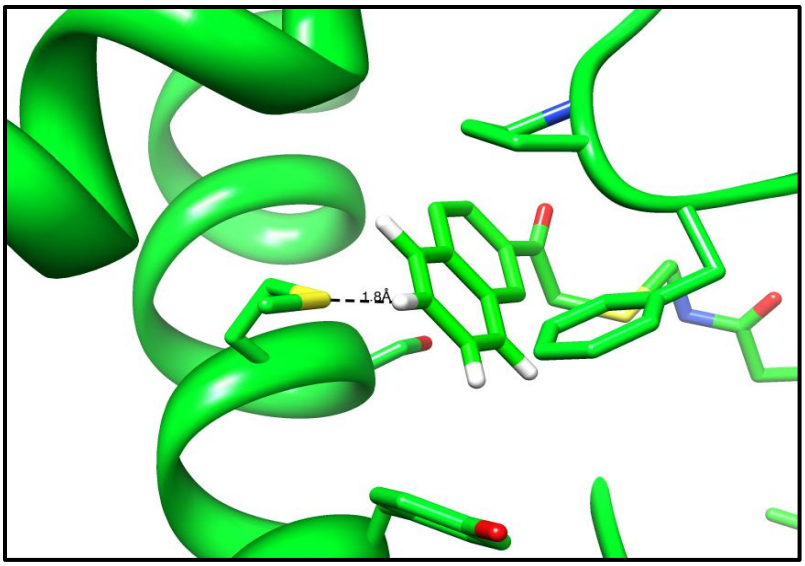

Figure 3.17: Crystal structure of the active site of the YdiI with napthoyl-CoA modeled from the existing phenacyl-CoA and the mutant V68M modeled by Chimera.

	Benzoyl-CoA		Lauroyl-CoA		DHNA-CoA	
Variant	**k_{cat} (s^{-1})**	**k_{cat}/K_M ($s^{-1}\mu M^{-1}$)**	**k_{cat} (s^{-1})**	**k_{cat}/K_M ($s^{-1}\mu M^{-1}$)**	**k_{cat} (s^{-1})**	**k_{cat}/K_M ($s^{-1}\mu M^{-1}$)**
WT YbdB	2.2 ± 0.1	1.8×10^5	$(2.81 \pm 0.03) \times 10^{-2}$	6.2×10^2	$(9.3 \pm 0.2) \times 10^{-3}$	5.8×10^2
M68V	1.75 ± 0.04	7.3×10^4	$(4.6 \pm 0.4) \times 10^{-2}$	4.5×10^3	$(1.6 \pm 0.2) \times 10^{-1}$	2.7×10^4
WT YdiI	18 ± 1	7.2×10^5	0.74 ± 0.01	3.4×10^5	1.58 ± 0.03	2.0×10^5
V68M	28 ± 1	1.0×10^6	0.77 ± 0.03	2.8×10^4	0.8 ± 0.1	4.0×10^5
Y71A	28 ± 1	4.6×10^5	0.95 ± 0.02	2.8×10^5	-	-

Table 3.3 - Steady-state kinetic constants for YbdB or YdiI binding pocket mutant catalyzed hydrolysis of benzoyl-CoA, lauroyl-CoA, or DHNA-CoA thioesters; measured using DTNB spectrophotometric assay at pH 7.5 and 25 ^oC.

Looking further into the binding pocket, the mutant YdiI Y71A demonstrated a increase in K_m by 2-fold as well as an increase in k_{cat} by approximately 1.5 fold towards benzoyl-CoA. The increase in K_m can be associated by the loss of favorable non-polar interactions and possibly the loss of the ability to pi-stack between the Tyr residue and the aromatic substrate. The increase in k_{cat} cannot be readily explained.

3.3.8 Inhibition of WT YdiI and YbdB

To gain further insight into the structural determinants of substrate recognition, the binding affinities of inert substrate analogs were measured. The binding affinities were accessed from the inhibition constants measured using steady-state kinetic techniques. The results are reported in Table 3.4. The K_i measured for the substrate

analog phenacyl-CoA is in good agreement with the K_m value measured for the substrate counterpart benzoyl-CoA. In addition there is no significant difference in the K_i values measured for YbdB and YdiI. In contrast, the K_i value measured for 2,4 dihydroxyphenacyl-CoA inhibition of ydiI is 2.5 μM vs 65 μM measured for Ybdb. The YdiI binding site is better at accommodating the ring hydroxyl groups than is that of the YbdB.

The CoASH binding affinity was evaluated by measuring its K_i value as a product inhibitor vs 4-HB-CoA. The K_i measured with YdiI (16 μM) is significantly smaller than that measured with YbdB (210 μM). This is consistent with the YdiI specialization towards a CoA thioester substrate and YbdB specialization towards a *holo*ACP domain (in EntB) thioester substrate.

	Ki (μM)	
Inhibitors	YbdB (EntH)	YdiI
2,4-dihydroxyphenacyl-CoA	65 ± 6	2.5 ± 0.2
Phenacyl-CoA	5.9 ± 0.3	7.8 ± 0.4
HS-CoA	210 ± 10	16.0 ± 1

Table 3.4. Inhibition constants for various inhibitors on YbdB or YdiI catalyzed hydrolysis of 4-Hydroxybenzoyl-CoA monitored at 310 nm and 25 ^{o}C.

Specifically, the tighter inhibition of coenzyme A on YdiI might be explained by the protein-nucleotide interactions on the surface of the protein. As shown in Figure 3.18A, the phosphate groups of the phospho-panthothene arm and the ribose phosphate appear to have favorable interactions with the surface of YdiI. However, on the surface of YbdB (Figure 3.18 B) the favorable electrostatic interactions of the nucleotide are not longer present.

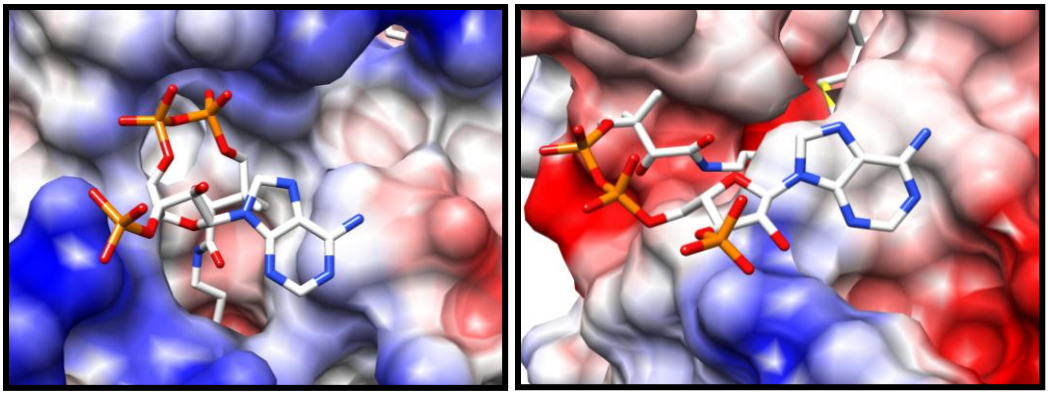

Figure 3.18 A - Surface electrostatic representation of YdiI (PDB unpublished) with the nucleotide unit of phenacyl-CoA substrate analog where blue is electropositive and red is electronegative. **B -** Surface electrostatic representation of YbdB (PDB unpublished) with the nucleotide unit of phenacyl-CoA substrate analog maintaining the same color distinguishments.

3.4 Conclusions

The *E. coli* hotdog-fold thioesterases YdiI and YbdB are an ideal system to monitor divergence from an evolutionary standpoint. The paralogs are closely related, especially amongst the fold family, having a 59% sequence identity, but have distinct physiological functions. The conservation of residues is best modeled in the active site where all catalytically active amino acids are conserved. Site direct mutagenesis on YdiI active site residues have identified Glu63, Gln48, His54 and His89 as major contributors to catalysis. The crystal structure with the phenacyl-CoA substrate analog has shown Glu63 3.8 Å from the thioester carbonyl, at the cusp of both nucleophilic and base catalysis. The remaining residues contribute to substrate activation (His54/Gln48) or to a hydrogen bonding network (His89). To determine the mode of catalysis, ^{18}O

incorporation reaction were carried out. Like the crystal structure, the mode of catalysis remains unclear due to the incorporation of both ^{16}O and ^{18}O with the latter being the majority.

Even though the ^{18}O incorporation experiment did not provide conclusive evidence towards the mode of catalysis, transient state kinetic rates were still sought after. The first attempt of elucidating the microscopic rates used stopped flow absorbance however the near A_{280} molar extinction coefficient did not allow for accurate modeling. However, the stopped flow results did provide a multiple turnover experiment that did not demonstrate "burst" kinetics. Rapid quench was used as a second more accurate attempt of determining the microscopic rate constants. Global fitting to a multiple turnover, single turnover and steady state reactions provided a reaction mechanism that does not utilize a substrate-enzyme intermediate and the following rates best describes the overall reaction; k_1 ~105 $\mu M^{-1}s^{-1}$, k_{-1} ~ 650 s^{-1}, k_2 ~ 18 s^{-1}, k_{-2} = 0 s^{-1}, k_3 ~ 700 s^{-1}, k_{-3} ~ 130 $\mu M^{-1}s^{-1}$, k_4 ~ 300 s^{-1}, and k_{-4} ~ 2 $\mu M^{-1}s^{-1}$. As expected, no single rate can best be fitted to the data, instead a range of rates fit the data within a reasonable error range.

The binding pockets of YdiI and YbdB are fairly conserved with the exception of YbdB Met68 and YdiI Val68. It was predicted that the Met68 residue restricts the binding pocket of YbdB thereby "screening" the substrates since the modeled crystal structure shows steric strain with the napthoyl-CoA substrate. This hypothesis was tested by making the YbdB M68V mutant and it's YdiI reciprocal. From the steady state analysis, the YbdB M68V mutant demonstrated an increase in efficiency with DHNA-CoA by ~ 10^2 $M^{-1}s^{-1}$. Although the YdiI V68M mutant was expected to have a similar

decrease in efficiency with the DHNA-CoA, it demonstrated no significant change. However, with lauroyl-CoA, the YdiI V68M mutant demonstrated a decrease in efficiency was ~ 10^2 $M^{-1}s^{-1}$, suggesting that the residue does play some role in substrate screening.

The fact that YdiI can distinguish between CoA substrates and protein partners (Chapter 2), led the investigation to look at CoA interactions with the protein. Inhibition experiments demonstrate the YdiI is affect much more by free CoA as compared to YbdB, by a factor of 15. This, with the protein discrimination, suggested that CoA must interact differently with YdiI and YbdB. The nucleotide of CoA does in fact interact with the surface of YdiI more favorably than with YdbB solidifying YdiI's substrate preference for acyl-CoA's.

Although very similiar, YdiI and YbdB have served as an excellent model to examine their evolutionary divergence that has led to their distinct physiological functions. Through site directed mutagensis, ^{18}O incorporation, and pre-steady state kinetic experiments, YdiI's kinetic model was elucidated. Mutagenesis of the binding pocket residues demonstrated substrate specificity with one amino acid. Lastly, YdiI discrimination against protein partners for acyl-CoA's could be explained by surface interactions.

References

1. Roberts, R. J. (2004) Identifying protein function--a call for community action., *PLoS Biology 2*, E42.

2. Pegg, S. C.-H., Brown, S. D., Ojha, S., Seffernick, J., Meng, E. C., Morris, J. H., Chang, P. J., Huang, C. C., Ferrin, T. E., and Babbitt, P. C. (2006) Leveraging enzyme structure-function relationships for functional inference and experimental design: the structure-function linkage database., *Biochemistry 45*, 2545-55.

3. Guo, Z.-F., Sun, Y., Zheng, S., and Guo, Z. (2009) Preferential hydrolysis of aberrant intermediates by the type II thioesterase in Escherichia coli nonribosomal enterobactin synthesis: substrate specificities and mutagenic studies on the active-site residues., *Biochemistry 48*, 1712-22.

4. Leduc, D., Battesti, A., and Bouveret, E. (2007) The hotdog thioesterase EntH (YbdB) plays a role in vivo in optimal enterobactin biosynthesis by interacting with the ArCP domain of EntB., *Journal of Bacteriology 189*, 7112-26.

5. Chen, D., Wu, R., Bryan, T. L., and Dunaway-Mariano, D. (2009) In vitro kinetic analysis of substrate specificity in enterobactin biosynthetic lower pathway enzymes provides insight into the biochemical function of the hot dog-fold thioesterase EntH., *Biochemistry 48*, 511-3.

6. Chen, D. (2010) Divergence of Thioesterase Function: Human BFIT2, Escherichia Coli EntH and ydiI. The University of New Mexico.

7. Merkel, S. M., Eberhard, a E., Gibson, J., and Harwood, C. S. (1989) Involvement of coenzyme A thioesters in anaerobic metabolism of 4-hydroxybenzoate by Rhodopseudomonas palustris., *Journal of Bacteriology 171*, 1-7.

8. Wu, R., and of New Mexico, T. U. (2007) Domain Movement and Substrate Recognition in 4-chlorobenzoate: Coenzyme A Ligase from Alcaligenes Sp. Strain AL3007. The University of New Mexico.

9. Song, F., Thoden, J. B., Zhuang, Z., Trujillo, M., Holden, H. M., and Dunaway-Mariano, Debra. The Catalytic Mechanism of the Hotdog-fold Enzyme Superfamily 4-Hydroxybenzoyl-CoA Thioesterase from *Arthrobacter sp*. Strain SU DB, *Unpublished*.

10. Song, F., Zhuang, Z., Finci, L., Dunaway-Mariano, D., Kniewel, R., Buglino, J. a, Solorzano, V., Wu, J., and Lima, C. D. (2006) Structure, function, and mechanism of the phenylacetate pathway hot dog-fold thioesterase PaaI., *The Journal of Biological Chemistry 281*, 11028-38.

CHAPTER FOUR
BIOLOGICAL RANGE AND DIVERGENCE OF FUNCTION IN THE HOTDOG-FOLD THIOESTERASE YDII

4.1 Introduction

In the previous chapters the structure and function of the *E. coli* hotdog-fold paralogs YbdB and YdiI were described. YbdB functions in the biosynthesis of the siderophore enterobactin (*1–3*). This biosynthetic pathway is specialized and thus found in a narrow range of bacterial species. YdiI on the other hand, functions in the menaquinone pathway, which is present in a wider range of bacteria. In this chapter I employ sequence identity and the structure determinants of YbdB and ydiI function to track orthologs.

Enzyme homologs present in different organisms and that share greater than 40% sequence identity are assumed to perform the same function. Function can be defined at the level of catalysis, i.e. substrate activities as assayed *in vitro*, as well as at the biological level, which entails the identification of the *in-vivo* substrate. The presence of two hotdog-fold thioesterases in *E. coli*, namely YbdB and YdiI, with 59% sequence identity in the is curious, especially when viewed in the context of the low pairwise sequence identities between other hotdog-fold thioesterases in this same organism. Nevertheless, YbdB and YdiI are the products of gene duplication. The linage of bacteria in which this event occurred can, in principle, be defined by the point of departure of the respective in biological ranges of *ybdB* and *ydiI*. By tracking the YbdB and YdiI orthologs I intended to define this point of departure.

Based on my analysis I show that ydiI has a wide biological range whereas ybdB is restricted to species of Enterobacteriales wherein enterobactin is synthesized. *YdiI* is present in organisms which synthesize menaquione, but remarkably, I found examples of putative YdiI orthologs in bacteria that do not synthesize menaquione. I experimentally characterized one such putative YdiI ortholog to show that it has diverged in substrate specificity to support a possible role in lipid metabolism. As with the shift in specificity documented in Chapter 2 with YbdB and ydiI, the shift in specificity between YdiI and the *Pseudomonas* homolog will be analyzed.

4.2 Methods and Materials

4.2.1 Materials

All restriction enzymes and T4 DNA ligase were purchased from Invitrogen. *Pfu Turbo* and *Deep Vent* DNA polymerases were purchased from Strategene. Oligonucleotide primers were custom-synthesized by Invitrogen. DNA sequencing was performed by the DNA Sequencing Facility of the University of New Mexico. Acetyl-CoA, benzoyl-CoA, propanoyl-CoA, hexanoyl-CoA, lauroyl-CoA, myristoyl-CoA, palmitoyl-CoA, oleoyl-CoA were purchased from Sigma. The thioester substrates 4-hydroxybenzyol-CoA, DHNA-CoA and coumaroyl-CoA were synthesized as previously reported (*1*, *3*).

4.2.2 Preparation of wild-type PA1618

The PA1618 gene was amplified by PCR using genomic DNA prepared from *P. aeruginosa* (ATCC) as template, commercial oligonucleotides as primers, and *Deep Vent*

as the polymerase. The PCR-products were digested by the restriction enzymes *NdeI* and *XhoI* and then purified by polyacrylamide gel electrophoresis. The genes were ligated to a *NdeI* and *XhoI- digested* pET-23a vector (Novagen) using T4 DNA ligase. The cloned genes were verified by DNA sequencing. The cloned plasmids were used to transform competent *E. coli* BL21(DE3) cells (Invitrogen) for gene expression. The *PA1618*/pET-23a or transformed *E. coli* BL21(DE3) cells were grown aerobically at 37 ^{o}C in LB media containing 50 µg/ml ampicillin. Production of C-terminal His_6-tagged PA1618 was induced with 0.4 mM isopropyl-β-$_D$-galactopyranoside (IPTG) once the cell density had reached $A_{600} \sim 0.6$. Following a 12 h induction period at 19 ^{o}C, the cells were harvested by centrifugation at 6,500 rpm for 10 min and then resuspended in 100 mL of 50 mM Tris buffer (pH 8.4), 50 mM imidazole, and 500 mM NaCl (Lysis Buffer). The cells were lysed using a French press at 1,200 psi and the lysate was centrifuged at 20,000 rpm for 15 min. The supernatant was loaded onto a 5 mL HisTrap FF column (GE Life Sciences) and the column was eluted at 4 ^{o}C with Lysis Buffer to remove non-tagged protein and then with 50 mM Tris (pH 8.4), 500 mM imidazole, and 500 mM NaCl (Elution Buffer) to elute the tagged protein. Column fractions were monitored by measuring solution absorbance at 280 nm and by carrying out SDS-PAGE analysis. The PA1618-containing fractions were combined and dialyzed at 4 ^{o}C against three changes of 1 L of 50 mM Tris (pH 8.4)/50 mM NaCl. Yield: 25 mg protein/g of wet cells.

4.2.3 Preparation of PA1617

The PA1617 gene was amplified by PCR using genomic DNA from *P. aeruginosa* PAO1 (ATCC), custom oligonucleotides (Invitrogen) as primers, and *Pfu*

Turbo (Stratagene) as polymerase. The PCR product was digested with *NdeI* and *BamHI* (New England Biolabs), and purified by polyacrylamide gel electrophoresis. The product was ligated into *NdeI* and *BamHI* digested pET28a vector (Novagen) using T4 ligase (New England Biolabs). The ligated product was transformed into chemically competent *E. coli* BL21 (DE3) RIPL cells (Stratagene) for gene expression. Production of the N-terminal His_6-tagged PA1617 followed the procedures described above. Yield: ~8 mg/g of wet cells.

4.2.4 PA1618 activity assays

Thioesterase activity was measured using the 5,5'-dithio-bis-(2-nitrobenzoic acid) (DTNB) coupled assay. Reactions were monitored at 412 nm ($\Delta\varepsilon$ = 13.6 $mM^{-1}\bullet cm^{-1}$) using a Beckman 640U Spectrometer. Reactions were carried out at 25 ^{o}C with 0.5 mL solutions containing 50 mM K^{+}HEPES (pH 7.5), 1 mM DNTB thioesterase and varying concentrations of thioester (0.5 – 5 x K_m). The catalyzed hydrolysis of 4-hydroxybenzoyl-CoA (4-HB-CoA) in 50 mM K^{+} HEPES (pH 7.5) was directly monitored at 300 nm ($\Delta\varepsilon$ = 11.8 $mM^{-1}cm^{-1}$).

The initial velocity data, measured as a function of substrate concentration, were analyzed using Enzyme Kinetics v 1.4 and equation 1

$$V = V_{max}[S]/([S]+K_m) \quad (1)$$

where V is initial velocity, V_{max} is maximum velocity, [S] is substrate concentration, and K_m is the Michaelis constant. The k_{cat} was calculated from $V_{max}/[E]$ where [E] is the total enzyme concentration as determined by the Bradford method.

4.2.5 PA1617 activity assays

Ligase activity was monitored by using a coupled assay. The 500 µL reactions contained varying concentrations of the carboxylic acid substrate (0.5 - 5 x K_m), 1 mM CoA, 3.5 mM ATP, 15 mM $MgCl_2$, 200 µM NADH, 2 mM PEP, 4 mM KCl, 11 U of adenylate kinase (EC 2.7.4.3), 9 U of pyruvate kinase (EC 2.7.1.40) and 9 U of lactate dehydrogenase (EC 1.1.1.27) in 50 mM K^+HEPES (25 ^oC, pH 7.5). The decrease in absorbance resulting from the oxidation of NADH was monitored at 340 nm ($\Delta\varepsilon$ = 6.2 $mM^{-1}cm^{-1}$).

The initial velocity data, measured as a function of substrate concentration, were analyzed using Enzyme Kinetics v 1.4 and equation 1

$$V = V_{max}[S]/([S]+K_m) \quad (1)$$

where V is initial velocity, V_{max} is maximum velocity, [S] is substrate concentration, and K_m is the Michaelis constant. The k_{cat} was calculated from V_{max}/[E] where [E] is the total enzyme concentration as determined by the Bradford method.

4.2.6 Bioinformatic analysis of YdiI and orthologues

Putative orthologs of *E. coli* K-12 YdiI were identified by a protein BLAST search utilizing the NCBI BLAST tool (http://blast.ncbi.nlm.nih.gov) with default parameters and the allowance of 5000 hits. Sequences were selected based on the requirement of a minimum of six of the YdiI ten specificity markers Met40, Val42, Gln48, Pro49, Phe/Tyr50, His54, Glu63, Ser/Thr64, Ser/Thr67 and His89 identified by analysis of the crystal structure (PDB ID: 1VH5) (Chapter 3). The sequences were aligned using the NCBI COBALT tool (http://www.ncbi.nlm.nih.gov/tools/cobalt) and displayed in ESPript (http://espript.ibcp.fr/ESPript/ESPript/). A phylogenetic tree was constructed using iTOL(interactive tree of life (http://itol.embl.de/)).

To determine the biological range of the menaquinone biosynthetic pathway in relationship to the biological range of YdiI, a protein BLAST search was carried out using the sequences of the *E. coli* menquinone pathway enzymes MenB and MenE as query. Species containing homologs of MenB and MenE that have sequence identities of >60% were judged to contain the menaquinone pathway. Genomes of the species with putative MenB and MenE orthologues that share 45-59% identity were further examined to determine if they possess homologs to the other *E. coli* menaquinone pathway enzymes.

4.3 Results and Discussion

4.3.1 Bioinformatic analysis of YdiI

Homologs to the E. coli YbdB (EntH) and YdiI were identified by BLAST searches using the respective amino acid sequences as query. Bacterial species that were found to possess two homologs where restricted to the order Enterobacteriales. The high pairwise sequence identities (>50%) indicated that these homologs are orthologs to the *E. coli* YbdB (EntH) and YdiI. The sequence makers for YbdB are: T64, M68, T15, F50 and F71. The Ybdb orthologs were found in the species of Escherichia, Shigella, Citrobacter, Dickeya, Klebsiella, Cronobacter, Enterobacter and Salmonella The enterobactin pathway genes were also found in these bacteria. Thus, the biological range of YbdB is restricted to those bacteria that produce the siderophore enterobactin, and is thus very small.

By comparison, the biological range of YdiI orthologs is quite large. The sequence identity among the YdiI orthologs in proteobacteria is reasonably high (>45%) and only in outside of proteobacteria where it localizes in the phylum Bacteroidetes and

more specifically in species of *Bacteroides* does it drop to 35-40%. The YdiI markers listed in the previous chapter were selected from structural analysis and sequence alignments with other known and characterized PaaI clade-like hotdog fold members. The potential catalytic residues Q48, H54, E63, and S/T64 were selected by previously reported data (*1*) and the remaining residues M40, V41, P49, F/Y50, S/T67 and H89 were selected by conservation amongst known homologues as shown in the crystal structure heat map (Figure 4.1**)** based on the multi-sequence alignment (Figure 4.2).

The range within proteobacteria is concentrated in the gama-subdivision with some respensentation in beta-subdivision (*Acidovorax species, Verminephrobacter eiseniae, Alicycliphilus denitrificans, Nitrosomonas eutropha, Variovoraz paradoxus, Polaromonas sp, Rhodoferax ferrireducens, Dechloromonas aromatic, and Comamonas testosterone*), delta-subdivision (*Pelobacter propionicus, Erythrobacter litoralis* and *Novosphingobium aromaticivorans*), and one case in Clamydiae (*Waddlia chondrophila*).

Within the gama-division of proteobacteria the representation of *ydiI* in the order of Enterobacteriales is pervasive. The YdiI orthologs accompany the YbdB orthologs in the species of *Escherichia, Shigella, Citrobacter, Dickeya, Klebsiella, Cronobacter, Enterobacter* and *Salmonella* and are represented in the order Enterobacteriales in species of *Yershina, Pantoea, Erwinia, Proteus, Pectobacterium, Edwardsiella, Serratia, Xenorahdbdus* and *Providencia*. Closely related hosts include species of *Shenwalla, Aeromonas, Psychromonas, Legionella, Marionobacter, Reinekea* and *Vibronales*.

YdiI occurrence can be tracked further within the gamma-subdivision of proteobacteria to the family Pasteurellaceae, where it is represented in species of *Pasteurella, Haemophilus, Mannheimia* and *Acintobacillus* and to the family

Pseudomonadaceae where it is represented in the genomes of the deposited species of *Pseudomonas* (*stutzeria, fluorescens, syringae, savastanol and aeruginosa*). Within the order of Vibrionaceae, only a small fraction of the deposited genomes contain the ydiI gene: *Vibrio vulnificus* and *Allivibrio salmonicida*. Within the order Xanthomonadaceae, *ydiI* appears to be pervasive. One notable species is *Xanthomonas albilineans*, which has two copies, one of which has Ala64 in place of the conserved Thr64.

Based on the comparison of the biological ranges of *ybdB* and *ydiI* it is evident that *ybdB* evolved via an ancestral *ydiI* gene duplicate within Enterobacteriales to function in the production of the siderophore enterobactin that is specific to certain species of Enterobacteriales proteobacteria. The larger biological range of *ydiI* suggests that it functions in a biochemical process that has is required by a larger range bacteria and/or that it might assume more than one type biochemical function.

Inspection of the genes that are neighbors to the *ydiI* gene in the various genomes provides clues as to its function (Figure 4.3). In Bacteroides genus, YdiI exists as a fusion protein or as a standalone protein encoded by a gene located with the menaquinone pathway gene cluster. The high catalytic efficiency towards thioester hydrolysis in the menaquinone pathway intermediate 1,4-dihydroxynapthoyl-CoA demonstrated for the *E. coli* ydiI (Chapter 2) indicates that it too functions in this role. Indeed, many but not all of the bacteria that possess *ydiI* contain genes that encode menaquinone pathway homologs indicating that YdiI is present to serve in the menaquinone pathway. The bacteria which do not produce menaquinone and hence do not contain menaquinone pathway genes, yet possess *ydiI* are of particular interest. This is the case with species of Pseudomonas and

as detailed in the following section, the function the YdiI from one such species was examined.

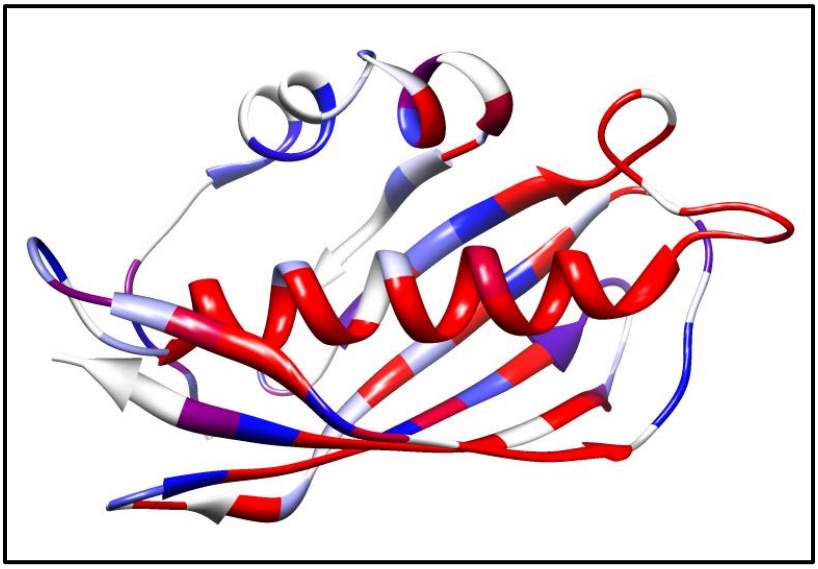

Figure 4.1: Conservation heat map of known YdiI homologues generated by Chimera. Red represents > 90% conservation.

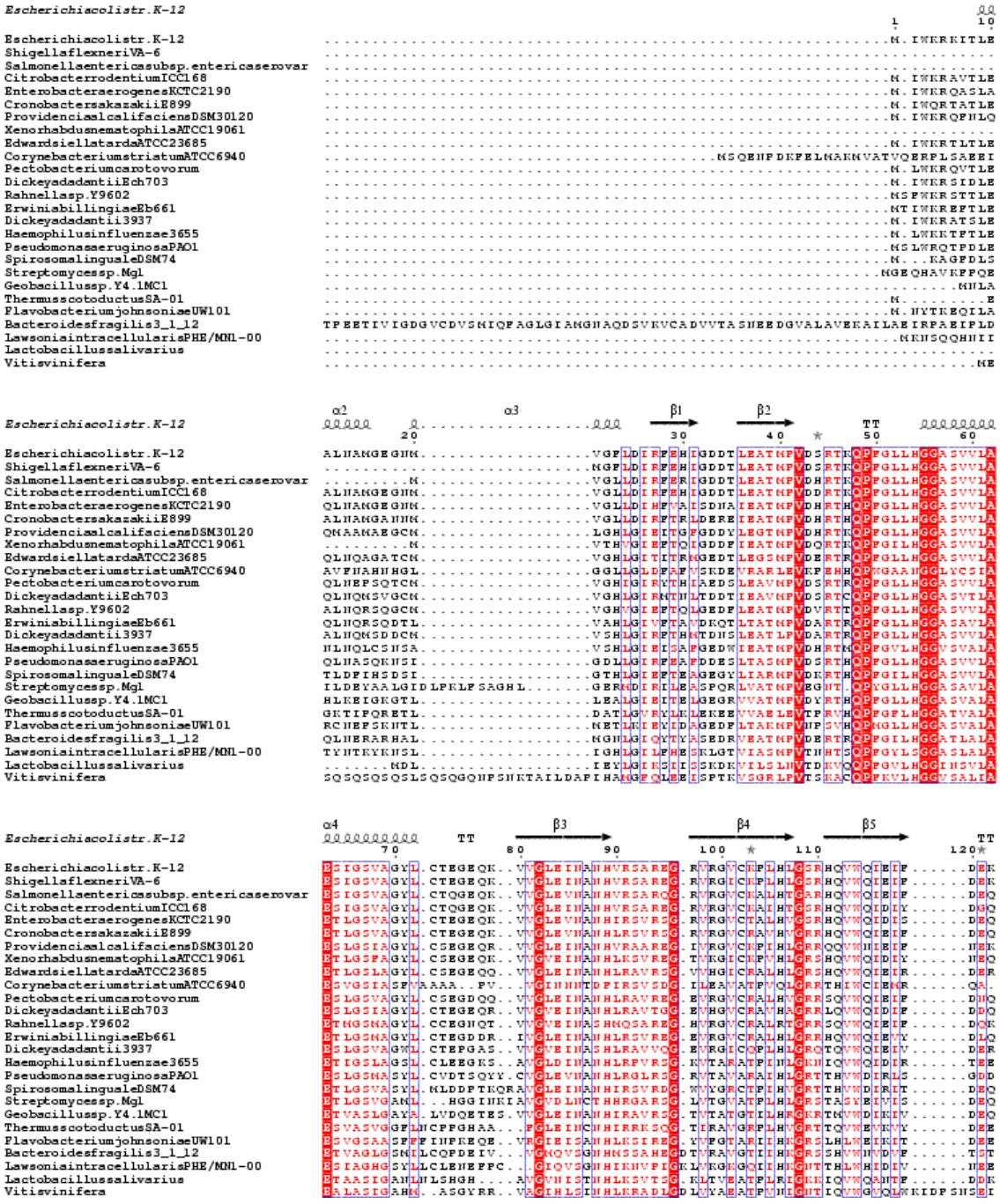

Figure 4.2: Cropped sequence (residues 1-120 of *E. coli* ydiI) alignment of 26 putative YdiI orthologues. Red background with white letters indicates complete conservation and white background red letters indicates mostly conserved residues.

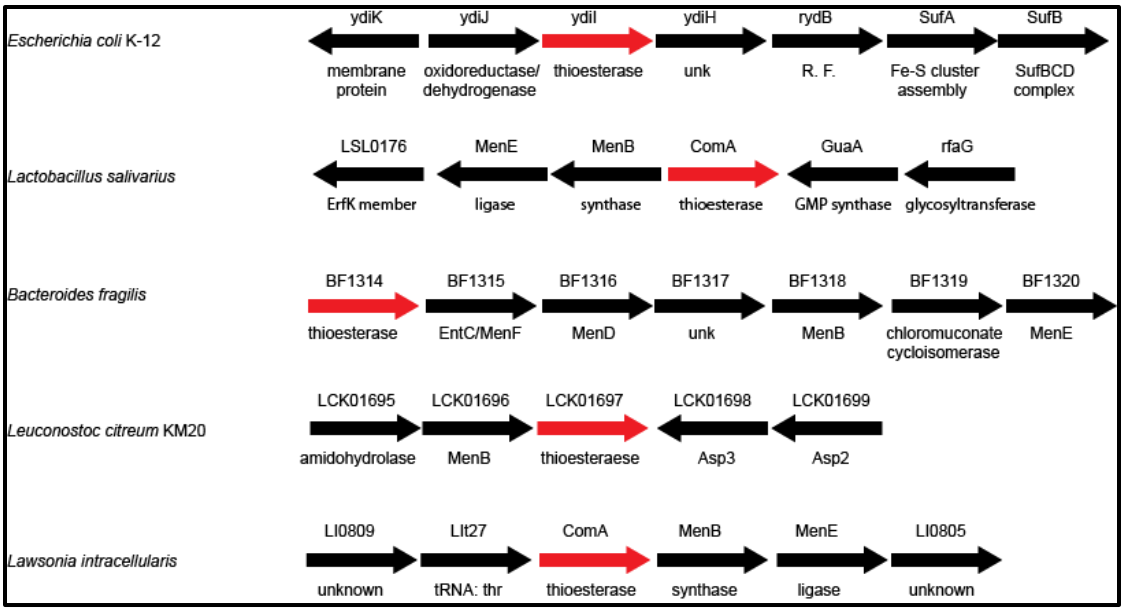

Figure 4.3: Gene map of YdiI homologues in species that contain the gene product co-localized with menaquinone pathway genes.

4.3.2 Substrate specificity profiles of the thioesterase PA1618 and ligase PA1617

This notion that YdiI could discriminate between ACP and CoA substrates was tested with an ortholog from *Pseudomonas aeruginosa*, PA1618. The ortholog PA1618 was selected because it demonstrated moderate sequence identity (52%), maintained all ten amino acid markers, and is located adjacent to a putative ligase, suggesting its partner is an acyl-/aroyl-CoA. PA1618 was subjected to the same substrate screen as EntH and YdiI, less the EntB substrate, and was in good agreement with the YdiI substrate preferences (See Table 4.1). From the screening, it appears that PA1618 prefers aroyl-CoA's with k_{cat}/K_M ranging from 10^6-10^5 $M^{-1}s^{-1}$. Additionally, like YdiI, PA1618 discriminates against the benzoyl-holo-ACP versus benzoyl-CoA by a factor of three when comparing the catalytic efficiencies. The ability of PA1618 to discriminate ACP or

CoA substrates reinforces the conclusion that the physiological substrate of YdiI is a CoA thioester.

	PA1618 Thioesterase		
Substrate	**k_{cat} (s^{-1})**	**K_M (μM)**	**k_{cat}/K_M ($M^{-1}s^{-1}$)**
Acetyl-CoA	$(4.31 \pm 0.1) \times 10^{-1}$	116 ± 8	3.7×10^3
Hexanoyl-CoA	$(1.04 \pm 0.02) \times 10^{-1}$	20 ± 2	5.2×10^3
Lauroyl-CoA	$(2.8 \pm 0.01) \times 10^{-1}$	60 ± 2	4.7×10^3
Myristoyl-CoA	$(9.1 \pm 0.2) \times 10^{-1}$	$156 \pm 34^*$	5.8×10^3
Oleoyl-CoA	$(3.9 \pm 0.2) \times 10^{-1}$	7 ± 6	1.1×10^4
Benzoyl-CoA	56 ± 1	12 ± 1	4.6×10^6
4-HB-CoA	9.3 ± 0.2	3.6 ± 0.3	3.1×10^6
1,4-DHN-CoA	$(5.5 \pm 0.5) \times 10^{-1}$	2.1 ± 0.1	2.8×10^5
Coumaroyl-CoA	2.5 ± 0.1	2.7 ± 0.2	9.3×10^5
2,4-DHB-EntB		ND	
Benzoyl-ACP	$(2.7 \pm 0.1) \times 10^{-1}$	174 ± 12	1.5×10^3

Table 4.1: Steady state kinetic parameters of PA1618 catalyzed hydrolysis of various acyl-CoA or acyl-ACP substrates monitored by direct absorbance changes or DTNB coupled reactions in 50 mM K^+HEPES at pH 7.5.

The promiscuity of PA1618 with acyl-CoA substrates provided ambiguity in proposing a physiological role. It was first hypothesized that the neighboring PA1617 ligase might synthesize a substrate for PA1618 in an analogous way that MenE synthesizes a precursor for *E. coli* YdiI. Therefore PA1617 was cloned, purified and

subjected to a modest substrate screen with various carboxylates. Considering PA1618's preference for aromatic compounds, PA1617 was first tested with benzoate and surprisingly, was inactive. The inactivity towards aromatics was confirmed with 4-hydroxybenzoate. The substrate screen was expanded to acyl-CoA's ranging from C4-C14. PA1617 demonstrated an increase in efficiency as the size of the acyl chain increased, starting at 10^2 $M^{-1}s^{-1}$ with butyrate and peaking at 10^6 $M^{-1}s^{-1}$ with laurate (See Table 4.2). Interestingly, PA1617's preference for long chain carboxylic acids conflicts with PA1618's discrimination towards long chain acyl-CoA's. In fact, PA1618 possess the Met69 (ydiI Val68 equivalent) "gate keeping" residue described in Chapter 3, suggesting that its role is to not catalyze long chain acyl-CoA's, rather to use its promiscuity to scavenge cellular CoA for PA1617.

	PA1617 Ligase		
Substrate	**k_{cat} (s^{-1})**	**K_M (μM)**	**k_{cat}/K_M ($M^{-1}s^{-1}$)**
Butyrate	1.0 ± 0.1	5800 ± 800	1.7×10^2
Hexanoate	2.3 ± 0.1	1300 ± 100	1.8×10^3
Octanoate	2.6 ± 0.1	50 ± 5	5.2×10^4
Decanoate	5.5 ± 0.15	7.2 ± 0.6	7.6×10^5
Laurate	6.1 ± 0.2	2.5 ± 0.2	2.4×10^6
Myristate	2.1 ± 0.1	2.5 ± 0.2	8.4×10^5
Benzoate	<0.0001		
4-HBA	<0.0001		

Table 4.2: Steady state kinetic constants for PA1617 ligase catalyzed reaction of carboxylate substrates with 1 mM CoA, 3.5 mM ATP, and 15 mM $MgCl_2$ in 50 mM K^+Hepes (25^oC, pH 7.5) using the coupling reactions described in Methods and Materials.

4.4 Conclusions

Through bioinformatic analysis, YdiI was tracked through Proteobacteria using known amino acid markers (Met40, Val42, Gln48, Pro49, Phe/Tyr50, His54, Glu63, Ser/Thr64, Ser/Thr67 and His89). YdiI was prevalent in the Proteobacteria phylum, concentrated in the gamma subdivision and having representation within the beta subdivision. When restricted to Enterobacteriales, bacterial species were found to possess two homologues. One homologue, YbdB is restricted to the Enterobacteriales family whereas the other homologue, YdiI, is pervasive in Proteobacteria and Bacteriodies phyla.

Inspection of gene neighbors in Bacteriodies showed YdiI within the context of the menaquinone gene cluster. The localization of ydiI in the menaquinone cluster in speicies of Bacteriodies coincides with the *E. coli* YdiI's high catalytic efficiency with DHNA-CoA as well as the gene knockout growth curves. Although YdiI was found as the DHNA-CoA thioesterase in *E. coli* and with strong evidence as the DHNA-CoA thioesterase in other bacterial species, it can also be found in bacterial species without a menaquinone pathway. This is the case in the Pseudomonadaceae family containing the species *Pseudomonas aeruginosa* where the YdiI homologue PA1618 is localized with a ligase.

The YdiI homologue PA1618 was cloned and subjected to the same substrate YdiI screening that was defined in Chapter 2. PA1618 maintained a high affinity towards aryl-CoA's, yet discriminated against long chain acyl-CoA's. PA1618 contains the gatekeeping residue Met69 described in Chapter 3, which could lead to PA1618's substrate specificity. To help determine the physiological role of PA1618, the neighboring ligase PA1617 was cloned and subjected to a modest substrate screen. Interestingly, PA1617 was found to favor long chain acyl-CoA's, in direct conflict of PA1618's discrimination towards the same substrates. Considering the evidence found here, PA1618 serves as CoA scavenger for PA1617.

References

1. Guo, Z.-F., Sun, Y., Zheng, S., and Guo, Z. (2009) Preferential hydrolysis of aberrant intermediates by the type II thioesterase in Escherichia coli nonribosomal enterobactin synthesis: substrate specificities and mutagenic studies on the active-site residues., *Biochemistry 48*, 1712-22.

2. Chen, D., Wu, R., Bryan, T. L., and Dunaway-Mariano, D. (2009) In vitro kinetic analysis of substrate specificity in enterobactin biosynthetic lower pathway enzymes provides insight into the biochemical function of the hot dog-fold thioesterase EntH., *Biochemistry 48*, 511-3.

3. Leduc, D., Battesti, A., and Bouveret, E. (2007) The hotdog thioesterase EntH (YbdB) plays a role in vivo in optimal enterobactin biosynthesis by interacting with the ArCP domain of EntB., *Journal of Bacteriology 189*, 7112-26.

CHAPTER FIVE
ANALYSIS OF THE PROTEIN-PROTEIN INTERACTIONS BETWEEN *ESCHERICHIA COLI* YBGC THIOESTERASE AND ACYL CARRIER PROTEIN

5.1 Introduction

The *Escherichia coli* hotdog-fold thioesterase YbgC is a 15.6 kDa homolog (21% sequence identity) of the 4-hydroxybenzoyl-CoA thioesterase from *Pseudomonas* sp strain CBS3 (*Ps.* 4HBT). The YbgC thioesterase is encoded by the first ORF of the *tol-pal* gene cluster found in most bacteria belonging to the α, β, and γ subdivision of Proteobacteria. Although the proteins encoded by the *tol-pal* operon have been extensively studied, how they function as a system remains unclear. Recently, it has been suggested that these proteins form a subcomplex of the cell division apparatus. This complex makes a transient *trans*-envelope connection at or near the septal ring and draws the outer membrane onto the enclosing inner membrane and peptidoglycan layers during constriction (*1*). *YbgC* is co-transcribed with the *tol-pal* genes however, whereas knockouts of each of the *tol-pal* operon genes result in a distinct phenotype the *E. coli* YbgC$^-$ does not (*2*). The role, if any that YbgC might play in relationship to the Tol-pal protein complex is not known.

The *E. coli* YbgC has been shown through tandem affinity purification, to interact with the *E. coli* acyl carrier protein (ACP) involved in fatty acid synthesis (*2*). Moreover, the same study showed that YbgC also co-purifies with the phospholipid synthesis proteins PlsB and PssA. Notably, PlsB is a *sn*-glycerol-3-phosphate acyltransferase that utilizes acyl-ACP as a substrate. ACP, encoded by the *E. coli* gene *acpP*, is a small (8.5

kDa) acidic protein that that serves as a fatty acid carrier for fatty acid synthesis and delivery (*3*). The residue Ser36 is modified post translationally to accommodate phosphopantatheine which serves as the thiol in thioester linkages of acyl-thioesters. The acyl-*holo*ACP serves as the thioester substrate for the fatty acid synthase. If YbgC functions in membrane synthesis/remodeling via a role that it might play in lipid metabolism, a possible connection between it and the tol-pal proteins might exist.

Recombinant *Haemophilus influenzae* YbgC has been reported to have thioesterase activity (*4*). However, although fatty acyl-CoA thioesters (C12 and C20) were tested activity was observed only with the short chain acyl-CoA thioesters propionyl-CoA and isobutyryl-CoA. In addition, the catalytic efficiency observed was atypically low (k_{cat} = 0.2-0.5 s^{-1}, K_m = 10-20 mM, $k_{cat}/K_m \sim 1 \times 10^3$ M^{-1} s^{-1}) suggesting that the physiological substrate had not been found (*4*). More recently, the thioesterase activity of recombinant *Helicobacter pylori* YbgC was reported (*5*). In this case, the short chain acyl-CoA thioesters (C2-C4) were not substrate active and the long chain acyl-CoA thioesters (C8-C18) were. However, once again the catalytic efficiency was too low to be considered physiologically significant (k_{cat} = 0.001-0.05 s^{-1}, K_m = 40-600 µM, $k_{cat}/K_m \sim 1 \times 10^2$ M^{-1} s^{-1}).

The *H. influenza, H. pylori* and *E. coli* YbgC genes conserve the *tol-pal* gene context and the protein products share significant sequence identity (53% and 37% pairwise identity with the *E. coli* YbgC, respectively), which includes the DTD motif that is found in the homolog 4-hydroxbenzoyl-CoA from *Pseudomomas* sp strain CBS3 (*Ps* 4HBT) (Figure 4.1). The *Ps* 4HBT catalytic Asp17 is contained in this motif.

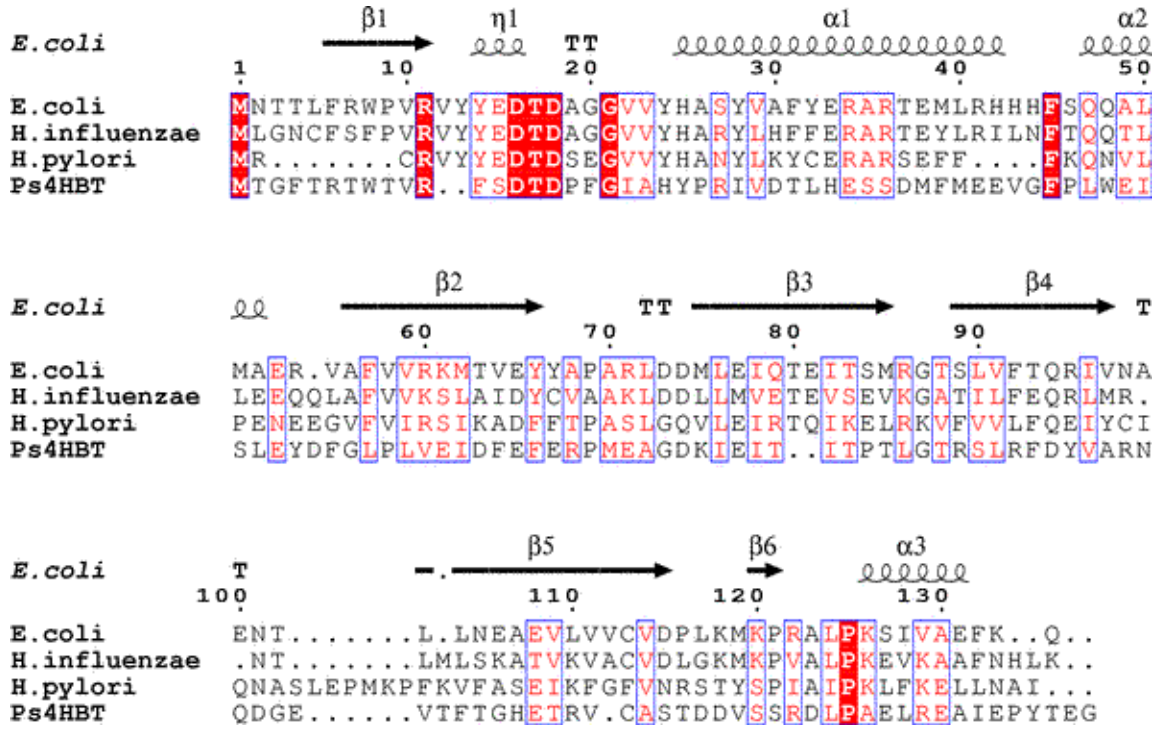

Figure 5.1: The sequence alignment of YbgC from *E. coli*, *H. influenzae*, and *Helicobacter pylori* and the *Pseudomonas sp.* strain CBS3 4-hydroxybenzoyl-CoA thioesterase generated by Cobalt and displayed in ESPript 2.2 (www.http://espript.ibcp.fr/ESPript/ESPript/index.php). Conserved residues are shown with white font against a red background and similar residues are shown in red font against a white background.

The crystal structure of *E. coli apo*-YbgC has been solved (PDB ID: 1S5U). It shows a conserved *Ps* 4HBT fold and conservation of the active site residue Asp17. However, unlike the *Ps* 4HBT, the YbgC has a solvent exposed substrate binding pocket (Figure 5.2 A). The active site should be able easily accommodate the long tails of fatty acyl-CoA thioesters. The X-ray crystal structure of *Helicobacter pylori apo*-YbgC (37%

identity to *E. coli* YbgC) has also been reported (PDB ID: 1VH5) (*5*) and it too shows a large solvent exposed active site. (Figure 5.2 B).

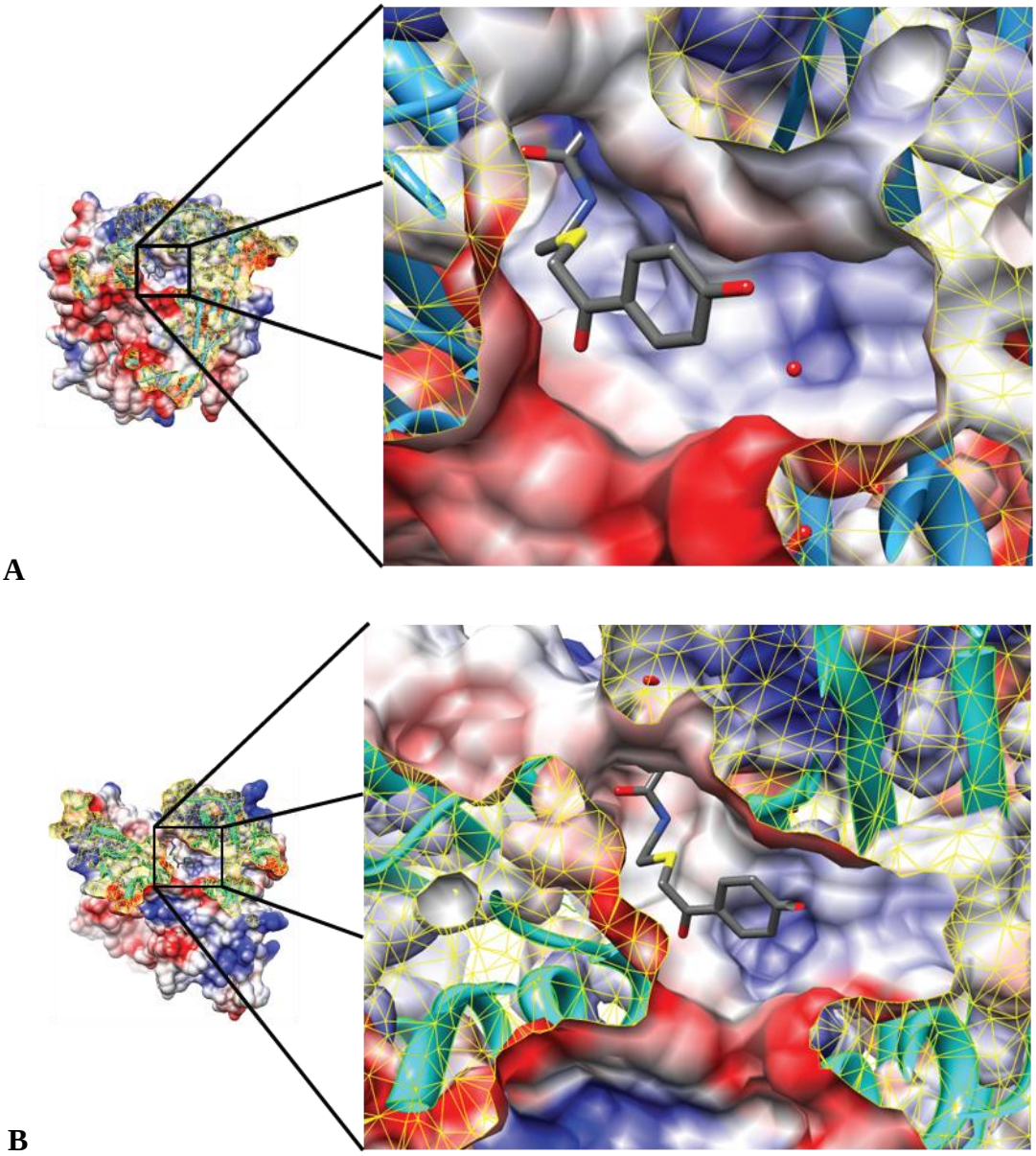

Figure 5.2: (**A) -** The *E. coli* YbgC binding pocket and (**B**) the *H. pylori* YbgC binding pocket cutaways generated by Chimera with 4-hydroxyphenacyl-CoA modeled from the superimposed structure of the *Pseudomonas sp.* strain CBS3(4-hydroxyphenacyl-CoA) complex.

The TAP experiment showing YbgC-ACP interactions has served as a starting point for my approach to a functional assignment to the *E. coli* YbgC. In this chapter I report and interpret the results from kinetic and structure-based probes of YbgC-ACP binding as well as from steady-state kinetic based substrate specificity analysis.

5.2 Materials and Method

5.2.1 Materials

All restriction enzymes and T4 DNA ligase were purchased from New England Biolabs. *Pfu Turbo* DNA polymerase was purchased from Strategene. Oligonucleotide primers were custom-synthesized by Invitrogen. DNA sequencing was performed by the DNA Sequencing Facility of the University of New Mexico. All chemicals were purchased from Sigma. The synthesis of β-ketopropanone-CoA from 1-chloro-2-propanone and coenzyme A was carried out according to published procedures. (*6*) *H. influenzea* YbgC was purified as previously described (*4*).

5.2.2 *E. coli* ybgC gene cloning and expression and protein purification

The wild-type *ybgC* gene was amplified via a PCR-based strategy using genomic DNA prepared from *E. coli* strain K-12 (ATCC) as template, commercial oligonucleotides as primers and *Pfu Turbo* as DNA polymerase. The PCR-products were digested by the restriction enzymes *NdeI* and *XhoI* and then purified by gel chromatography followed by T4 DNA ligase-catalyzed ligation to the pET-28a vector (Novagen) digested with *NdeI* and *XhoI*. The sequence of the cloned gene was verified by DNA sequencing. The clone was transformed into competent *E. coli* BL21(DE3) cells

(Invitrogen) for protein expression. The *ybgC*/pET-28a transformed *E. coli* BL21(DE3) cells were grown aerobically at 37 ^{o}C in LB media containing 100 µg/mL kanamycin. Production of the YbgC protein was induced at 19 ^{o}C with 0.4 mM isopropyl-β-D-galactopyranoside (IPTG) once the cell density reached A_{600} ~0.6. Following a 12 h induction period, the cells were harvested by centrifugation at 6,500 rpm for 10 min and then resuspended in 100 mL of 50 mM K^{+}HEPES buffer (pH 7.5), 50 mM imidazole, and 500 mM NaCl (Lysis Buffer). The cells were lysed using a French press at 1,200 psi and the lysate was centrifuged at 20,000 rpm for 15 min. The supernatant was purified by FPLC (AKTA) using a 5 mL HisTrap FF column (GE Life Sciences). The column was loaded with the clarified supernatant and was washed with Lysis Buffer at 4 ^{o}C to remove unbound protein and then with 50 mM K^{+}HEPES (pH 7.5), 500 mM imidazole, and 500 mM NaCl (Elution Buffer) to elute the tagged protein. Column fractions were monitored by their measuring absorbance at 280 nm and by carrying out SDS-PAGE analysis. The YbgC-containing fractions were combined and dialyzed three times against 1 L 50 mM K^{+}HEPES (pH 7.5) and 50 mM NaCl. Yield: ~ 15 mg/g of wet cells.

5.2.3 Steady-state kinetic constant determination

Thioesterase activity was measured using the 5,5'-dithio-bis-(2-nitrobenzoic acid) (DTNB) coupled assay. Reactions were monitored at 412 nm ($\Delta\varepsilon$ = 13.6 $mM^{-1}\bullet cm^{-1}$) using a Beckman 640U Spectrometer. Reactions were carried out in 50 mM K^{+}HEPES and 1 mM DTNB (pH 7.5, 25 ^{o}C) containing YbgC and varying concentrations of thioester (0.5 – 3 x K_m) in a total volume of 500 µL. For all measurements, the initial

velocity data, measured as a function of substrate concentration, were analyzed using Enzyme Kinetics v 1.4 and equation (1):

$$V = V_{max}[S]/([S]+K_m) \quad (1)$$

where V is initial velocity, V_{max} is maximum velocity, [S] is substrate concentration, and K_m is the Michaelis constant. The k_{cat} was calculated from $V_{max}/[E]$ where [E] is the total enzyme concentration as determined by the Bradford method.

5.2.4 Synthesis of acyl-*holo*ACP

Acetyl-, isobutyryl-, hexanoyl-, octanoyl-, myristoyl-, and β-ketopropanone-*holo*-ACP were synthesized using the *E.* coli strain DK574 *apo*ACP as the ACP unit. The *E.* coli strain DK574, genetically engineered to produce *apo*ACP (UniProt accession P0A6A8) (*7*) was a kind gift from Dr. John Cronan. *Apo*ACP was purified according to the published procedure (*7*) with slight modification. In brief, a 2 L mixture of LB broth containing 10 mL of starter culture, 15 µg/mL kanamycin, 50 µg/mL streptomycin and 10 µg/mL chloramphenicol was incubated with shaking at 23 ^{o}C to a cell density of A_{600} ~ 0.6, and then induced with 0.4 mM IPTG for ~15 h. The cells were harvested by centrifugation at 6500 rpm for 10 min. The cell pellet was suspended in 50 mM Tris-HCl pH 8.8, 25 mM $MgCl_2$, 1 mM DTT, 0.2 mM $MnCl_2$ and passed through a French press at 1200 PSIG. The lysate was centrifuged at 20,000 rpm for 20 min and the supernatant was decanted and then incubated at 37 ^{o}C for 2 h. The solution was dialyzed 3 times at 4 ^{o}C, for 1 h each in 1 L of K^+MES (pH 6.1). An equal volume of ice-cold isopropanol was added to the dialyzed solution with stirring for 1 h at 4 ^{o}C. The mixture was centrifuged at 20,000 rpm for 20 min. The *apo*ACP was purified from the supernatant by FPLC (AKTA) using a DEAE column (10 mL) equilibrated with 50 mM K^+MES (pH 6.1). The

column was washed with 5 void volumes of the equilibration buffer, followed by elution with a linear gradient of 0-0.5 M NaCl in the same buffer. The *apo*ACP eluted at ~ 0.4 M NaCl. The protein was dialyzed as previously described and then concentrated to ~10 mg/mL using 3500 MWCO centrifuge columns (Millipore). The concentration of the *apo*ACP was determined using the bicinchoninic acid (BCA) protein assay kit method (Sigma).

The acyl-*holo*ACP was prepared by incubating a reaction mixture (3-5 mL) initially containing 350 μM *apo*ACP, 400 μM acyl-CoA and 30 μL (18 mg/mL) BF1558 (*8*), 50 mM K^+HEPES (pH 7.5) and 5 mM $MgCl_2$ at 23 ^oC for 30 min. The resulting solution containing the acylated ACP was subjected to buffer exchange by FPLC (AKTA) using a HiPrep 16/60 Sephacryl S-200 HR (GE Life Sciences) size exclusion column and the previously described dialysis buffer. The acyl-*holo*ACP eluted at 75 mL and was concentrated to 1 mM using a 3,500 MWCO spin column (Millipore). The complete conversion of *apo*-ACP to acyl-*holo*ACP was confirmed by electrospray mass spectrometry (UNM Mass Spectrometry Facility). The molecular mass determinations by TOF-ESI-MS are as follows (calculated; observed): *apo*ACP (8507 Da; 8507.9 Da); acetyl-*holo*ACP (8890 Da, 8890 Da); β-ketopropanone-*holo*ACP (8904 Da, 8903.6 Da); isobutyryl-*holo*ACP (8918 Da, 8918.1 Da); hexanoyl-*holo*ACP (8946 Da, 9846.1 Da); octanoyl-*holo*ACP (8974 Da, 8974.1 Da); lauroyl-*holo*ACP (9030 Da, 9030.4 Da); myristoyl-*holo*ACP (9058 Da, 9058.1 Da) and palmitoyl-*holo*ACP: (9086 Da, 9086.6Da). The product of thioester hydrolysis is *holo*ACP (8847 Da).

5.2.5 Inhibition of YbgC-catalyzed hydrolysis of isobutyryl-CoA

Reactions were monitored using a continuous spectrophotometric assay. For β-ketopropanone-*holo*ACP, β-ketopropanoyl-CoA, and *apo*-ACP inhibition, YbgC catalyzed hydrolysis of isobutyryl-CoA was monitored using the DTNB assay as described above. The assay solution contained enzyme, varying concentrations of the substrate isobutyryl-CoA, and varying concentrations of inhibitor (0, 10, and 20 μM for β-ketopropanone-*holo*ACP; 0, 250 and 500 μM for *apo*-ACP; 0, 100, and 200 μM for β-ketopropanoyl-CoA). The inhibition constant K_i was obtained by fitting the initial rates to equation (2):

$$V = V_{max}[S]/[K_m (1+[I]/K_i) + [S]] \quad (2)$$

Where [I] = concentration of inhibitor and K_i = inhibition constant.

5.2.6 Small angle X-ray scattering analysis of the ybgC-β-ketopropanone-*holo*ACP complex

The YbgC and β-ketopropanone-*holo*ACP samples used for all SAXS experiments were frozen and shipped individually to the work site. The YbgC-β-ketopropanone-*holo*ACP complex was concentrated to 5 mg/mL at 4 ^{o}C. Synchrotron radiation X-ray scattering data were collected using the standard procedures on the X9 beamline at Brookhaven National Labs National Synchrotron Light Source. SAXS data were collected on a MarcCCD 165 located 3.4 m distance from the sample while simultaneously WAXS data were collected using a Photonic Science CCD located at 0.47 m from the sample. A 20 μL volume of sample was continuously pushed through a 1 mm diameter capillary for 30 s of measurement time and exposed to a 400 x 200 μm X-ray beam. Data collections were performed in triplicate. Beam intensity normalization, buffer subtraction and merging of data were carried out using PRIMUS (*9*). PRIMUS was also used to calculate a Guinier approximation, were a plot of ln[I(q)] and q^2 is

linear, as well as to calculate a radius of gyration (R_g) and distribution of distances. GNOM was used to generate a pair distribution function $|P(r)|$, maximum particle distribution (D_{max}), and an OUT file (*9*). DAMMIN and PDB2VOL were used to generate the low resolution solution structure employing the parameters defined in the OUT file (*10*, *11*). FOXS was used to generate the theoretical SAXS data of the YbgC- β-ketopropanone-*holo*ACP complex (*12*).

5.3 Results and Discussion

5.3.1 Preparation of acyl-*holo*ACP

In order to determine the specificity of YbgC towards acyl-*holo*ACP substrates, a robust method for synthesis was needed. The method previously used for the preparation of benzoyl-*holo*ACP (reported in Chapter 2) involved chemical reaction of *holo*ACP with an N-acyl-imidazole precursor. Because of the trichloroacetic acid induced ACP precipitation steps required and the limited solubility of the long chain N-acyl-imidazole precursors this method was deemed unsuitable. The synthetic method arrived at employed *apo*ACP in reaction with acyl-CoA catalyzed by the promiscuous pantetheinyl-phosphate transferase BF1558 previously characterized in our laboratory (*11*). The *apo*ACP was prepared in concentrations of >10 mg/mL by modification of the original procedure reported by Cronan *et al.* (*7*). The *apo*ACP was characterized by SDS-PAGE analysis (Figure 5.3**)** and by time of flight-electrospray ionization-mass spectrometry (TOF-ESI-MS) (Figure 5.4 A). The odd chromatographic behavior apoACP on the SDS-PAGE gel has been noted by others (*3*, *13*).

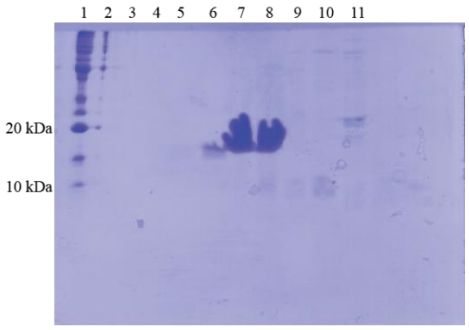

Figure 5.3: SDS-PAGE gel analysis of the *apo*ACP containing fractions pictured in the gel stained with Coomassie blue dye. Lane 1 shows the Invitrogen Benchmark protein ladder. Lanes 6-8 show DEAE fractions containing *apo*ACP.

The BF1558-catalyzed reaction between the apoACP and the acyl-CoAs was carried out at temperature. Within 1 h the reaction with the short-to-medium chain acyl-CoAs reached completion as demonstrated by TOF-ESI-MS (Figures 5.4 B-F). The myristoyl-*holo*ACP and lauroyl-*holo*ACP were also easily formed but in the case of palmitoyl-*holo*ACP limited solubility required greater dilution as precipitation occurred. (Figures 5.4 G and I).

A

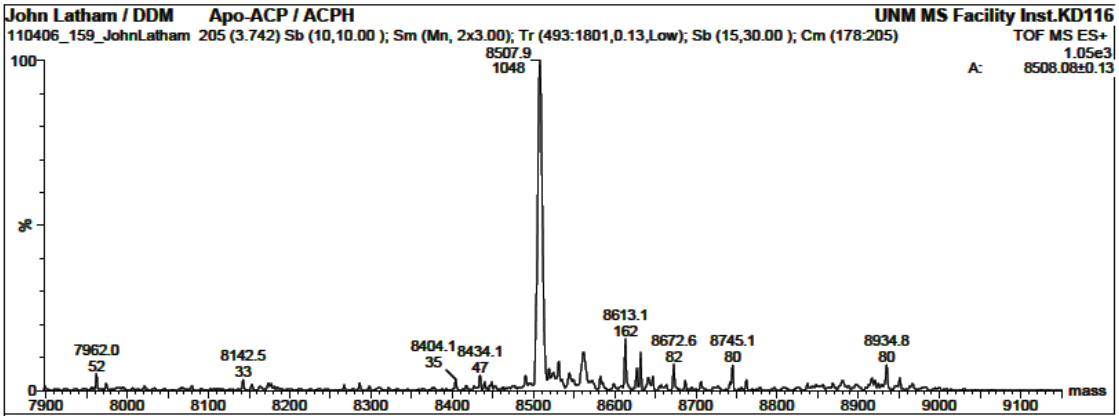

B

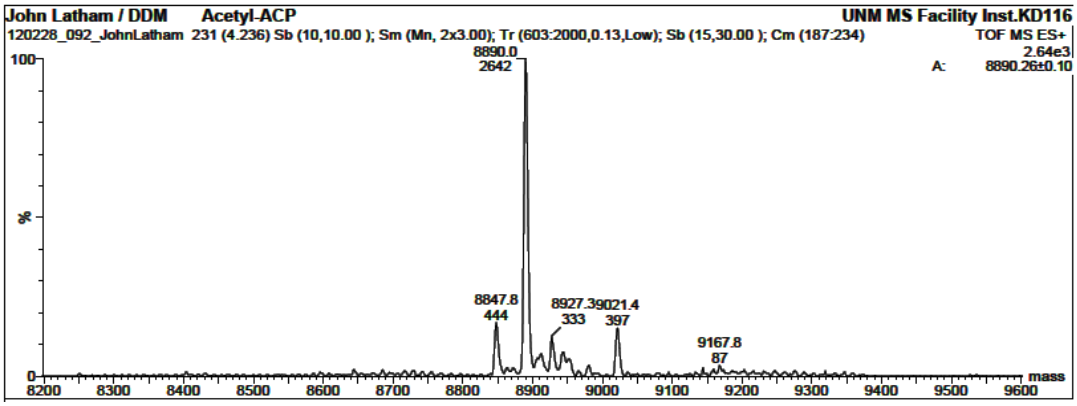
John Latham / DDM Acetyl-ACP
UNM MS Facility Inst.KD116
120228_092_JohnLatham 231 (4.236) Sb (10,10.00); Sm (Mn, 2x3.00); Tr (603:2000,0.13,Low); Sb (15,30.00); Cm (187:234)
TOF MS ES+
2.64e3
A: 8890.26±0.10
8890.0
2642
8847.8
444
8927.3
333
9021.4
397
9167.8
87
%
mass

C

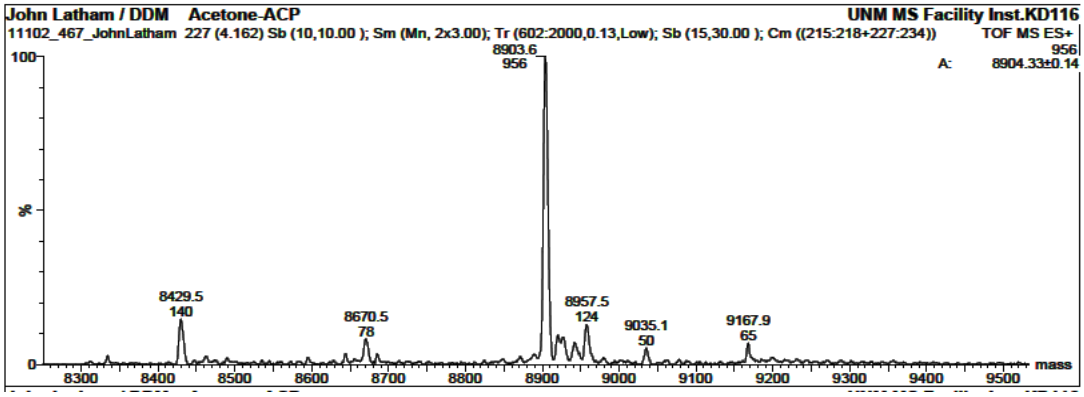
John Latham / DDM Acetone-ACP
UNM MS Facility Inst.KD116
11102_467_JohnLatham 227 (4.162) Sb (10,10.00); Sm (Mn, 2x3.00); Tr (602:2000,0.13,Low); Sb (15,30.00); Cm ((215:218+227:234))
TOF MS ES+
956
A: 8904.33±0.14
8903.6
956
8429.5
140
8670.5
78
8957.5
124
9035.1
50
9167.9
65
%
mass

D

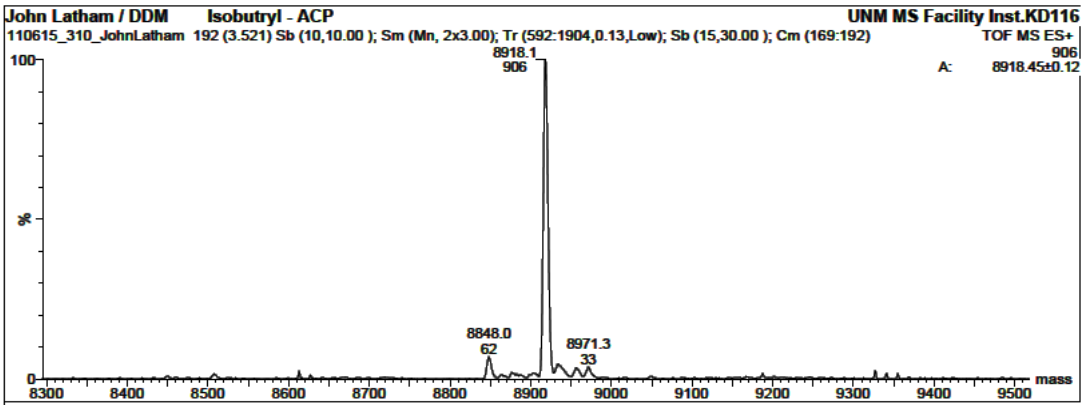
John Latham / DDM Isobutryl - ACP
UNM MS Facility Inst.KD116
110615_310_JohnLatham 192 (3.521) Sb (10,10.00); Sm (Mn, 2x3.00); Tr (592:1904,0.13,Low); Sb (15,30.00); Cm (169:192)
TOF MS ES+
906
A: 8918.45±0.12
8918.1
906
8848.0
62
8971.3
33
%
mass

E

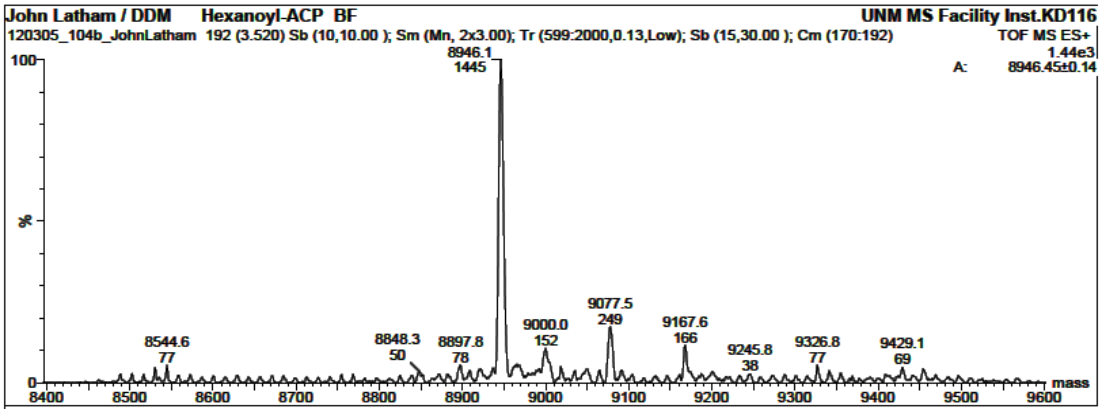
John Latham / DDM Hexanoyl-ACP BF
UNM MS Facility Inst.KD116
120305_104b_JohnLatham 192 (3.520) Sb (10,10.00); Sm (Mn, 2x3.00); Tr (599:2000,0.13,Low); Sb (15,30.00); Cm (170:192)
TOF MS ES+
1.44e3
A: 8946.45±0.14
8946.1
1445
9077.5
249
9000.0
152
9167.6
166
8544.6
77
8848.3
50
8897.8
78
9245.8
38
9326.8
77
9429.1
69
%
mass

F

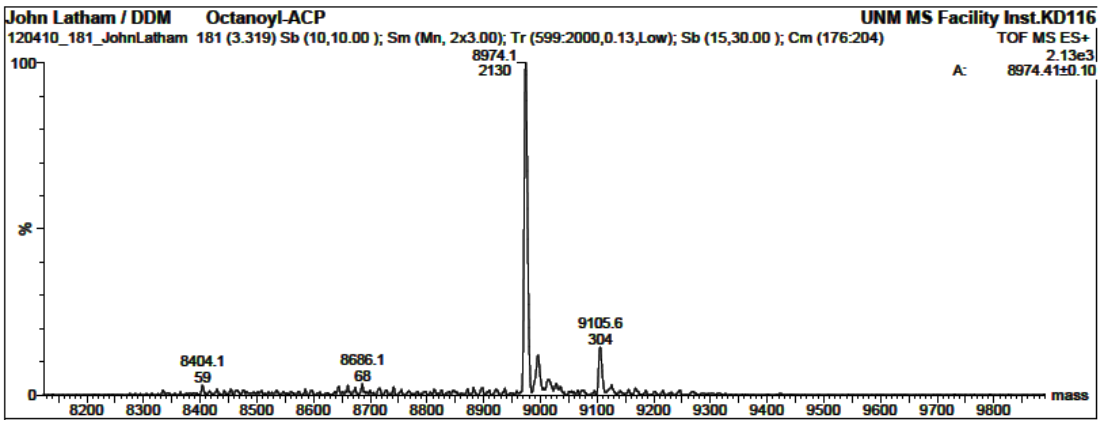
John Latham / DDM Octanoyl-ACP
UNM MS Facility Inst.KD116
120410_181_JohnLatham 181 (3.319) Sb (10,10.00); Sm (Mn, 2x3.00); Tr (599:2000,0.13,Low); Sb (15,30.00); Cm (176:204)
TOF MS ES+
2.13e3
A: 8974.41±0.10
8974.1
2130
9105.6
304
8404.1
59
8686.1
68
%
mass

G

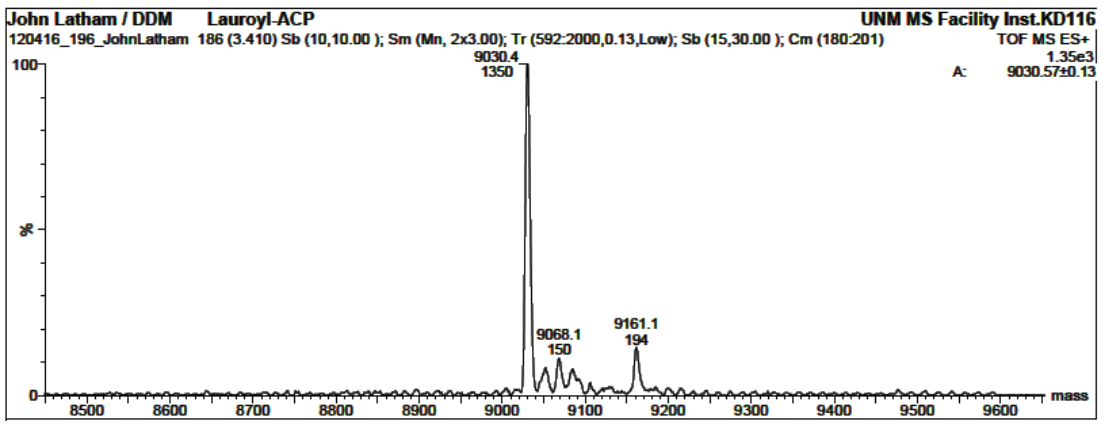
John Latham / DDM Lauroyl-ACP
UNM MS Facility Inst.KD116
120416_196_JohnLatham 186 (3.410) Sb (10,10.00); Sm (Mn, 2x3.00); Tr (592:2000,0.13,Low); Sb (15,30.00); Cm (180:201)
TOF MS ES+
1.35e3
A: 9030.57±0.13
9030.4
1350
9068.1
150
9161.1
194
%
mass

H

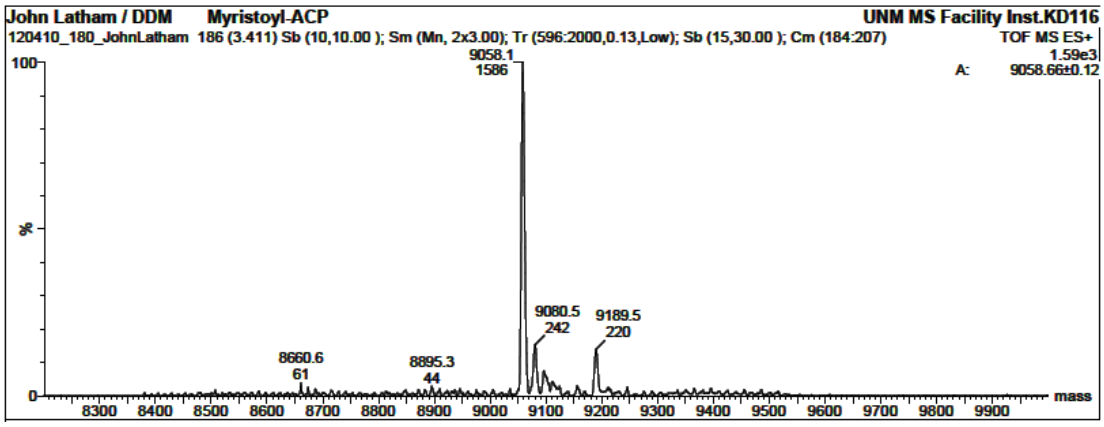

I

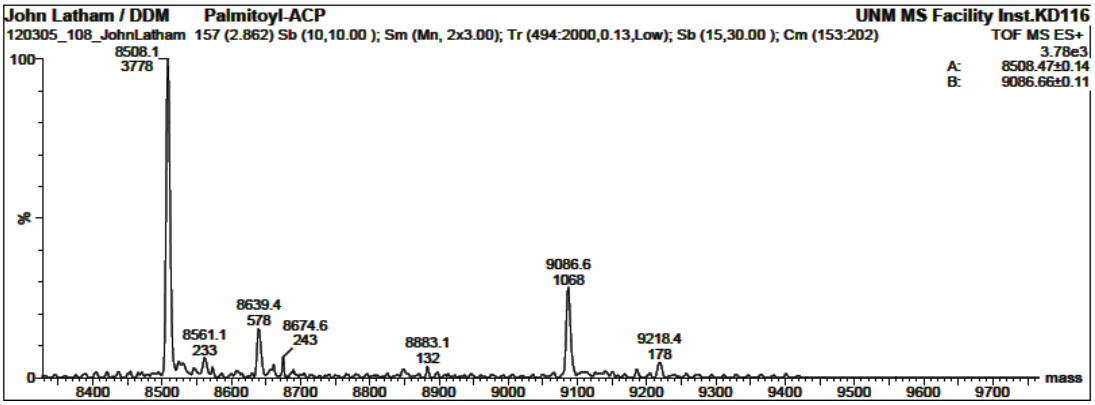

Figure 5.4: Exact molecular weight determination by TOF-ESI-MS of **A**- *apo*ACP (predicted MW = 8507 Da), **B-** acetyl-*holo*ACP (predicted MW = 8890 Da), **C**- β-ketopropanone-*holo*ACP (predicted MW = 8902 Da), **D** - isobutyryl-*holo*ACP (predicted MW = 8917 Da), **E** - hexanoyl-*holo*ACP (predicted MW = 8945 Da), **F** - octanoyl-*holo*ACP (predicted MW = 8974 Da), **G** - lauroyl-*holo*ACP (predicted MW = 9031 Da) **H** - myristoyl-*holo*ACP (predicted MW = 9059 Da) and **I** - palmitoyl-*holo*ACP (predicted MW = 9085 Da). The product of thioester hydrolysis is *holo*ACP (predicted MW = 8847 Da).

5.3.2 Substrate specificity of *E. coli* YbgC

The steady-state kinetic constants k_{cat} and K_m for *E. coli* YbgC-catalyzed hydrolysis of acyl-CoA and acyl-*holo*ACP thioesters were measured as a function of the length of the acyl group (C4-C14). The results are reported in (Table 5.1). The largest k_{cat} values (~1 s^{-1}) were observed for the short chain (C3-C4) acyl-CoA thioesters. In the case of the acyl-*holo*ACP thioesters, the largest k_{cat} (0.4 s^{-1}) was observed for catalyzed hydrolysis of the isobutyryl-*holo*ACP. Overall, the range of the k_{cat} values measured for the panel of thioesters is only ~10-fold. In contrast, the K_m value showed great variation. In case of the acyl-CoA thioester series, the K_m ranged from 10 mM (acetyl-CoA) to 5 μM (myristoyl-CoA). The general trend observed is the longer the acyl chain the smaller the K_m. The k_{cat}/K_m values measured for lauroyl-CoA and myristoyl-CoA (~1 x10^4 M^{-1} s^{-1}) are large enough to indicate that long chain fatty-acyl-CoA thioesters might be *in vivo* substrates. The K_m values for the short chain acyl-*holo*ACP thioesters are significantly smaller than those measured for the corresponding acyl-CoA thioesters. For example, the K_m value observed for acetyl-CoA is 10 mM and that for acetyl-holoACP is 33 μM, whereas the k_{cat} values are essentially the same (0.14 s^{-1} vs 0.11 s^{-1}). On the other hand, the K_m values for the long chain acyl-CoA and long chain acyl-*holo*ACP are both very small. However, Km values less than 5 μM are not accurately determined by the steady-state initial velocity method and thus K_m value (3-5 μM) for lauroyl-holoACP and myristoyl-holoACP might be significantly larger than the actual value. Such a small K_m value is consistent with the *in vivo* YbgC targeting long chain fatty-acyl-*holo*ACP formed during the course of fatty acid synthesis.

The activity of the *H. influenzea* YbgC with isobutyryl-*holo*ACP was measured and shown to be much greater (k_{cat}/K_m ~1 x10^4 $M^{-1}s^{-1}$) than the activity measured with the isobutyryl-CoA. Presumably, the K_m value (220 μM) measured with the native long chain fatty acyl-*holo*ACP (rather than the E. coli counterpart used here) would be significantly smaller.

	***E.coli* YbgC**			***H. influenzea* YbgC**		
Substrate	**k_{cat} (s^1)**	**K_M (mM)**	**k_{cat}/K_M ($s^{-1}\mu M^{-1}$)**	**k_{cat} (s^1)**	**K_M (mM)**	**k_{cat}/K_M ($s^{-1}\mu M^{-1}$)**
Acetyl-CoA	0.14 ± 0.01	10 ± 1	14		ND	
Propanoyl-CoA	1.38 ± 0.04	0.49 ± 0.04	2.8 x 10^3	0.44 ± 0.4*	11 ± 1*	40*
Butyryl-CoA	1.20 ± 0.02	0.70 ± 0.04	1.7 x 10^3	0.17 ± 0.03*	24 ± 7*	7*
Isobutyryl-CoA	1.3 ± 0.1	1.2 ± 0.1	1.1 x 10^3	0.54 ± 0.05*	16 ± 2*	34*
Hexanoyl-CoA	0.13 ± 0.01	2.8 ± 0.3	46		ND	
Octanoyl-CoA	0.037 ± 0.001	0.46 ± 0.05	80		ND	
Lauroyl-CoA	0.17 ± 0.01	0.014 ± 0.001	1.2 x 10^4		NA	
Myristoyl-CoA	0.24 ± 0.01	(5.3 ± 0.5) x 10^{-3}	4.8 x 10^4		ND	
Acetyl-*holo*ACP	0.11 ± 0.01	0.033 ± 0.002	3.3 x 10^3		ND	
Isobutyryl-*holo*ACP	0.43 ± 0.02	0.045 ± 0.005	9.6 x 10^3	2.1 ± 0.1	0.22 ± 0.02	9.5 x 10^3
Hexanoyl-*holo*ACP	(6.6 ± 0.1) x 10^{-2}	0.140 ± 10	4.7 x 10^2		ND	
Octanoyl-*holo*ACP	0.28 ± 0.01	0.043 ± 0.005	6.5 x 10^3		ND	
Lauroyl-*holo*ACP	0.18 ± 0.01	(3.5 ± 0.2) x 10^{-3}	5.1 x 10^4		ND	
Myristoyl-*holo*ACP	0.23 ± 0.01	(4.7 ± 5) x 10^{-3}	4.6 x 10^4		ND	

Table 5.1: Steady-state kinetic constants for *E. coli* or *H. influenzea* YbgC catalyzed hydrolysis of acyl-CoA and acyl-*holo*ACP thioesters measured using DTNB spectrophotometric assay at pH 7.5 and 25 ^{o}C. * Indicates as previously published. ND - Not determined. NA –No activity.

5.3.3 Inhibition of *E. coli* YbgC-catalyzed hydrolysis of isobutyryl-CoA by β-ketopropionyl-CoA, *apo*ACP, and β-ketopropionyl-*holo*ACP

The inert substrate analogs β-ketopropionyl-CoA and β-ketopropionyl-*holo*ACP were characterized as potential inhibitors and co-crystallization ligands. The presence of the methylene (-CH_2) in between the carbonyl and the S ether atom prevents YbgC-catalyzed hydrolytic cleavage. The binding affinities of the substrate analogs were determined by measuring their inhibition constants using the steady-state kinetics. As shown in Figure 5.5 A and B, the substrate analogs displayed competitive inhibition. Data fitting to equation 2 defines the β-ketopropionyl-CoA K_i = 85 ± 5 μM and the β-ketopropionyl-*holo*ACP K_i = 8 ± 0.4 μM (Table 5.2**)**. The 10-fold tighter binding of the ACP analog is evidence the *holo*ACP unit of the acyl-*holo*ACP binds to YbgC more strongly than does the CoA unit of the acyl-CoA.

To access if *apo*ACP binds to YbgC it was tested as an inhibitor vs isobutyryl-CoA. Competitive inhibition was observed which is consistent with the ACP is binding at the entrance to the active site thus blocking the substrate binding. The fitted inhibition constant for *apo*ACP was K_i = 190 ± 20 μM, approximately 25x less potent of an inhibitor as compared to β-ketopropanone-*holo*ACP. This result is in good agreement to the TAP assay conducted with the ACP S36C and S36T mutants which showed that the

YbgC-ACP interaction is not solely electrostatic and that the phosphopantatheine unit on ACP is necessary to interact with ybgC (*2*). The *holo*ACP inhibition could not be tested due to the nature of the DTNB assay and its interactions with the free thiol on the *holo*ACP.

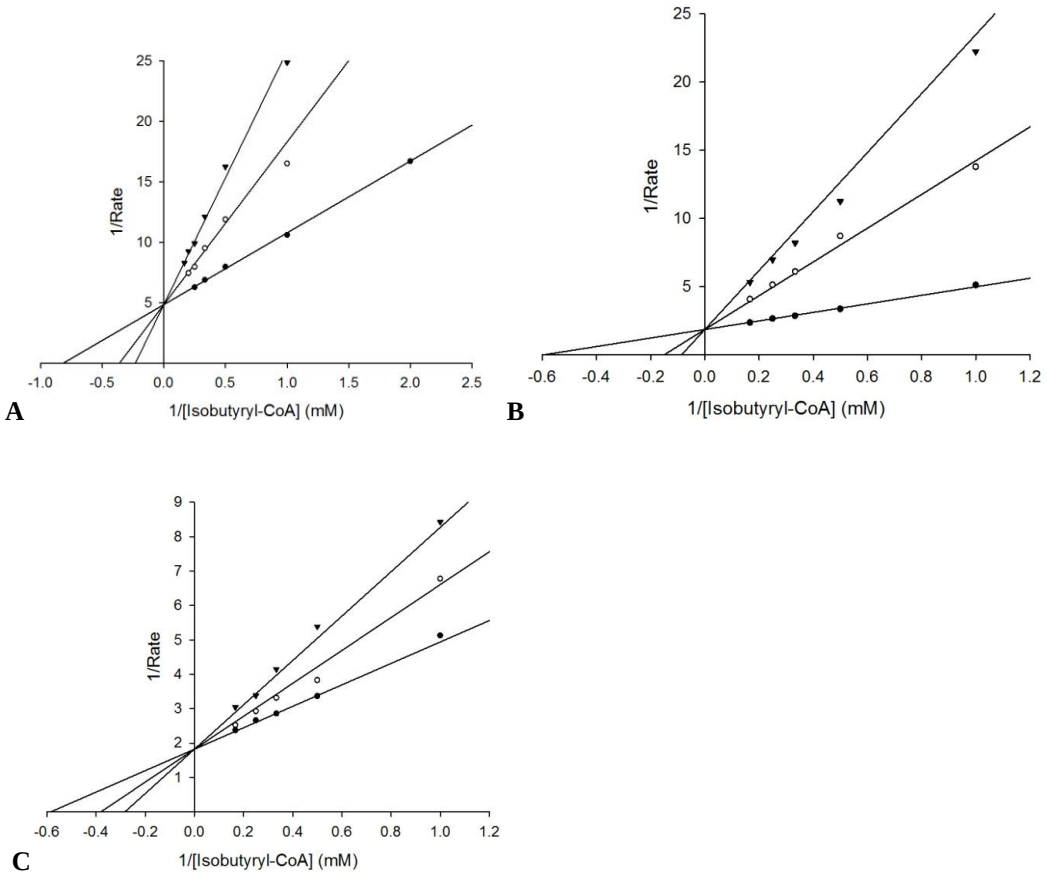

Figure 5.4: A - Competitive inhibition plots for β-ketopropanone-*holo*ACP monitored by DTNB assay using 0.16 µM *E. coli* YbgC, 0.5-6 mM isobutyryl-CoA, and 0 (●), 10 (o), or 20 (▼) µM inhibitior. **B** - Competitive inhibition plots for β-ketopropanone-CoA monitored by DTNB assay using 0.22 µM *E. coli* YbgC, 1-6 mM isobutyryl-CoA, and 0 (●), 250 (o), or 500 (▼) µM inhibitior. **C** - Competitive inhibition plots for *apo*-ACP

monitored by DTNB assay using 0.22 μM *E. coli* YbgC, 1-6 mM isobutyryl-CoA and 0 (●), 100 (o), or 200 (▼) μM inhibitior.

Inhibitors	K_i (μM)
β-ketopropanone-CoA	85 ± 5
Apo-ACP	190 ± 20
β-ketopropanone-*holo*ACP	8 ± 0.4

Table 5.2: Inhibition constants for *E. coli* YbgC catalyzed hydrolysis of isobutyryl-CoA determined by DTNB spectrophotomeric assay.

5.3.4 Small angle x-ray scattering of the YbgC-β-ketopropanone-*holo*ACP complex

It is important to note that the data presented here is only preliminary and that validation experiments must be carried out. Several SAXS experiments were conducted to determine the solution structure of the YbgC-ACP complex. Becuase the inhibitor β-ketopropanone-*holo*ACP displayed relatively tight binding, it was used as the substrate for YbgC rather than the loosely binding *apo*ACP. The complex demonstrated aggregation as can be seen in the steep decline of the initial data points when compared to theoretical SAXS data (Figure 5.5). In addition, the model generated by Chimera and FOXS diverges from the obtained data with a $\chi = 11.4$, out of the preferred range of 1-2. This could mean that the orientation of the predicted model must be further refined. However, the experimental data does show preference towards the complex as the χ values of predicted solo ACP and YbgC are 53 and 54 respectively. Additionally, the

size distribution of the SAXS data set is similar to that of the predicted complex set as shown in Figure 5.6 also suggesting that the solution structure is best represented by an YbgC-ACP complex.

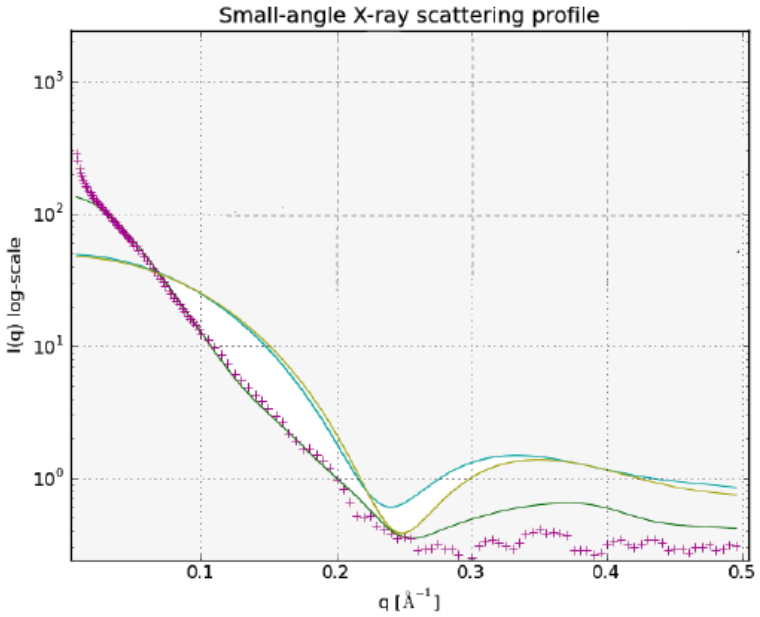

Figure 5.5: SAXS data for the YbgC-β-ketopropanone-*holo*ACP complex (+) overlaid with the predicted SAXS data for the complex (—), *apo*ybgC (—), and *apo*ACP (—).

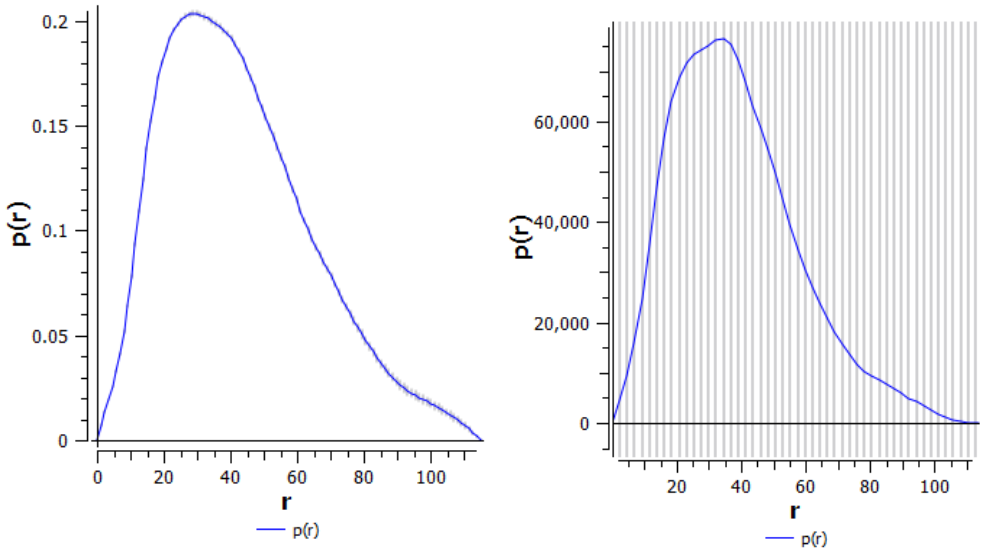

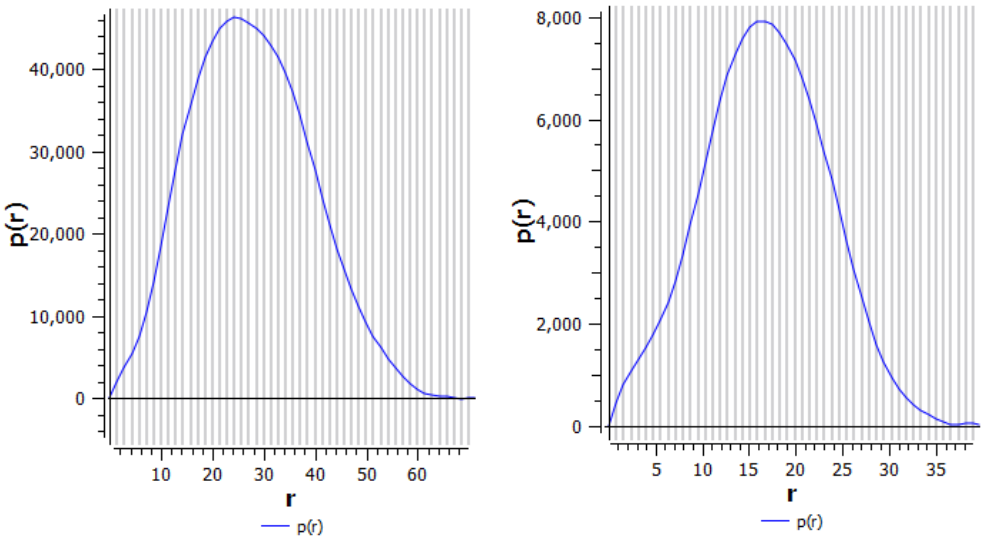

Figure 5.6: GNOM calculated size distributions of the experimental YbgC-β-ketopropanone-*holo*ACP complex (**A**) and the predicted YbgC-β-ketopropanone-*holo*ACP complex (**B**), *apo*YbgC (**C**), and *apo*ACP (**D**).

Even though the experimental data demonstrated signs of protein aggregation, enough acceptable data points were collected to construct a molecular envelope of the YbgC-β-ketopropanone-*holo*ACP complex. A DAMMIN script was used to generate 20 possible envelopes with χ values below 1.5. The 20 envelopes were averaged to generate a single molecular envelope with a χ value of 1.2. As shown in Figure 5.7, the molecular envelope is consistent with two ACP's binding to the dimeric YbgC, similar to other hotdog-fold proteins with acyl-CoA's in both active sites.

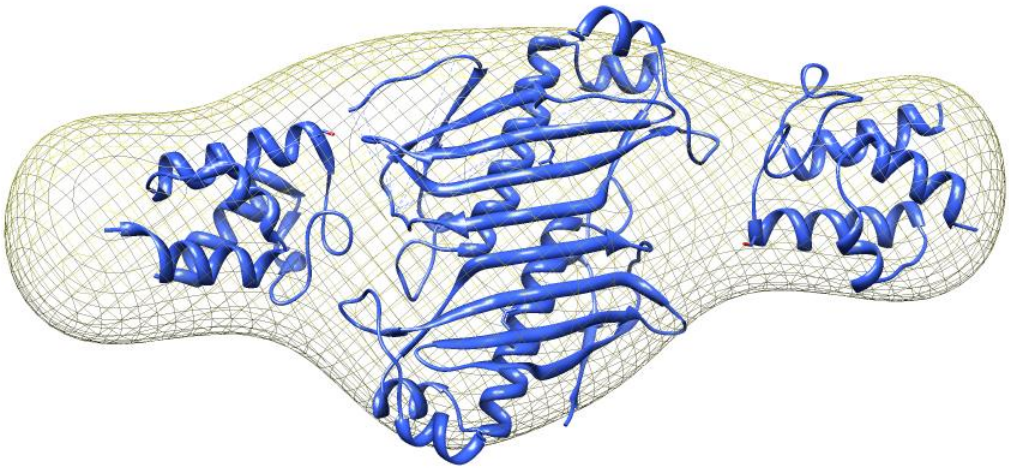

Figure 5.7: DAMMIN generated molecular envelope calculated from SAXS of the YbgC-β-ketopropanone-*holo*ACP complex (mesh) superimposed with the Chimera generated model of the ybgC-ACP complex.

5.4 Summary

The *Escherichia coli ybgC* gene was cloned, expressed and purified to homogeneity. Similar to the *H. Hyplori* YbgC, substrate activities of *E. coli* YbgC demonstrate preferences to long chain acyl-CoA's such as lauroyl- and myristoyl-CoA. Using the idea from previously reported TAP experiments showing that YbgC interacts with ACP, I wanted to test *E. coli* YbgC for acyl-*holo*ACP activity. To do this, a system to synthesize large quantities of acyl-*holo*ACP's was need. *Apo*ACP was purified to homogeneity at ~10 mg/mL and was verified by TOF-ESI-MS. The acyltransferase BF1558 was used to load various acyl-phosphopantetheine onto *apo*ACP to completion, verified by TOF-MSI-MS, to yield final products of 8-10 mg/mL. YbgC greater activity towards the acyl-*holo*ACP thioesters, favoring >C10 acyl-*holo*ACP, suggesting that its physiological substrate is a long chain fatty acyl-*holo*ACP. The inhibitor data both the

ACP and its pantetheine arm contribute to the substrate binding affinity. The correlation between K_m value and substrate acyl chain length (long chain having the smallest) of the acyl-CoA and acyl-*holo*ACP suggests that desolvation of the acyl chain contributes to the binding affinity.

The idea to synthesize the inert substrate analog β-ketopropanone-*holo*ACP was part of a larger idea to generate a co-crystal of the YbgC-ACP complex (which is underway in Professor Karen Allen's laboratory at Boston University). The substrate analog β-ketopropanone-*holo*ACP was synthesized and showed modest inhibition with a K_i ~ 8 μM, 25 times tighter than the *apo*ACP, and 10 times tighter than β-ketopropanone-CoA. Since currently only three different protein complex structure with ACP have been reported, P_{450}-ACP, FabI-ACP, and AcpS-ACP, small angle x-ray scattering seemed to be a useful tool to quickly examine the mode of binding between ACP and YbgC (*14–16*). Preliminary SAXS data of the YbgC-β-ketopropanone-*holo*ACP complex provided a first look at how ACP binds to the YbgC dimer, providing insight to how the two proteins interact. Verification of the SAXS data along with a co-crystal of the YbgC-ACP complex would further our understanding of how hotdog-fold thioesterases interact with acyl-*holo*ACP's. Although the exact biological function of YbgC was not determined, this work provides supporting evidence that YbgC does play a role in the phospholipid synthesis pathway as suggested by the TAP pull-down experiments. Specifically, YbgC is posited to support the synthesis of fatty acids by releasing the fatty acid from the *holo*ACP once it has reached a length of 14 or more carbon atoms.

References

1. Gerding, M. a, Ogata, Y., Pecora, N. D., Niki, H., and de Boer, P. a J. (2007) The trans-envelope Tol-Pal complex is part of the cell division machinery and required for proper outer-membrane invagination during cell constriction in E. coli., *Molecular Microbiology 63*, 1008-25.

2. Gully, D., and Bouveret, E. (2006) A protein network for phospholipid synthesis uncovered by a variant of the tandem affinity purification method in Escherichia coli., *Proteomics 6*, 282-93.

3. Rawlings, M., and Cronan, J. E. (1992) The gene encoding Escherichia coli acyl carrier protein lies within a cluster of fatty acid biosynthetic genes., *The Journal of Biological Chemistry 267*, 5751-4.

4. Zhuang, Z., Song, F., Martin, B. M., and Dunaway-Mariano, D. (2002) The YbgC protein encoded by the ybgC gene of the tol-pal gene cluster of Haemophilus influenzae catalyzes acyl-coenzyme A thioester hydrolysis., *FEBS Letters 516*, 161-3.

5. Angelini, A., Cendron, L., Goncalves, S., Zanotti, G., and Terradot, L. (2008) Structural and enzymatic characterization of HP0496, a YbgC thioesterase from Helicobacter pylori., *Proteins 72*, 1212-1221.

6. Luo, L., Taylor, K. L., Xiang, H., Wei, Y., Zhang, W., and Dunaway-Mariano, D. (2001) Role of active site binding interactions in 4-chlorobenzoyl-coenzyme A dehalogenase catalysis., *Biochemistry 40*, 15684-92.

7. Cronan, J. E., and Thomas, J. (2009) Bacterial fatty acid synthesis and its relationships with polyketide synthetic pathways., *Methods in Enzymology* 1st ed., pp 395-433. Elsevier Inc.

8. Huang, H. (2011) Functional assignment within the Haloacid Dehalogenase Superfamily. The University of New Mexico.

9. Konarev, P. V., Volkov, V. V., Sokolova, A. V., Koch, H. J., and Svergun, D. I. (2003) PRIMUS : a Windows PC-based system for small- angle scattering data analysis, *Journal of Applied Crystallography 36*, 1277-1282.

10. Svergun, D. I. (1999) Restoring low resolution structure of biological macromolecules from solution scattering using simulated annealing., *Biophysical Journal 76*, 2879-86.

11. Wriggers, W. (2010) Using Situs for the integration of multi-resolution structures., *Biophysical Reviews 2*, 21-27.

12. Schneidman-Duhovny, D., Hammel, M., and Sali, A. (2010) FoXS: a web server for rapid computation and fitting of SAXS profiles., *Nucleic Acids Research 38*, W540-4.

13. Cronan, J. E. (1982) Molecular properties of short chain acyl thioesters of acyl carrier protein., *The Journal of Biological Chemistry 257*, 5013-7.

14. Rafi, S., Novichenok, P., Kolappan, S., Zhang, X., Stratton, C. F., Rawat, R., Kisker, C., Simmerling, C., and Tonge, P. J. (2006) Structure of acyl carrier

protein bound to FabI, the FASII enoyl reductase from Escherichia coli., *The Journal of Biological Chemistry 281*, 39285-93.

15. Cryle, M. J., and Schlichting, I. (2008) Structural insights from a P450 Carrier Protein complex reveal how specificity is achieved in the P450(BioI) ACP complex., *Proceedings of the National Academy of Sciences 105*, 15696-701.

16. Halavaty, A.S., Minasov, G., Filippova, E.V., Dubrovska, I., Winsor, J., Shuvalova, L., Peterson, S.N., Anderson, W. F. (2012) 2.52 Angstrom resolution crystal structure of the acyl-carrier-protein synthase (AcpS)-acyl carrier protein (ACP) protein-protein complex from Staphylococcus aureus subsp. aureus COL, *Unpublished*.

CHAPTER SIX

BACILLUS HALODURANS GENTISYL-COA THIOESTERASE MECHANISM: PRE-STEADY STATE KINETICS, STEADY STATE KINETICS AND ACTIVE SITE PROPERTIES

6.1 Introduction

Pathways that lead to the mineralization of environmental aromatic compounds are found in a variety of bacteria (1-5). Examples include the 4-chlorobenzoate, benzoate, phenylacetate and gentisate (2,5-dihydroxybenzoate) degradation pathways. Because these aromatic compounds are formed as intermediates in the degradation of larger aromatic environmental pollutants (e.g., polychlorinated biphenyls, napthalenes and polyaromatics), the genes that encode the pathway enzymes can be used for engineering ("metabolic engineering") bacteria for use in pollutant bioremediation. In order to target a novel aromatic, the enzymes of a known pathway are engineered to redirect substrate specificity so that the novel pathway substrate and intermediates are processed. The starting point for enzyme engineering is the determination of the structural basis for substrate recognition and catalysis.

In this chapter, I examine the structure-function relationships in the hotdog-fold superfamily enzyme gentisyl-CoA thioesterase. Gentisyl-CoA is formed during biodegradation of naphthalene and hydroquinone as well as in the conversion of a variety of benzoates. The kinetic properties of the gentisyl-CoA thioesterase from *Bacillus halodurans* C-125 ("BH1999") was reported by the Dunaway-Mariano lab in 2004 (6). BH1999 shares 27% sequence identity with its closest known homolog, the *Pseudomonas*

sp. strain CBS3 4-hydroxybenzoyl-CoA thioesterase (*Ps.* 4HBT), and it conserves the active site residues Asp16, Asp31, and Arg108 which have counterparts in *Ps.* 4HBT (Figure 6.1).

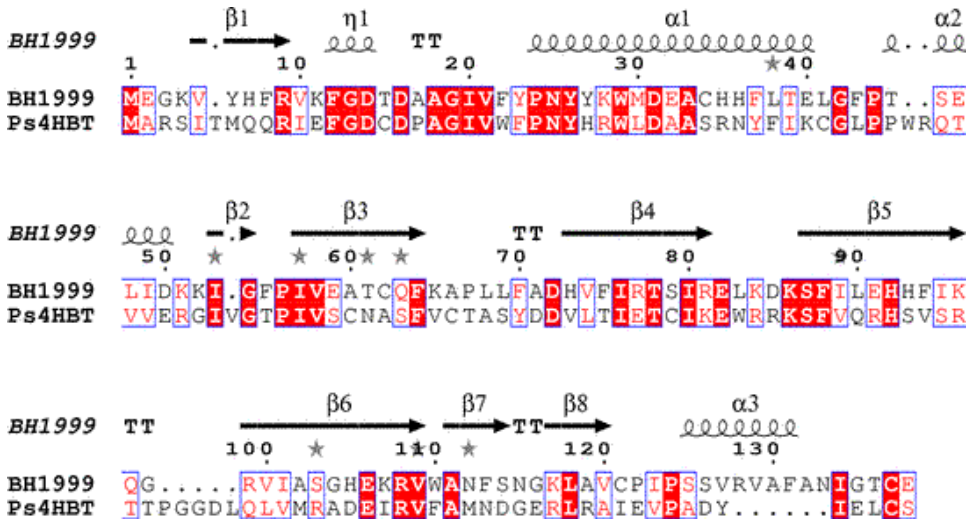

Figure 6.1: ESpript generated sequence alignment of BH1999 and *Pseudomonas sp*. Strain CBS3 4-HBT where white font and red backgrounds represent identical residues and red font white background represents similar residues.

Until recently, crystal structures of BH1999 have not been unavailable. In collaboration with Professor Karen Allen and Dr. Lorenzo Finci at Boston University the X-ray crystal structure of BH1999 bound with the inert substrate analog 2-hydroxyphenacyl-CoA was recently solved. As shown in Figure 6.2A, the first noticalble difference between BH1999 and *Ps.* 4HBT is the replacement of the active site Arg36 with a His residue. The second and perhaps more mechanistically important difference between the two active sites is the two ordered water molecules in the active site of BH1999, one of which is positioned close to what would correspond to the reaction site

of the bound substrate (Figure 6.2B). The X-ray crystal structures of the active site of *Ps.* 4HBT bound with the inert substrate analog 4-hydroxyphenacyl-CoA or the D17N mutant bound with the substrate 4-HB-CoA, do not include an ordered water molecule at the reaction site, nor does there appear to be room for one. In a previous paper we reported that the *Ps.*4HBT Asp17 functions in nucleophilic catalysis (*1*). The central question that I address in this chapter is whether the BH1999 Asp16 functions in nucleophilic or base catalysis. These two mechanisms, introduced in previous chapters are reviewed in Figure 6.3.

The X-ray structure of the 2-hydroxyphenacyl-CoA BH1999 complex supports both scenarios because the Asp16 assumes a pose that places it in the now familiar "near attack" conformation, and yet an ordered water molecule is present at the site and engaged in hydrogen bond formation with the Asp16 carboxylate group.

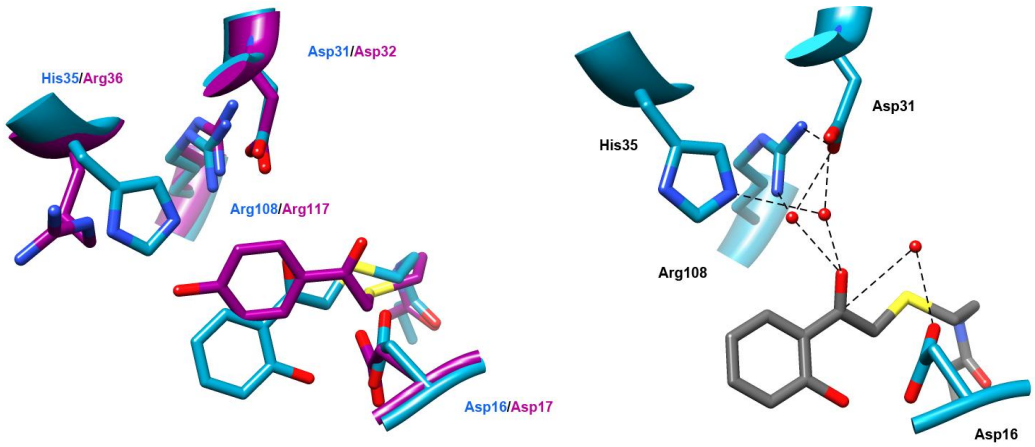

Figure 6.2: **A.** Active site alignment of *Ps.* 4HBT (violet - PDB ID: 1LO8) and BH1999 (blue - PDB ID: unpublished) with liganded 4-HP-CoA and 2-HP-CoA respectively. **B.** Active site of BH1999 with the 2-HP-CoA ligand showing the potential hydrogen bonding network with active site waters.

My objective was to use transient kinetic techniques to measure the time course for consecutive BH1666-catalyzed single-turnover reactions. If the BH1999 Asp16 functions in base catalysis one would expect a single-phase time course for the multiple-turnover reaction forgoing a "burst" phase, as discussed in Chapter 3. However, if BH1999 Asp16 functions in nucleophilic catalysis, similar to that of *Ps.* 4HBT, one would expect a biphasic time course for the multiple-turnover reaction consisting of the fast "burst" phase followed by a slower steady-state phase. In this chapter, I will present rapid quench data measured for the wild-type BH1999 along with the the results from an experiment aimed at trapping the covalent anhydride intermediate formed via the nucleophilic catalysis mechanistic pathway.

Base Catalysis:

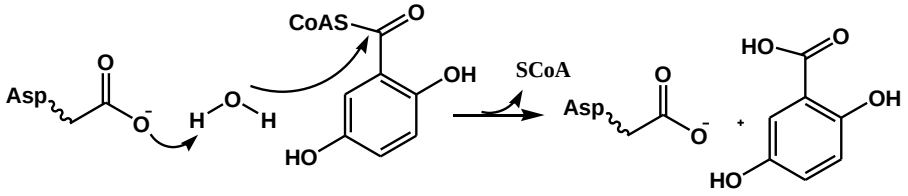

Nucleophilic Catalysis:

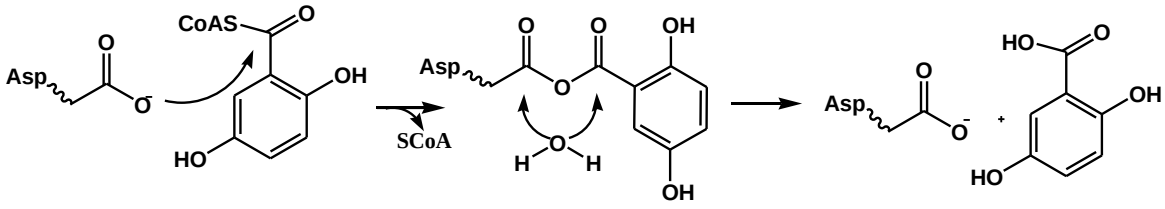

Figure 6.3. Illustration of the two possible roles of the Asp catalytic group in thioesterase catalysis.

6.2 Materials and Methods

6.2.1 Materials

All restriction enzymes and T4 DNA ligase were purchased from Invitrogen. *Pfu Turbo* DNA polymerases was purchased from Strategene. Oligonucleotide primers were custom-synthesized by Invitrogen. DNA sequencing was performed by the DNA Sequencing Facility of the University of New Mexico. 2,5-Dihydroxybenzoyl-CoA (2,5-DHB-CoA) and 3-hydroxybenzyol-CoA (3-HBA-CoA) were synthesized as previously reported (*2*).

6.2.2 Subcloning, expression, and purification

The wild-type (WT) *BH1999* gene was amplified by PCR using the native *BH1999*/pET23a plasmid as template, commercial oligonucleotides as primers, and *Deep Vent* as the DNA polymerase. (*3*) The PCR-products were digested by the restriction enzymes *NdeI* and *XhoI* and then purified by polyacrylamide gel electrophoresis. The gene was ligated to an *Nde I* and *XhoI* -digested pET23a vector (Novagen) to include the C-terminal His_6 tag. The cloned gene was verified by DNA sequencing. The cloned plasmid was used to transform competent *E. coli* BL21(DE3) cells (Invitrogen) for expression. The *BH1999*/pET-23a transformed *E. coli* BL21(DE3) cells were grown aerobically at 37 ^{o}C in LB media containing 50 µg/ml ampicillin. Production of the C-terminal His_6 tagged BH1999 was induced with 0.4 mM isopropyl-β-$_D$-galactopyranoside (IPTG) once the cell density reached A_{600} ~ 0.6. Following a 12 h induction period at 22 ^{o}C, the cells were harvested by centrifugation at 6,500 rpm for 10 min and then resuspended in 100 mL of 50 mM K^+HEPES buffer (pH 7.5), 50 mM imidazole, and 500

mM NaCl (Lysis Buffer). The cells were lysed using a French press at 1,200 psi and the lysate was centrifuged at 20,000 rpm for 15 min. The supernatant as loaded onto a 5 mL HisTrap FF column (GE Life Sciences) and the column was washed with Lysis Buffer at 4 ^{o}C to remove non-tagged protein and then with 50 mM K^{+}HEPES (pH 7.5), 500 mM imidazole, and 500 mM NaCl (Elution Buffer) to elute the tagged protein. Column fractions were monitored by their measuring absorbance at 280 nm and by carrying out SDS-PAGE analysis. The BH1999 containing fractions were combined and dialyzed three times against 1 L 50 mM K^{+}HEPES (pH 7.5) and 50 mM NaCl. Yield: ~ 18 mg/g of wet cells.

Site-directed mutagenesis was carried out to create the D16E mutant using the Quick Change PCR strategy (Stratagene) with the WT-*BH1999*/pET-23a plasmid, commercial primers, and *Pfu Turbo* polymerase. The PCR products were purified by polyacrylamide gel electrophoresis and treated with *DpnI* to degrade the wild-type plasmid. The *Nde I* and *XhoI* digested recombinant mutant plasmid was used to transform competent *E. coli* BL21 (DE3) cells (Invitrogen) for expression. The sequence of the mutated gene was confirmed by DNA sequencing. The mutant protein was purified to homogeneity (as determined by SDS-PAGE analysis) by the same procedure used for the wild-type BH1999. Yield: ~19 mg/g of wet cells.

6.2.3 Steady-state kinetic analysis of the WT BH1999 and the D16E mutant

Thioesterase activity was measured using the 5,5'-dithio-bis-(2-nitrobenzoic acid) (DTNB) coupled assay. Reactions were monitored at 412 nm ($\Delta\varepsilon$ = 13.6 $mM^{-1}\bullet cm^{-1}$) using a Beckman 640U Spectrometer. Reactions were carried out in 50 mM K^{+}HEPES

and 1 mM DTNB (pH 7.5, 25 ^{o}C) containing thioesterase and varying concentrations of thioester (0.5 – 3 x K_m) in a total volume of 500 µL. For all measurements, the initial velocity data, measured as a function of substrate concentration, were analyzed using Enzyme Kinetics v 1.4 and equation (1).

$$V = V_{max} [S]/([S]+K_m) \quad (1)$$

where V is initial velocity, V_{max} is maximum velocity, [S] is substrate concentration, and K_m is the Michaelis constant. The k_{cat} was calculated from V_{max}/[E] where [E] is the total enzyme concentration as determined by the Bradford method.

6.2.4 Synthesis of ^{14}C radiolabled 3-hydroxybenzyol-CoA

[^{14}C]-3-HB-CoA was synthesized enzymatically by using the 4-hydroxybenozoic acid ligase (4HBAL) from *Rhodopseudomonas palustris.* 4HBAL was purified using the procedure reported in Chapter 3 (*4*). The [^{14}C]-3-hydroxybenzoic acid (specific activity of 50 mCi/mol; American Radiolabeled Chemicals Inc.) was converted to the sodium salt by the addition of 100 µL 0.1 M NaOH and then added to a final concentration of 2 µM to a 1 mL solution comprised of 100 mM K^+HEPES, 5 mM $MgCl_2$, 13 mM coenzyme-A, 13 mM ATP, 8 U inorganic pyrophosphatase and 5 µM 4HBAL. The reaction mixture was incubated at room temperature overnight and then acidified by the addition of 50 µL of 1 M HCl. The precipitated protein was separated by centrifugation at 14,000 rpm for 5 min. [^{14}C]-3-HB-CoA was purified from the supernatant by chromatography on a semi-prep Ultra Aqueous C-18 reverse phase HPLC column (RESTEK) eluted with a linear gradient of 50% 20 mM KH_2PO_4 (pH 6.1) and 66% CH_3CN at a flow rate of 3 mL/min. The chromatography was monitored by an in-line SPD-20AV UV/Vis detector

(Shimadzu) at 260 and 310 nm. The target compound eluted at ~15 min. The desired fractions were combined and lyophilized to a powder and then resuspended in water. The yield of 25% was calculated from the absorbance at 261 nm (ε_{261} = 21.3 $M^{-1}cm^{-1}$) (*5*).

6.2.5 Rapid-quench studies of the WT BH1999 and D16E mutant catalyzed hydrolysis of 3-hydroxybenzoyl-CoA under single and multiple turnover conditions

A rapid-quench instrument from KinTek Instruments was used to combine buffered wild-type thioesterase with buffered [^{14}C]3-HB-CoA to initiate the reaction, and then to add 0.2 M HCl to terminate the reaction. For the multiple turnover reactions, mixtures initially contained 10 μM enzyme and 50 μM [^{14}C]3-HB-CoA in 100 mM NaCl/50 mM K^+HEPES (pH 7.5, 25 °C), whereas for the single turnover reactions, enzyme and [^{14}C]3-HB-CoA concentrations were 50 μM and 30 μM, respectively. The protein was removed from the quenched reaction solution using a 10,000 MWCO centrifuge column prior to carrying out the separation of the [^{14}C]3-HB-CoA and [^{14}C]3-HB on a C18-reversed phase analytical column (RESTEK), eluted using a linear gradient of 50% 20 mM KH_2PO_4 (pH 6.1) and 66% CH_3CN at a flow rate of 1 mL/min. The radioactivity of the substrate and product fractions was quantified using an in-line β-RAM4 (Lab Logic) scintillation counter. Peak integrations were performed by Laura software (Lab Logic) and the progress curves were fitted by simulation using the KinTek Corp. Global Kinetic Explorer computer program.

6.2.6 Trapping the catalytic aspartate with hydroxylamine

Thioesterase activity was monitored using the DTNB assay described above. Reactions contained 0.07 µM WT BH1999 thioesterase, 70 µM 3-HB-CoA and 100 mM hydroxylamine. Control reactions with substrate, substrate and enzyme, hydroxylamine, and hydroxylamine and substrate were also conducted. A stock solution of protein incubated with 100 mM hydroxylamine was prepared to ensure that hydroxylamine was not modifying the enzyme directly without catalytic turnover. An aliquot of the equilibrated BH1999 was used in a reaction void of hydroxylamine to demonstrate no loss in activity. The final control reaction containing 100 mM hydroxylamine and 70 µM CoA was carried out to verify that CoA reacts with DTNB in the presence of hydroxylamine.

6.3 Results and Discussion

6.3.1 Steady-state kinetic analysis of wild-type BH1999 and the mutant D16E

The recombinant *Bacillus halodurans* thioesterase BH1999 was subjected to steady-state kinetic analysis to verify the previously reported activity (7). The current BH1999 preparation proved to be slightly more active (~2-fold increase in k_{cat}) than the previous preparation (Table 5.1) (*3*).

In order to determine the impact of altering the length of the side chain of the catalytic carboxylate residue (Asp16) on the catalytic efficiency, the D16E mutant was prepared for kinetic analysis. The BH1999 X-ray structure shows that the Asp16 carboxylate group is engaged in hydrogen bond interaction (2.6 Å) with the active site water molecule but it is not pinned into position by an active site enzyme residue. It is expected that the additional methylene group of the Glu side chain will perturb the

orientation of the carboxylate group relative to the substrate thioester group. If the Asp16 functions as a nucleophile, its orientation will be especially important because of the steric requirements for the attack of a nucleophile on a carbonyl carbon. Likewise, if the carboxylate group, in the role of base catalyst, orients the water nucleophile for attack at the substrate thioester group the extension of the side chain by the additional methylene group might cause misalignment of the water nucleophile. As shown in Table 5.1, the k_{cat} (and not the K_m) value determined for BH1999 D16E catalyzed hydroylis of gentisyl-CoA is altered. However, the 63-fold reduction compared to 500 and 5,000-fold reduction in the k_{cat} values reported for the D16N and D16A mutants (7), suggests that the carboxylate group of the D16E mutant retains a majority of the function of the Asp16 of the wild-type enzyme.

Enzyme	**Substrate**	**k_{cat} (s^{-1})**	**K_M (μM)**	**k_{cat}/K_M ($M^{-1}s^{-1}$)**
Wild-type	4-HB-CoA	$(4.2 \pm 0.2) \times 10^{-2}$	120 ± 20	3.6×10^{2}
Wild-type	Gentisyl-CoA	15 ± 1	5.3 ± 0.5	2.9×10^{6}
Wild-type	Benzoyl-CoA	$(6.8 \pm 0.3) \times 10^{-2}$	330 ± 40	2.1×10^{2}
Wild-type	3-HB-CoA	4.5 ± 0.2	5.0 ± 0.4	9.0×10^{5}
D16E	Gentisyl-CoA	0.24 ± 0.01	8.5 ± 0.9	2.8×10^{4}
D16E	3-HB-CoA	0.30 ± 0.01	5.9 ± 0.6	5.0×10^{4}
D16A*	Gentisyl-CoA	3×10^{-3}	ND	ND
D16N*	Gentisyl-CoA	$(2.8 \pm 0.3) \times 10^{-2}$	9 ± 2	3.1×10^{3}

***** Data was taken from reference (6).

Table 6.1: Steady-state kinetic constants for BH1999-catalyzed hydrolysis of acyl-CoA and and aroyl-CoA thioesters measured using DTNB spectrophotometric assay at pH 7.5 and 25 ^{o}C. ND - not determined.

6.3.2 Kinetic analysis of wild-type BH1999

Global fitting of steady-state, single-turnover, and multiple-turnover time courses for wild-type BH1999-catalyzed 3-HB-CoA was carried out to define microscopic rate constants for the reaction steps. This particular substrate was chosen because 4HBAL does not catalyze the ligation of 2,5-dihydroxybenzoic acid (2,5-DHB) to CoA and the chemical synthesis of the 2,5-DHB-CoA requires large quantities of starting material. The time course for the steady-state reaction was measured by monitoring of the hydrolysis of the 3-HB-CoA thioester at 310 nm. The absorbance was converted to 3-HB-CoA concentration using $\Delta\varepsilon = 2.18\ mM^{-1}cm^{-1}$. The time course data were fitted by simulation assuming the kinetic model shown in Scheme 6.1 and by restricting the values of $k_{1,}$ k_{-3} and k_{-4} to 1000 s^{-1} and the value of k_{-2} to 0 s^{-1}.

$$\mathbf{E + S} \underset{k_{-1}}{\overset{k_1}{\rightleftharpoons}} \mathbf{ES} \underset{k_{-2}}{\overset{k_2}{\rightleftharpoons}} \mathbf{EPQ} \overset{k_3}{\rightarrow} \mathbf{Q} \quad \mathbf{EPQ} \underset{k_{-3}}{\rightleftharpoons} \mathbf{EP} + \mathbf{(Q)} \quad \mathbf{EP} \underset{k_{-4}}{\overset{k_4}{\rightleftharpoons}} \mathbf{E + P} \qquad \textbf{(Scheme 6.1)}$$

The K_M (k_{-1}/k_1) was calculated to be ~1 µM as compared to the K_M value of 5 µM determined from steady-state initial velocity data measured as a function of substrate concentration (and fitted to the Michaelis-Menten equation). The K_i for CoA (k_3/k_{-3}) was calculated to be ~300 µM and the K_i (k_4/k_{-4}) for 3-HBA acid was calculated to be ~ 800 µM. The k_{cat} was in found to be 3-fold larger than the steady state derived k_{cat}, ~14 versus 4.5 s^{-1} respectively.

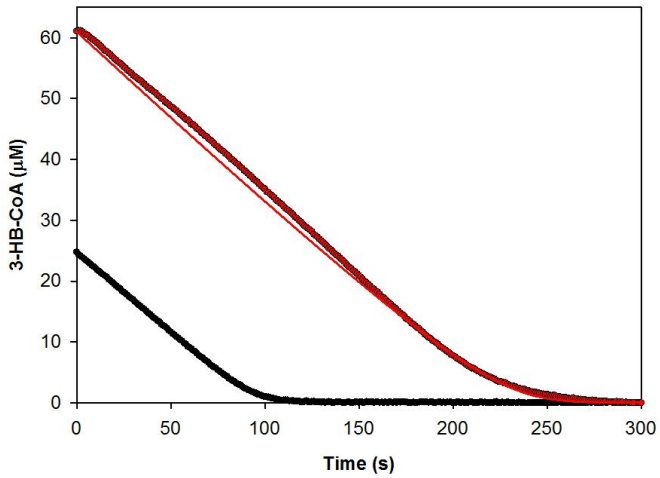

Figure 6.3: Experimental and simulated time courses for the steady state reaction containing 0.035 µM wild type BH1999 and 14 (●) or 24 µM (●) 3-HB-CoA in 50 mM K^+HEPES (pH 7.5, 25 ^oC). Data was obtained by observing the hydrolysis of 3-HB-CoA at 310 nm ($\Delta\varepsilon$ = 2.18 $mM^{-1}cm^{-1}$). The simulated curves were generated using the kinetic model in Scheme 1 and assuming k_1 = 160 $\mu M^{-1}s^{-1}$, k_{-1} = 100 s^{-1}, k_2 = 14 s^{-1}, k_{-2} = 0 s^{-1}, k_3 = 150 s^{-1}, k_{-3} = 0.5 s^{-1}, k_4 = 110 $\mu M^{-1}s^{-1}$, k_{-4} = 6 s^{-1}.

The time course measured for the multiple-turnover reaction of 10 µM BH1999 and 50 µM [^{14}C] 3-HB-CoA did not demonstrate a "burst" phase in contrast to the time course measured for *Ps.* 4HBT (*1*). Instead the reaction time course appears to have a single linear phase as shown in Figure 6.4. The time course was fitted by simulation using the by KinTek Corp. Global Kinetic Explorer computer program in conjunction with the kinetic model shown in Scheme 6.1 and the following rate constants: k_1 = 200-700 $\mu M^{-1}s^{-1}$, k_{-1} = 100-300 s^{-1}, k_2 = 14-16 s^{-1}, k_{-2} = 0 s^{-1}, k_3 = > 200 s^{-1}, k_{-3} = < 0.5 s^{-1}, k_4 = 90-150 $\mu M^{-1}s^{-1}$, k_{-4} = 5-20 s^{-1} (Figure 6.4A) The kinetic model was expanded to that shown in Scheme 5.2 and using the kinetic constants k_1 = 175-700 $\mu M^{-1}s^{-1}$, k_{-1} = 180-400

s^{-1}, k_2 = 15.5 -18 s^{-1}, k_{-2} = 0 s^{-1}, k_3 = 40-100 s^{-1}, k_{-3} = 0 s^{-1}, k_4 = >200 $\mu M^{-1}s^{-1}$, k_{-4} = <20 s^{-1}, k_5 = >200 $\mu M^{-1}s^{-1}$, k_{-5} = <10 s^{-1} a time course was simulated to match the experimental time course (Figure 6.4B).

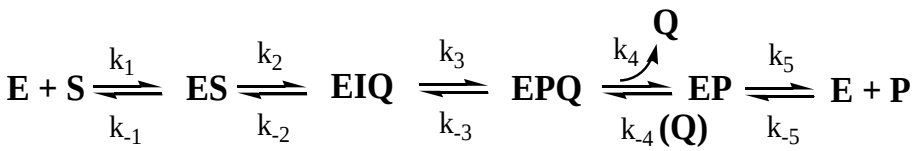

(Scheme 6.2)

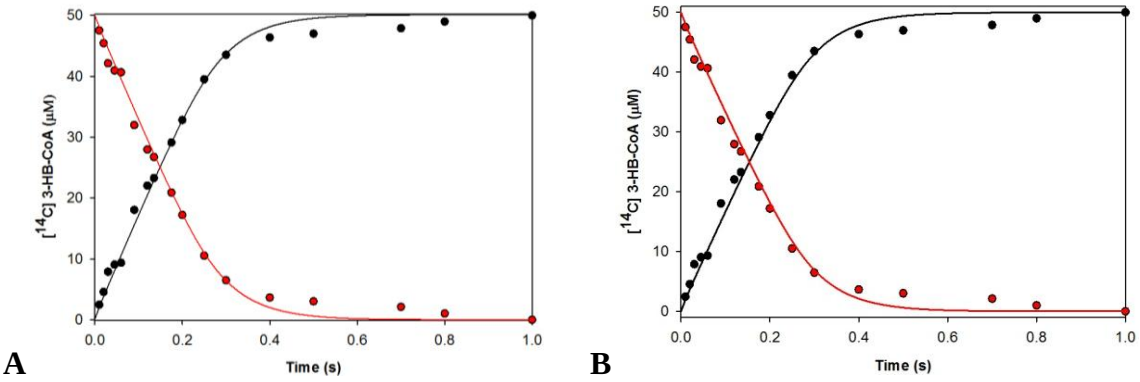

Figure 6.4: Experimental and simulated time courses for the multiple turnover reaction containing 10 μM wild type BH1999 and 50 μM [^{14}C] 3HB--CoA in 50 mM K^+Hepes (pH 7.5, 25 ^{o}C). The time point data [^{14}C] 3-HB-CoA (●) and [^{14}C] 3-hydroxybenzoic acid (●) were calculated from the fraction of [^{14}C] 3-HB-CoA and [^{14}C] 3-hydroxybenzoic acid present in the acid quenched reaction. (**A.**) The simulated curves were generated using the kinetic model in Scheme 6.1 using the rate constants k_1 = 160 $\mu M^{-1}s^{-1}$, k_{-1} = 100 s^{-1}, k_2 = 14 s^{-1}, k_{-2} = 0 s^{-1}, k_3 = 150 s^{-1}, k_{-3} = 0.5 s^{-1}, k_4 = 110 $\mu M^{-1}s^{-1}$, k_{-4} = 6 s^{-1}. (**B**) The simulated curves were generated using the kinetic model of Scheme 6.2 using the rate constants k_1 = 250 $\mu M^{-1}s^{-1}$, k_{-1} = 400 s^{-1}, k_2 = 14.5 s^{-1}, k_{-2} = 0 s^{-1}, k_3 = 75 s^{-1}, k_{-3} = 0 s^{-1}, k_4 =325 $\mu M^{-1}s^{-1}$, k_{-4} = 1.5 s^{-1}, k_5 = 300 $\mu M^{-1}s^{-1}$, k_{-5} = 2.5 s^{-1}.

The single-turnover reaction of 50 µM BH1999 and 30 µM [^{14}C]3-HB-CoA was conducted for the purpose of circumscribing the time course to reflect only the substrate binding step (k_1 and k_{-1}) and the chemical step (concerted reaction; Kinetic model of Scheme 6.1; k_2 and k_{-2}) or chemical steps (concerted reaction; Kinetic model of Scheme 6.2 ; k_2, k_{-2}, k_3 and k_{-3}) of the reaction. The time course for the single turnover reaction is shown in Figure 6.5A fitted with curves simulated assuming the kinetic model of Scheme 6.1 and setting $k_{-3} = 0$ s^{-1}. The fitted data provided the following ranges: $k_1 = >100$ $\mu M^{-1}s^{-1}$, $k_{-1} = <300$ s^{-1}, $k_2 = 13\text{-}15$ s^{-1} and $k_{-2} = 0$ s^{-1}. The time course for the single turnover reaction is shown in Figure 6.5B fitted with curves simulated assuming the kinetic model of Scheme 6.2 and setting $k_{-3} = 0$ s^{-1}. The fitted data provided the following ranges: $k_1 = >100$ $\mu M^{-1}s^{-1}$, $k_{-1} = >300$ s^{-1}, $k_2 = 13\text{-}15$ s^{-1} and $k_{-2} = 0$ s^{-1}.

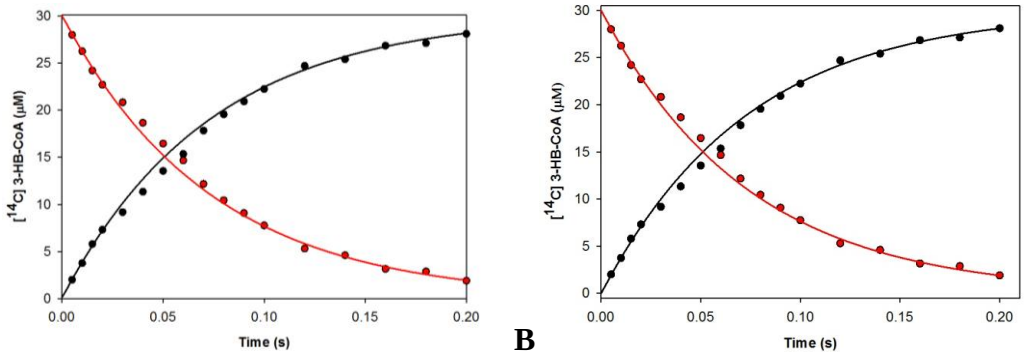

Figure 6.5: Experimental and simulated time courses for the single turnover reaction containing 50 µM wild type BH1999 and 30 µM [^{14}C]3-HB-CoA in 50 mM K^+HEPES (pH 7.5, 25 ^{o}C). The time point data [^{14}C]3-HB-CoA (●) and [^{14}C]3-hydroxybenzoic acid (●) were calculated from the fraction of [^{14}C] 3-HB-CoA and [^{14}C] 3-hydroxybenzoic acid present in the acid quenched reaction. (A) The simulated curves were generated using the kinetic model in Scheme 6.1 using the rate constants $k_1 = 160$

$\mu M^{-1}s^{-1}$, k_{-1} = 100 s^{-1}, k_2 = 14 s^{-1}, k_{-2} = 0 s^{-1}, k_3 = 150 s^{-1}, k_{-3} = 0.5 s^{-1}, k_4 = 110 $\mu M^{-1}s^{-1}$, k_{-4} = 6 s^{-1}. (B) The simulated curves were generated using the kinetic model of Scheme 6.2 using the rate constants k_1 = 250 $\mu M^{-1}s^{-1}$, k_{-1} = 400 s^{-1}, k_2 = 14.5 s^{-1}, k_{-2} = 0 s^{-1}, k_3 = 75 s^{-1}, k_{-3} = 0 s^{-1}, k_4 =325 $\mu M^{-1}s^{-1}$, k_{-4} = 1.5 s^{-1}, k_5 = 300 $\mu M^{-1}s^{-1}$, k_{-5} = 2.5 s^{-1}.

6.3.3 - Trapping the covalent enzyme intermediate by reaction with hydroxylamine

The absence of the "burst" phase in the in the time course measured for the multiple turnover reaction of 3-HB-CoA is consistent with a single chemical step involving Asp16 base catalysis as well as a two-step reaction (involving Asp16 nucleophilic catalysis) in which the first step (anhydride intermediate formation) is rate-limiting. To distinguish between these two scenarios we measured the time course for BH1999-catalyzed hydrolysis of 3-HB-CoA hydrolysis in the presence of the nucleophile hydroxylamine. Hydroxylamine as a more reactive nucleophile than is water and thus can potentially compete with an active site water molecule for attack at the electrophilic center. Hydroxylamine has previously been shown to trap a ubiquitin-carboxylase mixed anhydride by forming the carboxylase-hydroxamate (*6*). Reaction of the hydroxylamine at the carbonyl carbon of the acylated Asp16 would displace the 3-HB and convert the Asp16 carboxylate group to a hydroxyamide adduct, and thus inactive the enzyme (see Figure 6.6). Alternatively, if the attack occurs at the 3-hydroxybenzoyl carbonyl carbon no inactivation will be observed.

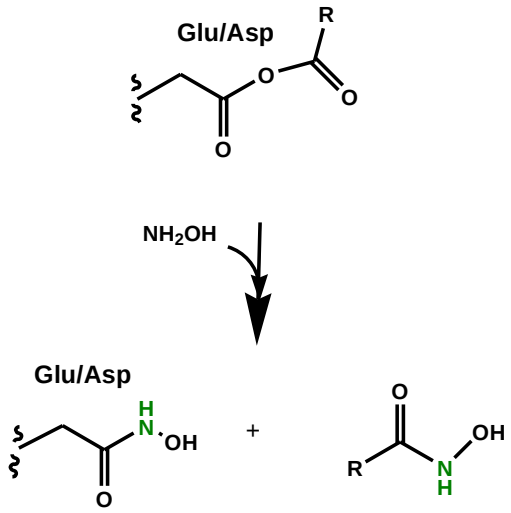

Figure 6.6. Reaction scheme showing the products of the hydroxylamine incorporation into the mixed anhydride.

The inactivation experiment was carried out in parallel with several control experiments. Accordingly, the time course for the hydrolysis of 70 µM 3-HB-CoA catalyzed by 0.07 µM BH1999 was measured using the DTNB coupled assay in the presence (in duplicate) and absence of 100 mM hydroxylamine. The results are presented in Figure 6.7. Absorbance changes that might result from DTNB in combination with 70 µM 3-HB-CoA or 100 mM hydroxylamine were ruled out in the respective control reactions. Likewise, inactivation by reaction of the 100 mM hydroxylamine with the BH1999 in the absence substrate was eliminated on the basis of the control reaction which contained 0.07 µM BH1999 that had been subjected to preincubation with 100 mM hydroxylamine prior to reaction with 70 µM 3-HB-CoA. Lastly, a control reaction was carried out to show that the 100 mM hydroxylamine does not inhibit the reaction of DTNB with the CoA.

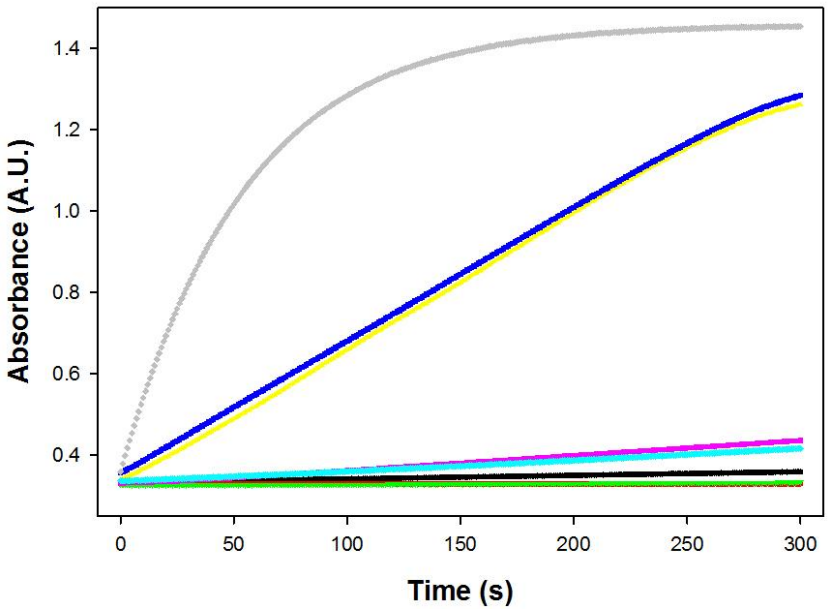

Figure 6.7. All reaction solutions contained 1 mM DTNB in 50 mM K^+HEPES (pH 7.5, 25 ^oC). Test Reactions: (—) 70 µM 3-HB-CoA and 0.07 µM BH1999; (—,—) 70 µM 3-HB-CoA, 100 mM hydroxylamine, and 0.07 µM BH1999; Control Reactions: (—) 70 µM 3-HB-CoA and 0.07 µM BH1999 preincubated with 100 mM hydroxylamine; (—) 70 µM CoA and 100 mM hydroxylamine; (—) 70 µM 3-HB-CoA; (—)100 mM hydroxylamine; (—)70 µM 3-HB-CoA and 100 mM hydroxylamine.

6.4 Conclusion: Catalytic Mechanism

Like the AA clade prototype *Ps* 4HBT, BH1999 forms a tetrameric structure in which each central helix is located inside the interfaced dimer of dimer (Figure 6.8A). Furthermore, the active site thioester-polarizing residue and the catalytic carboxylate residue are contributed by one of the paired subunits that form the active site (Figure

6.8B) (the AB clade is distinguished by one of the subunits contributing the catalytic carboxylate residue and the other the thioester-polarizing residue). The X-ray structure of the *Ps* 4HBT complexed with the inert substrate analog 4-hydroxyphenacyl-CoA revealed the same alignment of reaction center with catalytic residues as did the X-ray structure of the substrate (4-hydroxybenzoyl-CoA) complex with the catalytically inert *Ps* 4HBT mutant, in with the catalytic Asp17 was replaced with Asn. The structures of the liganded active sites revealed the following key features: (1) the Asp17 carboxylate group is in near-attack conformation relative the thioester C=O, (2) the thioester carbonyl is positioned for hydrogen bond formation with the backbone amide NH of the central α-helix N-terminal residue, (3) the thioester group is tightly encased such that there is room for a solvent molecule, (4) there is no polar residue in the vicinity of the thioester S atom to function in acid catalysis and (5) there is no polar residue in the correct position to function in base catalysis of the anhydride intermediate.

A

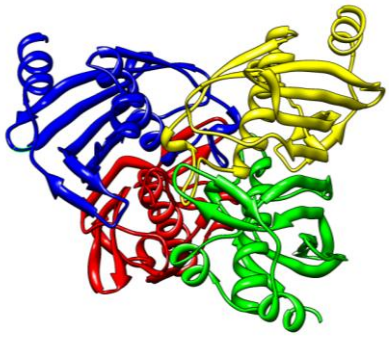

B

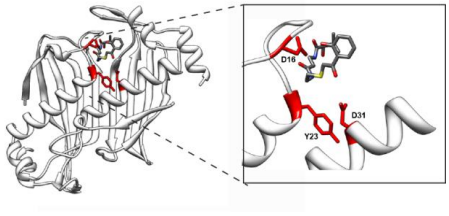

Figure 6.8. (A). The cartoon representation of the BH1999 tetramer with subunits colored green, yellow, red and blue. **(B)** The BH1999 dimer showing the truncated 2-hydroxyphenacyl-CoA ligand in grey stick and the Asp16 and Tyr23 in red stick. The Asp31 located on the opposing subunit (red stick), is conserved in the *Ps* 4HBT.

The alignment of BH1999 catalytic residues with the substrate thioester group suggested by the structure of BH1999 bound with the inert substrate analog 2-hydroxyphenacyl-CoA deviates from the pattern observed with *Ps* 4HBT. Specifically, whereas the catalytic scaffolds of the two thioesterases superimpose very well, the ligand 2-hydroxyphenacyl group does not align with the 4-hydroxyphenacyl group of the *Ps* 4HBT (Figure 6.2). The change in pose is stabilized by a network of hydrogen bonds formed with active site water molecules that function as bridges between ligand and active site residues. The C=O is pulled away from the Asp16 carboxylate group. This created the room for a solvent water molecule, which engages both oxygen atoms in hydrogen bond formation.

The BH1999 X-ray structure provides a snapshot of the active site which captured the Asp16 carboxylate group engaging a water molecule for attack at the thioester C=O as defined by inert substrate analog. This picture served as the starting point for the application of kinetic experiments that had been used earlier to demonstrate the catalytic mechanism of *Ps* 4HBT. The result of the transient kinetic test of the two-step pathway associated with Asp16 functioning in nucleophilic catalysis did not prove or disprove either mechanism. On the other hand, the chemical trapping experiment provides strong

evidence that the BH1999 catalyzed reaction is a two-step reaction in which Asp16 functions in nucleophilic catalysis.

References

1. Zhuang, Z., Latham, J., Song, F., Zhang, W., Trujillo, M., and Dunaway-Mariano, D. (2012) Investigation of the catalytic mechanism of the hotdog-fold enzyme superfamily Pseudomonas sp. strain CBS3 4-hydroxybenzoyl-CoA thioesterase., *Biochemistry 51*, 786-94.

2. Guo, Z.-F., Sun, Y., Zheng, S., and Guo, Z. (2009) Preferential hydrolysis of aberrant intermediates by the type II thioesterase in Escherichia coli nonribosomal enterobactin synthesis: substrate specificities and mutagenic studies on the active-site residues., *Biochemistry 48*, 1712-22.

3. Zhuang, Z., Song, F., Takami, H., and Dunaway-Mariano, D. (2004) The BH1999 Protein of Bacillus halodurans C-125 Is Gentisyl-Coenzyme A Thioesterase The BH1999 Protein of Bacillus halodurans C-125 Is Gentisyl-Coenzyme A Thioesterase, *Journal of Bacteriology 186*.

4. Wu, R., and of New Mexico, T. U. (2007) Domain Movement and Substrate Recognition in 4-chlorobenzoate: Coenzyme A Ligase from Alcaligenes Sp. Strain AL3007. The University of New Mexico.

5. Webster Jr., L. T., Mieyal, J. J., and Siddiqui, A. (1974) Benozyl and Hydroxybenzoyl Esters of Coenzyme A, *The Journal of Biological Chemistry 249*, 2641-2645.

6. Pickart, C. M., and Rose, A. (1986) Mechanism of Ubiquitin Carboxyl-terminal Hydrolase, *The Journal of Biological Chemistry 261*, 10210-10217.

APPENDIX

A.1 Published Collaborative Work

A1.1 Regioselectivity of Enzymatic and Photochemical Single Electron Transfer Promoted Carbon-Carbon Bond Fragmentation Reactions of Tetrameric Lignin Model Compounds

[a]Dae Won Cho[*], [a]John A. Latham, [b]Hea Jung Park, [b]Ung Chan Yoon, [c]Paul Langan, [a]Debra Dunaway-Mariano, [a]Patrick S. Mariano[*]

[a]Department of Chemistry and Chemical Biology, University of New Mexico, Albuquerque, New Mexico, 87131

[b]Department of Chemistry and Chemistry Institute for Functional Materials, Pusan National University, Busan 609-735, Korea

[c]Bioscience Division, Los Alamos National Laboratory Los Alamos, NM 87545, USA

Abstract

New types of tetrameric lignin model compounds, which contain the common β-O-4 and β-1 structural subunits found in natural lignins, have been prepared and carbon-carbon bond fragmentation reactions of their cation radicals, formed by photochemical (9,10-dicyanoanthracene) and enzymatic (lignin peroxidase) SET-promoted methods, have been explored. The results show that cation radical intermediates generated from the tetrameric model compounds undergo highly regioselective C-C bond cleavage in their β-1 subunits. The outcomes of these processes suggest that, independent of positive charge and odd electron distributions, cation radicals of lignins formed by SET to excited states of sensitizers or heme-iron centers in enzymes degrade selectively through bond cleavage reactions in β-1 *vs.* β-O-4 moieties. In addition, the findings made in the enzymatic studies demonstrate that the sterically large tetrameric lignin model compounds undergo lignin peroxidase catalyzed cleavage via a mechanism involving preliminary formation of an enzyme-substrate complex.

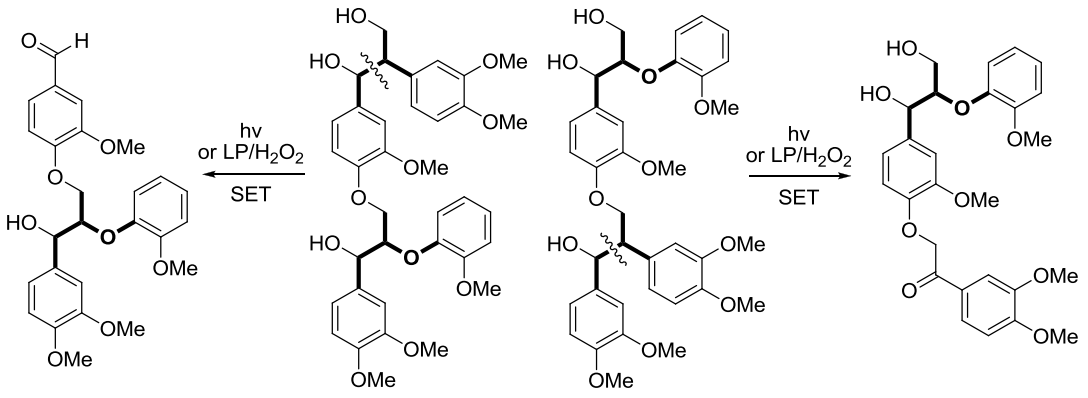

A.1.2 Investigation of the Catalytic Mechanism of the Hotdog-fold Enzyme Superfamily *Pseudomonas sp*. strain CBS3 4-Hydroxybenzoyl-CoA Thioesterase[+]

Zhihao Zhuang[1#], John Latham[1], Feng Song[1#], Wenhai Zhang[1#], Michael Trujillo[2#] and Debra Dunaway-Mariano[1*]

[1]Department of Chemistry and Chemical Biology, University of New Mexico, Albuquerque, NM 87131; [2]Scientific Laboratory Division, New Mexico Department of Health, Albuquerque, NM 87131

Abstract

The 4-hydroxybenzoyl-CoA (4-HB-CoA)[1] thioesterase from *Pseudomonas* sp strain CBS3 catalyzes the final step of the 4-chlorobenzoate degradation pathway, which is the hydrolysis of 4-hydroxybenzoyl-CoA (4-HB-CoA) to coenzyme A (CoA) and 4-hydroxybenzoate. In previous work, X-ray structural analysis of the substrate-bound thioesterase provided evidence for the role of an active site Asp17 in nucleophilic catalysis (Thoden, J. B., Holden, H. M., Zhuang, Z., Dunaway-Mariano, D. (2002) X-ray crystallographic analyses of inhibitor and substrate complexes of wild-type and mutant 4-hydroxybenzoyl-CoA thioesterase. *J. Biol. Chem. 277*, 27468-27476.). In the present study, kinetic techniques were used to test the catalytic mechanism that was suggested by the X-ray structural data. The time course for the multiple-turnover reaction of 50 μM

[^{14}C]4-HB-CoA catalyzed by 10 μM thioesterase supported a two-step pathway in which the second step is rate-limiting. Steady-state product inhibition studies revealed that CoA (K_{is} = 250 ± 70 μM, K_{ii} = 900 ± 300 μM) and 4-HB (K_{is} = 1.2 ± 0.2 mM) binding is weak, suggesting that product release is not rate-limiting. A substantial D_2O solvent kinetic isotope effect (3.8) on the steady-state k_{cat} value (18 s^{-1}) provided evidence that a chemical step involving proton transfer is the rate-limiting step. Taken together, the kinetic results support a two-chemical pathway. The microscopic rate constants governing the formation and consumption of the putative aspartyl17-(4-hydroxybenzoyl)anhydride intermediate were determined by simulation-based fitting of a kinetic model to time courses for the substrate binding reaction (5.0 μM 4-HB-CoA and 0.54 μM thioesterase), single-turnover reaction (5 μM [^{14}C]4-HB-CoA catalyzed by 50 μM thioesterase), steady-state reaction (5.2 μM 4-HB-CoA catalyzed by 0.003 μM thioesterase) and transient-state multiple-turnover reaction (50 μM [^{14}C]4-HB-CoA catalyzed by 10 μM thioesterase). Together with the results obtained from solvent ^{18}O-labeling experiments, the findings are interpreted as evidence for the formation of an aspartyl17-(4-hydroxybenzoyl)anhydride intermediate that undergoes rate-limiting hydrolytic cleavage at the hydroxybenzoyl carbonyl carbon atom.

A.2 Manuscript of Collaborative Work Submitted for Publication

A2.1 Regioselectivity of Enzymatic and Photochemical Single Electron Transfer Promoted Carbon-Carbon Bond Fragmentation Reactions of Tetrameric Lignin Model Compounds

[a]Dae Won Cho[*], [a]John A. Latham, [b]Hea Jung Park, [b]Ung Chan Yoon, [c]Paul Langan, [a]Debra Dunaway-Mariano, [a]Patrick S. Mariano[*]

[a]Department of Chemistry and Chemical Biology, University of New Mexico, Albuquerque, New Mexico, 87131

[b]Department of Chemistry and Chemistry Institute for Functional Materials, Pusan National University, Busan 609-735, Korea

[c]Bioscience Division, Los Alamos National Laboratory Los Alamos, NM 87545, USA

(daewon@unm.edu, mariano@unm.edu)

Introduction

The cellulose found in plant cell walls can be transformed to glucose, the starting materials for fermentation that efficiently yields bioethanol. However, a large barrier exists to accessing and hydrolytically cleaving cellulose in most plant materials, owing to its encasement in networks comprised of lignin. Lignin is a natural, heterogeneous

arylpropanoid polymer that is biosynthesized in plants in order to provide structural rigidity and prevent hydrolysis of cellulose and, thereby, to protect plants from external chemical and/or biological attack.[1,2] As a result, a large effort is underway to develop mild, non-energy-intensive and eco-friendly methods to bring about delignification of plant materials so that cellulose can be easily converted to glucose, the precursor of bioethanol.

One approach to delignification employs fungi (*eg.*, the white rot fungus *Phanerochaete chrysosporium*) that excrete iron-heme containing enzymes, such as lignin peroxidase (LP) and manganese peroxidase (MnP), which catalyze oxidation reactions that lead to cleavage of C-C bonds in lignin.[3] The cleavage reactions result in a decrease of the structural integrity and an increase in the permeability of the arylpropanoid polymer. The mechanistic pathway for LP induced degradation of lignin involves initial single electron transfer (SET) from the aromatic groups in the polymer to the doubly oxidized form of LP (*i.e.*, LP I) to generate lignin radical cations, which undergo carbon-carbon bond cleavage (Scheme 1).[4-13] An alternative route has been suggested that involves mediation by small molecules (*eg.*, veratryl alcohol) whose cation radicals formed by SET to LP I are responsible for one electron oxidation of lignin.

Studies are underway in our laboratory to gain fundamental information about how the composition of lignins might govern the efficiencies of delignification reactions that proceed via SET pathways. We believe that this information is potentially relevant to ethanol production

Scheme 1.

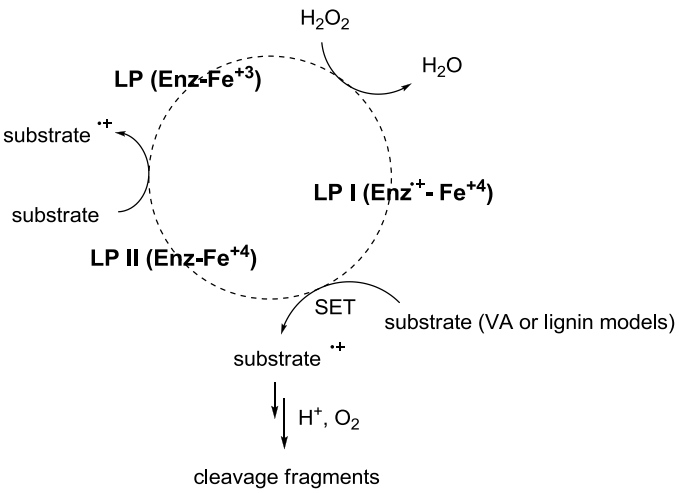

from plant materials[14,15] since it could provide a framework for the genetic design of plants[16,19] that have the type of lignin that are more readily cleaved by enzymatic or other oxidative processes. Prior to our efforts in this area, nothing was known about the C-C bond cleavage reactivity of sites in lignin where radical cation formation can take place. This is an extremely important issue since it is possible that SET from lignin to either LP I directly and/or to hole carrier mediator cation radicals produces a mixture of intermediates that differ in the site where the cation radical center exists and that these intermediates undergo rapid and reversible interconversion by an electron hopping mechanism. As we have shown in previous investigations,[20] in this event, the site(s) at which cation radical C-C bond cleavage takes place more rapidly will strongly influence the nature and overall efficiency of the lignin cleavage process.

In an earlier study,[21] information was gained about the efficiencies/rates of C-C bond cleavage of arylpropanoid units in lignin. For this purpose, SET photochemical, Ce(IV), and LP promoted oxidation reactions were carried out on dimeric lignin model compounds **1** and **4** that represent the β-1 (1,2-diarylpropanoid) and β-O-4 (1-aryl-2-aryloxypropanoid) groups that are present in the lignin skeleton (Scheme 2). The

observations made in that effort show that, regardless of the method used for their generation, cation radicals derived by SET oxidation of β-1 lignin model undergo C-C bond cleavage more rapidly than do those produced from β-O-4 model compounds.

Scheme 2.

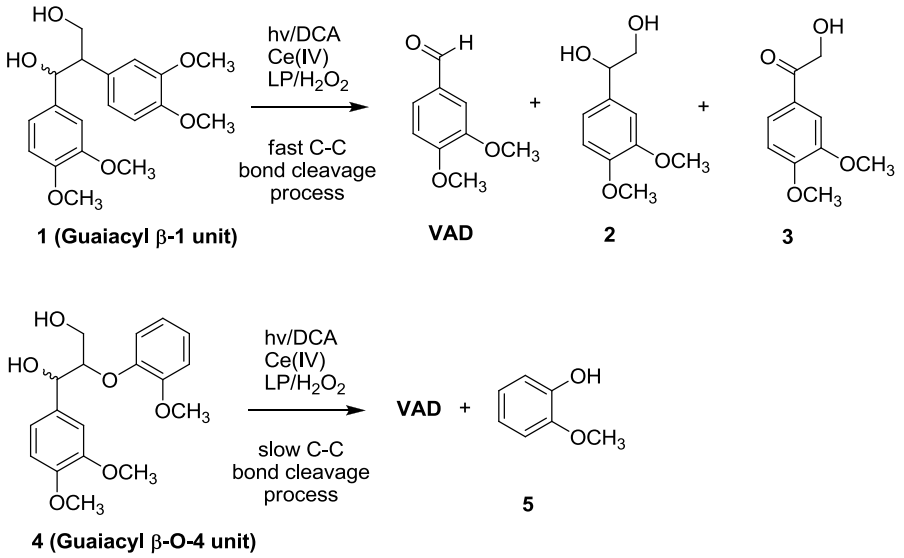

Another approach to assessing how structure governs the C-C bond cleavage reactivity of lignin cation radicals involves the use of the more complex lignin models. This approach was employed in an earlier study of trimeric lignin models by Baciocchi and his coworkers.[22] The results of that investigation showed that LP generated radical cations of trimeric models composed of two β-O-4 units degrade by C-C or benzyl C-H bond cleavage processes to give aldehyde and β-hydroxyketone products by pathways that mimic fragmentation patterns seen in dimeric model compounds. To our knowledge, no investigation has been conducted using more complex lignin models that contain different arylpropanoid units to assess the sites at which cation radical C-C bond cleavage takes place more efficiently.

As part of our continuing efforts in this area we have designed a study of SET-photochemical and LP-catalyzed reactions of tetrameric lignin model compounds that are comprised of both β-1 and β-O-4 moieties. We envisaged that analysis of products produced in low conversion reactions of these models would yield information about the relative rates of C-C bond cleavage in interconverting radical cations in which the charge and odd electron is distributed over β-1 and β-O-4 moieties. For example, if the β-1 > β-O-4 reactivity pattern observed in our earlier investigation with dimeric models is general, it is anticipated that cation radicals of mixed β-1 and β-O-4 tetrameric models will undergo predominant cleavage of 1,2-diaryl rather than 1-aryl-2-aryloxy C-C bonds.

To probe this feature, two tetrameric lignin model compounds, **6EE** and **7TE** (Scheme 3), in which β-1 and β-O-4 groups are connected via an ether linkage in a manner that mimics arylpropanoid arrays in the natural polymer, were prepared. Studies of the time courses of SET-promoted photochemical and LP enzymatic reactions of these substances were carried out. The results of this effort demonstrate that the most rapid reaction pathways followed by **6EE** and **7TE** involve C-C bond cleavage of β-1 units within their tetrameric skeletons. These findings along with observations made in probing the kinetics of the LP processes are described and discussed below.

Scheme 3.

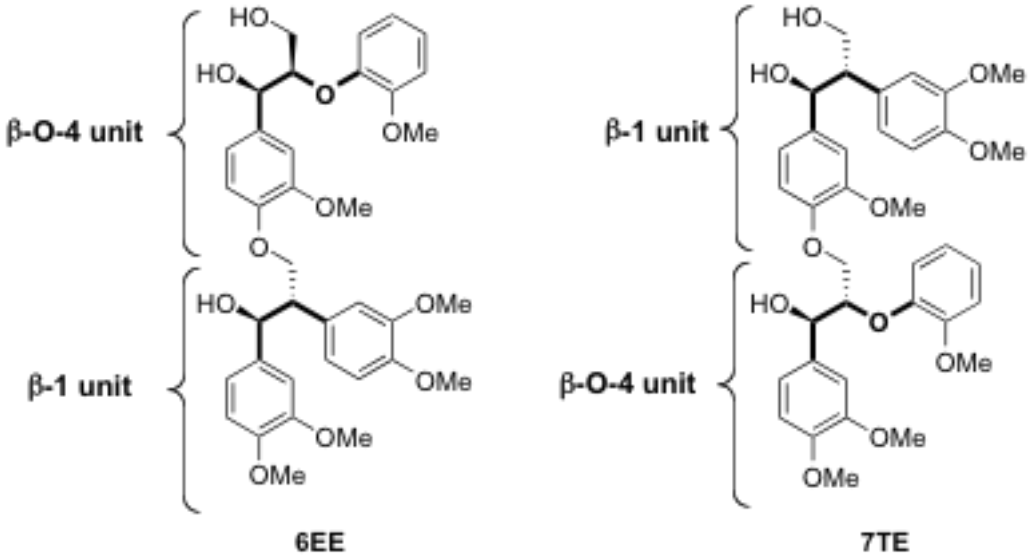

6EE **7TE**

Results

Synthesis of Tetrameric Lignin Models. A convergent strategy was used for the preparation of the tetrameric model compounds **6EE** and **7TE** (Scheme 4). The approach involves the preparation and coupling of the selectively protected, diastereomerically pure phenols **12E** and **16T** with the respective primary tosylates **23E** and **24E**. The synthesis of **12E** was initiated by aldol condensation of the aryloxyacetate **8** with the selectively protected veratraldehyde derivative **9** (Scheme 4). This process afforded a separable mixture of the diastereomeric esters **10T** and **10E**, the latter of which was treated with $LiAlH_4$ followed by acetonide protection of the resulting 1,3-diol to form the erythro phenol **12E**. A similar route beginning with the arylacetate **13** was employed to generate the threo phenolic acetonide **16T**. The stereochemical assignments to these substances were made by comparison of their spectroscopic properties with those previously reported for closely related compounds whose stereochemistry was determined by using X-ray crystallographic analysis.[21,23,24]

Scheme 4.

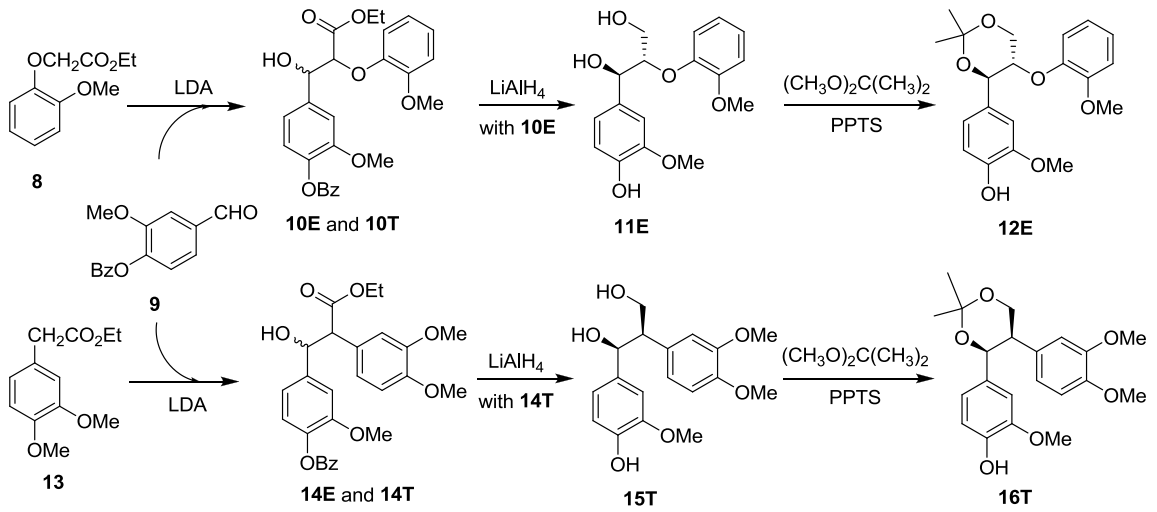

The tosylate coupling partners **23E** and **24E** were synthesized by using processes developed in our earlier effort[21] beginning with MOM protection of the erythro β-hydroxyesters **17E** and **18E**. The protected hydroxyesters were then transformed to the respective target tosylates **23E** and **24E** by sequential treatment with $LiAlH_4$ and *p*-toluenesulfonyl chloride (Scheme 5).

Scheme 5.

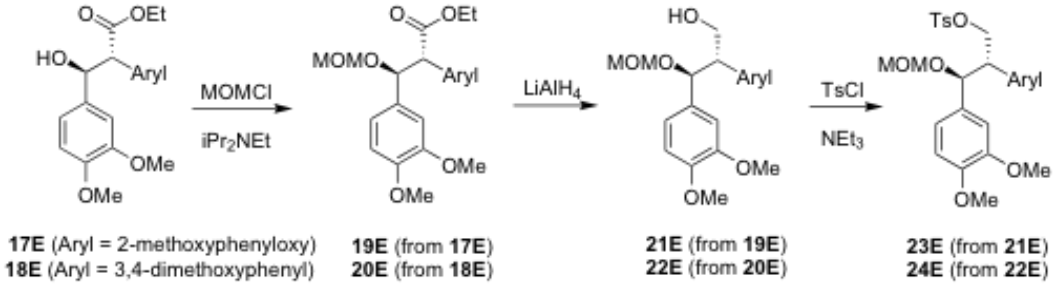

Scheme 6.

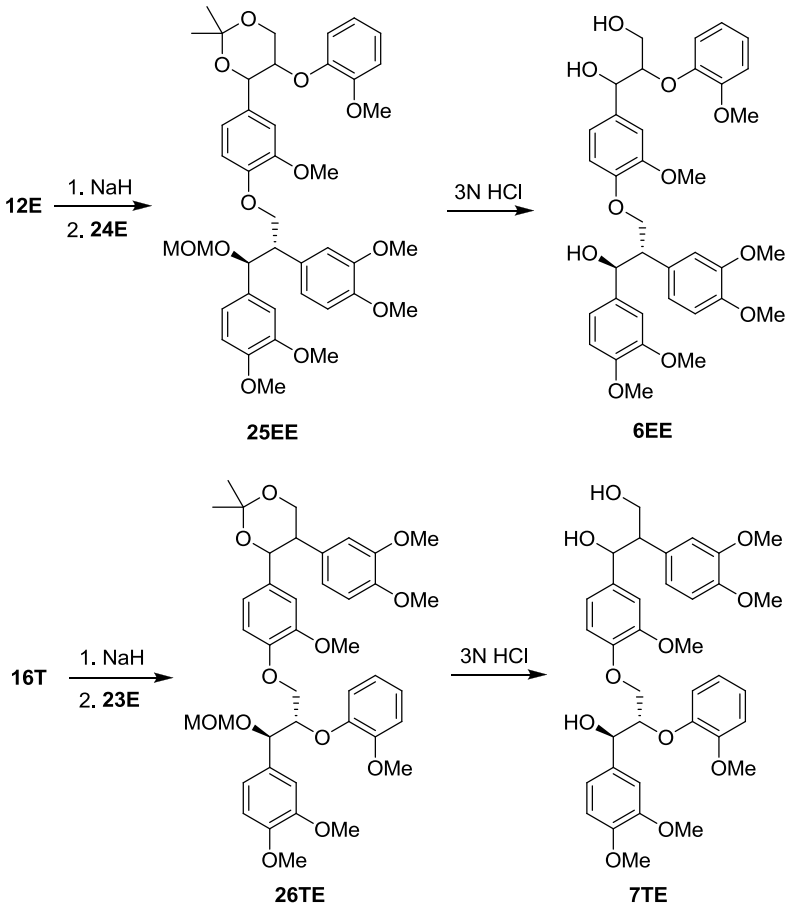

Preparation of the tetrameric lignin model compounds **6EE** and **7TE** was accomplished by using respective hetero-coupling reactions of the β-O-4 phenol **5E** with the β-1 tosylate

24E, and of the β-1 phenol **16T** with the β-O-4 tosylate **23E** (Scheme 6). These processes were promoted by treatment of the phenol derivatives with NaH. The products of these reactions, **25EE** and **26TE**, were then treated with 3*N* HCl to remove the acetonide and MOM protecting groups and furnish the desired tetrameric models **6EE** and **7TE**. Owing to the fact that enantiomeric mixtures of the phenol and tosylate subunits were used in the coupling reactions, **6EE** and **7TE** are produced as *ca.* 1:1 mixtures of inseparable diastereomers.

DCA-Promoted Photoreaction of Tetrameric Lignin Models. One method employed for the generation of cation radicals of the tetrameric lignin model compounds **6EE** and **7TE** involves SET-photosensitization with the acceptor 9,10-dicyanoanthracene (DCA). Prior to beginning photochemical studies, the oxidation potentials and rates of DCA fluorescence quenching were determined for **6EE** and **7TE** (see Supporting Information for fluorescence spectra and Stern-Volmer plots). The results of these experiments show that SET from tetrameric lignin models to the singlet excited state of DCA ($E_{1/2}$(-) DCA^{S1} = +2.8 V) is both predicted and observed to take place at diffusion controlled rates (Table 1).

Table 1. Oxidation potentials and DCA-fluorescence quenching rate constants of tetrameric models **6EE** and **7TE**.

Substrate	Oxidation Potentials $E_{1/2}$(+) (V *vs* Ag/AgCl)	DCA Fluorescence Quenching rate Constants k_q x 10^{-10} ($M^{-1}s^{-1}$)[a]
6EE	1.38	1.15
7TE	1.38	1.06

[a] τ_{DCA} = 14.9 ns

Photochemical reactions of **6EE** and **7TE** using DCA as the electron acceptor were performed on oxygenated 5% aqueous acetonitrile solutions. Inspection of the results displayed in Scheme 7 and Table 2 shows that low conversion (18%) SET-photochemical reaction of the β-O-4 (top) β-1 (bottom) tetramer **6EE** takes place cleanly to form nearly equal amounts of veratrylaldehyde (**VAD**) and aryloxyketone **27E**. In a similar manner,

DCA sensitized, low conversion (32%) photoreaction of the β-1 (top) β-O-4 (bottom) tetramer **7TE** in the presence of O_2 produces aldehyde **28E** as the major product along with minor amounts of **VAD** and the ketol **3** (Scheme 7 and Table 2).

Scheme 7.

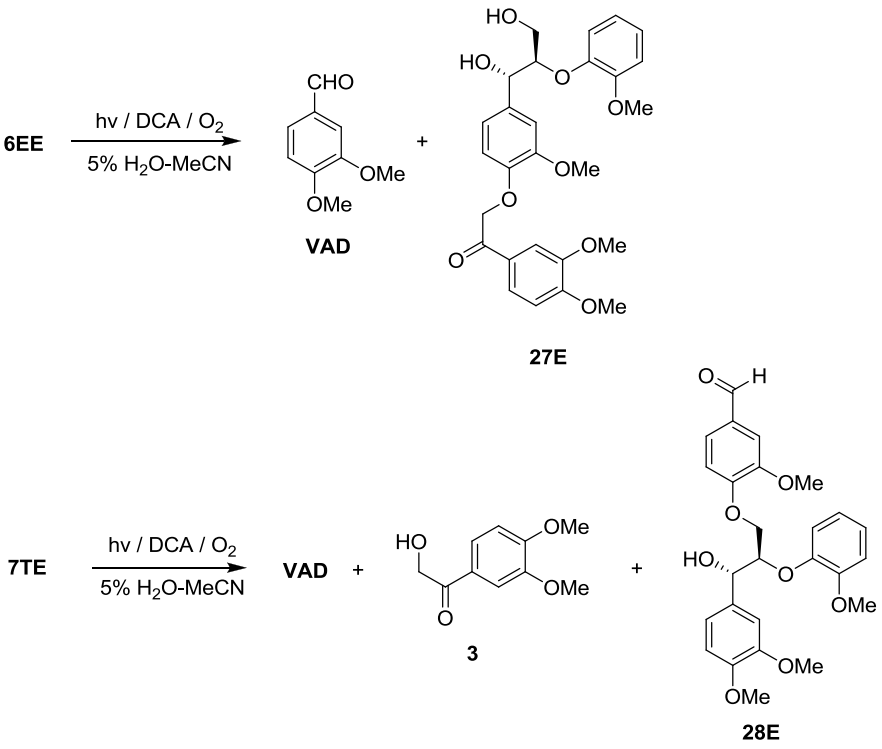

Table 2. Products and yields of DCA-promoted photoreactions of tetrameric models **6EE** and **7TE.**[a]

Substrate	Percent Conversion[b]	Product (Percent Yield)[c]			
		VAD	**27E**	**3**	**28E**
6EE	18	79	83	-	-
7TE	32	16	-	6	59

[a]Uranium glass filtered light irradiation (0.5 h) of O_2 satd 5% aq. MeCN solutions of DCA (0.27 mM) and substrate (0.22 mM of **6EE**, 0.46 mM of **7TE**). [b]Based on recovered substrates determined by HPLC analysis. [c]Determined by HPLC analysis and based on amounts of substrates reacted.

Structural assignments to photoproducts **27E** and **28E** were made by comparing their spectroscopic data to those of independently synthesized substances. The route employed to prepare ketone **27E** (Scheme 8) involves condensation of phenol **12E** and 3,4-dimethoxyphenacyl bromide to form the aryloxyketone **30E**. Removal of the acetonide protecting group then furnishes photoproduct **27E**. An authentic sample of the aldehyde photoproduct **28E** was produced by using a sequence starting with condensation of vanillin with tosylate **23E** to yield aldehyde **34E**, followed by MOM-deprotection (Scheme 9). Another possible product that could arise by cleavage of the β-1 C-C bond in tetrameric model **6EE** (see below) is the benzylic alcohol **31E**. This substance was independently prepared (Scheme 8) in order to unambiguously rule out its presence by inspection of the product mixture produced by DCA irradiation of **6EE**. Likewise, the aryloxyketone **32**, a possible product of β-O-4 C-C bond cleavage reaction of the initially formed photoproduct **27E**, produced by irradiation of **6EE**, was prepared (Scheme 8) to demonstrate that it does form in a secondary reaction. Finally, it is important to note that careful ^{1}H NMR and HPLC analysis of the crude mixtures arising by DCA promoted photoreactions of **6EE** and **7TE** failed to reveal the presence of products other than those displayed in Scheme 7.

Scheme 8.

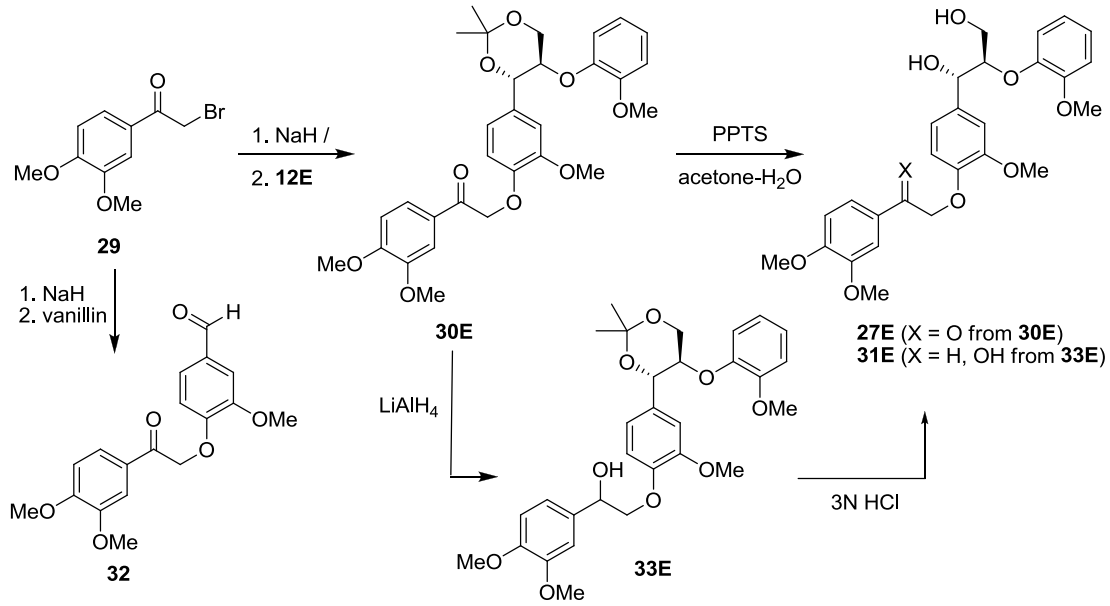

Scheme 9.

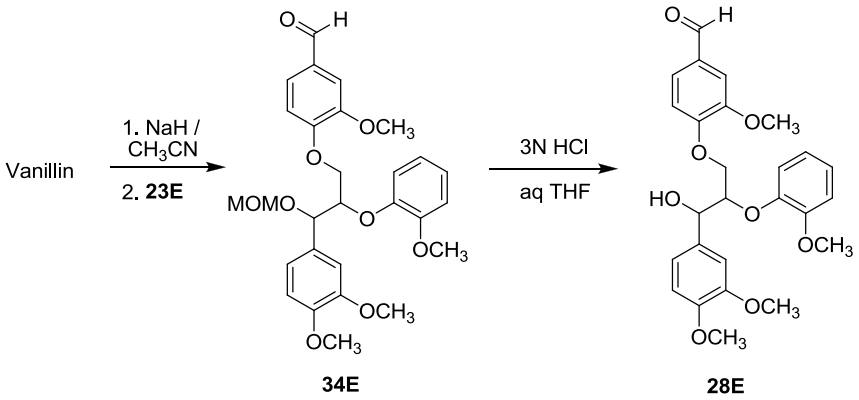

Monitoring product distributions generated in the DCA-sensitized photoreactions of **6EE** and **7TE** as a function of irradiation time gives more detailed information about preferences displayed in C-C bond cleavage processes (Figure 1). The time course of low conversion (<10%) reaction of **6EE** shows that C-C bond cleavage in the β-1 subunit takes place **e**xclusively to form **VAD** and ketone **27E** (Figure 1A). Thereafter, formation of **VAD** increases continuously but production of **27E** reaches a maximum at *ca.* 50% conversion of tetramer **6EE**. This observation suggests that both reactant **6EE** and

fragment **27E** undergo SET-induced photoreactions that generate **VAD,** as the only detectable product in the latter case. Importantly, even though secondary SET reaction of **27E** might have been expected to undergo β-O-4 C-C bond cleavage, ketone **32** that would have formed by such a pathway is not observed (see above).

Study of the time dependence of the product distributions in photoreaction of the tetrameric model **7TE** (Figure 1B) showed that at low conversion (<40%), **28E**, **VAD** and ketol **3** were formed in ratios that were invariant with time. At higher conversions, the initially formed β-1 C-C bond cleavage product **28E** slowly disappears while the amount of **VAD** gradually increases.

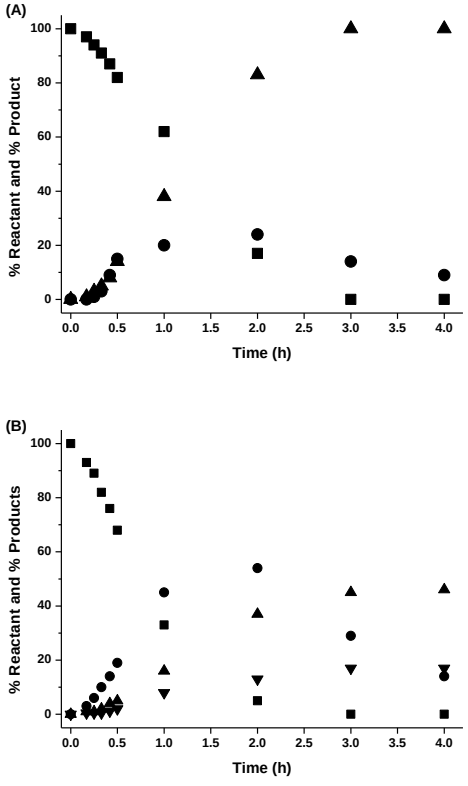

Figure 1. Plots of percentages of reactants remaining (**6EE** and **7TE** (■)) and products formed (**VAD** (▲) and **27E** (●), and **VAD** (▲)**, 3** (▼) and **28E** (●) in DCA-promoted photoreactions of **6EE** (A) and **7TE** (B) in O_2 saturated conditions as functions of irradiation times.

A brief study was carried out to explore the reactivity of the ketone **27E**, a product of SET-induced cleavage of **6EE**. Irradiation of a DCA and O_2 saturated solution of this substance in 5% aqueous MeCN with Uranium glass filtered light leads to clean production of the acetophenone derivative **35** (10%) and 1,4-diketone **36**[25] (70%) (Scheme 10). This process appears to be initiated by direct excitation of **27E**, which absorbs light, albeit weakly, in the wavelength region transmitted by the Uranium glass filter, followed by documented[25] α-aryloxyketone homolytic cleavage. The α–acyl radical produced in this manner undergoes H-atom abstraction and coupling to form the respective products **35** and **36**.

Scheme 10.

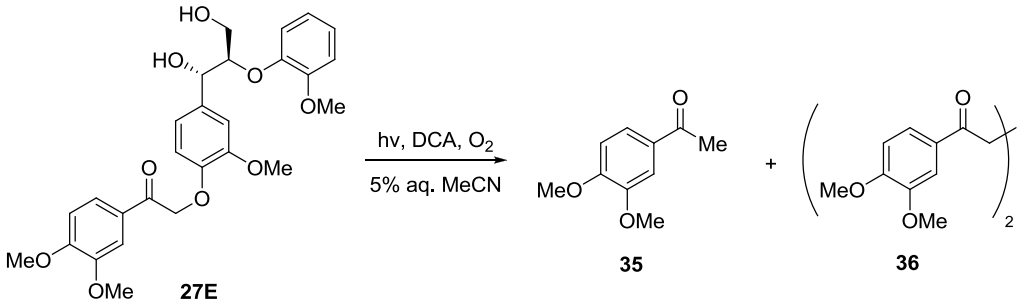

The observation that **VAD** and ketol **3** are generated in the C-C bond cleavage reaction of the β-1 unit in **7TE** is interesting since these substances would need to arise via a radical intermediate produced in this process or through secondary reaction of the initially formed diol **2**, which we have observed earlier[21] as a minor product in reactions of related β-1 model compounds. To explore the latter possibility, diol **2** was subjected to the DCA-sensitized photochemical reaction conditions. As shown in Scheme 11, under these conditions **2** is efficiently converted to **VAD** and ketol **3**.

Enzymatic Reactions of Tetrameric Lignin Model Compounds. Low conversion, lignin peroxidase catalyzed reactions of **6EE** and **7TE** initiated by H_2O_2 were performed

in tartrate buffer solutions (pH 3.4) containing 17% acetonitrile. HPLC analysis of the product mixtures

Scheme 11.

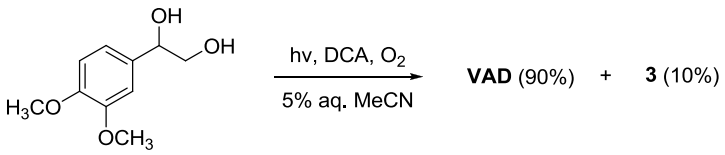

2

provided the results listed in Table 3. As can be seen by viewing the data, the LP-catalyzed reaction generate the same products in the same relative yields as those arising from DCA-promoted photoreactions of **6EE** and **7TE** by way of selective C-C bond cleavage in the β-1 unit.

Table 3. LP-catalyzed reaction of tetramers **6EE** and **7TE**

Substrate	Percent Conversion[a.b]	Products (Percent Yield)[c]		
		VAD	**27E**	**28E**	**3**
6EE	16	100	13	-	-
6EE	31	81	26	-	-
7TE	7	14	-	57	-
7TE	18	22	-	67	6

[a] LP (8 μM), **6EE** and **7TE (**0.2 mM), and H_2O_2 (1.2 mM) in 17% MeCN-buffer solution (pH 3.4) were used. [a] Percent conversion based on recovered substrate determined by HPLC analysis. [c]Determined by HPLC and based on amounts of substrates reacted.

Steady state kinetic constants for the LP catalyzed bond cleavage reactions of **6EE** and **7TE** were determined. As can be seen by the results displayed in Figure 2A, **6EE** and **7TE** form complexes with LP, in which SET takes place to produce cation radicals that undergo β-1 bond breaking. Comparing the k_{cat} values of the LP catalyzed reaction with

6EE and **7TE** shows that both substances react at about the same rate a 2-fold rate increase for the **6EE** compound. However, regardless of the K_M and k_{cat} differences between **6EE** and **7TE**, their catalytic efficiencies (k_{cat}/K_M) are approximately the same. Furthermore, in agreement to previously reported results by other groups,[22,26,27] the catalytic efficiency is influenced by the size of the lignin model compounds. Specifically, the tetrameric models have lower catalytic efficiencies than dimeric models as compared to our previous studies.[21]

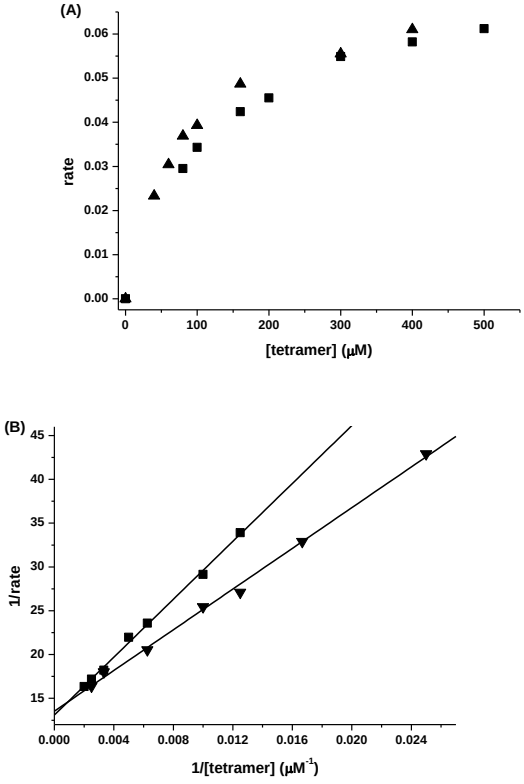

Figure 2. Plots of the (A) rate *vs*. tetrameric model concentrations in LP catalyzed reactions of **6EE** (▪) and **7TE** (▾), and (B) Lineweaver Burke plots of the reciprocals of rates *vs*. reciprocals of concentration of **6EE** (▪) and **7TE** (▾).

.

Table 4. Steady state kinetic constants of the LP-catalyzed reaction of tetramers **6EE** and **7TE**.[a]

Substrate	k_{cat} (s^{-1})	K_M (μM)	k_{cat}/K_M ($M^{-1}s^{-1}$)
6EE	0.39±0.01	130	3.0×10^3
7TE	0.30±0.01	80	3.8×10^3

[a] 20-300 μM substrates in 25% MeCN-tartrate buffer solution (50 mM, pH 3.4, 25°C), 0.26 μM of LP, 50 μM H_2O_2 were used.

Conclusions

As stated in the Introduction, one of the major hurdles that needs to be surmounted in the conversion of plant materials to ethanol is related to the development of efficient and low energy requiring pretreatment methods that facilitate access of cellulase enzymes to cellulose that is encased in lignin networks in plant cell walls. An interesting approach to this problem relies on the use of microbial or enzyme based lignin degradation processes. It is known that wood rotting fungi (*eg.*, the white rot fungus *Phanerochaete chrysosporum*) secrete enzymes like LP that catalyze depolymerization of lignin[3] through SET-promoted C-C bond cleavage pathways. Being a complex heterogeneous polymer, lignin is comprised of several major types of dimeric structural units containing propanoid moieties with 1-aryl-2-aryloxy (β-O-4), 1,2-diaryl (β-1), benzofuran (β-5) and spirodienone structural frameworks (see below). It should be noted that the β-5 unit is a cyclized form of the β-1 structure and that spirodienone units[28] likely convert to β-1 moieties under the highly acidic conditions present in LP containing secretions of wood rotting the fungi.

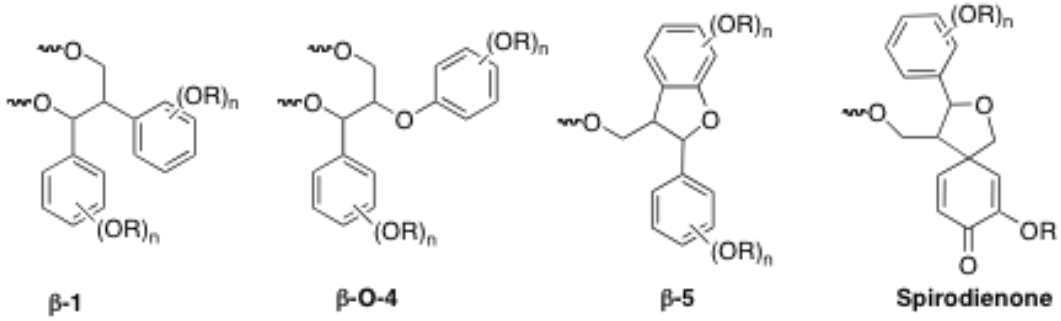

Cation radicals arising by SET from alkoxyaryl sites in lignin to the oxidized form of LP (termed LP I) are believed to undergo C-C bond cleavage to generate cation and radical intermediates, the latter of which are further oxidized under aerobic conditions. It is highly probable that the lignin cation radicals are comprised of a mixture of potentially rapidly interconverting species that differ in the location of the arene ring delocalized positively charged radical centers. As we have demonstrated in earlier studies[20] with more simple polydonor derived cation radicals, the sites at which bond cleavage reactions take place more rapidly in systems of this type is governed by the rates of the processes and not the relative populations of the interconverting species. An example taken from this earlier effort that demonstrates this principle is found in the SET promoted photochemical reaction of the thioether linked, α-silymethansulfonamide terminated phthalimide **37** (Scheme 12). In this system, SET from the two possible heteroatom donor sites to the phthalimide excited state gives rise to two interconverting zwitterionic biradicals **38** and **39**, whose population is governed by differences in the oxidation potentials of the thioether (*ca.* +1.4 V)[29] and sulfonamide (*ca.* +2.5 V).[30] As a result, **38** is heavily favored at equilibrium. However, as product yield determinations show, the exclusive reaction pathway followed involves α-desilylation of **39** to form biradical **41**, which then undergoes cyclization to yield **40**. Thus, the much larger rate of methanol

promoted α-desilylation at the methansulfonamide cation radical site *vs.* α-deprotonation at the thioether cation radical site is the major factor controlling the nature of the SET process.[31]

Scheme 12.

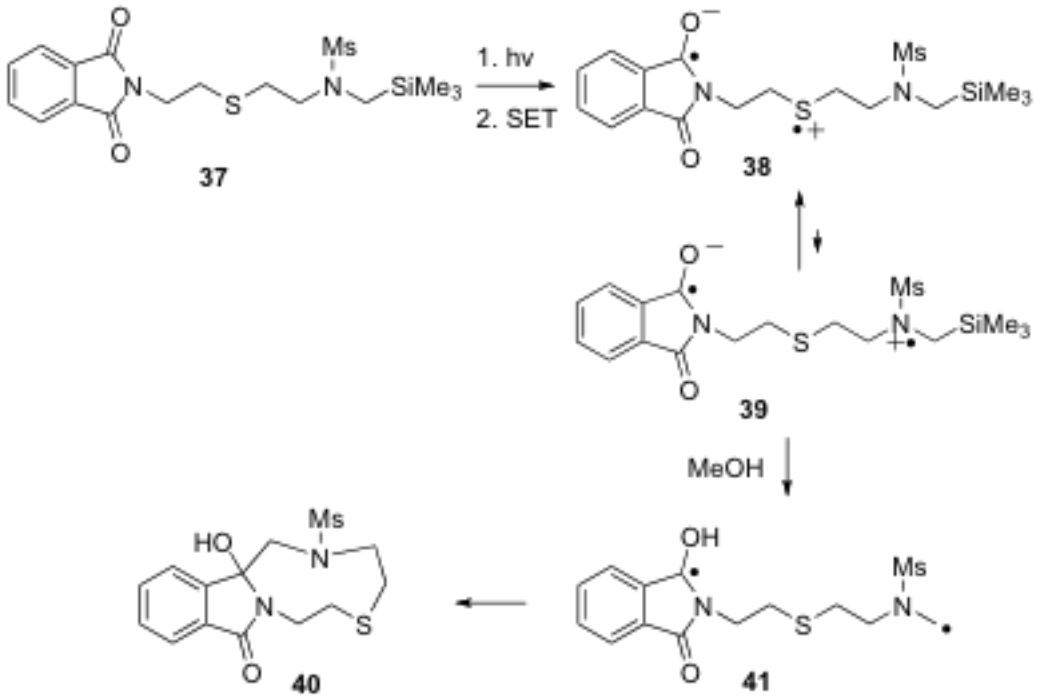

An example in which the rates of bond cleavage are important in governing product profiles of reactions proceeding through the intermediacy of competitively formed cation radicals that arise by SET from sites of differing oxidation potential, is found in studies by Baciocchi and his coworkers.[22] Specifically the major product produced in LP promoted reaction of the tetrameric lignin model **42** (Scheme 13) is aldehyde **43**, formed by C-C bond cleavage at the monoalkoxy substituted β-O-4 center, which in contrast to the dialkoxy substituted unit, has a higher oxidation potential.

Scheme 13.

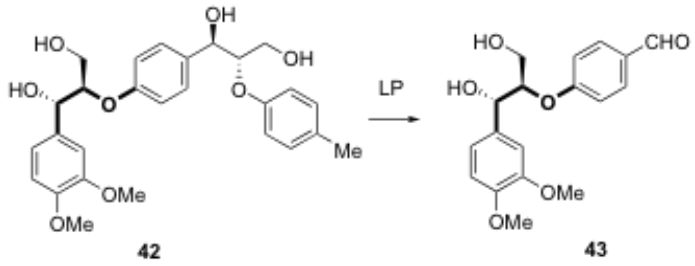

42 43

In the same manner, it is expected that preferences for C-C bond cleavage in reactions of lignin cation radicals will be governed by reactivity rather than population factors. In an earlier effort,[21] we probed reactions of cation radicals of simple dimeric lignin model compounds that possess either β-1 or β-O-4 structures that were generated by using DCA-photosensitized, CAN and LP initiated SET processes. The results showed that β-1 cation radicals undergo C-C bond cleavage at rates that far exceed those of their β-O-4 counterparts. We also determined that these findings are consistent with the results of DFT calculations, which indicate that the C1-C2 bond dissociation energies of β-1 cation radicals are significantly lower than those of similarly substituted β-O-4 analogs.

The major aim of the current effort was to determine if the reactivity profiles observed using dimeric models can be employed to predict the site(s) of C-C bond cleavage in more complex lignin cation radicals. For this purpose, the tetrameric models **6EE** and **7TE**, which contain both β-1 and β-O-4 units, were prepared and subjected to SET promoted reactions using DCA-photosensitization and LP catalysis. It is important to note that **6EE** and **7TE** contain an array of alkoxy-substituted arene rings that should have nearly the same oxidation potentials. As a result, cation radicals of these substances are expected to exist as mixtures of interconverting, near equal energy positively charged radical species (Scheme 14).

Scheme 14.

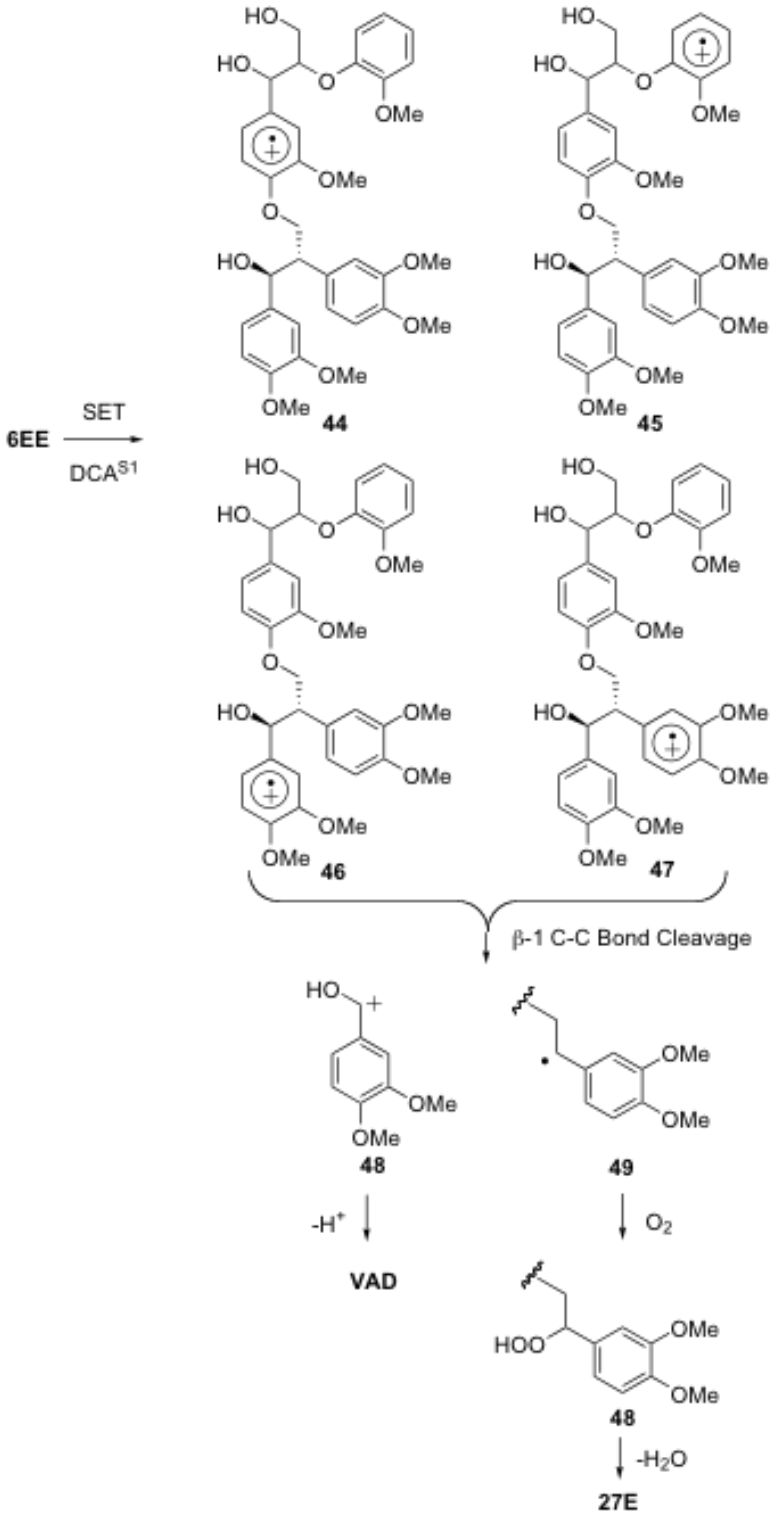
6EE
SET
DCA^S1
44
45
46
47
β-1 C-C Bond Cleavage
48
49
-H+
O2
VAD
48
-H2O
27E

Reaction Mechanism. The photosensitized reactions are initiated by SET from **6EE** and **7TE** to the singlet excited state of DCA, processes that take place at diffusion controlled rates as judged by the results of fluorescence quenching studies summarized in Table 1. Using **6EE** as an example, SET forms a mixture of four interconverting radical cations (**44**-**47**, Scheme 14) that differ in the arene ring where the odd electron and positive charge are localized. Two of the four cation radicals, **46** and **47**, are capable of undergoing β-1 type C-C bond cleavage to generate the cation radical pair **49**+**49**, while one (**42**) could undergo β-O-4 type bond cleavage. That the former reaction pathway dominates in the SET-photoreaction of **6EE** is reflected in the exclusive formation of **VAD** and α-aryloxyketone **27E**. **VAD** arises by deprotonation of cation **48** while **27E** is produced by reaction of radical **49** with oxygen followed by loss of water from the resulting hydroperoxide **50**. Importantly, the failure to detect substances that would have been formed by β-O-4 type C-C bond cleavage of cation radical **44** further evidences the exclusive operation of β-1 type cleavage in **6EE**.

In a similar fashion, β-1 C-C bond fragmentation in the cation radical arising from **7TE** leads to formation of the radical cation pair **51**+**52** (Scheme 15). The major products formed in this process are aldehyde **28E**, coming from proton loss from cation **52**, and ketol **3**, arising by oxygen capture of radical **51** followed by dehydration of the resulting hydroperoxide. The production of **VAD** in this process is interesting since this substance could arise by β-O-4 type cleavage. However, another reasonable route exists for the formation of **VAD** following β-1 C-C bond cleavage of the **7TE** cation radical. This proposal is based on the results of unpublished studies with unsymmetrically substituted dimeric β-1 lignin model compounds (Scheme 16), which show that cation radical C-C

bond cleavage gives aldehydes that originate from both aryl moieties. This observation suggests that the β-hydroxy-hydroperoxides **54** formed by oxygen addition to the C2 radical fragment **53**, are capable of undergoing retro-aldol type cleavage in competition with dehydration to yield aldehyde products. Thus, radical **51**, produced by cation radical β-1 bond fragmentation (Scheme 15) is likely one source of **VAD** in the DCA photosenstitized reaction of **7TE**.

Scheme 15.

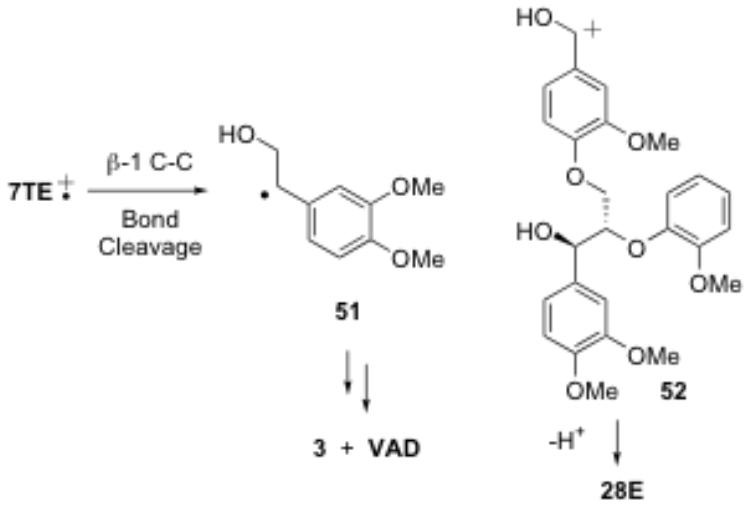

Scheme 16.

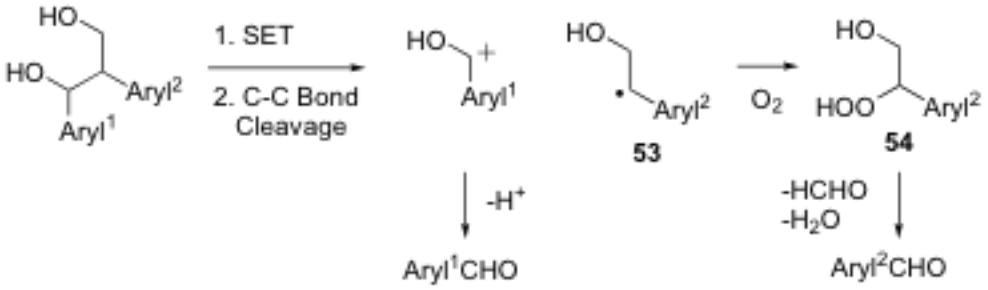

LP Catalyzed Processes. The outcomes of LP catalyzed reactions of tetrameric lignin models **6EE** and **7TE** are remarkably similar to those of the DCA-sensitized processes, despite the fact that the reactions are carried out under quite different conditions. For example, LP promoted reaction of **7TE**, occurring in pH 3 aq. tartrate

buffer containing 15% MeCN, produces a *ca.* 1:2.4-4 ratio of **VAD**+**3** and aldehyde **28E**. In contrast, a *ca.* 1:3 ratio of these products is generated in the DCA sensitized photoreaction in 5% aq. MeCN. Furthermore, although differences exist in the relative amounts of **VAD** and α-aryloxyketone **27E** formed in the photochemical (*ca.* 1:1) and LP (*ca.* 3-8:1) reactions of **6EE**, the reduced amount of **27E** generated in the former process is a likely consequence of its highly efficient photochemical reactivity (Scheme 10) and uv-spectroscopic properties (λmax 278 and 310 nm with absorption extending to 330 nm) that enable it to absorb light competitively with DCA under the photochemical reaction conditions. Very closely related direct irradiation reactions of 3,4-dimethoxyphenacyl phenol ethers have been observed to take place to generate the acetophenone derivative **35** and 1,4-diketone **36**. However, it is possible that a DCA SET sensitized reaction of **27E** is responsible for the formation of **35** and **36**.

The chemical mechanism of the LP catalyzed C-C bond cleavage reactions of **6EE** and **7TE** are the same as those for the DCA-sensitized processes. However, an interesting difference exists in the way the reactive cation radical intermediates are produced. In the photochemical process, SET occurs from the tertrameric substrates to the singlet excited state of DCA in a diffusion governed manner. However, as the kinetic data displayed in Figure 2 and Table 4 show, SET in the enzymatic reactions occurs in LP-substrate complexes. The K_M values for LP promoted reactions of **6EE** (130 μM) and **7TE** (80 μM) reflect reasonably tight binding of these substrates that resemble those for C-C bond cleavage of simple dimeric lignin model compounds (50-250 μM)[21] and for oxidation of the mono-arene ring containing substrate veratrylalcohol (72 μM).[6] It should be noted that, by using a resonant mirror biosensor system, it has been shown that a synthetic

lignin formed by polymerization of coniferyl alcohol binds reversibly to both LP and its oxidized form LP I with respective dissociation constants of 330 and 350 μM.[12] The k_{cat} values for LP catalyzed cleavage of **6EE** and **7TE** fall in the range of 0.3-0.4 s^{-1} and are approximately one order of magnitude smaller that those of simple β-1 dimeric model compounds (*ca.* 4-9 s^{-1}*).*[21]

Based on these observations, a plausible enzymatic mechanism for the β-1 C-C bond cleavage reactions involves SET in complexes of **6EE** and **7TE** with LPI. Since no structures of LP or LP I complexed with substrates or substrate analogs have been determined thus far, the exact manner in which the tetrameric models bind to LP I is not known. However, it is reasonable to expect that only one of the four arene rings of these substances is positioned close to the porphyrin-π-cation, which serves as the electron acceptor in LP I. The results of x-ray crystallographic studies conducted by Poulos and his coworkers[32] suggest that the heme moiety in LP is buried in the protein skeleton but modeling shows that the active site could accommodate the aromatic ring of verytrylalcohol. In addition, kinetic studies[33,34] have led to the conclusion that LP oxidizes natural lignins through a long range SET pathway much in the same way that cytochrome-c peroxidase oxidizes its substrates.[35,36] In any event, SET from the tetrameric models to LPI generates cation radicals that are initially localized in one arene ring but that can undergo delocalization by intramolecular SET. Two of the four possible cation radicals derived from either **6EE** or **7TE** (exemplified by **44** and **45** for **6EE** in Scheme 13) can participate in β-1 C-C bond fragmentation, whereas one of the other two (*eg.,* **42** for **6EE**) can only undergo less efficient β-O-4 cleavage. Since C-C bond cleavage in these cation radicals is expected to compete with back SET to regenerate LPI

and nonoxidized substrate, the fact that less- or un-reactive species comprise the mixture of cation radicals arising from **6EE** and **7TE** could be one of the reasons why the k_{cat} values for LP promoted reactions of the tetrameric substrates are lower than those for dimeric β-1 models in which all cation radicals are reactive.

Summary. The results of this effort have provided interesting information about the regioselectivities of C-C bond cleavage reactions of cation radical intermediates formed by SET from tetrameric lignin model compounds that contain both β-1 and β-O-4 structural units. The findings could be relevant to LP catalyzed reactions of natural lignins and, consequently, to the genetic design of plants that contain lignins that more efficiently undergo microbial and/or enzymatic delignification.

Experimental

General. All reagents were obtained from commercial sources and used without further purification and solvents were dried using standard procedures. ^{1}H and ^{13}C NMR (500 MHz) spectra were recorded on $CDCl_3$ solutions and the chemical shifts of resonances are reported in parts per million relative to $CHCl_3$ (7.24 ppm in ^{1}H-NMR, 77.0 ppm in ^{13}C-NMR) serving as an internal standard. HRMS data were obtained by using electrospray ionization or fast atom bombardment. Photochemical reactions were conducted with an apparatus consisting of a 450 W Hanovia medium vapor pressure mercury lamp surrounded by a uranium glass filter in water-cooled quartz immersion well and quartz glass tubes containing solutions of substrates in merry-go-round photoreactor. All products were isolated as oils unless otherwise specified and the purity of each was determined to be >90% by ^{1}H and ^{13}C NMR analysis. Column

chromatography was performed using 230–400 mesh silica gel. Identification of products from photochemical and enzymatic reactions was identified by comparing their spectroscopic and chromatographic properties with those of independently synthesized or commercially available compounds. Product yields were obtained by using HPLC analysis (a 4.6mm diameter Restek Ultra Aqueous C-18 reverse phase column with pore size 5μm, and a MeOH/H_2O gradient) based on calibration curves constructed by using known or synthesized substances.

Synthesis of *Erythro*-1-(4-hydroxy-3-methoxyphenyl)-2-(2-methoxyphenoxy)-1,3-diol Acetonide 12E.

Diastereomeric Ethyl 3-(4-(benzoyloxy)-3-(methoxyphenyl)-2-(2-methoxy-phenoxy)-3-hydroxypropionate (10E and **10T)**. A solution of diisopropylamine (4.6 mL, 32.8 mmol) in dry THF (40 mL) containing 13 mL (33 mmol) of 2.5 *M* nBuLi at -78 ^oC and stirred for 30 min. Acetate ester **8** (6.9 g, 32.8 mmol) was added dropwise and the resulting solution was stirred over for 1 h followed by addition of aldehyde **9** (7.0 g, 27.3 mmol). After 3 h additional stirring at the same temperature, the mixture was diluted with H_2O and extracted with EtOAc. The organic layer was dried and evaporated in *vacuo* to give a residue which was subjected to column chromatography (EtOAc:hexane 1:3) to yield erythro **10E** (3.2 g, 25 %) and threo **10T** (2.9 g, 20 %).

10E: ^{1}H-NMR ($CDCl_3$) 1.15 (t, 3H, *J* = 7.5 *Hz*), 3.80 (s, 3H), 3.84 (s, 3H), 4.13 (q, 2H, *J* = 7 *Hz*), 4.75 (d, 1H, *J* = 5 *Hz*), 5.21 (d, 1H, *J* = 5 *Hz*), 6.83-7.19 (m, 7H), 7.48 (t, 2H, *J* = 7.5 *Hz*), 7.61 (t, 1H, *J* = 7.5 *Hz*), 8.19 (d, 2H, *J* = 7.5 *Hz*); ^{13}C-NMR ($CDCl_3$) 14.0, 55.8, 55.9, 61.3, 73.7, 83.7, 111.3, 112.4, 119.1, 119.2, 121.1, 122.5, 124.0, 128.5,

129.5, 130.3, 133.4, 138.1, 139.7, 147.1, 150.6, 151.1, 164.6, 169.2; HRMS (ES) *m/z* 489.1515 (M+Na, $C_{26}H_{26}O_8Na$ requires 489.1525).

10T: ^{1}H-NMR ($CDCl_3$) 1.11 (t, 3H, *J* = 7 *Hz*), 3.80 (s, 3H), 3.85 (s, 3H), 4.08 (q, 2H, *J* = 7 *Hz*), 4.51 (d, 1H, *J* = 6.5 *Hz*), 5.13 (d, 1H, *J* = 7 *Hz*), 6.84-7.13 (m, 7H), 7.48 (t, 2H, *J* = 8 *Hz*), 7.61 (t, 1H, *J* = 7.5 *Hz*), 8.19 (d, 2H, *J* = 8 *Hz*); ^{13}C-NMR ($CDCl_3$) 13.8, 55.7, 55.9, 61.3, 74.7, 85.0, 111.2, 112.3, 118.3, 119.3, 121.0, 122.5, 123.9, 128.4, 129.3, 130.2, 133.3, 137.3, 139.9, 147.2, 150.3, 151.3, 164.5, 169.3; HRMS (ES) *m/z* 489.1522 (M+Na, $C_{26}H_{26}O_8Na$ requires 489.1525).

***Erythro*-1-(4-hydroxy-3-methoxyphenyl)-2-(2-methoxyphenoxy)-1,3-diol 11E**.[37] To solution of THF (50 mL) containing 1.0 *M* $LiAlH_4$ (7.0 mL, 7.0 mmol) was added **10E** (1.6 g, 3.4 mmol) at room temperature. After 3 h stirring, H_2O (20 mL) and 1 *N* HCl (20 mL) were added at 0 ^oC and the solution was extracted with CH_2Cl_2. The organic extracts were dried and concentrated in *vacuo* to give a residue which was subjected to column chromatography (EtOAc:hexane 1:1) to yield **11E** (0.8 g, 73 %). ^{1}H-NMR ($CDCl_3$) 3.64 and 3.89 (dd, 2H, *J* = 3.5 *Hz*, 12 *Hz*), 3.86 (s, 3H), 3.87 (s, 3H), 4.14 (m, 1H), 4.95 (d, 1H, *J* = 4.5 *Hz*), 5.58 (s, 1H), 6.80-7.06 (m, 7H).

***Erythro*-1-(4-hydroxy-3-methoxyphenyl)-2-(2-methoxyphenoxy)-1,3-diol Acetonide 12E**. A solution of **11E** (4.7 g, 14.7 mmol) in CH_2Cl_2 (80 mL) containing pyridinium p-toluenesulfonate (0.74 g, 3.0 mmol) and 2,2-dimethoxypropane (7.64 g, 73.4 mmol) was stirred at room temperature for 8 h and concentrated in *vauco* to give a residue which was portioned between CH_2Cl_2 and sat $NaHCO_3$. The organic layer was dried and concentrated in *vacuo* to give a residue, which was subjected to column chromatography (EtOAc:hexane 1:3) to yield **12E** (3.76 g, 71 %). ^{1}H-NMR ($CDCl_3$) 1.49

(s, 3H), 1.62 (s, 3H), 3.74 (s, 3H), 3.81 (s, 3H), 3.98-4.01 (m, 1H), 4.11-4.17 (m, 2H), 4.88 (d, 1H, *J* = 9 *Hz*), 5.55 (s, 1H), 6.48 (d, 1H, *J* = 8 *Hz*), 6.69 (t, 1H, *J* = 8 *Hz*), 6.77 (d, 1H, *J* = 8 *Hz*), 6.83-6.88 (m, 2H), 6.98 (s, 1H), 7.02 (d, 1H, *J* = 8 *Hz*); ^{13}C-NMR 19.6, 28.5, 55.7, 55.8, 62.9, 74.6, 99.4, 109.9, 112.1, 114.0, 117.4, 120.5, 120.8, 122.7, 131.1, 145.4, 146.2, 147.1, 150.4; HRMS (ES) *m/z* 397.1630 (M+Na, $C_{21}H_{26}O_6Na$ requires 397.1627).

Synthesis of *Erythro*-2-(2-methoxyphenoxy)-3-(3,4-dimethoxyphenyl)-3-methoxymethyloxy-1-tosyl propane 23E.

Ethyl *Erythro*-2-(2-methoxyphenoxy)-3-(3,4-dimethoxyphenyl)-3-methoxymethyloxypropionate 19E. A solution of the **17E**[21] (0.64 g, 1.7 mmol) in THF (40 mL) containing diisopropylethylamine (2.4 mL, 13.6 mmol) and methoxymethyl ether (2.7 g, 34 mmol) was stirred at room temperature for 15 h and concentrated in *vauco* to give a residue which was portioned between CH_2Cl_2 and H_2O. The organic layer was dried and concentrated in *vacuo* to give a residue, which was subjected to column chromatography (EtOAc:hexane 1:3) to yield **19E** (3.76 g, 71 %). ^{1}H-NMR ($CDCl_3$) 1.24 (t, 3H, *J* = 7 *Hz*), 3.31 (s, 3H), 3.71 (s, 3H), 3.85 (s, 3H), 3.86 (s, 3H), 4.22 (q, 2H, *J* = 7 *Hz*), 4.57 (s, 2H), 4.66 (d, 1H, *J* = 7.5 *Hz*), 5.03 (d, 1H, *J* = 7.5 *Hz*), 6.59 (d, 1H, *J* = 8 *Hz*), 6.72 (t, 1H, *J* = 7.5 *Hz*), 6.78-6.83 (m, 2H), 6.89 (t, 1H, *J* = 8 *Hz*), 7.00 (d, 1H, *J* = 8 *Hz*), 7.05 (s, 1H); ^{13}C-NMR ($CDCl_3$) 14.2, 55.7, 55.8, 61.2, 82.4, 93.9, 110.5, 111.0, 112.5, 117.3, 120.7, 120.8, 123.1, 129.8, 147.3, 148.7, 149.0, 150.4, 170.0; HRMS (ES) *m/z* 443.1689 (M+Na, $C_{22}H_{28}O_8Na$ requires 443.1682).

Ethyl *Erythro*-2-(2-methoxyphenoxy)-3-(3,4-dimethoxyphenyl)-3-methoxymethyloxy-1-propanol 21E. To solution of THF (50 mL) containing 1.0 *M*

$LiAlH_4$ (8.6 mL, 8.6 mmol) was added **19E** (3.6 g, 8.6 mmol) at room temperature. After 3 h stirring, H_2O (20 mL) and 1 *N* HCl (20 mL) were added at 0 ^oC and the solution was extracted with CH_2Cl_2. The organic extracts were dried and concentrated in *vacuo* to give a residue which was subjected to column chromatography (EtOAc:hexane 1:2) to yield **21E** (2.1 g, 66 %). ^{1}H-NMR ($CDCl_3$) 3.39 (s, 3H), 3.80 (s, 3H), 3.80 (s, 3H), 3.82 (s, 3H), 3.82-3.94 (m, 2H), 4.10-4.13 (m, 1H), 4.59 (s, 2H), 4.88 (d, 1H, *J* = 7 *Hz*), 6.54 (d, 1H, *J* = 8 *Hz*), 6.75 (t, 1H, *J* = 7.5 *Hz*), 6.83 (d, 2H, *J* = 8 *Hz*), 6.93-6.96 (m, 3H); ^{13}C-NMR ($CDCl_3$) 55.7, 55.8, 55.9, 61.4, 76.3, 87.0, 94.1, 110.5, 110.8, 112.0, 120.4, 120.5, 121.3, 123.6, 131.2, 147.6, 148.7, 148.9, 151.1; HRMS (ES) *m/z* 401.1578 (M+Na, $C_{20}H_{26}O_7Na$ requires 401.1576).

***Erythro*-2-(2-methoxyphenoxy)-3-(3,4-dimethoxyphenyl)-3-methoxymethyloxy-1-tosyl-propane 23E**. To solution of CH_2Cl_2 (70 mL) containing **21E** (3.67 g, 9.7 mmol) was added triethylamine (4.1 mL, 29.0 mmol) at 0 ^oC. After 1 h stirring, TsCl (2.8 g, 14.5 mmol) was added and the solution was stirred for 10 h at room temperature. The solution was extracted with CH_2Cl_2 and sat. $NaHCO_3$. The organic extracts were dried and concentrated in *vacuo* to give a residue which was subjected to column chromatography (EtOAc:hexane 1:2) to yield **23E** (3.7 g, 72 %). ^{1}H-NMR ($CDCl_3$) 2.40 (s, 3H), 3.31 (s, 3H), 3.67 (s, 3H), 3.80 (s, 3H), 3.84 (s, 3H), 4.30-4.33 (m, 1H), 4.37-4.40 (m, 1H), 4.45-4.48 (m, 1H), 4.52-4.56 (m, 2H), 4.84 (d, 1H, *J* = 6 *Hz*), 6.61 (d, 1H, *J* = 7 *Hz*), 6.70 (t, 1H, *J* = 7 *Hz*), 6.76 (d, 2H, *J* = 8 *Hz*), 6.84-6.90 (m, 3H), 7.24 (d, 2H, *J* = 8 *Hz*), 7.68 (d, 2H, *J* = 8 *Hz*); ^{13}C-NMR ($CDCl_3$) 21.6, 55.6, 55.8, 55.8, 55.9, 68.5, 76.2, 81.3, 94.4, 110.6, 110.7, 112.3, 118.8, 120.5, 120.8, 123.1, 128.0, 129.7, 129.8, 132.8, 144.6, 147.1, 148.8, 150.7; HRMS (ES) *m/z* 555.1666 (M+Na, $C_{27}H_{32}O_9NaS$ requires 555.1665).

Synthesis of *Erythro*-2,3-(3,4-dimethoxyphenyl)-3-methoxymethyloxy-1-tosylpropane 24E.

Ethyl *Erythro*-2,3-(dimethoxyphenyl)-3-methoxymethyloxypropionate 20E. A solution of the **18E**[21] (2.5 g, 6.4 mmol) in THF (40 mL) containing diisopropylethylamine (8.9 mL, 51.2 mmol) and methoxymethyl ether (10.3 g, 128.1 mmol) was stirred at room temperature for 15 h and concentrated in *vauco* to give a residue which was portioned between CH_2Cl_2 and H_2O. The organic layer was dried and concentrated in *vacuo* to give a residue, which was subjected to column chromatography (EtOAc:hexane 1:3) to yield **20E** (2.0 g, 72 %). ^{1}H-NMR ($CDCl_3$) 1.26 (t, 3H, *J* = 7 *Hz*), 3.34 (s, 3H), 3.72 (s, 3H), 3.73 (s, 3H), 3.75 (s, 3H), 3.76 (s, 3H), 3.84-3.86 (m, 1H), 4.11-4.16 (m, 1H), 4.21-4.26 (m, 1H), 4.51 (s, 2H), 5.03 (d, 1H, *J* = 10.5 *Hz*), 6.54-6.61 (m, 5H), 6.67 (s, 1H); ^{13}C-NMR ($CDCl_3$) 14.1, 55.7, 55.7, 55.9, 58.8, 60.9, 79.9, 94.0, 110.0, 110.3, 110.6, 111.5, 120.5, 121.2, 127.2, 130.6, 148.2, 148.4, 148.5, 148.6, 172.6; HRMS (ES) *m/z* 457.1837 (M+Na, $C_{23}H_{30}O_8Na$ requires 457.1838).

***Erythro*-2,3-(dimethoxyphenyl)-3-methoxymethyloxy-1-propanol 22E**. To solution of THF (50 mL) containing 1.0 *M* $LiAlH_4$ (4.9 mL, 4.9 mmol) was added **20E** (2.1 g, 4.8 mmol) at room temperature. After 3 h stirring, H_2O (20 mL) and 1 *N* HCl (20 mL) were added at 0 ^{o}C and the solution was extracted with CH_2Cl_2. The organic extracts were dried and concentrated in *vacuo* to give a residue which was subjected to column chromatography (EtOAc:hexane 1:1) to yield **22E** (1.05 g, 62 %). ^{1}H-NMR ($CDCl_3$) 3.04-3.07 (m, 1H), 3.43 (s, 3H), 3.71 (s, 3H), 3.74 (s, 3H), 3.78 (s, 3H), 3.79 (s, 3H), 3.91-3.96 (m, 1H), 4.15-4.19 (m, 1H), 4.49-4.53 (m, 2H), 4.78 (d, 1H, *J* = 10 *Hz*), 6.43 (s, 1H), 6.52-6.55 (m, 2H), 6.61-6.66 (m, 3H); ^{13}C-NMR ($CDCl_3$) 54.5, 55.7, 55.8, 56.0,

66.0, 82.0, 93.8, 110.0, 110.3, 110.9, 111.8, 120.3, 120.5, 131.5, 131.8, 147.7, 148.4, 148.5, 148.6; HRMS (ES) *m/z* 415.1735 (M+Na, $C_{21}H_{28}O_7Na$ requires 415.1733).

***Erythro* 2,3-(3,4-dimethoxyphenyl)-3-methoxymethyloxy-1-tosylpropane 24E**. To solution of CH_2Cl_2 (60 mL) containing **22E** (1.6 g, 4.1 mmol) was added triethylamine (1.7 mL, 12.2 mmol) at 0 ^oC. After 1 h stirring, TsCl (1.2 g, 6.1 mmol) was added and the solution was stirred for 10 h at room temperature. The solution was extracted with CH_2Cl_2 and sat. $NaHCO_3$. The organic extracts were dried and concentrated in *vacuo* to give a residue which was subjected to column chromatography (EtOAc:hexane 1:1) to yield **24E** (1.5 g, 66 %). ^{1}H-NMR ($CDCl_3$) 2.34 (s, 3H), 3.17-3.21 (m, 1H), 3.29 (s, 3H), 3.64 (s, 3H), 3.70 (s, 3H), 3.78 (s, 6H), 4.41-4.51 (m, 2H), 4.46 (s, 2H), 4.68 (d, 1H, *J* = 8.5 *Hz*), 6.33 (s, 1H), 6.39 (d, 1H, *J* = 7.5 *Hz*), 6.51-6.62 (m, 4H), 7.21 (d, 2H, *J* = 8 *Hz*), 7.57 (d, 2H, *J* = 8 *Hz*); ^{13}C-NMR ($CDCl_3$) 21.6, 51.2, 55.6, 55.7, 56.0, 70.7, 78.1, 94.0, 110.1, 110.3, 110.5, 111.7, 120.3, 121.2, 127.8, 129.6, 129.8, 131.0, 132.8, 144.5, 147.8, 148.3, 148.4, 148.5; HRMS (ES) *m/z* 569.1808 (M+Na, $C_{28}H_{34}O_9NaS$ requires 569.1821).

Synthesis of tetrameric model β-O-4 (top)-β-1 (bottom) 6EE.

Tetrameric model β-O-4 actonide (top)-β-1 MOM (bottom) 25EE. To solution of CH_3CN (60 mL) containing **12E** (3.9 g, 10.8 mmol) was added NaH (60 % in mineral oil) (450 mg, 11.3 mmol) at room temperature. After 1 h stirring at 80 ^oC, **24E** (3.94 g, 7.2 mmol) was added and the solution was stirred for 24 h at the same temperature. The solution was concentrated following extraction with CH_2Cl_2 and H_2O. The organic extracts were dried and concentrated in *vacuo* to give a residue which was subjected to column chromatography (EtOAc:hexane 1:1) to yield diastereomeric mixture **25EE** (2.54

g, 48 %). (diastereomeric mixture)**:** ^{1}H-NMR ($CDCl_3$) 1.49 (s, 3H), 1.62 (s, 3H), 3.22 (s, 3H), 3.32-3.36 (m, 1H), 3.66 (s, 3H), 3.72 (s, 6H), 3.74 (s, 3H), 3.76 (s, 3H), 3.78 (s, 3H), 3.98-4.01 (m, 1H), 4.08-4.17 (m, 2H), 4.23-4.25 (m, 1H), 4.46-4.50 (m, 1H), 4.50 (s, 2H), 4.88 (d, 1H, *J* = 8.5 *Hz*), 4.98-5.01 (m, 1H), 6.45 (d, 1H, *J* = 8 *Hz*), 6.51 (d, 1H, *J* = 8 *Hz*), 6.55 (s, 1H), 6.59-6.66 (m, 4H), 6.75-6.85 (m, 4H), 7.00 (s, 2H); ^{13}C-NMR ($CDCl_3$) 19.6, 28.5, 51.5, 55.6, 55.9, 62.8, 69.3, 74.5, 77.1, 78.1, 94.1, 99.4, 110.2, 110.4, 111.4, 112.0, 112.6, 113.1, 117.3, 117.4, 119.8, 119.9, 120.3, 121.4, 122.6, 131.7, 132.0, 147.0, 147.5, 148.1, 148.3, 149.4, 150.3; HRMS (ES) *m/z* 757.3195 (M+Na, $C_{41}H_{50}O_{12}Na$ requires 757.3200).

Tetrameric model β-1 (top)-β-O-4 (bottom) 6EE. To solution of THF (60 mL) containing **25EE** (1.2 g, 1.63 mmol) was added 3*N* HCl (20 mL) at room temperature and the solution was stirred for 12 h at the room temperature. The solution was concentrated following extraction with CH_2Cl_2 and 1*N* HCl. The organic extracts were dried and concentrated in *vacuo* to give a residue which was subjected to column chromatography (EtOAc:hexane 2:1) to yield diastereomeric mixture **6EE** (230 mg, 22 %). (diastereomeric mixture)**:** ^{1}H-NMR ($CDCl_3$) 3.32-3.36 (m, 1H), 3.69 (s, 3H), 3.72 (s, 3H), 3.77 (s, 3H), 3.78 (s, 3H), 3.85 (s, 6H), 3.85-3.91 (m, 1H), 4.11-4.17 (m, 2H), 4.28-4.31 (m, 1H), 4.41-4.43 (m, 1H), 4.94-4.97 (m, 1H), 5.18 (d, 1H, *J* = 5 *Hz*), 6.61-7.05 (m, 13H); ^{13}C-NMR ($CDCl_3$) 52.3, 55.6, 557, 55.8, 55.9, 60.6, 72.6, 77.5, 87.2, 109.5, 109.7, 110.4, 110.8, 112.1, 112.2, 114.1, 118.4, 119.1, 120.8, 121.6, 124.2, 131.7, 133.9, 135.1, 146.7, 147.8, 148.0, 148.1, 148.4, 148.4, 149.7, 151.5; HRMS (ES) *m/z* 673.2632 (M+Na, $C_{36}H_{42}O_{11}Na$ requires 673.2625).

Synthesis of tetrameric model β-1 (top)-β-O-4 (bottom) 7TE.

Tetrameric model β-1 acetonide (top)-β-O-4 MOM (bottom) 26TE. To solution of CH_3CN (60 mL) containing **16T** (1.34 g, 3.6 mmol) was added NaH (60 % in mineral oil) (143 mg, 3.6 mmol) at room temperature. After 1 h stirring at 80 ^oC, **23E** (1.6 g, 3.0 mmol) was added and the solution was stirred for 24 h at the same temperature. The solution was concentrated following extraction with CH_2Cl_2 and H_2O. The organic extracts were dried and concentrated in *vacuo* to give a residue which was subjected to column chromatography (EtOAc:hexane 1:1) to yield diastereomeric mixture **26TE** (1.2 g, 55 %). (diastereomeric mixture)**:** ^{1}H-NMR ($CDCl_3$) 1.62 (s, 3H), 1.64 (s, 3H), 3.30 (s, 3H), 3.49 and 3.51 (s, 3H), 3.65 and 3.66 (s, 3H), 3.75 (s, 6H), 3.77 and 3.78 (s, 3H), 3.83 (s, 3H), 3.75-3.78 (m, 1H), 4.08 (d, 1H, *J* = 7 *Hz*), 4.10-4.15 (m, 1H), 4.18-4.22 (m, 1H), 4.50-4.53 (m, 1H), 4.57-4.64 (m, 2H), 4.71-4.75 (m, 1H), 5.02 (d, 1H, *J* = 5 *Hz*), 5.28 (d, 1H, *J* = 3 *Hz*), 6.37 (d, 1H, *J* = 16.5 *Hz*), 6.50-6.61 (m, 4H), 6.76-6.78 (m, 3H), 6.86-6.98 (m, 4H), 7.10 (s, 1H); ^{13}C-NMR ($CDCl_3$) 18.8, 29.9, 45.0, 55.6, 55.8, 65.4, 67.9, 73.6, 82.0, 94.4, 99.3, 110.0, 110.4, 110.9, 112.1, 112.8, 112.9, 113.2, 118.2, 118.2, 120.5, 120.6, 120.7, 122.0, 122.3, 130.2, 130.3, 132.5, 133.5, 147.2, 147.3, 147.9, 147.9, 148.5, 148.6, 149.0, 150.6; HRMS (ES) *m/z* 757.3190 (M+Na, $C_{41}H_{50}O_{12}Na$ requires 757.3200).

Tetrameric model β-1 (top)-β-O-4 (bottom) 7TE. To solution of THF (60 mL) containing **26TE** (0.24 g, 0.33 mmol) was added 3*N* HCl (10 mL) at room temperature and the solution was stirred for 12 h at the room temperature. The solution was concentrated following extraction with CH_2Cl_2 and 1*N* HCl. The organic extracts were dried and concentrated in *vacuo* to give a residue which was subjected to column chromatography (EtOAc:hexane 2:1) to yield diastereomeric mixture **7TE** (43 mg, 21 %). (diastereomeric mixture)**:** ^{1}H-NMR ($CDCl_3$) 3.00-3.05 (m, 1H), 3.70 (s, 3H), 3.78, (s,

3H), 3.81 (s, 3H), 3.84 (s, 6H), 3.88 (s, 3H), 3.92-3.94 (m, 1H), 3.98-4.00 (m, 1H), 4.12-4.21 (m, 2H), 4.53-4.57 (m, 1H), 4.87-4.90 (m, 1H), 4.97-5.01 (m, 1H), 6.45-6.56 (m, 2H), 6.64-6.82 (m, 5H), 6.87-6.91 (m, 3H), 6.97-7.05 (m, 2H), 7.15-7.18 (m, 1H); ^{13}C-NMR ($CDCl_3$) 54.5, 55.4, 55.7, 55.8, 64.2, 66.3, 68.2, 68.3, 72.9, 75.6, 79.3, 84.8, 109.5, 110.0, 110.8, 111.0, 111.3, 112.1, 112.2, 118.7, 118.9, 120.4, 120.9, 121.1, 121.4, 123.9, 130.8, 132.1, 147.3, 147.6, 148.3, 148.6, 148.8, 149.0, 149.2, 149.5, 151.4; HRMS (ES) *m/z* 673.2628 (M+Na, $C_{36}H_{42}O_{11}Na$ requires 673.2625).

Synthesis of potential degradation products of tetrameric models compounds 27E, 28E, 31E and 32.

Compound 30E. To solution of CH_3CN (60 mL) containing **12E** (2.5 g, 6.94 mmol) was added NaH (60 % in mineral oil) (280 mg, 6.94 mmol) at room temperature. After 1 h stirring at 80 ^{o}C, **29** (2.7 g, 10.4 mmol) was added and the solution was stirred for 24 h at the same temperature. The solution was concentrated following extraction with CH_2Cl_2 and H_2O. The organic extracts were dried and concentrated in *vacuo* to give a residue which was subjected to column chromatography (EtOAc:hexane 1:3) to yield **30E** (2.1 g, 55 %). ^{1}H-NMR ($CDCl_3$) 1.45 (s, 3H), 1.61 (s, 3H), 3.71 (s, 3H), 3.82 (s, 3H), 3.90 (s, 3H), 3.93 (s, 3H), 3.95-4.01 (m, 1H), 4.10-4.12 (m, 1H), 4.12-4.16 (m, 2H), 4.88 (d, 1H, *J* = 8.5 *Hz*), 5.22 (s, 2H), 6.45 (d, 1H, *J* = 8 *Hz*), 6.66 (t, 1H, *J* = 7.5 *Hz*), 6.75-6.77 (m, 2H), 6.83-6.87 (m, 2H), 6.99 (d, 1H, *J* = 8.5 *Hz*), 7.03 (s, 1H), 7.56 (s, 1H), 7.63 (d, 1H, *J* = 8.5 *Hz*); ^{13}C-NMR ($CDCl_3$) 19.6, 28.5, 55.7, 55.8, 56.0, 56.1, 62.8, 72.1, 74.4, 99.4, 110.1, 110.4, 111.2, 112.0, 114.2, 117.4, 119.7, 120.7, 122.7, 122.8, 127.8, 133.4, 147.0, 147.2, 149.1, 149.3, 150.3, 153.7, 193.2; HRMS (ES) *m/z* 561.2098 (M+Na, $C_{30}H_{34}O_9Na$ requires 561.2101).

Compound 27E. A solution of **30E** (0.54 g, 1.0 mmol) in acetone:H_2O (v/v 3:2) 30 mL containing pyridinium *p*-toluenesulfonate (0.76 g, 3.0 mmol) was stirred at 80 ^oC for 10 h and concentrated in *vauco* to give a residue which was portioned between EtOAc and sat. $NaHCO_3$. The organic layer was dried and concentrated in *vacuo* to give a residue, which was subjected to column chromatography (EtOAc:hexane 1:1) to yield **27E** (0.38 g, 77 %). ^{1}H-NMR ($CDCl_3$) 3.62 (d, 1H, *J* = 12 *Hz*), 3.86 (s, 3H), 3.86-3.88 (m, 1H), 3.91 (s, 3H), 3.93 (s, 3H), 4.10-4.14 (m, 1H), 4.95 (d, 1H, *J* = 4 *Hz*), 5.26 (s, 2H), 6.76-6.81 (m, 2H), 6.87-6.94 (m, 4H), 6.98 (s, 1H), 7.03-7.06 (m, 1H), 7.56(s, 1H), 7.64 (d, 1H, *J* = 8.5 *Hz*); ^{13}C-NMR ($CDCl_3$) 55.9, 56.0, 56.1, 60.7, 72.0, 72.6, 87.4, 109.9, 110.1, 110.3, 112.1, 114.3, 118.3, 121.2, 121.6, 122.7, 124.3, 127.7, 133.9, 146.8, 146.9, 149.2, 149.7, 151.6, 153.8, 193.1; HRMS (ES) *m/z* 521.1799 (M+Na, $C_{27}H_{30}O_9Na$ requires 521.1788).

Compound 33E. To solution of 50 mL THF containing 1.0 *M* $LiAlH_4$ (4.0 mL, 4.0 mmol) were added **30E** (2.0 g, 3.7 mmol) at room temperature. After stirring for 3 h, 20 mL H_2O and 20 mL 1 *N* HCl solution at 0 ^oC were added and the solutions were extracted with CH_2Cl_2. The extracts were dried and concentrated in *vacuo* to afford a residue which was subjected to column chromatography (EtOAc:hexane 1:2) to yield **33E** (1.52 g, 76 %). ^{1}H-NMR ($CDCl_3$) 1.50 (s, 3H), 1.62 (s, 3H), 3.74 (s, 3H), 3.82 (s, 3H), 3.85 (s, 3H), 3.87 (s, 3H), 3.88-3.93 (m, 1H), 4.00-4.02 (m, 1H), 4.08-4.10 (m, 1H), 4.11-4.18 (m, 2H), 4.91 (d, 1H, *J* = 9 *Hz*), 4.98 (d, 1H, *J* = 7.5 *Hz*), 6.47 (d, 1H, *J* = 6.5 *Hz*), 6.69 (t, 1H, *J* = 7.5 *Hz*), 6.77 (d, 1H, *J* = 8.5 *Hz*), 6.82-6.90 (m, 4H), 6.96 (s, 1H), 7.04-7.06 (m, 2H); ^{13}C-NMR ($CDCl_3$) 19.6, 25.6, 28.5, 55.7, 55.8, 55.8, 55.9, 62.8, 68.0, 71.9, 74.4, 76.6, 99.5, 109.3, 110.9, 111.1, 111.2, 112.1, 115.8, 115.9, 117.3, 118.5, 119.9, 120.0, 120.7, 122.7,

132.0, 133.7, 147.0, 147.6, 147.6, 148.7, 149.0, 149.8, 150.3; HRMS (ES) *m/z* 563.2262 (M+Na, $C_{30}H_{36}O_9Na$ requires 563.2257).

Compound 31E. A solution of **33E** (1.54 g, 2.85 mmol) in acetone:H_2O (v/v 3:2) 80 mL containing pyridinium *p*-toluenesulfonate (2.15 g, 8.6 mmol) was stirred at 80 ^oC for 24 h and concentrated in *vauco* to give a residue which was portioned between EtOAc and sat. $NaHCO_3$. The organic layer was dried and concentrated in *vacuo* to give a residue, which was subjected to column chromatography (EtOAc:hexane 1:1) to yield **31E** (1.15 g, 81 %). ^{1}H-NMR ($CDCl_3$) 3.62 (dd, 1H, *J* = 3 *Hz*, 12.5 *Hz*), 3.84 (s, 3H), 3.85 (s, 3H), 3.86 (s, 3H), 3.87 (s, 3H), 3.89-3.91 (m, 1H), 3.94 (dd, 1H, *J* = 4 *Hz*, 10 *Hz*), 4.09-4.14 (m, 2H), 4.96 (d, 1H, *J* = 5 *Hz*), 5.02 (d, 1H, *J* = 9.5 *Hz*), 6.82-7.06 (m, 10H); ^{13}C-NMR ($CDCl_3$) 55.8, 55.9, 60.6, 72.0, 72.5, 76.2, 87.3, 109.3, 109.7, 111.0, 112.1, 115.3, 118.6, 121.0, 121.6, 124.3, 132.1, 134.1, 146.7, 147.3, 148.7, 149.0, 149.9, 151.6; HRMS (ES) *m/z* 523.1942 (M+Na, $C_{27}H_{32}O_9Na$ requires 523.1944).

Compound 34E. To solution of CH_3CN (50 mL) containing vanillin (0.4 g, 2.6 mmol) was added NaH (60 % in mineral oil) (105 mg, 2.6 mmol) at room temperature. After 1 h stirring at 80 ^oC, **23E** (0.93 g, 1.75 mmol) was added and the solution was stirred for 24 h at the same temperature. The solution was concentrated following extraction with CH_2Cl_2 and H_2O. The organic extracts were dried and concentrated in *vacuo* to give a residue which was subjected to column chromatography (EtOAc:hexane 1:3) to yield **34E** (680 mg, 76 %). ^{1}H-NMR ($CDCl_3$) 3.34 (s, 3H), 3.68 (s, 3H), 3.79 (s, 3H), 3.83 (s, 3H), 3.85 (s, 3H), 4.34-4.37 (m, 1H), 4.42-4.45 (m, 1H), 4.65 (dd, 2H, *J* = 7 *Hz*, 26.3 *Hz*), 4.75-4.78 (m, 1H), 5.08 (d, 1H, *J* = 5 *Hz*), 6.80 (d, 3H, *J* = 8 *Hz*), 6.89-6.96 (m, 5H), 7.35-7.37 (m, 2H); ^{13}C-NMR ($CDCl_3$) 55.6, 55.7, 55.8, 68.0, 82.4, 94.6, 109.2,

110.6, 111.8, 112.1, 118.8, 120.3, 120.8, 122.8, 126.6, 130.1, 130.2, 147.8, 148.7, 148.8, 150.0, 150.8, 153.9190.9; HRMS (ES) *m/z* 535.1935 (M+Na, $C_{28}H_{32}O_9Na$ requires 535.1944).

Compound 28E. To solution of THF (60 mL) containing **34E** (0.64 g, 1.2 mmol) was added 3*N* HCl (10 mL) at room temperature and the solution was stirred for 12 h at the room temperature. The solution was concentrated following extraction with CH_2Cl_2 and 1*N* HCl. The organic extracts were dried and concentrated in *vacuo* to give a residue which was subjected to column chromatography (EtOAc:hexane 2:1) to yield diastereomeric mixture **28E** (240 mg, 43 %). ^{1}H-NMR ($CDCl_3$) 3.79 (s, 3H), 3.84 (s, 3H), 3.86 (s, 3H), 3.87 (s, 3H), 4.11-4.14 (m, 1H), 4.30-4.33 (m, 1H), 4.61-4.64 (m, 1H), 5.02 (d , 1H, *J* = 3.5 *Hz*), 6.79-6.83 (m, 2H), 6.88-6.94 (m, 4H), 6.98 (s, 1H), 7.03-7.07 (m, 1H), 7.21-7.23 (m, 1H), 7.34-7.38 (m, 1H), 9.82 (s, 1H); ^{13}C-NMR ($CDCl_3$) 29.7, 55.7, 55.8, 55.8, 55.9, 67.8, 72.5, 84.9, 109.2, 109.3, 110.9, 111.8, 112.1, 118.5, 121.2, 121.5, 124.2, 126.6, 130.3, 131.7, 147.1, 148.4, 148.9, 149.9, 151.5, 153.6, 190.9; HRMS (ES) *m/z* 491.1684 (M+Na, $C_{26}H_{28}O_8Na$ requires 491.1682).

Compound 32.[38] To solution of CH_3CN (50 mL) containing vanillin (2.2 g, 14.5 mmol) was added NaH (60 % in mineral oil) (580 mg, 14.5 mmol) at room temperature. After 1 h stirring at 80 ^{o}C, **29** (2.5 g, 9.6 mmol) was added and the solution was stirred for 24 h at the same temperature. The solution was concentrated following extraction with CH_2Cl_2 and H_2O. The organic extracts were dried and concentrated in *vacuo* to give a residue which was subjected to column chromatography (EtOAc:hexane 1:3) to yield **32** (2.2 g, 70 %). ^{1}H-NMR ($CDCl_3$) 3.92 (s, 3H), 3.95 (s, 6H), 5.42 (s, 2H), 6.83 (d, 1H, *J* = 8.5 *Hz*), 6.90 (d, 1H, *J* = 8 *Hz*), 7.36 (d, 1H, *J* = 8 *Hz*), 7.43 (s, 1H), 7.63 (s, 1H), 7.63

(d, 1H, *J* = 8.5 *Hz*), 9.82 (s, 1H); ^{13}C-NMR ($CDCl_3$) 56.0, 56.0, 56.1, 71.1, 109.7, 110.1, 110.2, 112.4, 122.6, 126.3, 127.3, 130.8, 149.3, 149.9, 152.8, 154.1, 190.8, 191.8; HRMS (ES) *m/z* 353.0996 (M+Na, $C_{18}H_{18}O_6Na$ requires 353.1001).

Photoreaction of 27E. A DCA saturated, O_2 purged solution of **27E** (150 mg, 0.3 mmol) in 150 mL of 5% aqueous MeCN was irradiated by using Uranium glass filtered light for 6 h (50% conversion). Concentration of the photolysate gave a residue, which was subjected to silica gel chromatography (1:3 EtOAc-hexane) to yield **35** (3 mg, 10%) and **36**[25,39] (38 mg, 70%).

DCA Fluorescence quenching by tetrameric lignin models 6EE and 7TE. Fluorescence spectra were recorded on 2 mL of MeCN solutions of DCA (5.4×10^{-6} M) each containing 0, 0.25, 0.5, 1.0, 2.0 mM of the respective tetrameric lignin model compounds. The excitation wavelength was 400 nm.

DCA-promoted photoreactions of tetrameric lignin models 6EE and 7TE. Independent DCA saturated, O_2 purged solutions containing each tetrameric lignin model compounds (0.22 mM of 7TE, 0.46 mM of 6EE) in 4 mL of 5 % aqueous MeCN in quartz tubes were simultaneously irradiated by using uranium filtered light in a merry-go-round apparatus for time periods of 0.5, 1, 1.5, 2, 3, 4 and 5 h. Each photolysate was subjected to HPLC analysis, giving the yields reported in Table 2 and Figure 1.

Lignin peroxidase (LP) catalyzed reactions of tetrameric lignin models 6EE and 7TE. To 200 μL of 50 mM tartrate buffer (pH 3.4) were added 200 μL of tetrameric lignin models (0.5 mM dissolved in 17% MeCN-tartrate buffer, final concentration 0.2 mM) and 40 μL of lignin peroxidase (100.5 μM, final concentration 8 μM, 17.2 units per mL). After 60 μL of H_2O_2 (10 mM, final concentration 1.2 mM) was added, the solutions

were agitated for 30 min and then subjected to HPLC analysis to give the results included in Table 3 and Figure 2.

Determination of steady state kinetic constants of LP Reactions of tetrameric model compounds 6EE and 7TE. LP reactions were carried out by monitoring the formation of bond cleavage products at 310 nm. Reactions were performed in 50 mM tartate buffer (pH 3.4 at 25 ^{o}C) with fixed concentrations of LP (0.26 μM of 17.2 units per mL) and varying concentrations of **6EE** and **7TE** dissolved in 25 % MeCN-buffer solution, and initiated by the addition of a fixed concentration of H_2O_2 (50 μM). For all measurements, the initial velocity data, measured as a function of substrate concentration, were analyzed using following equations: $V = V_{max}[S]/([S]+K_M)$, where V is initial velocity, V_{max} is maximum velocity, [S] is substrate concentration, and K_M is the Michaelis constant. The k_{cat} was calculated from $V_{max}/[E]$ where [E] is the total enzyme concentration.

Acknowledgement

This research was supported financially in part by a subcontract to DDM from a U.S. Department of Energy grant to Paul Langan (20080001DR) through the LANL/LDRD program and a National Research Foundation of Korea Grant (2009-0072585) to UCY. Also, we are grateful to David Fox for generously providing the lignin peroxidase used in this effort.

Supporting Information

Contained in this are ^{1}H and ^{13}C NMR spectra of all previously unidentified compounds, and fluorescence quenching plots. This material is available free of charge via the Internet at http://pubs.acs.org/.

References

1. Adler, E. *Wood Sci. Technol.* **1977**, *11*, 169-218.
2. Sarkanen, K. V. *Lignins: Occurrence, Formation, Structure and Reactions*: Sarkanen, K. V., Ludwig, C. H., Eds.; Wiley-Interscience: New York, 1971; p 95-495.
3. Hammel, K. E.; Jensen, K. A.; Mozuch, M. D.; Landucci, L. L.; Tien, M.; Pease, E. A. *J. Biol. Chem.*, **1993**, *268*, 12274.
4. Tien, M.; Kirk, T. K. *Science* **1983**, *221*, 661.
5. Harvey, P. J.; Schoemaker, H. E.; Bowen, R. M.; Palmer, J. M. *FEBS Lett*. **1985**, *183*, 13.
6. Tien, M.; Kirk, T. K.; Bull, C.; Fee, J. A. *J. Biol. Chem*. **1986**, *261*, 1687.
7. Schmidt, H. W.; Haemmerli, S. D.; Schoemaker, H. E.; Leisolar, M. S. *Biochemistry*. **1989**, *28*, 1776.
8. Hammel, K. E.; Kalyanaraman, B.; Kirk, T. K. *Proc. Natl. Acad. Sci. U.S.A.* **1986**, *83*, 3708.
9. Glenn, J. K.; Morgan, M. A.; Mayfield, M. B.; Kuwahara, M.; Gold, M. H. *Biochem. Biophys. Res. Commun*. **1983**, *114.* 1077.
10. Umezawa, T.; Higuchi, T. *FEBS Lett*. **1987**, *218*, 255.

11. Kawai, S.; Shoji, S. I.; Nabeta, K.; Okuyama, H.; Higuchi, T. *Mokuzai Gakkaishi* **1990**, *36*, 126.

12. Johjima, T.; Itoh, N.; Kabuto, M.; Tokimura, F.; Nakagawa, T.; Wariishi, H.; Tanaka, H. *Proc. Natl. Acad. Sci. U.S.A.* **1999**, *96*, 1989.

13. Have, R. T.; Teunissen, P. J. M. *Chem. Rev*. **2001**, *101*, 3397.

14. de Wild, P.; Van der Laan, R.; Kloekhorst, A.; Heeres, E. *Environ. Prog. Sustainable energy*. **2009**, *28*, 461.

15. Dabo, P.; Cyr, A.; Lessard, J.; Brossard, L.; Menard, H. *Can. J. Chem*. **1999**, *77*, 1225.

16. Hu, W. J.; Kawaoka, A.; Tsai, C. J.; Lung, J.; Osakabe, K.; Ebinuma, H.; Chiang, V. L. *Proc. Natl. Acad. Sci. U.S.A.* **1998**, *95*, 5407.

17. Ralph, J.; MacKay, J. J.; Hatfield, R. D.; O'Malley, D. M.; Whetten, R. W. *Science*. **1997**, *277*, 235.

18. Ralph, J.; Kim, H.; Peng, J.; Lu, F. *Org. Lett*. **1999**, *1*, 323.

19. Tsai, C. J.; Podila, G. K.; Chiang, V. L. *Plant Cell Rep*. **1994**, *14*, 94.

20. Yoon, U. C.; Kwon, H. C.; Hyung, T. G.; Choi, K. H.; Oh, S. W.; Yang, S.; Zhao, Z.; Mariano, P. S. *J. Am. Chem. Soc*. **2004**, *126*, 1110.

21. Cho, D. W.; Parthasarathi, R.; Pimentel, A. S.; Maestas, G. D.; Park, H. J.; Yoon, U. C.; Dunaway-Mariano, D.; Gnanakaran, S.; Langan, P.; Mariano, P. S. *J. Org. Chem*. **2010**, *75*, 6549.

22. Baciocchi, E.; Fabbri, C.; Lanzalunga, O. *J. Org. Chem*. **2003**, *68*, 9061.

23. Langer, V.; Lundquist, K. *Acta Crystallogr. Sect. E.-Struct Rep. Online*, **2002**, *E58*(4), 433.

24. Stomberg, R.; Lundquist, K. *Nord. Pulp Paper Res. J.* **1994**, *9*(1), 37.

25. Castellan, A.; Zhu, J. H.; Colombo, N.; Nourmamode, A.; Davidson, R. S.; Dunn, L. *J. Photochem. Photobiol. A: Chem*. **1991**, *58*, 263.

26. Ciofi-Baffoni, S.; Banci, L.; Brandi, A. *J. Chem. Soc., Perkin Trans. 1*. **1998**, *1*, 3207.

27. Banci, L.; Ciofi-Baffoni, S.; Tien, M. *Biochemistry*. **1999**, *38*, 3205.

28. Setala, H.; Pajunen, A.; Rummakko, P.; Brunow, G. *J. Chem. Soc., Perkin Trans. 1***,** **1999**, *461*.

29. Cottrell, P. T.; Mann, C. K. *J. Electrochem. Soc.*, **1969**, *116*, 1499.

30. Yoon, U. C.; Kim, J. W.; Ryu, J. Y.; Cho, S. J.; Oh, S. W. *J. Photochem. Photobiol. A*, **1997**, *106*, 145.

31. Su, Z.; Mariano, P. S.; Falvey, D. E.; Yoon, U. C.; Oh, S. W. *J. Am. Chem. Soc*. **1998**, *120*, 10676.

32. Poulos, T. L.; Edwards, S. L.; Warishi, H.; Gold, M. H. *J. Biol. Chem.*, **1993**, *268*, 4429.

33. Shoemaker, H. E.; Lundell, T. K.; Hataka, A. I.; Piontek, K. *FEMS Microbiol. Rev.*, **1994**, *13*, 321.

34. Wariishi, H.; Sheng, D.; Gold, M. H. *Biochemistry* **1994**, *33*, 5545.

35. Beratan, D. N.; Onuchic, J. N.; Winkler, J. R.; Gray, H. B. *Science* **1992**, *258*, 1740.

36. Moser, C. C.; Keske, J. M.; Waruche, K.; Farid, R. S.; Dutton, L. *Nature (London)* **1992**, *355*, 796.

37. Pardini, V. L.; Smith, C. Z.; Utley, J. H. P.; Vargas, R. R.; Viertler, H. *J. Org. Chem.* **1991**, *56*, 7305.

38. Criss, D. L.; Fisher, T, H.; Schultz, T. P. *Holzforschung* **1998**, *52*, 57.

39. Nishiyama Y.; Kobayashi, A. *Tetrahedron Lett*. **2006**, *47*, 5565.

A2.2 Investigation of the Catalytic Mechanism of the Hotdog-fold Enzyme Superfamily *Pseudomonas sp*. strain CBS3 4-Hydroxybenzoyl-CoA Thioesterase[+]

Zhihao Zhuang[1#], John Latham[1], Feng Song[1#], Wenhai Zhang[1#], Michael Trujillo[2#] and Debra Dunaway-Mariano[1*]

[1]*Department of Chemistry and Chemical Biology, University of New Mexico, Albuquerque, NM 87131;* [2]*Scientific Laboratory Division, New Mexico Department of Health, Albuquerque, NM 87131*

Running Title: 4-Hydroxybenzoyl-CoA Thioesterase

Key Words: 4-Hydroxybenzoyl-CoA thioesterase, nucleophilic catalysis, base catalysis, solvent kinetic isotope effects, transient kinetics, thioester hydrolysis, hotdog-fold family, divergent evolution, enzyme mechanism.

[+]This work was supported by N.I.H. grant GM 28688

[#]Current Addresses: Z .Z.: 214A Drake Hall, Department of Chemistry and Biochemistry, University of Delaware, Newark DE 19716; F. S.: 3054 E, Syngenta Crop Protection, LLC, Research Triangle Park, NC 27709; W.Z.: Millennium Pharmaceuticals, Cambridge, MA 02139; M.T.: New Mexico Department of Health 1101 Camino de Salud, Albuquerque, NM 87106

*To whom correspondence should be addressed: Debra Dunaway-Mariano, Department of Chemistry and Chemical Biology, University of New Mexico, Albuquerque, NM 87111, Tel: (505) 277-3383, Email: dd39@unm.edu, Fax: (505) 277-6202

Footnotes

[1]Abbreviations used are: coenzyme A (CoA), 4-hydroxybenzoyl-CoA (4-HB-CoA), 4-hydroxybenzoyl-3'-dephospho-CoA (4-HB-3'-dephospho-CoA), 4-hydroxyphenacyl-CoA (4-HP-CoA), 2-(N-morpholino)ethanesulfonate (MES); N-(2-hydroxyethyl)piperzine-N'-2-ethanesulfonate (HEPES); N-tris(hydroxymethyl)methyl-3-aminopropane sulfonate (TAPS); 3-(cyclohexylamino)-2-hydroxy-1-propanesulfonate (CAPSO).

Cellular carboxylic acids are activated for acyl transfers, Michael additions and Claisen condensations by conversion to the corresponding thioester. The thiol unit is typically coenzyme A (CoA)[1] or an acyl carrier protein (ACP) modified at a serine residue with a pantetheine phosphate unit. Following the conversion of the thioester, the CoA or *holo*-ACP is released *via* hydrolysis, a reaction that is catalyzed by a thioesterase. The majority of these thioesterases belong to the hotdog-fold enzyme superfamily (*1*). The 4-hydroxybenzoyl-CoA (4-HB-CoA) thioesterase from *Pseudomonas* sp strain CBS3 was the first hotdog-fold thioesterase to be characterized (*2*). This particular thioesterase is used in the three-step pathway that converts 4-chlorobenzoate to the metabolite 4-hydroxybenzoate (Scheme 1) (*3*).

The X-ray structure of the *apo Pseudomonas* 4-HB-CoA thioesterase revealed a homotetrameric structure comprised of a dimer of dimer (*4*). The subunits consist of a five-stranded anti-parallel sheet that wraps an elongated α-helix. The ensuing atomic resolution X-ray structure determinations of the tetrameric thioesterase, bound with substrate (4-HB-CoA) or a substrate analog (4-hydroxybenzyl-CoA; 4-hydroxyphenacyl-CoA) (PDB accession codes 1LO7, 1LO8 and 1LO9), showed that the active sites are

located at the subunit-subunit interfaces (Figure 1A) (*5*). The structure of the active site suggested a unique catalytic mechanism for thioester hydrolysis, as well as a strict order for product release.

The catalytic scaffold, which is quite minimal, consists of the N-terminal region of the elongated α-helix and its connecting loop (Figure 1B). The loop Asp17 carboxylate oxygen atom (at 3.7 Å from the thioester C=O carbon atom) is optimally positioned for nucleophilic addition to the substrate. Notably, there is no room for a water molecule to bind in between the Asp17 carboxylate group and thioester moiety (Figure 1C). The amide NH of the α-helix N-terminal residue Tyr24 is within hydrogen bond distance (3.2 Å) of the thioester C=O oxygen atom (Figure 1B). Also, the positive pole of the α-helix macrodipole is directed at the thioester group. Raman spectral analysis has shown that these electrostatic interactions orient and polarize the thioester C=O for nucleophilic attack (*6*).

There are no electropositive side chains located near the substrate thioester sulfur atom. Thus, the CoA leaving group appears to be displaced by the Asp17 as a "naked" thiolate anion, stabilized only by the electrostatic field emanating from the α-helix macrodipole. Notably, the catalytic site is devoid of a basic amino acid side chain to perform the role of base in the activation the water molecule for hydrolysis of the anhydride intermediate. It is conceivable that the CoA thiolate serves this function, and once protonated it dissociates from its binding site allowing the exit of the 4-HB, which is otherwise trapped at the bottom of the active site (Figure 1D).

The kinetic studies reported herein, were carried out to test and explore the catalytic mechanism of thioesterase-catalyzed 4-HB-CoA hydrolysis suggested by the

structural data, and to define the microscopic rate constants that govern the kinetic mechanism. Below we report and interpret the results from steady-state and transient-state kinetic analyses, solvent kinetic isotope effect measurements and solvent ^{18}O-labeling experiments.

Materials and Methods

Materials

Recombinant wild-type *Pseudomonas* sp. strain CBS3 4-HB-CoA thioesterase was prepared from the *E. coli* clone as previously described (*7*). 4-HP-CoA, 4-HB-3'-dephospho-CoA, and 4-HB-CoA were prepared according to published procedures (*8*). 4-Methoxybenzoyl-CoA was synthesized from the corresponding benzoyl chloride derivatives and the CoA lithium salt according to the procedures described by Liang et al (1993) (*9*). [^{14}C]4-HB-CoA was prepared as previously described (*10*).

Steady-state kinetic constant determinations from initial velocity data

4-HB-CoA thioesterase-catalyzed hydrolysis of 4-HB-CoA ($\Delta\varepsilon$ = 11.8 $mM^{-1}cm^{-1}$) was monitored using a direct spectrophotometric assay in which the decrease in absorbance at 300 nm associated with the hydrolysis of the thioester substituent is monitored. Reaction solutions initially contained thioesterase, 4-HB-CoA, KCl (0.2 M) and 50 mM K^+HEPES (pH 7.5, 25 ^oC). Initial velocity data were measured as a function of substrate concentration (K_m to $10K_m$) and were fitted to equation 1 using KinetAsyst (IntelliKinetics, PA) to determine the V_{max} and K_m values. The k_{cat} was calculated from the V_{max}/[E] where [E] is the total enzyme active site concentration (determined using the

Bradford method (*11*)).

$$V = V_{max} [S] / ([S] + K_m) \qquad \text{eq. 1}$$

Where V = initial velocity, V_{max} = maximum velocity, [S] = substrate concentration and K_m= Michaelis constant.

Initial velocity data were measured in the absence or presence ($1K_i$, $2K_i$ and $3K_i$) of 4-HB or CoA and were fitted to equation 2 (to define the competitive inhibition constant K_{is}) or to equation 3 (to define the kinetic constants for noncompetitive inhibition K_{ii} and K_{is}), respectively.

$$V = V_{max} [S] / [K_m (1+[I]/K_{is}) + [S]] \qquad \text{eq. 2}$$

$$V = V_{max} [S] (1+[I]/K_{ii}) / [K_m (1+[I]/K_{is}) + [S]] \qquad \text{eq. 3}$$

Where [I] = inhibitor concentration, K_{is} = the slope inhibition constant and K_{ii} = the intercept inhibition constant.

Steady-state multiple turnover time courses

The full time courses for 0.003 μM thioesterase-catalyzed 4-HB-CoA hydrolysis of 4-HB-CoA (1.4, 3.5 and 5.2 μM) in 50 mM K^+HEPES (pH 7.5, 25 ^oC) were monitored at 300 nm ($\Delta\varepsilon = 11.8\ mM^{-1}s^{-1}$). To determine the k_{cat} and K_m values, the data were fitted by curve simulation using the kinetic model:

$$\mathbf{E + S} \underset{k_{-1}}{\overset{k_1}{\rightleftharpoons}} \mathbf{ES} \underset{k_{-2}}{\overset{k_2}{\rightleftharpoons}} \mathbf{E + P}$$

and the definitions: $k_{cat} = k_2$ and $K_m = (k_{-1} + k_2)/k_1$

The KinTek Corporation Global Kinetic Explorer *(*www.kintek-corp.com/KGExplorer/index.php*)* was used to generate the simulations (*12*).

Determination of the Solvent Kinetic Isotope Effect on k_{cat}

The pH rate profiles for thioesterase-catalyzed hydrolysis of 4-HB-CoA in H_2O and D_2O solvent were measured using a dual buffer system consisting of 50 mM acetate and 50 mM MES (pH 4.0 – 5.6); 50 mM MES and 50 mM HEPES (pH 5.6-8.0); 50 mM HEPES and 50 mM TAPS (pH 8.0-9.1); 50 mM TAPS and 50 mM CAPSO (pH 9.1-9.6). The enzyme activity at overlapping pH values was measured to ensure equal enzyme activity in the different buffer systems. The stability of the thioesterase at the acidic and basic pH values was verified by carrying out pre-incubation tests. The k_{cat} pH profile was fitted using equation 4.

$$\log Y = \log [C (1 + H/K_{a1})/(1 + H/K_{a2})] \qquad \text{eq. 4}$$

where Y is the steady-state kinetic constant k_{cat}, H is the proton concentration of the reaction solution, K_a and K_b are the apparent ionization constants of the acidic and basic groups, C is the constant value of Y where it does not change with the solution pH.

Rapid quench transient kinetic determinations

A rapid-quench instrument from KinTek Instruments was used to combine buffered wild-type thioesterase with buffered [^{14}C]4-HB-CoA to initiate the reaction, and then to add 0.2 M HCl to terminate the reaction. For the multiple turnover reactions, mixtures initially contained 10 μM enzyme and 50 μM [^{14}C]4-HB-CoA in 0.15 M KCl/50 mM K^+HEPES (pH 7.5, 25 °C), whereas for the single turnover reactions, enzyme and [^{14}C]4-HB-CoA concentrations were 50 μM and 5 μM, respectively. The enzyme was precipitated from the quenched reaction solution by vigorous mixing with 200 μL CCl_4 using a Vortex mixer, and then pelleted by (micro)centrifugation of the mixture (14,000 rpm for 1 min). The water phase was injected into an HPLC for separation of the [^{14}C]4-HB-CoA and [^{14}C]4-HB as described previously (*13*). The eluent was collected using a fraction collector and analyzed by liquid scintillation counting. Control reactions (lacking enzyme) were carried out in parallel to establish the background radioactivity associated with the [^{14}C]4-HB fraction. The background (~2%) was taken into account when calculating the concentrations of substrate and product remaining in each quenched reaction mixture. The amounts of radioactivity (in CPM) contained in the [^{14}C]4-HB-CoA and [^{14}C]4-HB HPLC fractions were used in conjunction with the specific activity (CPM/micromole) of the substrate to calculate the concentration of substrate remaining and product formed in the reaction mixture for each time point. The time courses for [^{14}C]4-HB-CoA consumption and [^{14}C]4-HB formation were plotted and then fitted by simulation using the KinTek Corporation Global Kinetic Explorer. The initial estimate of an apparent rate constant governing a single turnover of substrate was determined by fitting the single-turnover time course data to equation 5.

$$\ln [S] = -k\, t + \ln [S]_o \qquad \text{eq. 5}$$

where [S] is the substrate concentration at time "t" , $[S]_o$ is the initial substrate concentration and *k* is the apparent first order rate constant.

4-HB-CoA and 4-HP-CoA binding to wild-type thioesterase measured by stopped-flow fluorescence spectroscopy.

Kinetic experiments were performed with an Applied Photophysics DX.17MV sequential stopped-flow spectrophotometer (optical path length 1 cm, mixing time ~3 ms) fitted with a 340 nm cutoff filter. The excitation wavelength was 280 nm. The measurement of the time-dependent quenching of the wild-type thioesterase (0.54 μM) fluorescence by 4-HP-CoA (5.3 μM) or 4-HB-CoA (5.0 μM) was carried out under pseudo-first-order conditions. The observed pseudo-first-order rate constant, k_{obs}, was obtained by fitting the data to equation 6 using the software package provided by Applied Photophysics.

$$\ln (F_0 - F_t)/(F_0 - F_\infty) = -k_{obs}t \qquad \text{eq. 6}$$

Where F_t = the fluorescence at time "t", F_0 = initial fluorescence , F_∞ = final fluorescence, k_{obs} = the observed first-order rate constant.

To measure the association rate constant (k_{on}) and dissociation rate constant (k_{off}) of 4-HP-CoA or 4-HB-CoA binding to wild-type thioesterase, time courses for fluorescence quenching were measured as a function of ligand concentration at fixed enzyme concentration. The resulting k_{obs} values were plotted against the ligand concentrations ([L]) and the data were fitted to equation 7 in order to define the k_{on} and k_{off} values.

$$k_{obs} = k_{on}[L] + k_{off} \qquad \text{eq. 7}$$

^{18}O-Incorporation into 4-hydroxybenzoate (4-HBA) during wild-type thioesterase catalyzed hydrolysis in ^{18}O-enriched water

A 320 μL solution of 1.9 mM wild-type thioesterase in 10 mM K^+HEPES (pH 7.5) containing 0.2 M KCl and 1 mM DTT was lyophilized. To the resulting powder 230 μL of 95% $H_2{}^{18}O$ (Aldrich) was added. After a 30 min incubation period at 25 ˚C, the enzyme solution in $H_2{}^{18}O$ buffer was assayed to ensure that catalytic activity was retained. Next, 20 μL of $H_2{}^{18}O$ was added to a sample of 4-HB-CoA powder obtained by lyophilization of 20 μL of 3.0 mM 4-HB-CoA in natural isotopic abundance water. A 5 μL aliquot of the 4-HB-CoA in $H_2{}^{18}O$ solution was mixed with the enzyme solution at room temperature. After ~ 1 min a second 5 μL aliquot was added. This was repeated twice more. The final enzyme concentration in the reaction solution was 2.4 mM, whereas the final substrate concentration was 0.24 mM ([E]:[S]=10:1). After incubation at room temperature for 15 min, the reaction solution was filtered using a 10 kDa micro separation filter (Pall Filtron). The filtrate was acidified by adding 5 μL of 6 N HCl and extracted four times with 1 mL portions of ethyl acetate. The ethyl acetate extracts were combined, dried over anhydrous sodium sulfate and the solvent was evaporated *in vacuo*. The solid was dissolved in 100 μL of absolute methanol and subjected to GC-MS analysis using a Saturn GC-MS spectrometer equipped with a Restek XTI-5 column.

Results and Discussion

Detection of the Anhydride Intermediate

Experimental design. Enzyme covalent intermediates can usually be captured by using a fast quench technique or a steady-state chemical trap (*14-15*). However, in view

of the intrinsic chemical reactivity of anhydrides it was not surprising that our attempts to isolate the putative aspartyl17-(4-hydroxybenzoyl)anhydride intermediate by using C-14 labeled 4-HB-CoA, in conjunction with rapid quench techniques and enzyme separation, failed. An attempt to trap the anhydride intermediate with the nucleophilic reagent hydroxylamine was also unsuccessful.

Stopped-flow spectroscopy provides a noninvasive method to observe enzyme intermediates provided that their spectral properties are easily distinguished from those of the bound substrate and product. Although stopped-flow *UV*-absorbance proved to be an effective method to monitor the consumption of 4-HB-CoA (at 300 nm $\Delta\varepsilon = 11.8\ mM^{-1}\ cm^{-1}$), the signal from the anhydride intermediate was found to be obscured by those emanating from the substrate and product complexes. Ultimately, we relied on the accurate measurement of radiolabeled substrate and product to reveal, via kinetic analyses, the anhydride intermediate. Based on this strategy, the kinetic experiments reported below were designed and executed.

The kinetic "burst" experiment. The time course for the multiple-turnover of [^{14}C]4-HB-CoA (50 μM) catalyzed by wild-type thioesterase (10 μM) was measured using rapid (acid) quench techniques coupled with HPLC separation and quantitation of the [^{14}C]4-HB-CoA and [^{14}C]4-HB present in the quenched reaction mixtures (Figure 2). The acid quench denatures the enzyme, thereby releasing the bound substrate and product. The anhydride is hydrolyzed to form [^{14}C]4-HB which contributes to the "product pool" of [^{14}C]4-HB (i.e., $[4\text{-HB}]_{observed}$ = [enzyme anhydride intermediate] + [enzyme(CoA)(4-HB)] + $[4\text{-HB}]_{free}$). Providing that the anhydride intermediate is formed at a rate that exceeds the rate of its hydrolysis, the first catalytic turnover of

substrate will be observed to take place faster than will the subsequent turnovers. Indeed, the measured time course for the first few catalytic turnovers shows an initial "burst phase" of [^{14}C]4-HB-CoA consumption, which roughly corresponds to one half of the active sites initially present in the reaction solution. The burst phase is followed by a slower, linear phase of substrate consumption that takes place during the subsequent catalytic turnovers (Figure 2).

Although the observed time course is consistent with the intermediacy of the anhydride intermediate as proposed, so too is a single-step reaction pathway that proceeds with rate-limiting CoA and/or 4-HB product release. Consequently, further experimentation was undertaken to distinguish between rate-limiting anhydride intermediate hydrolysis and rate-limiting product release. To this end, the D_2O solvent kinetic isotope effect (SKIE) on k_{cat} was measured. Product release is typically isotope insensitive whereas a rate-limiting hydrolysis step is expected to give rise to a significant SKIE. Accordingly, the k_{cat} pH profile (Figure 3) was measured in D_2O solvent as well as in H_2O solvent so that the SKIE could be accurately determined. The pH profile shows a double wave, indicative of slowly exchanging substrate and proton (*16*). The kinetic data were fitted to equation (4) to define a break at 5.15 ± 0.09 and C_1 = 5.0 ± 0.1 and a break at 7.70 ± 0.08 and C_2 = 55 ± 4 for catalysis in buffered H_2O, and a break at 5.1 ± 0.1 and C_1 = 1.3 ± 0.2 and a break at 8.0 ± 0.1 and C_2 = 15 ± 1 for catalysis in buffered D_2O. The pH independent isotope effect was calculated from the ratio of the respective C_1 or C_2 values to be 3.8 or 3.7.

Together, the substantial SKIE of 3.7-3.8 and the observed burst-phase kinetic time course (Figure 2), constitute strong evidence for the proposed two-step chemical

pathway. Our next step was to define the microscopic rate constants governing thioesterase catalysis by fitting these and additional kinetic data to a kinetic model representing a two-step chemical pathway.

Substrate binding and product release. The X-ray structure of the D17N thioesterase(4-HB-CoA) complex reveals a "worm-hole"-like active site in which the CoA pantetheine arm fills the tunnel leading to a tight pocket that accommodates the 4-hydroxybenzoyl unit, while the CoA nucleotide units sits at the entrance to this tunnel (Figure 1D) (*5*). In earlier work, we measured the K_d values for the wild-type thioesterase(4-hydroxyphenacyl-CoA) inhibitor complex and the inert D17N thioesterase(4-HB-CoA) complex to be 0.33 and 0.14 μM, respectively by using steady-state fluorescence quenching techniques (*5*). In the present study, stopped-flow fluorescence quenching techniques were used to measure the corresponding binding rates. In Figure 4A, the time course for the binding reaction of 5.3 μM 4-hydroxyphenacyl-CoA with 0.54 μM thioesterase is shown, whereas Figure 4B shows the time course for the binding reaction of 4.0 μM 4-HB-CoA with 0.54 μM thioesterase. The values of the respective apparent pseudo-first order rate constants k_{obs} = 350 ± 4 s^{-1} and 280 ± 30 s^{-1} were obtained by data fitting (equation 6). The plots of k_{obs} vs ligand concentration, shown as insets to Figures 4A and 4B, defined a linear correlation. The association (k_{on}) and dissociation (k_{off}) rate constants were determined by fitting the data to equation 7. For 4-hydroxyphenacyl-CoA, k_{on} = 59 ± 1 $\mu M^{-1}s^{-1}$ and k_{off} = 20 ± 5 s^{-1} define the microscopic rate constants for substrate binding and dissociation. Indeed, the ratio k_{off}/k_{on} = 0.33 μM is in perfect agreement with the independently measured K_d = 0.33 μM (*5*). For 4-HB-CoA, we note that only if the substrate binding step is in rapid

equilibrium do the k_{on} = 65 ± 2 $\mu M^{-1}s^{-1}$ and the k_{off} = 13 ± 5 s^{-1} values accurately define the microscopic rate constants for substrate binding and dissociation. The ratio k_{off}/k_{on} = 0.20 μM falls halfway in between the 4-HB-CoA K_m = 0.26 μM (*vide infra*) and the independently measured K_d = 0.14 μM (*5*).

The quantitative analysis of product binding was limited (for technical reasons) to the determination of the steady-state inhibition constants for thioesterase-catalyzed hydrolysis of 4-HB-CoA. CoA proved to be a weak noncompetitive inhibitor (K_{is} = 250 ± 70 μM, K_{ii} = 900 ± 300 μM) and 4-HB, a weak competitive inhibitor (K_{is} = 1.2 ± 0.2 mM). The competitive inhibition observed for 4-HB (binds only to the free enzyme), and the noncompetitive inhibition (binds to the free enzyme (slope effect) and to the enzyme-anhydride intermediate and/or enzyme(4-HB) complex (intercept effect)) observed for CoA are consistent with CoA departure preceding that of 4-HB, as was predicted from the X-ray structure the D17N thioesterase(4-HB-CoA) complex.

Reaction time course analysis. In order to define the microscopic rate constants for thioesterase catalysis, the measurement of time courses, which would supplement the transient-state, multiple-turnover time course (Figure 2) and the time course for substrate binding (Figure 4) was pursued. Firstly, the time course for a single-turnover reaction was measured by using 50 μM wild-type thioesterase to catalyze the hydrolysis of 5 μM [^{14}C]4-HB-CoA (Figure 5). Secondly, steady-state multiple-turnover time courses were measured using 1.4, 3.5 or 5.2 μM 4-HB-CoA and 0.003 μM thioesterase (Figure 6).

The simulation-based fitting of the four sets of time-course data was carried out using the kinetic model shown in Scheme 2. This model assumes includes the substrate-

binding step, the two chemical steps and the two (ordered) product release steps. A more complex model in which CoA dissociates prior to the hydrolysis of the anhydride intermediate was also considered. However, the divergence observed in the sets of microscopic rate constants used to generate optimal fits to the respective time courses, was comparatively large. For this reason, the model was not carried forward.

To initiate the simulation process, estimates of the microscopic rate constants were obtained by conventional fitting of the individual data sets (see Material and Methods). The values of the microscopic rate constants were varied individually, and in combination, until the simulated curve matched the experimental time course. The simulated curves are shown in Figures 2, 4, 5 and 6 along with the values of the microscopic rate constants used in the simulation. During the process of fitting the four time courses we discovered, as one might anticipate, that there is some variation in the extent to which the allowed range of a given microscopic rate constant can be confined. For instance, the value of k_3 (governs the rate-limiting anhydride hydrolysis step) was inconsequential to the simulation of the substrate-binding time course, whereas it could not deviate more that 10% without noticeably compromising the respective fits of the simulated curves to the other time courses. On the other hand, the values of the microscopic rate constants governing the product release steps had a limited impact on the simulation process.

Everything considered, the rate microscopic rate constants governing the substrate-binding step and the two chemical steps are reasonably well defined. We show in Figure 5, along with the simulated single-turnover time course data, the simulated curves representing the anhydride intermediate and the 4-HB product. At 25 ms the

anhydride intermediate peaks at ~40% and then slowly declines. The slow onset of 4-HB formation (*i.e.*, initial lag in the simulated time course colored green) is the reflection of the rate-limiting hydrolysis step. In the section that follows, we report the ^{18}O-solvent labeling experiment that was used to determine the regiochemistry of hydrolysis of the anhydride intermediate.

Regiochemistry of the Hydrolysis of the Anhydride Intermediate

The attack of the water nucleophile at the anhydride intermediate formed in the first step of thioesterase catalysis can potentially occur at either the benzoyl carbonyl carbon or the aspartyl carbonyl carbon. In order to determine the regiochemistry of the hydrolysis step, single turnover reactions were carried out in 95% $H_2{}^{18}O$ solvent. If the Asp17 carbonyl carbon is attacked, the 4-HB product will not contain the solvent-derived ^{18}O atom in its carboxylate group, but instead it will contain the Asp17-derived ^{16}O atom. On the other hand, if the benzoyl carbonyl carbon is attacked, the 4-hydroxybenzoate product will contain the ^{18}O atom derived from solvent. The mass spectrum of the 4-hydroxybenzoic acid standard (see Figure 7A) contains the parent ion (M*) peak at 138 m/z, parent ion fragment (M*-OH) peak at 121 m/z (note that the OH group lost is from the carboxylic acid group, not the aromatic ring), a fragment (M*-COOH) at 93 m/z and lastly, a fragment at 65 m/z (not assigned). The parent ion (M*) and parent ion fragment (M*-OH) contain oxygen from the carboxylic acid group, and can thus be used to measure the oxygen-18 incorporation.

The mass spectrum of the 4-hydroxybenzoic acid isolated from the single turnover reaction of 4-HB-CoA (0.24 mM) catalyzed by the wild-type thioesterase (2.4

mM) in 95% $H_2{}^{18}O$ revealed that >90% of the parent ion peak occurs at 140 m/z (see Figure 7B), which means that the vast majority of the 4-hydroxybenzoic acid is labeled at the carboxylic acid group with one ^{18}O atom and one ^{16}O atom. The equal probability of losing either carboxylic acid oxygen atom in the parent ion resulted in an equal amount of (M*-OH) specie at 121 and 123 m/z. These findings demonstrate that hydrolysis occurs at the benzoyl carbonyl carbon of the Asp17-(4-hydroxybenzoyl)anhydride intermediate.

Conclusions

In Figure 8 we propose a reaction mechanism for 4-HB-CoA catalysis, which integrates the findings from earlier investigations (*5, 6*) with those presented here. The reaction begins with very tight substrate binding. The catalytic site is located at the end of a narrow tunnel that leads from solvent to an enclosed, largely hydrophobic pocket (Figure 1D). The conformation of the thioesterase, and the substrate-binding site in particular, is unchanged by substrate binding. Thus, a "lock-in-key" model of substrate binding is applicable. The substrate-binding rate (k_1 ~ 70 $\mu M^{-1}s^{-1}$) is about average, however the dissociation rate is slow (k_{-1} ~15 s^{-1}) and therefore the K_d = 0.14 μM is quite small. The substrate 4-hydroxybenzoyl unit is immobilized by tight packing with the surrounding side chains, several of which are aromatic. The single hydrogen bond formation with the benzoyl ring hydroxyl group involves the indole NH of Trp47 (Figure 1B).

At the catalytic site, the substrate thioester C=O is oriented and activated for nucleophilic attack by the Asp17 carboxylate group. The range for a pre-transition state conformation (*i.e*, "near-attack-conformation") of a carboxylate oxygen anion and the

carbonyl carbon electrophile, posited by Lightstone and Bruice (*17*), is depicted in Figure 8 alongside the orientation of the Asp17 observed in the thioesterase X-ray structures (5). The Asp17 thus appears to be in a "near-attack-conformation". Substitution of the Asp17 with a Glu extends the side chain by one methylene group, which we expect would offset the alignment of the carboxylate oxygen anion with the 4-HB-CoA thioester C=O. Indeed, the magnitude of the rate reduction observed for the D17E thioesterase is ~1000-fold (*6*), is consistent with a significant perturbation of the ground state.

The displacement of the CoA thiolate anion is assumed to be a concerted reaction. This is because the pK_a of the conjugate acid (= 9.7) is low enough to fall well within the limit prescribed for concerted ester hydrolysis (*18*). The CoA thiolate anion is not within reach of an active site residue, yet it could favorably interact with electropositive field generated by the α-helix N-terminus. If the CoA does not depart before the ensuing hydrolysis step, it might serve to orient and activate the water molecule for attack at the 4-hydroxybenzoyl carbonyl carbon. This scenario is depicted in Figure 8, with the caveat that we have provided little in the way of supporting evidence. Additional work will be required in order to define the mechanism of the rate-limiting step of thioesterase catalysis.

The proposed mechanism of the *Pseudomonas* 4-HB-CoA thioesterase catalysis deviates from the mechanisms employed by the thioesterases of the α/β-fold hydrolase enzyme superfamily, which are centered on covalent catalysis by the Ser of the Ser-His-Asp/Glu catalytic triad, and on electrophilic catalysis by an oxyanion hole (*19*). In contrast, the thioesterase of the crotonase enzyme superfamily (3-hydroxyisobutyryl-CoA thioesterase) shares with the 4-HB-CoA thioesterase the use of a carboxylate residue

(Glu143) in nucleophilic catalysis and the use of the N-terminus (positive pole) of an α-helix in electrophilic catalysis (*20)*. A detailed comparison of the catalytic mechanisms of hotdog-fold thioesterases, including the 4-HB-CoA thioesterase, is planned for a separate publication. Nevertheless, to date the 4-HB-CoA thioesterase is the only member of the hotdog-fold family known to use the catalytic carboxylate group in nucleophilic catalysis.

Acknowledgements

The authors thank Drs. Zhibing Lu and Karen Allen for preparing Figure 1C and W. W. Cleland for critically reading the manuscript. Also, we say "thank you" to a very helpful reviewer.

References

1. Dillon, S. C., and Bateman, A. (2004) The Hotdog fold: wrapping up a superfamily of thioesterases and dehydratases. *BMC Bioinformatics 5*, 109.
2. Scholten, J. D., Chang, K. H., Babbitt, P. C., Charest, H., Sylvestre, M., and Dunaway-Mariano, D. (1991) Novel enzymic hydrolytic dehalogenation of a chlorinated aromatic. *Science 253*, 182-185.
3. Dunaway-Mariano, D., and Babbitt, P. C. (1994) On the origins and functions of the enzymes of the 4-chlorobenzoate to 4-hydroxybenzoate converting pathway. *Biodegradation 5*, 259-276.
4. Benning, M. M., Wesenberg, G., Liu, R., Taylor, K. L., Dunaway-Mariano, D., Holden, H. M. (1998) The three-dimensional structure of 4-hydroxybenzoyl-CoA thioesterase from *Pseudomonas* sp. Strain CBS-3. *J. Biol. Chem. 273*, 33572-33579.
5. Thoden, J. B., Holden, H. M., Zhuang, Z., Dunaway-Mariano, D. (2002) X-ray crystallographic analyses of inhibitor and substrate complexes of wild-type and mutant 4-hydroxybenzoyl-CoA thioesterase. *J. Biol. Chem. 277*, 27468-27476.
6. Zhuang, Z., Song, F., Zhang, W., Taylor, K., Archambault, A., Dunaway-Mariano, D., Dong, J., Carey, P. R.. (2002) Kinetic, Raman, NMR, and site-directed mutagenesis studies of the *Pseudomona*s sp. strain CBS3 4-hydroxybenzoyl-CoA thioesterase active site. *Biochemistry 41,* 11152-11160.
7. Chang, K. H., Liang, P. H., Beck, W., Scholten, J. D., and Dunaway-Mariano, D. (1992) Isolation and characterization of the three polypeptide components of 4-

chlorobenzoate dehalogenase from *Pseudomonas* sp. strain CBS-3. *Biochemistry 31*, 5605-5610.

8. Luo, L., K. L. Taylor, H. Xiang, Y. Wei, W. Zhang, and D. Dunaway-Mariano. (2001) Role of active site binding interactions in 4-chlorobenzoyl-coenzyme A dehalogenase catalysis. *Biochemistry 40*, 15684-15692.
9. Liang, P. H., G. Yang, and D. Dunaway-Mariano. (1993) Specificity of 4-chlorobenzoyl coenzyme A dehalogenase catalyzed dehalogenation of halogenated aromatics. *Biochemistry 32*, 12245-12250.
10. Zhuang, Z., Gartman, K-H, Eichenlaub, R. and Dunaway-Mariano, D. (2003) Characterization of the 4-hydroxybenzoyl-coenzyme A thioesterase from *Arthrobacter* sp. strain SU. Appl. *Environ. Microbiol. 69*, 2707-2711.
11. Bradford, M. M. (1976) A rapid and sensitive method for the quantitation of microgram quantities of protein utilizing the principle of protein-dye binding. *Anal Biochem 72*, 248-254.
12. Johnson, K. A. (2009) Fitting enzyme kinetic data with KinTek Global Kinetic Explorer. Methods Enzymol. 467, 601-626.
13. Zhang, W., Wei, Y., Luo, L., Taylor, K. L., Yang, G., Dunaway-Mariano, D., Benning, M. M., and Holden, H. M. (2001) Histidine 90 function in 4-chlorobenzoyl-coenzyme A dehalogenase catalysis. *Biochemistry 40*, 13474-13482.
14. Johnson, K. A. (2003) *Kinetic Analysis of Macrolecules. A Practical Approach*.
15. Purich, D. Covalent enzyme-substrate compounds: detection and catalytic competence. (2002) *Methods Enzymol*. *354*, 1-27.

16. Cleland, W. W. (1977) Determining the chemical mechanisms of enzyme-catalyzed reactions by kinetic studies. *Adv. Enzymol. Relat. Areas Mol. Biol. 45*, 273-387.

17. Lightstone, F. C., Bruice, Thomas C. (1996) Ground state conformations and entropic and enthalpic factors in the efficiency of intramolecular and enzymic reactions. 1. Cyclic anhydride formation by substituted glutarates, succinate, and 3,6-endoxo-D4-tetrahydrophthalate monophenyl esters. *J. Amer. Chem. Soc. 118*,2595-2605.

18. Hess, R.A, Hengge, A.C., and Cleland, W.W. (1998) Isotope effects on enzyme-catalyzed acyl transfer from p-nitrophenyl acetate: Concerted mechanisms and increased hyperconjugation in the transition state. *J. Amer. Chem. Soc. 120*, 2703-2709.

19. OLLIS, D. L., CHEAH E., CYGLER M., DIJKSTRA B., FROLOW F., FRANKEN S. M., HAREL M, REMINGTON S. J., SILMAN I., SCHRAG J., SUSSMAN, J. L., VERSCHUEREN, K.H. G., AND GOLDMAN, A. (1992) THE ALPHA/BETA HYDROLASE FOLD. *PROTEIN ENG.* *5*, 197-211.

20. WONG, B. J. AND GERLT, J. A. (2003) DIVERGENT FUNCTION IN THE CROTONASE SUPERFAMILY: AN ANHYDRIDE INTERMEDIATE IN THE REACTION CATALYZED BY 3-HYDROXYISOBUTYRYL-COA HYDROLASE. *J. AMER. CHEM. SOC*. *125*, 12076-12077.

Scheme 1. The three chemical steps of the 4-chlorobenzoate degradation pathway catalyzed by 4-chlorobenzoate: CoA ligase, 4-chlorobenzoyl-CoA dehalogenase and 4-hydrobenzoyl-CoA thioesterase, respectively.

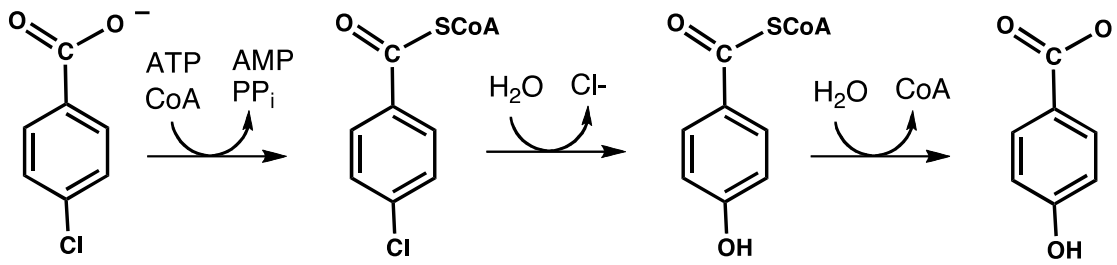

Scheme 2. The kinetic model representing 4-HB-CoA thioesterase catalysis. Abbreviations: E, thioesterase; EI, thioesterase-anhydride intermediate; S, 4-HB-CoA; P, CoA; Q, 4-HB.

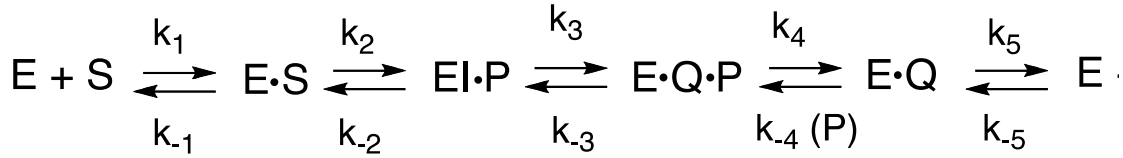

Figure Legends

Figure 1. The structure of D17N *Pseudomonas* sp. strain CBS3 4-HB-CoA thioesterase bound with 4-HB-CoA (PDB accession code 1LO9). (**A.**) The tetramer shown in Pymol cartoon with the 4-HB-CoA ligands shown in yellow stick. (**B**.) The active site structure wherein the 4-HB-CoA has been truncated for better viewing and the Asn17 has been mutated *in silico* to Asp17. Hydrogen bonds are indicated in gray or black dashed lines. The 3.7 Å distance between the Asp17 carboxylate group oxygen atom and the 4-HB-CoA ring carbonyl carbon atom is represented by the magenta dashed line. The nitrogen atoms are colored blue, the oxygen atoms red, the sulfur atom yellow and the enzyme carbons atoms are colored gray whereas the 4-HB-CoA carbon atoms are colored cyan. (**C.)** Stereo figure of the active site solvent cage generated from the empty active site cavity produced in VOIDOO (teal colored mesh). The 4-HB-CoA ligand fills the cage. Carbon atoms are shown in gray, oxygen atoms in red, nitrogen atoms in blue and sulfur atoms in yellow. (**D**) The surface representation of the thioesterase substrate-binding site. The 4-HB-CoA ligand is shown in stick with carbon atoms colored cyan. The Asp17 side chain and Tyr24 amide unit are shown in stick with carbon atoms colored green.

Figure 2. A plot of the experimental and simulated time courses for the transient-state multiple-turnover reaction of 10 μM wild-type thioesterase and 50 μM [^{14}C]4-HB-CoA in 50 mM K^+HEPES (pH 7.5, 25 ^{o}C). The time point data ([^{14}C]4-HB-CoA (•) and [^{14}C]4-HB (**O**)) were calculated from the fraction of [^{14}C]4-HB-CoA or [^{14}C]4-HB present in the acid-quenched reaction mixture multiplied by the initial concentration of

[^{14}C]4-HB-CoA present in the reaction. The simulated curves were generated using the kinetic model shown in Scheme 2 and the following set of rate constants: k_1 = 71 μM^{-1} s^{-1}, k_{-1} = 12 s^{-1}, k_2 = 290 s^{-1}, k_{-2} = 67 s^{-1}, k_3 = 23 s^{-1}, k_{-3} = 0 s^{-1}, k_4 /k_{-4} = 300 μM and k_5 /k_{-5} = 1200 μM. The simulated curve-coloring scheme is as follows: E-I(CoA) + E(4-HB)(CoA) + E(4-HB) + 4-HB (red); E(4-HB-CoA) + 4-HB-CoA (black).

Figure 3. A plot of log k_{cat} vs reaction solution pH measured for wild *Pseudomonas* sp. strain CBS3 4-HB-CoA thioesterase-catalyzed hydrolysis of 4-HB-CoA in H_2O solvent (●) or D_2O solvent (○).

Figure 4. (**A**) Time-dependent fluorescence change associated with the binding reaction between 5.3 μM 4-HP-CoA and 0.54 μM thioesterase in 50 mM K^+HEPES (pH 7.5, 25 ^oC). The data were fitted to equation 6 to define the observed rate constant k_{obs} as 350 ± 4 s^{-1}. Inset: a plot of the k_{obs} vs 4-HP-CoA concentration (1.0 - 5.3 μM). The data were fitted to equation 7 to define the association rate constant k_{on} as 59 ± 1 $\mu M^{-1}s^{-1}$ and the dissociation rate constant k_{off} as 20 ± 5 s^{-1}. (**B.**) Time-dependent fluorescence change associated with the binding reaction between 5.0 μM 4-HB-CoA and 0.54 μM thioesterase in 50 mM K^+HEPES (pH 7.5, 25 ^oC). The data were fitted to equation 6 to define the observed rate constant k_{obs} as 280 ± 30 s^{-1}. Inset: a plot of the k_{obs} vs 4-HB-CoA concentration (1.0 - 5.0 μM). The data were fitted to equation 7 to define the

association rate constant k_{on} as 65 ± 2 $\mu M^{-1}s^{-1}$ and the dissociation rate constant k_{off} as 13 ± 5 s^{-1}. (**C**) The time course for the binding reaction between 3.0 μM 4-HB-CoA and 0.54 μM thioesterase in 50 mM K^+HEPES (pH 7.5, 25 ^oC). The simulated curved was generated using the kinetic model shown in Scheme 2 and the rate constants k_1 = 70 $\mu M^{-1}s^{-1}$ and k_{-1} = 15 s^{-1}.

Figure 5. The experimental and simulated time courses for the single-turnover reaction of 50 μM wild-type thioesterase and 5 μM [^{14}C]4-HB-CoA in 50 mM K^+HEPES (pH 7.5, 25 ^oC). The time point data ([^{14}C]4-HB-CoA (•) and [^{14}C]4-HB (O)) were calculated from the fraction of [^{14}C]4-HB-CoA or [^{14}C]4-HB present in the acid-quenched reaction mixture multiplied by the initial concentration of [^{14}C]4-HB-CoA present in the reaction. The simulated curves were generated using the kinetic model shown in Scheme 2 and the following set of rate constants: k_1 = 79 μM^{-1} s^{-1}, k_{-1} = 20 s^{-1}, k_2 = 76 s^{-1}, k_{-2} = 50 s^{-1}, k_3 = 26 s^{-1}, k_{-3} = 0 s^{-1}, k_4 /k_{-4} = 300 μM and k_5 /k_{-5} = 1200 μM. The simulated curve-coloring scheme is as follows: E-I(CoA) + E(4-HB)(CoA) + E(4-HB) + 4-HB (red); E(4-HB-CoA) + 4-HB-CoA (black); E-I(CoA) (yellow); E(4-HB)(CoA) + E(4-HB) + 4-HB (green).

Figure 6. The time courses for the steady-state multiple-turnover reactions of 1.4 (black), 3.5 (red) or 5.2 (green) μM 4-HB-CoA catalyzed by 0.003 μM thioesterase in 50 mM K^+HEPES (pH 7.5, 25 ^oC). The 300 nm absorbance traces (dotted lines) are shown in the context of the calculated concentration of 4-HB-CoA (ε = 11.8 mM^{-1} cm^{-1}) present in the reaction mixture (y-axis) as a function of reaction time (x-axis). The simulated curves

(solid lines) were generated using the kinetic model shown in Scheme 2 and rate constants: $k_1 = 71\ \mu M^{-1}\ s^{-1}$, $k_{-1} = 12\ s^{-1}$, $k_2 = 290\ s^{-1}$, $k_{-2} = 67\ s^{-1}$, $k_3 = 23\ s^{-1}$, $k_{-3} = 0\ s^{-1}$, $k_4 /k_{-4} = 300\ \mu M$ and $k_5 /k_{-5} = 1200\ \mu M$.

Figure 7. The GC-MS analysis of the 4-HB product generated in the single turnover reaction of 4-HB-CoA (0.24 mM) catalyzed by the wild-type thioesterase (2.4 mM) in 95% $H_2{}^{18}O$ containing 50 mM K^+HEPES (pH 7.5, 25 ^oC) (**A.**) GC-MS spectrum of the 4-hydroxybenzoic acid standard. (**B.**) GC-MS spectrum of the 4-hydroxybenzoic acid isolated the quenched reaction mixture.

Figure 8. A cartoon representation of the proposed mechanism of 4-HB-CoA thioesterase catalysis. The rates shown over the arrows correspond to the range of values obtained for the microscopic rate constants via the time course simulations. The boxed content: (left) an adaptation of a figure from reference (*17*), which depicts the ranges of optimal positions for nucleophilic attack of a carboxylate oxygen anion at a carbonyl carbon as posited by Lightstone and Bruice and (right) the distance and angle of attack of the Asp17 carboxylate oxygen atom at the 4-HB-CoA carbonyl carbon as inferred from the X-ray structure of the D17N thioesterase(4-HB-CoA) complex (PDB accession code 1LO9).

Figure 1

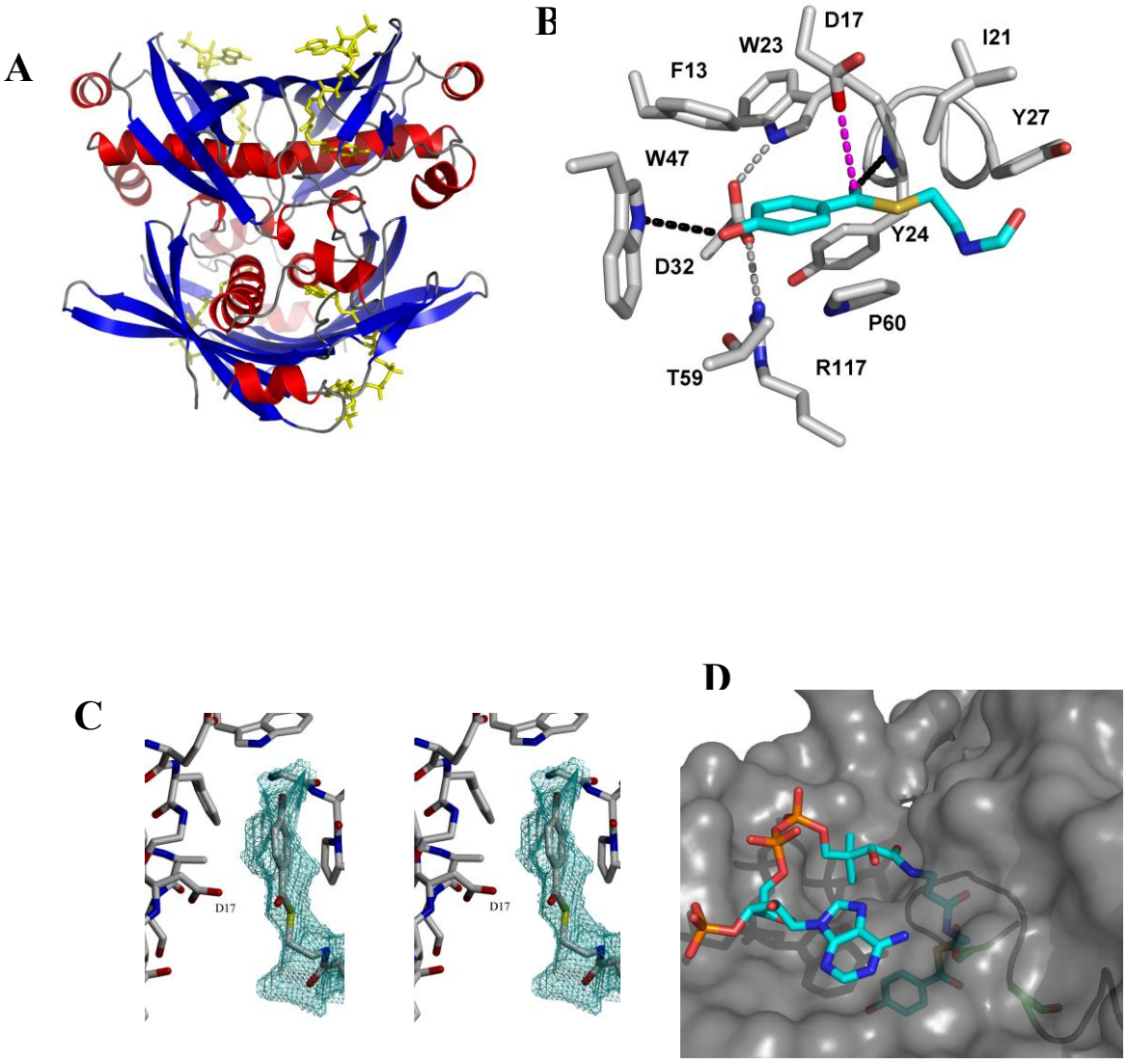

Figure 2

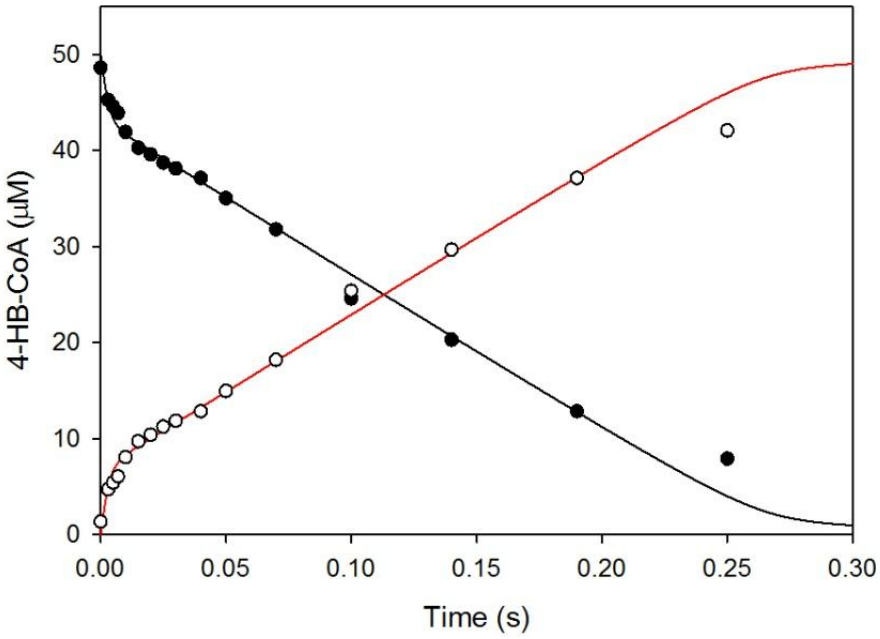

Figure 3

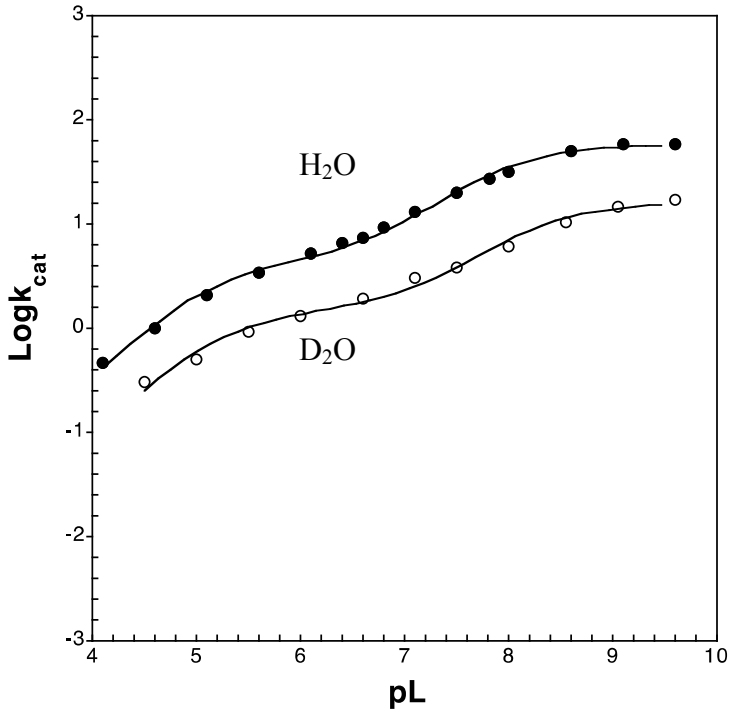

Figure 4

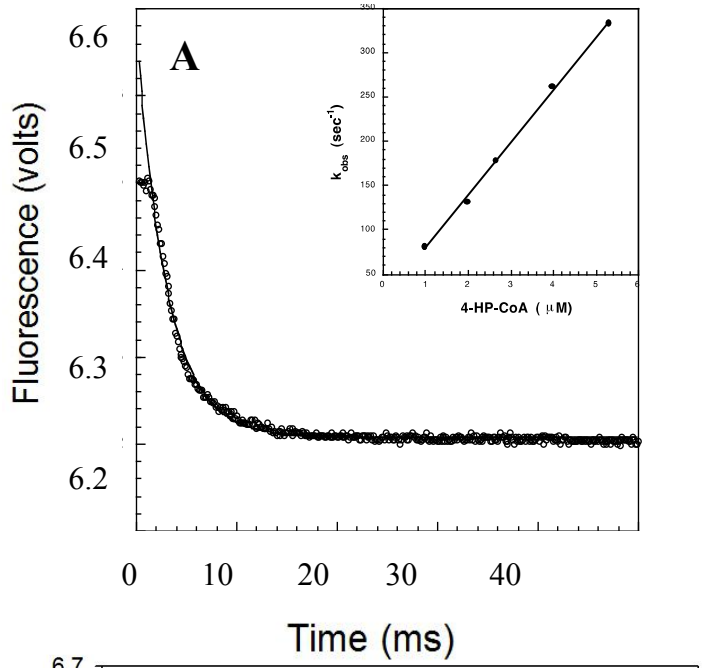
A
Fluorescence (volts)
6.6
6.5
6.4
6.3
6.2
0
10
20
30
40
Time (ms)
k_{obs} (sec^{-1})
4-HP-CoA (μM)

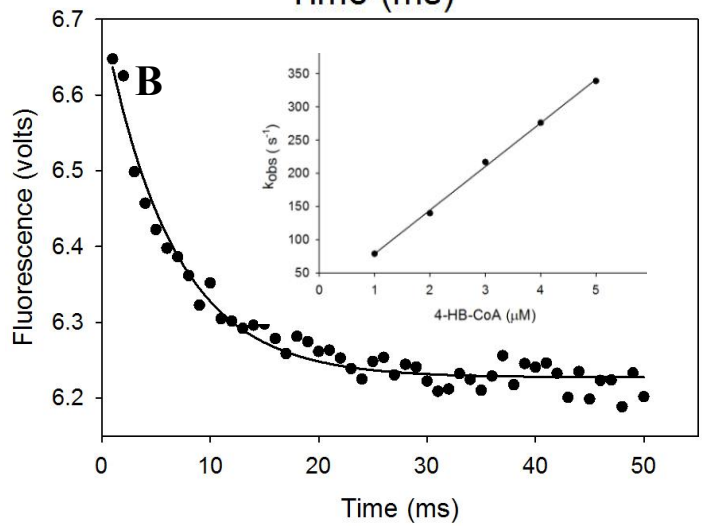
B
Fluorescence (volts)
6.7
6.6
6.5
6.4
6.3
6.2
0
10
20
30
40
50
Time (ms)
k_{obs} (s^{-1})
4-HB-CoA (μM)

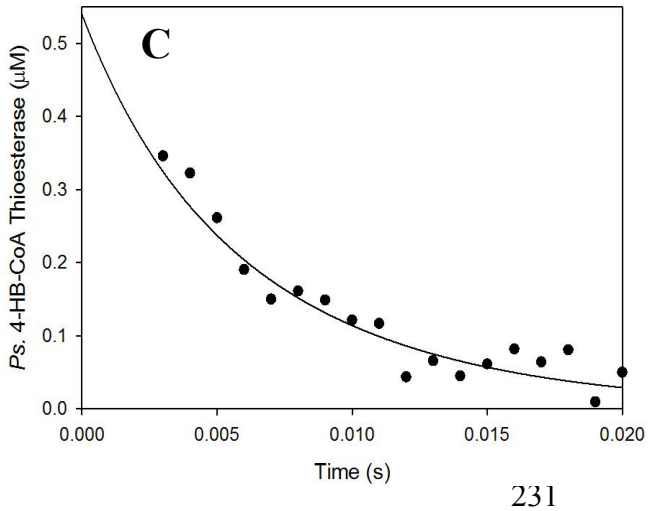
C
Ps. 4-HB-CoA Thioesterase (μM)
0.5
0.4
0.3
0.2
0.1
0.0
0.000
0.005
0.010
0.015
0.020
Time (s)

Figure 5

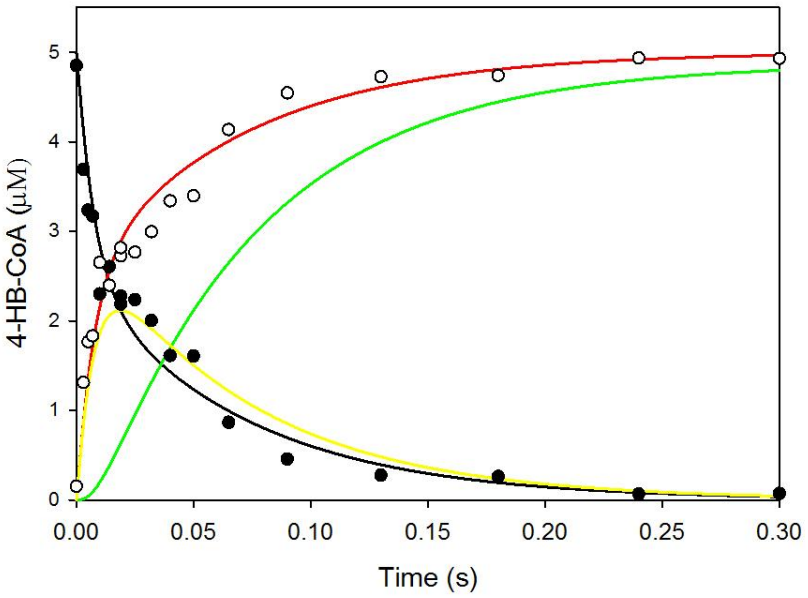

Figure 6

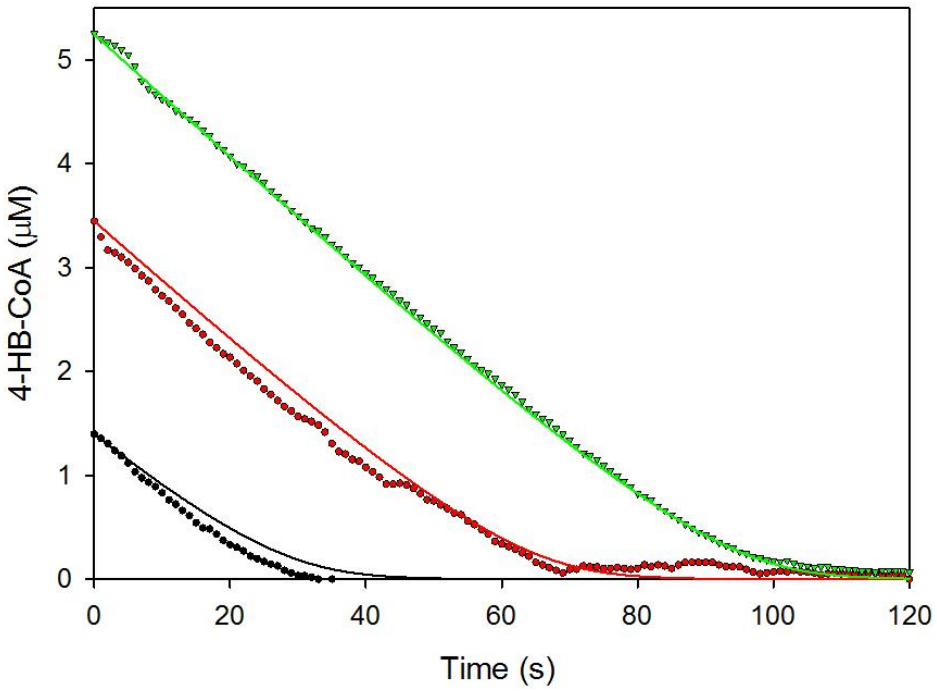

Figure 7

A

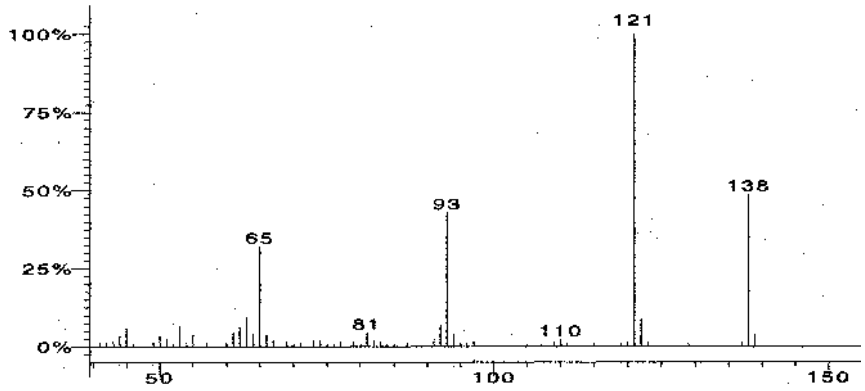

m/z

B m/z

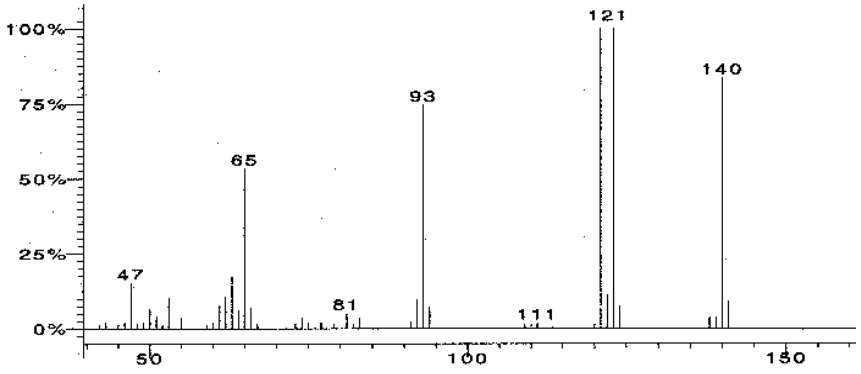

m/z

Figure 8

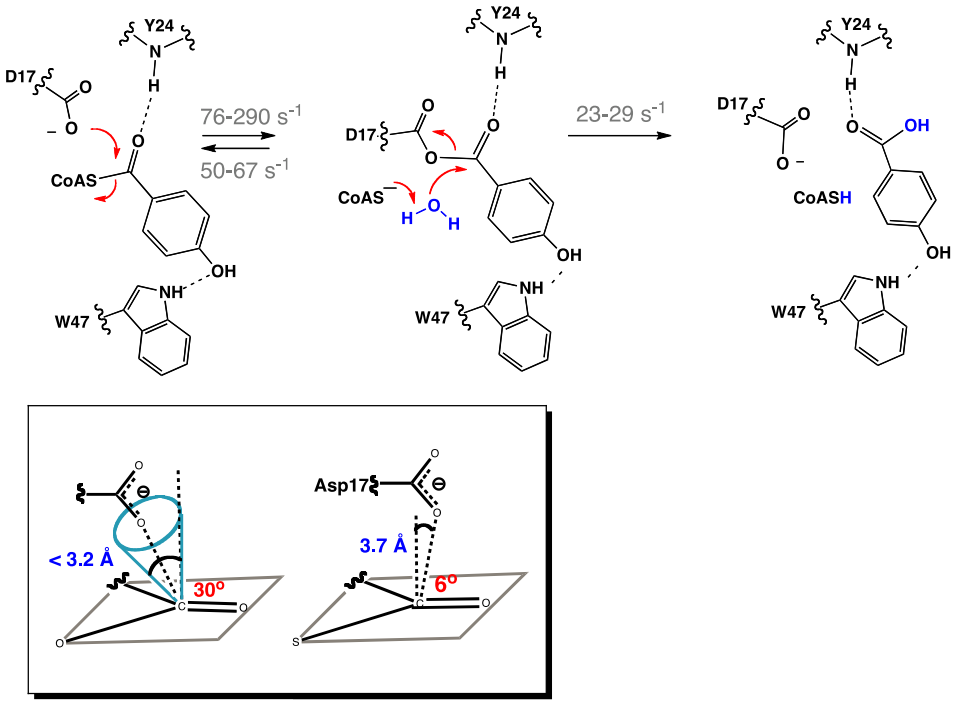
Y24
D17
CoAS
W47
76-290 s-1
50-67 s-1
23-29 s-1
CoASH
OH
NH
Asp17
< 3.2 Å
30°
3.7 Å
6°

For Table of Contents use only

Investigation of the Catalytic Mechanism of the Hotdog-fold Enzyme Superfamily *Pseudomonas sp.* strain CBS3 4-Hydroxybenzoyl-CoA Thioesterase[+]

Zhihao Zhuang[1], John Latham[1], Feng Song[1], Wenhai Zhang[1], Michael Trujillo[2] and Debra Dunaway-Mariano[1*]